

Erosive and Accretive Coastal Profile Response

Report

April 2008

Erosive and Accretive Coastal Profile Response

Claartje Hoyng

M.sc. Thesis

April 2008

Graduation Committee

Prof. dr. ir. M.J.F. Stive

Prof. dr. ir. L.C. van Rijn

Dr. J.E.A. Storms

Ir. D.J.R. Walstra

Preface

The M.Sc. thesis is the final step of my study at Delft, University of Technology, Faculty of Civil Engineering and Geosciences, section Hydraulic Engineering.

During the summer months of 2007, I co-operated with the physical model tests carried out in the Scheldt flume of WL|Delft Hydraulics. Within the framework of the project SANDS, morphological tests were set-up to advance the mobile-bed scaling laws and to test new instruments. The other project VOP aims at establishing and quantifying the dominant physical processes that are affected by the presence of a shoreface nourishment. I would like to thank WL|Delft Hydraulics for the opportunity to be involved in these experiments.

I would like to thank my graduation committee, Prof. dr. ir. M.J.F. Stive (Delft University of Technology), Prof. dr. ir. L.C. van Rijn (WL | Delft Hydraulics), Dr. J.E.A. Storms (Delft University of Technology) and especially Ir. D.J.R. Walstra (WL | Delft Hydraulics) for their enthusiastic support. Also, I would like to thank Pieter-Koen Tonnon and John Coolegem, who were also involved in the tests carried out in the Scheldt flume.

Furthermore, I would like to thank my fellow graduate students for the very pleasant time we had at WL | Delft Hydraulics. Finally, I would like to show gratitude to all my friends and family for their support and the good times during the last seven years. A special thanks goes to Bram, who was my biggest support and helped me through the tough times.

Claartje Hoyng,

Delft, April 2008

Short summary

Project SANDS

To advance the mobile bed scaling laws and to test new instruments, identical tests are carried out on different scale levels in three hydraulic facilities; Hannover GWK Flume, Barcelona Flume and Delft Scheldt Flume. Data obtained in Hannover and Barcelona are not yet available. Focus is on the Delft data; bed profile development and distorted models.

The initial bed slopes were fixed, respectively 1/20, 1/15 and 1/10. Two wave time series are run consecutively, the erosive ($H_s = 0.17 \text{ m} / T_p = 2.3 \text{ s}$) and the accretive wave condition ($H_s = 0.1 \text{ m} / T_p = 3.0 \text{ s}$). The bed profiles exposed to an accretive wave condition show a shoreward migration of the breaker bar, caused by a dominant seaward transport by undertow. The profiles subject to an erosive condition show an offshore migration, caused by a dominant landward transport by wave asymmetry. No equilibrium profile is reached. It may be possible that the process stops, if the decay of the wave height over the surf zone is sufficiently large. The length between the breaker bar and the coastline should be very large, in order to be able to reduce the wave height to such an extent. Such a profile is not likely to occur. Profiles exposed to an accretive condition, did not reach an equilibrium either.

Distorted models are physical models in which the horizontal length scale and the vertical length scale are different. Distorted hydraulic models are used because of limitations on the available space in the flume, or because of a lack of control over the modelling materials and conditions. Erosion and deposition volumes are analysed to find the morphological time scale factor ($n_{Tm} = (n_l / n_h)^{b+1} (n_{d50})^d (n_{s-1})^e / (n_h)^{0.5-0.5a+0.5c}$). The morphological time scale factor of test 1:15 is 2-2.5 and for test 1:10 the average time scale factor is 8. By means of the time scale factor, erosion and deposition volumes of the erosive tests 1:10 and 1:15 are re-calculated and correspond fairly well to the original erosion and deposition volumes of test 1:20. However, the bed profiles of test 1:10 and 1:15 translated to the reference test do not correspond with the reference test. The distortion scale should be as small as possible, to prevent the generation of scale effects.

Project VOP

The Dutch coast is maintained by sand nourishment. This study focusses on shoreface nourishment. At this moment, no hydrodynamic measurements or data on sediment transports are available. A low and a high nourishment design are implemented in the Scheldt flume. Test results will enhance knowledge of efficiency of shoreface nourishment designs by linking process-based measurements with bed profile development. The bed profiles with the nourishment designs and the reference profile are exposed to two wave conditions, similar to the SANDS experiments. The low Nourishment Design 1, leads to a relative increase of sand volume, 20% for the accretive condition and 40% for the erosive condition in the coastal zone. The high Nourishment Design 2, results in the largest relative increase of sand volume, 60% for both wave conditions.

The presence of a shoreface nourishment significantly affects the wave height, the wave-induced return flow, the wave asymmetry and the sediment transport, whereas it does not have a clear relation with the sediment concentration. The presence of a shoreface nourishment has a combined relative effect. On one hand, the shoreward sediment transport is reduced due to the decreased wave-induced return flow. On the other hand, the landward sediment transport is increased because of an increased wave asymmetry.

Summary

Within the framework of the project SANDS and VOP, during three months, experiments have been conducted in the Scheldt flume of WL |Delft Hydraulics.

Background SANDS

Presently, mobile bed tests are designed with scaling laws which are only applicable to a certain extent. Beach profile tests under wave action are designed with the Froude similitude law, suitable for the scaling of wave motion. However, Froude scaling does not result in correctly scaled bed shear stresses, which distort the bottom boundary layer. In addition, effects like turbulence are not considered in Froude scaling. This unscaled processes establish unknown uncertainties in the representativeness of the tests. Moreover, existing instruments are not able to observe turbulent and intra-wave fluid-sediment interactions over the entire boundary layer. Most of the available observational equipment disturbs the water and sediment fluxes and has limited accuracy and limited efficiency. Therefore the uncertainties in hydraulic experiments lead to results that contain unquantified errors.

To advance the mobile bed scaling laws and to test new instruments, identical tests are carried out on three different scale levels in three hydraulic facilities; Hannover GWK Flume, Barcelona Flume (CIEM) and Delft Scheldt Flume.

At this moment, the data obtained in Hannover and Barcelona are not available and therefore this study will focus on the results from Delft.

Background VOP

In the Netherlands, a large part of the mainland is protected from the sea by dunes. The dunes and the coastline used to be erosive at many locations. In 1990 the Dutch government decided to maintain the coastline of 1990 (BKL, Basic Coast Line) by means of nourishments. Different types of shore nourishments exist, depending on where the sediment is placed. This can be on the first dune row, at the duneface, on the beach, in the surf zone or at the shoreface (Hamm et al., 2002). Presently, the Dutch coast is maintained by sand nourishment at the beach and at the shoreface. This method has relatively small negative effects to adjacent areas and has a relatively low impact on the ecology.

Shoreface nourishments have the advantage of reduced cost: natural forces are assumed to redistribute the sediment shoreward, so that there is no need to scrape the beach. The use of the beach is also not hindered while the nourishment is placed and there is no need to put sediment directly on land. (Van Leeuwen et al., 2006)

Within the framework of project VOP (Voortschrijdend Onderzoek Programma) experiments are performed focussing on shoreface nourishment. To have further insight into the morphological behaviour of shoreface nourishments, two designs are implemented in the Scheldt flume. Test results will enhance knowledge of efficiency of shoreface nourishment designs.

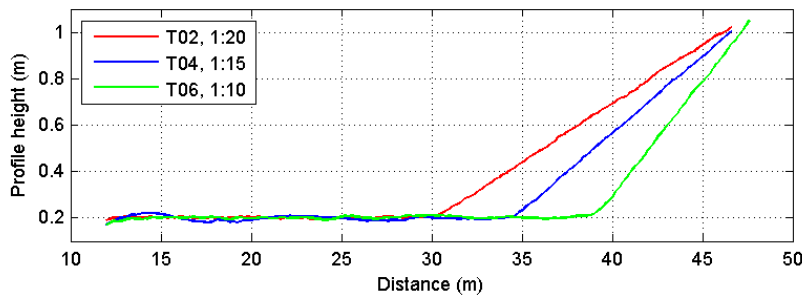
Objectives

The main objectives of this study are:

- improvement of morphological scaling laws for coastal profile evolution
- quantification of beach profile development
- improvement of knowledge of shoreface nourishment in the surf zone

Experimental set-up SANDS

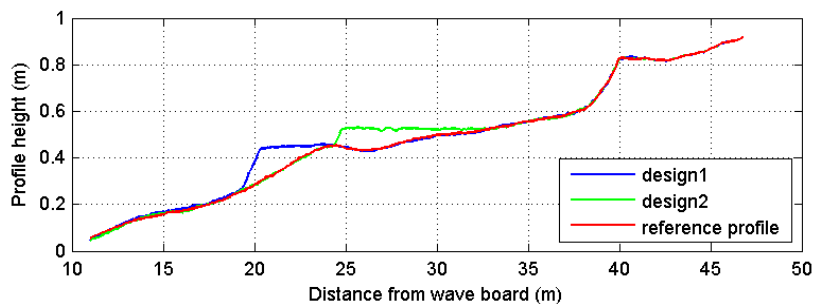
Identical tests are carried out on three different scale levels in three hydraulic facilities; Hannover GWK Flume, Barcelona Flume (CIEM) and Delft Scheldt Flume. The experiments in the Hannover flume are referred to as prototype scale 1. The initial bed slopes were fixed, respectively 1/20, 1/15 and 1/10. Two wave time series are run consecutively, first the erosive conditions ($H_s = 0.17$ m and $T_p = 2.3$ s) and secondly without reshaping the beach slope the accretive wave conditions ($H_s = 0.1$ m and $T_p = 3.0$ s).



Experimental set-up VOP

The position of a shoreface nourishment in the profile is considered an important design parameter (Walstra et al, 2006). The effect of a shoreface nourishment on the bed profile development largely depends on its position in the profile. Therefore, two nourishment designs are tested: one design positioned seawards of the breaker bar and one located higher up in the coastal profile. The high nourishment design is located on top of the original breaker bar and covers the original trough. The two nourishment designs have identical volumes, which amounts to 400 m³/m on prototype scale.

The bed profiles with the nourishment designs and the reference profile are exposed to two wave conditions; an averaged wave condition ($H_s = 0.1$ m and $T_p = 3.0$ s) and a storm wave condition ($H_s = 0.17$ m and $T_p = 2.3$ s), also referred to as the accretive wave condition and the erosive wave condition. The three profiles and two wave conditions result in six tests.



Instruments and process-based measurements

Several instruments are mounted on a carriage, which can roll over the flume. The sediment concentrations are measured by means of an ASTM and a Transverse Suction System. The ASTM was re-calibrated. The flow velocities are measured by an ADV, EMS and ASTM. The EMS is used in the analysis, since this device functioned most reliably. Along the flume some wave gauges measure the water elevation. At several fixed intervals, the bed profile is measured by the profiler.

Results SANDS experiments

Beach profile development

The bed profiles exposed to an accretive wave condition show a shoreward migration of the breaker bar, whereas the bed profiles subject to an erosive wave condition show an offshore migration of the breaker bar. The net cross-shore sediment transport in coastal areas is a balance between landward transport by wave asymmetry and seaward transport by undertow. In case of a landward migration, the transport by wave asymmetry is dominant, whereas the seaward transport by undertow dominates when the bed profile is subject to an erosive condition.

Analysis of the development of sediment volumes in time indicates that no equilibrium profile is reached. Even after 48 hours of propagating erosive waves on the initial 1:15 slope, the bed profile changes. It may be possible that the process stops, if the decay of the wave height over the surf zone is sufficiently large, that the sediment transport due to the undertow does not dominate over the sediment transport caused by wave asymmetry. The length between the breaker bar and the coastline should be very large, in order to be able to reduce the wave height to such an extent. Such a profile is not likely to occur. Profiles exposed to an accretive condition, did not reach an equilibrium either. Contrary to the profile development of the erosive tests, it could be possible, that the profile development of the accretive tests reaches an equilibrium. This is not substantiated by the measured bed profiles.

Morphological time scale for distorted tests

Distorted models are physical models in which the horizontal length scale and the vertical length scale are different. Non-distorted models with the same scale in both the horizontal and vertical directions, are by far preferable. Still distorted hydraulic models may have to be used because of limitations on the available space in which to construct the model, or because of a lack of control over the modelling materials and conditions. The distortion scale is expressed as n_l/n_h .

The morphological time scale can be represented by

$$n_{Tm} = (n_l / n_h)^{b+1} (n_{d50})^d (n_{s-1})^e / (n_h)^{0.5-0.5a+0.5c}$$

Using $n_h = 1$, $n_{d50} = 1$ and $n_{s-1} = 1$, this yields,

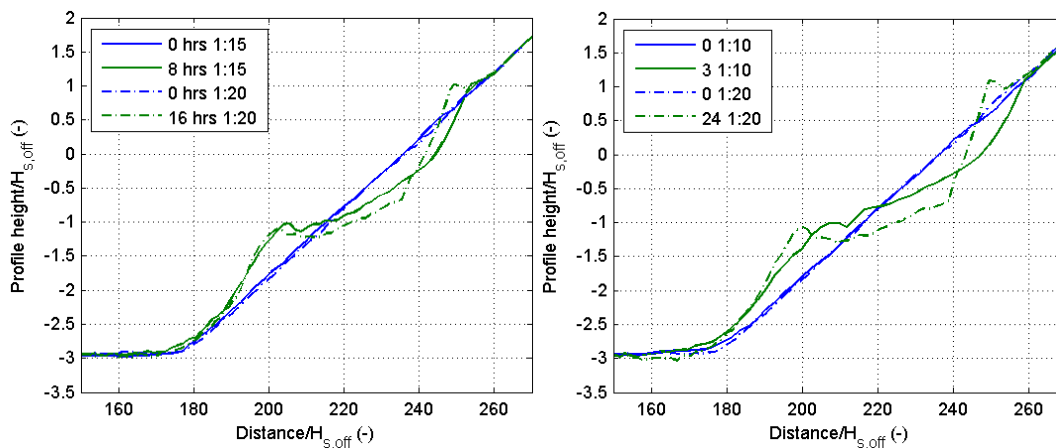
$$n_{Tm} = (n_l)^{b+1} = (n_l)^\beta$$

Factor β is assumed to lie between 1.5 and 3.5 (Van Rijn, 2007). Erosion and deposition volumes are analysed to find the exponent β . The morphological time scale factor of test 1:15 is approximately 2-2.5. For test 1:10, no single value for the time scale factor can be observed. As more sediment is deposited or eroded, the time scale factor initially increases and subsequently decreases again. The time scale factor varies from 6 to 10, with an average of approximately 8.

The tests do not have equal time scale factors. The exponents β of 2.4 for test 1:15 and 3 for test 1:10 both lie between 1.5 and 3.5, as Van Rijn predicted.

Time scale factors 8 for test 1:10 and 2 for test 1:15 are applied to the volumes of prototype test 1:20. The re-calculated erosion and deposition volumes of the erosive tests 1:10 and 1:15 correspond fairly well to the original erosion and deposition volumes of test 1:20.

The obtained time scale factors are checked by analysis of the profile development of test 1:10 and 1:15 with the reference test 1:20. A time scale factor of 2 implies that profile 1:20 after 16 hours should approximately be equal to profile 1:15, translated to profile 1:20, after 8 hours. The correspondence of the two profiles is relatively good, particularly in the vicinity of the breaker bar.



By means of the time scale factor for translation of test 1:10 to prototype test 1:20, test 1:10 after 3 hours should correspond with test 1:20 after 24 hours. It can be concluded that these similarities are not that good in comparison with the prototype test 1:20 and test 1:15. However, the bulk erosion values are approximately equal. For test 1:10 no swashbar is present.

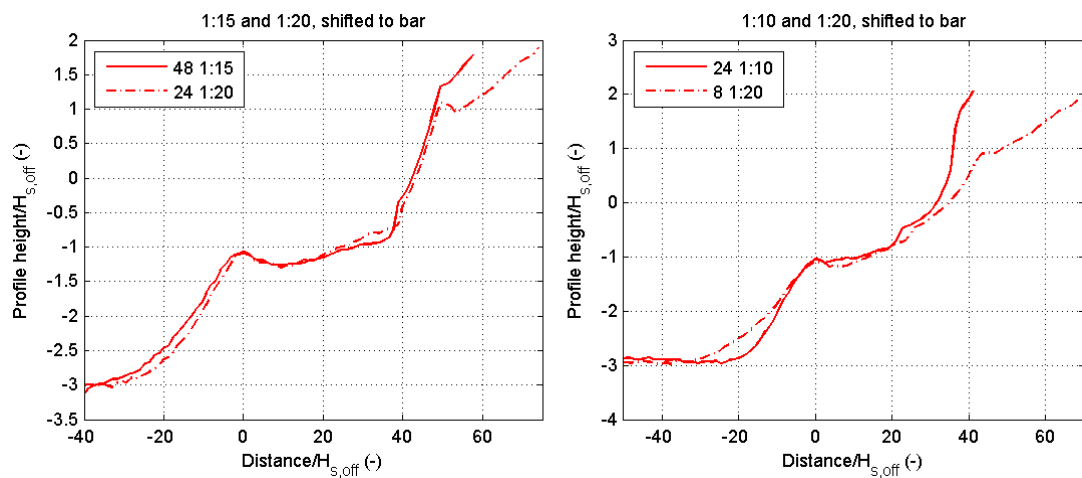
The distortion scale should be as small as possible, to prevent the generation of scale effects. Applying a distorted scale the wave breaking and wave run-up processes are overestimated, which results in overestimated erosion around the swash zone. The scale effects can be attributed to the fact that scale laws like the surf similarity parameter ($n_r = (n_h)^{0.5} (n_l / n_h)$) and fall velocity parameter ($n_{ws} = (n_h)^{0.5} (n_l / n_h)^{-1}$) are not lived up to.

Geometric characteristics

Extensive analysis is done to define and quantify parameters describing profile change. Geometric parameters are made non-dimensional to be able to draw a parallel between tests at all scale levels.

Analysis of beach slope, slope of outer bar, length of the surf zone, bar height, trough height and bar height show similar values for test 1:20 after 24 hours and 1:15 after 48 hours. Just the height of the swash bar differs. This implies that, after a certain period, the initial profile is not of importance in the profile development. From that moment on, it can be expected that the profile development will be more or less equal. As a result, a time scale factor can not be applied in the infinity, because this value will amount to one in time.

For test 1:10 such great similarities with prototype test 1:20 can not be found. Although comparable sediment transports with respect to test 1:20 and test 1:15 are found at the end of the test, little similarity between beach profiles is displayed. Especially higher up in the profile, deviations are significant; no swash bar can be found and the beach slope considerably differs. It can be expected that at a certain moment in time, the bed profile will be more or less equal to the bed profile of test 1:20. However, it is not evident, when this will be about to happen. It can be assumed that it will take more time for profile 1:10 than profile 1:15 to 'catch up' with test 1:20, because the initial profile of test 1:10 is more out of equilibrium compared to the initial profile of test 1:15.



To be able to compare the results of the three flume tests, it is recommended that the data of Hannover and Barcelona are analysed in a similar way as the data obtained in the Scheldt flume are analysed.

Results VOP experiments

Effect of nourishment designs

To obtain better insight into the effects of the nourishments on the bed profile development, the relative increase of sand volume in the coastal zone, defined as the range from 32 m from the wave board to the end of the profile, is computed. The low Nourishment Design 1, leads to a relative increase of sand volume, 20% for the accretive condition and 40% for the

erosive condition. The high Nourishment Design 2, however, results in the largest relative increase of sand volume, 60% for both wave conditions.

Effect of the presence of a shoreface nourishment on physical processes

The following effects are expected to occur as a consequence of the placement of a shoreface nourishment (Van Duin and Wiersma, 2002). Large waves break at the seaward side of the shoreface nourishment. Remaining shoaling waves generate onshore transport due to wave asymmetry over the nourishment area. The smaller waves in the leeside generate less stirring of the sediment and the wave-induced return flow (cross-shore currents) reduces. This results in an increase of the onshore sediment transport and a reduction of the offshore sediment transport. Both effects lead to an enhanced onshore transport behind the shoreface nourishment area.

Analysis of the data indicates that the presence of a shoreface nourishment significantly affects the wave height, the wave-induced return flow, the wave asymmetry and the sediment transport, whereas the presence of a shoreface nourishment does not have a clear relation with the sediment concentration. The physical processes that are affected by the presence of the nourishment are strongly connected. A reduced wave height leads to a reduced return flow, which in its turn leads to a reduced sediment transport.

The presence of a shoreface nourishment has a combined relative effect. On one hand, the shoreward sediment transport is reduced due to the decreased wave-induced return flow. On the other hand, the landward sediment transport is increased because of an increased wave asymmetry.

The presence of the high nourishment and the low nourishment both positively affect the bed profile development. The high nourishment, however, is far more effective than the low nourishment. An important aspect in the design of a nourishment seems to be the height of the nourishment. This can be explained by the fact that, due to the presence of the high nourishment, also smaller waves are not able to pass the breaker zone and break already on top of the nourishment instead of closer to the coastline.

Sediment characteristics

Analysis of the samples of the bed sediments taken at different positions along the flume, showed that on top of the breaker bar of the profiles of the reference tests and tests with the low nourishment, a slightly more coarse grain size is present compared to the grain size adjacent to the breaker bar.

Comparison results physical model tests and results UNIBEST-TC

The correlation coefficients between the measured and modelled flow velocities, wave heights and sediment concentrations are considerably high. However, the sediment transports are not simulated properly. The differences between the measured bed profile development with and without a shoreface nourishment are not comparable with the differences between the modelled bed profile development. Modelled sediment transports are significantly underestimated. This could be due to the fact that the tests are simulated on a very small (flume)scale.

Additional modelling efforts are required, particularly for the sediment transport simulations. It is recommended to upscale the measured data and simulate this in UNIBEST-TC.

Contents

List of Tables

List of Figures

List of Symbols

1	Introduction	1-4
1.1	Background SANDS	1-4
1.2	Background VOP	1-4
1.3	Objectives	1-5
1.4	Methodological approach	1-5
2	Description of tests and instruments	2-7
2.1	Description of physical model tests	2-7
2.1.1	Scheldt flume	2-7
2.1.2	Model schematisation, scale relations and design of set-up tests	2-8
2.1.3	Sediment	2-13
2.2	Instruments including calibrations	2-13
2.3	Methodology of process-based measurements	2-23
3	Results of SANDS experiments	3-1
3.1	Introduction	3-1
3.2	Beach profile development	3-1
3.2.1	Profile 1:20	3-3
3.2.2	Profile 1:15	3-7
3.2.3	Profile 1:10	3-11
3.2.4	Development of sediment volumes	3-15
3.3	Analysis of morphological time scale for distorted tests	3-19
3.4	Geometric characteristics of beach profiles	3-26
3.4.1	Vertical positions	3-27
3.4.2	Horizontal positions	3-30
3.4.3	Slopes	3-34
3.4.4	Erosion and deposition volumes	3-37
3.4.5	Conclusions on bed profile development	3-39
3.5	Wave height and water level	3-42
3.6	Flow velocities	3-47
3.7	Concentrations	3-58
3.8	Sediment transport	3-60
3.8.1	Sediment transport derived from verticals	3-60
3.8.2	Sediment transport derived from bed level change	3-63
3.8.3	Comparison of results	3-65

4	Analysis of shoreface nourishments (VOP)	4-1
4.1	Introduction	4-1
4.2	Bed profile development	4-2
4.2.1	Effect of nourishment designs	4-5
4.3	Analysis of effects nourishment designs	4-8
4.3.1	Wave height	4-9
4.3.2	Flow velocities and velocity moments	4-14
4.3.3	Concentrations	4-26
4.3.4	Sediment transport	4-29
4.4	Sediment characteristics	4-34
4.5	Conclusions	4-36
5	Comparison UNIBEST-TC and test results	5-1
5.1	Introduction	5-1
5.2	Computational set-up	5-1
5.2.1	Input	5-2
5.3	Calibration procedure	5-4
5.3.1	Calibration of wave model	5-4
5.3.2	Calibration of flow model	5-5
5.3.3	Calibration of concentrations	5-5
5.4	Comparison UNIBEST-TC and physical model tests	5-6
5.4.1	Wave height	5-6
5.4.2	Flow velocities	5-8
5.4.3	Concentrations	5-10
5.4.4	Sediment transport	5-12
5.4.5	Bed profile development VOP	5-14
5.4.6	Bed profile development SANDS	5-17
6	Conclusions & recommendations	6-1
6.1	Conclusions	6-1
6.1.1	Results of SANDS experiments	6-1
6.1.2	Analysis of shoreface nourishments (VOP)	6-4
6.1.3	Comparison UNIBEST-TC and physical model tests	6-5
6.2	Recommendations	6-6
7	References	7-1

Appendices

A	SANDS, overview of scaling laws	A-1
A.1	Froude number	A-1
A.2	Reynolds number	A-1
A.3	Dynamic similarity number	A-2
A.4	Surf similarity number	A-3
A.5	Fall velocity parameter	A-4
A.6	Suspended transport	A-4
B	SANDS, shifted bed profiles	B-1
C	Sediment transport	C-1
D	Description of UNIBEST-TC	D-1
D.1	Schematic representation of UNIBEST TC model	D-1
D.1.1	Wave propagation model	D-2
D.1.2	Mean current profile model	D-3
D.1.3	Wave orbital velocity model	D-4
D.1.4	Bed load and suspended load transport model	D-6
	Bed load transport	D-6
D.1.5	Bed level change model	D-8

List of Tables

Table 2.1 Wave conditions SANDS	2–9
Table 2.2 Flume dimensions and the experimental characteristics	2–9
Table 2.3 Overview of important scale relations	2–10
Table 2.4 Translation of Hannover flume parameters to Scheldt flume parameters	2–11
Table 2.5 Overview of SANDS tests.....	2–11
Table 2.6 Wave conditions VOP	2–12
Table 2.7 Overview of VOP tests.....	2–12
Table 2.8 Changes in calibration factors during the experiments	2–18
Table 3.1 Values of distortion scales	3–19
Table 3.2 Dimensionless profiles by division with offshore water depth and wave height...3– 26	
Table 3.3 Feature numbers 1-6	3–27
Table 3.4 Definition of erosion and deposition volumes	3–37
Table 5.1 Run parameters	5–2
Table 5.2 Erosion/deposition volumes	5–14

List of Figures

Figure 2.1 Scheldt flume of WL Delft Hydraulics	2–8
Figure 2.2 Initial profiles SANDS	2–8
Figure 2.3 Initial profiles VOP	2–12
Figure 2.4 Grain size distribution of the sediment in the Scheldt flume.	2–13
Figure 2.5 General overview tests.....	2–14
Figure 2.6 Bed profiler with three probes.....	2–14
Figure 2.7 Lay-out of the suction tubes.....	2–15
Figure 2.8 From left to right: TSS, EMS, reference rod, WHM, ASTM, ADV	2–16
Figure 2.9 Schematisation of reference rod and positioning of TSS.....	2–17
Figure 2.10 Scatter plot measured concentrations from suction tubes against ASTM output	2–18
Figure 2.11 Clustering data.....	2–19
Figure 2.12 New non-linear calibration curve through average concentrations and error margins of clustered TSS data against ASTM output	2–19
Figure 2.13 Calibration of VAT.....	2–20
Figure 2.14 Time series of velocity measurements at 10 cm above bed level. The upper plot shows the series obtained at 19.9 m for the accretive test T04 (Design 1). The lower plot represents the series obtained at 24.9 m for the erosive test T05 (Design 1).....	2–21
Figure 2.15 Comparison of velocity verticals measured by ASTM, EMS and ADV.....	2–22
Figure 3.1 Sinusoidal waves development into waves with peaked wave crest and flat trough	3–2
Figure 3.2 Profile development of SANDS test T04, 1:15	3–3
Figure 3.3 Profile development T02, 1:20, erosive condition	3–4
Figure 3.4 Profile development T07, 1:10, accretive condition.....	3–4
Figure 3.5 Dimensionless profiles T02	3–5
Figure 3.6 Dimensionless profiles T03	3–6
Figure 3.7 Profile development T04, 1:15, erosive condition	3–7
Figure 3.8 Profile development T05, 1:15, accretive condition.....	3–8
Figure 3.9 Dimensionless profiles T04	3–9
Figure 3.10 Dimensionless profiles T05.....	3–10
Figure 3.11 Profile development T06, 1:10, erosive condition.....	3–11
Figure 3.12 Profile development T07, 1:10, accretive condition.....	3–12
Figure 3.13 Dimensionless profiles T06.....	3–13

Figure 3.14 Dimensionless profiles T07	3–14
Figure 3.15 Development of erosion/deposition volumes in time, divided into three parts: 28-36, 36-40, 40-47	3–16
Figure 3.16 Development of erosion/deposition volumes in time, divided into three parts: 28-36, 36-40, 40-47	3–16
Figure 3.17 Development of erosion/deposition volumes in time, divided into three parts: 31-39, 39-43, 43-47	3–17
Figure 3.18 Development of erosion/deposition volumes in time, divided into three parts: 31-39, 39-43, 43-47	3–17
Figure 3.19 Development of erosion/deposition volumes in time, divided into three parts: 37-42, 42-45, 45-47	3–18
Figure 3.20 Development of erosion/deposition volumes in time, divided into three parts: 37-42, 42-45, 45-47	3–18
Figure 3.21 Definition of erosion and deposition volumes used for the determination of the time scale factor.....	3–20
Figure 3.22 On the left measured erosion areas. On the right these are converted to prototype values.....	3–21
Figure 3.23 Time scale factor for tests 1:10 and 1:15	3–22
Figure 3.24 Re-calculation of the erosion and deposition volumes by means of multiplication of the values of the erosion/deposition volumes of the reference tests and the time scale factors for test 1:10.....	3–23
Figure 3.25 Comparison test 1:15 after 16 hours and test 1:20 after 24 hours.....	3–23
Figure 3.26 Comparison test 1:10 after 3 hours and test 1:20 after 24 hours.....	3–24
Figure 3.27 Test 1:15 scaled up to test 1:20	3–25
Figure 3.28 Test 1:10 scaled up to test 1:20	3–25
Figure 3.29 Distinct features of beach profile.....	3–26
Figure 3.30 Definition of geometric vertical parameters	3–27
Figure 3.31 Evolution of bar height in time	3–28
Figure 3.32 Evolution of trough height in time	3–29
Figure 3.33 Evolution of swash bar height	3–29
Figure 3.34 Evolution of maximum erosion point in time	3–30
Figure 3.35 Definition of geometric horizontal parameters	3–31
Figure 3.36 Evolution of bar length in time	3–31
Figure 3.37 Evolution of trough length in time	3–32
Figure 3.38 Evolution of swash bar length in time.....	3–33
Figure 3.39 Evolution of length of the surf zone in time	3–34
Figure 3.40 Definition of geometric slope parameters.....	3–34

Figure 3.41 Evolution of slope of breaker bar in time	3–35
Figure 3.42 Evolution of beach slope in time	3–36
Figure 3.43 Definition of bar migration	3–36
Figure 3.44 Migration breaker bar in time	3–37
Figure 3.45 Definition of erosion and deposition volumes	3–37
Figure 3.46 Evolution of erosion and deposition volumes in time	3–38
Figure 3.47 Evolution of sediment transport in time.....	3–39
Figure 3.48 Comparison profiles of test 1:20 after 24 hours and test 1:15 after 48 hours	3–40
Figure 3.49 Profiles shifted on top of each other with reference to top of bar	3–40
Figure 3.50 Comparison profiles of test 1:20 after 8 hours and test 1:10 after 24 hours ..	3–41
Figure 3.51 Profiles shifted on top of each other with reference to top of bar	3–41
Figure 3.52 Wave height and water level variation along the flume, T02 (1:20), erosive condition.....	3–44
Figure 3.53 Wave height and water level variation along the flume, T04 (1:15), erosive condition.....	3–45
Figure 3.54 Wave height and water level variation along the flume, T06 (1:10), erosive condition.....	3–46
Figure 3.55 The shape of the total mean velocity profile under waves	3–47
Figure 3.56 Flow velocity verticals for erosive test T04, experiment 19-35	3–48
Figure 3.57 Flow velocity verticals for accretive test T05, experiment 39-52	3–49
Figure 3.58 Flow velocity verticals for erosive test T06, experiment 57-68	3–49
Figure 3.59 Depth-averaged velocities of erosive test T04, experiment 19-35	3–50
Figure 3.60 Depth-averaged velocities of accretive test T05, experiment 39-52.....	3–51
Figure 3.61 Depth-averaged velocities of erosive test T06, experiment 57-68	3–51
Figure 3.62 Development of the variance density spectrum of T04, subject to an erosive condition. The long waves are represented by the blue line, the short waves by the red line.	3–53
Figure 3.63 Development of the variance density spectrum of T05, subject to an accretive condition. The long waves are represented by the blue line, the short waves by the red line.	3–54
Figure 3.64 Development of the variance density spectrum of T06, subject to an erosive condition. The long waves are represented by the blue line, the short waves by the red line.	3–55
Figure 3.65 Third order velocity moments of T04, T05 and T06 along the profile, separated in the contribution of the short wave velocities (guss) and the contribution of the long wave velocities (guls).	3–57
Figure 3.66 Concentration verticals for erosive test T04, experiment 19-35.....	3–59

Figure 3.67 Concentration verticals for accretive test T05, experiment 39-52	3-59
Figure 3.68 Concentration verticals for erosive test T06, experiment 57-68	3-60
Figure 3.69 On the left, the concentration vertical of experiment 27, T04, at $x = 35.6$ is shown for three different interpolation methods. The concentration vertical is multiplied by the velocity vertical (second plot) resulting in the sediment transport.	3-61
Figure 3.70 Sediment transport using three different methods for all SANDS experiments 3-61	
Figure 3.71 Profile evolution and sediment transport of test 1:20.....	3-62
Figure 3.72 Profile evolution and sediment transport of test 1:15.....	3-62
Figure 3.73 Profile evolution and sediment transport of test 1:10.....	3-63
Figure 3.74 Sediment transport derived from changes in bed level for T04	3-64
Figure 3.75 Corrected sediment transport.....	3-65
Figure 4.1 The reference profile (red line) with the two nourishment designs (blue and green line).....	4-1
Figure 4.2 Beach profile development of T02, T04 and T06, the accretive tests	4-3
Figure 4.3 Beach profile development of T03, T05 and T07, the erosive tests	4-4
Figure 4.4 Differences between reference bed profile development and development of nourishment design profiles	4-6
Figure 4.5 On the left, erosion volume of the accretive tests, T02, T04 and T06 in the range from 32 m-47.7 m. On the right, development of the sand volume, relative to the reference test.....	4-7
Figure 4.6 On the left, erosion volume of the erosive tests, T03, T05 and T07 in the range from 32 m -47.7 m. On the right , development of the sand volume, relative to the reference test.....	4-7
Figure 4.7 Wave height variation along the flume for the accretive tests (T02, T04 and T06)	4-10
Figure 4.8 Wave height variation along the flume for the erosive tests (T03, T05 and T07) 4-11	
Figure 4.9 The upper plot shows the ratio between the wave height of T04 (Nourishment Design 1 test) and T02 (reference test) for the accretive condition. The lower plot shows the ratio between the wave height of T06 (Nourishment Design 2 test) and T02 for the accretive condition.	4-12
Figure 4.10 The upper plot shows the ratio between the wave height of T05 (Nourishment Design 1 test) and T03 (reference test) for the erosive condition. The lower plot shows the ratio between the wave height of T07 (Nourishment Design 2 test) and T03 for the erosive condition.....	4-12
Figure 4.11 Overview of positions of process-based measurements	4-14
Figure 4.12 On the left, the undertow of the accretive tests, on the right, the erosive tests measured by the EMS	4-15

- Figure 4.13 On the left, the undertow of the accretive tests, on the right, the erosive tests measured by the ASTM..... 4-16
- Figure 4.14 Depth-averaged velocities for all tests for the ASTM. The upper plot shows data for the accretive condition, the lower plot for the erosive condition..... 4-18
- Figure 4.15 Ratio between depth-averaged velocities of nourishment design tests and the reference tests 4-18
- Figure 4.16 Wave-induced flow velocities derived from the wave mass flux (Phillips, 1977). The upper plot shows data for the accretive condition, the lower plot for the erosive condition..... 4-19
- Figure 4.17 Development of the variance density spectrum of T02 and T03, the reference tests. On the left, the accretive test T02 is shown. On the right, the erosive test T03 is shown. The long wave velocities are represented by the red line, the short wave velocities by the blue line..... 4-21
- Figure 4.18 Development of the variance density spectrum of T04 and T05, the tests with Design 1. On the left, the accretive test T04 is shown. On the right, the erosive test T05 is shown. The long wave velocities are represented by the red line, the short wave velocities by the blue line. 4-22
- Figure 4.19 Development of the variance density spectrum of T06 and T07, the tests with Design 2. On the left, the accretive test T06 is shown. On the right, the erosive test T07 is shown. The long wave velocities are represented by the red line, the short wave velocities by the blue line. 4-23
- Figure 4.20 Third order velocity moments along the profile, separated in the contribution of the short wave velocities (guss) and the contribution of the long wave velocities (guls). On the left, the accretive tests are shown and on the right, the erosive tests..... 4-25
- Figure 4.21 The upper plot shows the ratios between the accretive tests with a nourishment design and the reference tests. The lower plot shows the ratios between the erosive tests with a nourishment design and the reference tests. 4-26
- Figure 4.22 On the left, the concentration verticals of the accretive tests, on the right the erosive tests 4-28
- Figure 4.23 Sediment transport using three different methods for all VOP experiments.. 4-29
- Figure 4.24 Sediment transports (derived from velocity and concentration verticals and derived from bed level change) for the accretive tests T02, T04 and T06 .. 4-31
- Figure 4.25 Sediment transport (derived from velocity and concentration verticals and derived from bed level change) for the erosive tests T03, T05 and T07 . 4-32
- Figure 4.26 Ratio between sediment transport of nourishment design tests and the reference tests. Ratio of test with Design 1 and the reference test (solid lines). Ratio of test with Design 2 and the reference tests (dotted lines). 4-33
- Figure 4.27 Cross-shore distribution of sediments of T03, reference test subject to an erosive condition..... 4-34

Figure 4.28 Upper plot shows last profile measurements of VOP test T02 up to T05, lower plots indicate distribution of D_{10} , D_{50} and D_{90} along the profile.....	4–35
Figure 5.1 Set-up of model UNIBEST-TC.....	5–1
Figure 5.2 Scatter plot modelled wave height versus measured wave height	5–4
Figure 5.3 Scatter plot modelled velocities versus measured velocities	5–5
Figure 5.4 Scatter plot modelled concentrations versus measured concentrations.....	5–6
Figure 5.5 Measured (dotted lines) and modelled (solid lines) wave height development. The upper plot shows the accretive tests, the lower plot the erosive tests.	5–7
Figure 5.6 Measured (dotted lines) and modelled (solid lines) flow velocities.....	5–9
Figure 5.7 Measured (dotted lines) and modelled (solid lines) sediment concentrations.	5–11
Figure 5.8 Measured (dotted lines) and modelled (solid lines) sediment transports for the accretive tests	5–13
Figure 5.9 Measured (dotted lines) and modelled (solid lines) sediment transports for the erosive tests	5–13
Figure 5.10 Measured (blue line) and modelled (red line) bed profile development for the accretive tests	5–15
Figure 5.11 Measured (blue line) and modelled (red line) bed profile development for the erosive tests	5–16
Figure 5.12 Measured (blue line) and modelled (red line) bed profile development for the erosive SANDS tests.....	5–17
Figure B.1 Dimensionless profiles T02 and T04, shifted on top of breaker bar.....	B–1
Figure B.2 Dimensionless profiles T02 and T06, shifted on top of breaker bar.....	B–2
Figure B.3 Dimensionless profiles T02 and T04, shifted to water level.....	B–3
Figure B.4 Dimensionless profiles T02 and T06, shifted to water level.....	B–4
Figure C.1 Extrapolation of velocity profiles.....	C–1
Figure C.2 Extrapolation of concentration profiles	C–2
Figure D.1 Set-up of model UNIBEST-TC.....	D–1
Figure D.2 Three layers, according De Vriend and Stive (1987)	D–4

List of Symbols

Symbol	Unit	Description
a	m	thickness of bed load layer
a_n	m	amplitude in orbital velocity formulation
a_m	m	amplitude in orbital velocity formulation
A	m^2	area of a roller
B_j	m/s	amplitude in orbital velocity formulation
c_a	kg/m^3	time and space averaged sediment concentration
c_g	m/s	wave group velocity
C_r	-	correlation coefficient between wave envelope and long wave surface variation in orbital velocity formulation
C	kg/m^3	sediment concentration
c	kg/m^3	time and space averaged sediment concentration
d	m	water depth (to mean surface level)
D^*	-	dimensionless particle parameter
D_{50}	m	geometric mean sediment diameter; grain size diameter such that 50% of the grains by mass are smaller than $D = D_{50}$
D_{90}	m	grain size diameter such that 90% of the grains by mass are smaller than $D = D_{90}$
D_{10}	m	grain size diameter such that 10% of the grains by mass are smaller than $D = D_{10}$
Diss	W/m^2	dissipation of roller energy
D_w	W/m^2	wave energy dissipation rate due to breaking
D_f	W/m^2	wave energy dissipation rate due to bottom friction
E	J/m^2	wave energy per unit area
E_r	J/m^2	roller energy
f_w	-	bottom friction factor
f'_{cw}	-	weighted friction factor, accounting for both wave and current friction
g	m/s^2	gravitational acceleration
G_{nm}	-	transfer function in orbital velocity formulation
H_s	m	significant wave height
h_{off}		offshore water depth
$H_{s,off}$		offshore significant wave height
H_{m0}	m	spectral 'significant wave height', $H_{m0} = 4\sqrt{m_0}$
H_{max}	m	maximum height of a wave of permanent form of given length or period in a given waterdepth
H_{rms}	m	root mean square wave height
$H_{rms,0}$	m	root mean square wave height at seaward boundary of model
h_r	m	local water depth
j	-	counter in orbital velocity formulation
k	m^{-1}	wave number
L	m	length of a roller
m	$kg/m/s$	landward directed mass flux above mean wave trough level
m_0	m^2	variance of the surface elevation
n	-	ratio of wave group and phase velocity ($=c_g/c$)
n	-	number in orbital velocity formulation

n	-	scale factor $\left(= \frac{P_p}{P_m} \right)$
n_H	-	wave height scale factor
n_L	-	wave length scale factor
n_{ws}	-	fall velocity scale factor
n_h	-	depth scale factor
n_{Tm}	-	morphological time scale factor
n_T	-	wave period scale factor
n_g	-	gravitational constant scale factor
n_{rho}	-	mass density scale factor (fluid)
n_{mu}	-	viscosity scale factor
n_{d50}	-	mean sediment diameter scale factor
n_{s-1}	-	mass density scale factor (sediment)
n_l	-	length scale factor
p	-	porosity of sediment
q_b	$m^3/m/s$	bed load transport rate including pores
q_s	$kg/m/s$	suspended sediment transport rate
$q_{s,c}$	$m^3/m/s$	current related suspended sediment transport including pores
$q_{s,c}$	$kg/m/s$	current related suspended sediment transport
S_{xx}	$m^3/m/s$	(time averaged) depth integrated sediment transport per unit width
S_{xx}	J/m^2	radiation stress in x-direction through x-plane
T	-	dimensionless bed shear stress parameter
T	-	wave period
t	s	time
t	s	time
u	m/s	time averaged value of horizontal component of velocity field
u_b	m/s	near bottom velocity in bed load transport formulation
u_{orb}	m/s	amplitude of wave orbital velocity
U_1	m/s	orbital velocity
U_2	m/s	orbital velocity
U_2'	m/s	orbital velocity
U_3	m/s	orbital velocity
U_4	m/s	orbital velocity
x	m	horizontal cross-shore coordinate
z_b	m	vertical coordinate of the bed profile with respect to the reference level
α	-	dissipation coefficient
β	-	slope of the face of the wave in roller dissipation equation
β_s	-	slope factor
γ	-	dissipation coefficient
Δ	-	relative density of sediment with respect to water $\left(= \frac{\rho_s - \rho}{\rho} \right)$
$\epsilon_{s,cw}$	m^2/s	sediment mixing coefficient for combined current and waves
$\epsilon_{s,c}$	m^2/s	current related mixing coefficient
$\epsilon_{s,w}$	m^2/s	wave related mixing coefficient
$\bar{\eta}$	m	(time averaged) mean elevation of the water level above the mean level h due to wave set-up or set-down

θ	rad	angle of wave attack with respect to shore normal
θ'	-	dimensionless effective shear stress
θ_{cr}	-	dimensionless critical shear stress
ξ_a	m	amplitude in orbital velocity formulation
μ	kg/m/s	viscosity
ρ	kg/m ³	mass density of fluid (water)
ρ_s	kg/m ³	mass density of sediment
$\tau_{s,wave}$	N/m ²	shear stress in direction of wave propagation, introduced by surface roller
φ	rad	phase difference between bound wave and short wave in orbital velocity formulation
Φ_{bd}	-	non-dimensional bed load transport vector
ω	rad/s	angular frequency ($=2\pi/T$)

I Introduction

I.1 Background SANDS

Presently, mobile bed tests are designed with scaling laws, which are only applicable to a certain extent. Beach profile tests under wave action are designed with the Froude similitude law (ratio of inertial to gravity forces), suitable for the scaling of wave motion. However, Froude scaling does not result in correctly scaled bed shear stresses, which distort the bottom boundary layer, which is important in morphodynamics. In addition, effects like turbulence are not considered in Froude scaling and establish unknown uncertainties in the accuracy of the tests. Moreover, existing instruments are not able to observe turbulent and intra-wave fluid-sediment interactions over the entire boundary layer. Most of the available observational equipment disturbs the water and sediment fluxes, has limited accuracy and limited efficiency. Therefore the uncertainties in hydraulic experiments lead to results that contain unquantified errors.

To advance the mobile bed scaling laws and to test new instruments, identical tests are carried out on three different scale levels in three hydraulic facilities; Hannover GWK Flume, Barcelona Flume (CIEM) and Delft Scheldt Flume.

The data obtained in Hannover and Barcelona are not available at this moment and therefore this study will focus on the results from Delft.

I.2 Background VOP

In the Netherlands, a large part of the mainland is protected from the sea by dunes. The dunes and the coastline used to be erosive at many locations. In 1990 the Dutch government decided to stop further coastal retreat and to maintain the coastline of 1990 (BKL, Basic Coast Line) by means of nourishments. Different types of shore nourishments exist, depending on where the sediment is placed. This can be on the first dune row, at the duneface, on the beach, in the surf zone or at the shoreface (Hamm et al., 2002). Presently, the Dutch coast is maintained by sand nourishment at the beach and at the shoreface. This method has relatively small negative effects to adjacent areas and has a relatively low impact on the ecology. The traditional hard measures like seawalls and groynes that not only are expensive to construct and maintain, but also show adverse side effects, are replaced by nourishments.

Shoreface nourishments have the advantage of reduced cost: natural forces are assumed to redistribute the sediment shoreward, so that there is no need to scrape the beach. The use of the beach is also not hindered while the nourishment is placed and there is no need to put sediment (generally mined offshore) directly on land. Any reduction in costs is desirable as shoreface nourishments, like all shore nourishments, are expensive. Nourishments in general are an ongoing commitment, incurring monitoring expenses as well as those of repeated nourishment. (Van Leeuwen et al., 2006)

Within the framework of project VOP (Voortschrijdend Onderzoek Programma) experiments are performed focussing on shoreface nourishment. To have further insight into the morphological behaviour of shoreface nourishments, two nourishment designs are implemented in the Scheldt flume. Test results will enhance knowledge of efficiency of nourishment designs.

1.3 Objectives

The main objectives of this study are:

- improvement of morphological scaling laws for coastal profiles
- quantification of beach profile development
- improvement of knowledge of shoreface nourishment in the surf zone

1.4 Methodological approach

From June until August, experiments are carried out in the Scheldt flume. The first six and half weeks focused on the SANDS experiments and the second six and half weeks on the VOP experiments. The set-up of the morphological tests can be found in Chapter 2.

The results of the tests are analysed in Chapter 3 and Chapter 4. The SANDS experiments are dealt with in Chapter 3. The development of the beach profile is discussed in Section 3.2. In addition, the focus is on the scale relationships within the Scheldt flume tests, since at this moment no data are available on the tests in Hannover and Barcelona. The 1:10 and 1:15 tests in the Scheldt flume can be seen as the distorted tests of 1:20. In Section 3.3, research is done concerning distortion scale and morphological time scale.

In Section 3.4, several geometric characteristics of the beach profiles, which were subject to an erosive wave condition, are studied. The features of the profiles are discussed and the profiles are made dimensionless to be able to compare with the tests in Hannover and Barcelona for future research.

Analysis of wave height and water level variation along the flume can be found in Section 3.5. Flow velocities, sediment concentrations and sediment transport are discussed in Section 3.6, 3.7 and 3.8 respectively.

Chapter 4 concerns the analysis of the VOP experiments. This chapter aims at establishing and quantifying the dominant physical processes that are affected by the presence of a shoreface nourishment. The results of the tests with the two nourishment designs are compared to the results obtained for the reference tests. In Section 4.2, the effects of the two shoreface nourishment designs on the morphology are analysed. One design is found to be most effective. Furthermore, detailed comparisons are made between the results for the nourishment designs and the reference profile using the process-based measurements. As a result, an overview of the dominant processes, which are affected by the presence of a shoreface nourishment, is presented in Section 4.5.

In Chapter 5, the UNIBEST-TC model is applied to simulate the physical model tests focussing on the physical processes involved in implementation of a shoreface nourishment.

In Chapter 6, the conclusions and recommendations are presented.

2 Description of tests and instruments

This chapter gives a description of the experimental set-up of the physical model tests carried out in the Scheldt flume. Furthermore, the performance of the instruments and the methodology of the process-based measurements are discussed. For a more detailed description of the experimental set-up and results of the physical model tests, see Data report flume experiments VOP (2007) and Data report flume experiments SANDS (2007).

2.1 Description of physical model tests

2.1.1 Scheldt flume

The experiments have been conducted in the Scheldt flume of WL |Delft Hydraulics. The flume, consisting of an iron bottom and glass walls, has an overall length of 56 m, width of 1 m and depth of 1.2 m. The wave generator located at the beginning of the flume is equipped with an online Active Reflection Compensation (ARC). This means that waves propagating towards the wave board are measured and that the wave board compensates for these reflected waves. In this way, these undesired waves do not re-reflect towards the beach and do not disturb the measurements. In addition, the wave board is equipped with second order wave steering to compensate for spurious waves.

For the location of the instruments in the facility, the following co-ordinate system is adopted:

- The x-direction is parallel to the length of the flume, the positive x-direction is from the wave-board towards the “beach face”, and $x = 0$ is located at the position of the wave board in rest.
- The y-direction is parallel to the width of the flume, the positive y-direction is to the right when looking from the wave board to the “beach face”, and $y = 0$ is located inside the channel at the glass window.
- The z-direction is directed vertically upward, with $z = 0$ located at the top of the horizontal iron bottom part of the flume.



Figure 2.1 Scheldt flume of WL|Delft Hydraulics

2.1.2 Model schematisation, scale relations and design of set-up tests

SANDS

Identical tests are carried out on three different scale levels in three hydraulic facilities; Hannover GWK Flume, Barcelona Flume (CIEM) and Delft Scheldt Flume. The experiments in the Hannover flume are referred to as prototype scale 1. The initial bed slopes were fixed, respectively 1/20, 1/15 and 1/10, see Figure 2.2. Two wave time series are run consecutively, first the erosive conditions ($H_s = 1.0$ m and $T_p = 5.7$ s) and secondly without reshaping the beach slope the accretive wave conditions ($H_s = 0.6$ m and $T_p = 7.5$ s), see Table 2.1.

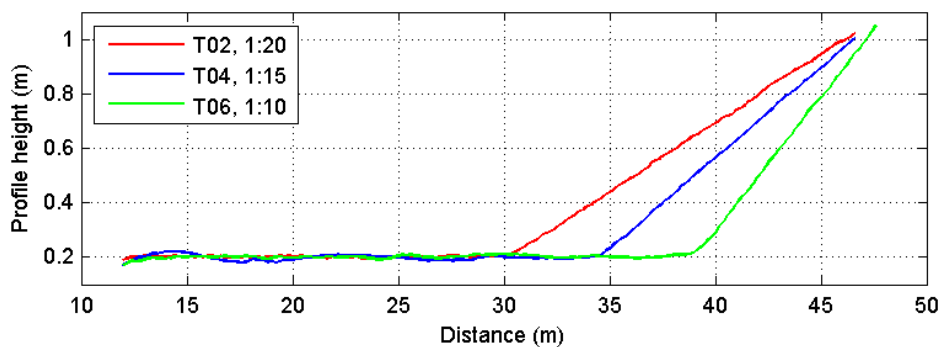


Figure 2.2 Initial profiles SANDS

Table 2.1 Wave conditions SANDS

Hannover Flume	Condition	Hs	Tp
Time Series 1	Erosive	1.0 m	5.7 s
Time Series 2	Accretive	0.6 m	7.5 s

Scheldt flume	Condition	Hs	Tp
Time Series 1	Erosive	0.17 m	2.3 s
Time Series 2	Accretive	0.10 m	3.0 s

Wave board steering files for both erosive and accretive wave conditions are generated from scaled-down (wave height and generation frequency) prototype time series provided by UPC, Barcelona. The file of the erosive time series and the file of the accretive time series consist of 500 waves. During the tests, these wave time series of 500 waves are consecutively run.

The experiments in Hannover are scaled down taking into account geometrically undistorted models and using Froude scaling in the scaled tests. The flume parameters and scale relations in the different flumes are presented in Table 2.2. All tests in the Scheldt flume are carried out with a water level at 0.7 m above the flume bottom.

Table 2.2 Flume dimensions and the experimental characteristics

	Length (m)	Depth (m)	Width (m)	D₅₀ (mm)	Slopes	Scale
Hannover	300	7	5	0.35	1/15	Prototype
Barcelona	100	5	3	0.25	1/10; 1/15	1.7
Delft (Scheldt)	56	1.2	1	0.130	1/10; 1/15; 1/20	6

Parameters are scaled down from prototype Hannover to the Scheldt flume based on existing scaling laws. Correct representation of the physical processes requires that dimensionless numbers are the same in all three flumes. Important dimensionless numbers are Froude number, Reynolds' number, surf similarity parameter, suspension parameter and Shields parameter and are discussed in Appendix A. For correct scale modelling it is sufficient that these numbers are in a certain range, and thus not impose a fixed value.

The basic parameters in physical modelling are generally much smaller than the corresponding values in nature. The ratio of the value in prototype and in the laboratory model is expressed by the scale parameter:

$$n = \frac{P_p}{P_m} \quad (2.1)$$

in which,

p_p is the parameter value in prototype

p_m is the value in laboratory model.

In Table 2.3, an overview of the important scale relations is given (see Appendix A).

Table 2.3 Overview of important scale relations

Scale law	Scale relation
Froude number	$\frac{n_v}{\sqrt{n_s n_L}} = 1$ (A.4)
Reynolds number	$\frac{n_v n_L n_p}{n_\mu} = 1$ (A.6)
Dynamic similarity number	$n_u = n_T = (n_L)^{0.5} = (n_H)^{0.5} = (n_h)^{0.5}$ (A.13)
Surf similarity parameter	$n_T = (n_h)^{0.5} (n_l / n_h)$ (A.16)
Fall velocity parameter	$n_{ws} = (n_h)^{0.5} (n_l / n_h)^{-1}$ (A.19)
Suspend transport parameter	$n_{Tm} = (n_l / n_h)^{b+1} (n_{d50})^d (n_{s-1})^e / (n_h)^{0.5-0.5a+0.5c}$ (A.26)

Basic parameters of non-distorted tests for the Scheldt flume, with respect to prototype Hannover, are determined by applying the scale relations listed in Table 2.3. All geometric lengths are scaled by the same ratio, i.e. $n=6$. Froude scaling is applied for determination of the wave period.

Since large quantities of sand are required for the Hannover flume, it is preferred to use available beach sand ($D_{50} = 33$ mm in Hannover). For the Scheldt flume, the available sand had $D_{50} = 0.13$ mm.

Based on the suspend transport parameter (equation (A.26) in Appendix A):

$$n_{Tm} = (n_l / n_h)^{b+1} (n_{d50})^d (n_{s-1})^e / (n_h)^{0.5-0.5a+0.5c} \quad (A.26)$$

Morphological time scale is proposed to be $n_{Tm} = n_{d50}$, assuming $d=1$, $e=1$, $a=2$ and $c=1$.

The translation from the prototype flume parameters into the Scheldt flume parameters are illustrated in Table 2.4. An overview of SANDS tests is given in Table 2.5.

Table 2.4 Translation of Hannover flume parameters to Scheldt flume parameters

Scale Parameter	Hannover Accretive	Hannover Erosive	Scheldt flume Accretive	Scheldt flume Erosive
Vertical	$n_h = 1$ depth at deep water = 3m	$n_h = 1$ depth at deep water = 3m	$n_h = 6$ depth at deep water = 0.5 m	$n_h = 6$ depth at deep water = 0.5 m
Horizontal	$n_l = 1$	$n_l = 1$	$n_l = 6$	$n_l = 6$
Distortion	$n_l / n_h = 1$	$n_l / n_h = 1$	$n_l / n_h = 1$	$n_l / n_h = 1$
Waveheight	$n_H = 1$ Hs = 1m	$n_H = 1$ Hs = 0.6 m	$n_H = 6$ Hs = 0.167m	$n_H = 6$ Hs = 0.10 m
Wave period	 $T_p = 5.7$ s	 $T_p = 7.5$ s	$n_T = (n_h)^{0.5}$ = 2.45 $T_p = 2.32$ s	$n_T = (n_h)^{0.5}$ = 2.45 $T_p = 3.06$ s
Morphological time scale	$n_{Tm} = 1$ t = 20 hrs	$n_{Tm} = 1$ t = 20 hrs	$n_{Tm} = n_{d50}$ = 2.53 t = 7.9 hrs	$n_{Tm} = n_{d50}$ = 2.53 t = 7.9 hrs
Median sand size	 $d_{50} = 0.33$ mm	 $d_{50} = 0.33$ mm	$n_{d50} = (n_h)^{0.5}$ = 2.45 $d_{50} = 0.13$ mm	$n_{d50} = (n_h)^{0.5}$ = 2.45 $d_{50} = 0.13$ mm

Table 2.5 Overview of SANDS tests

Test nr	Hs	Tp	Condition	Slope	Profile measurement (hrs)
T02	0.17 m	2.3 s	Erosive	1:20	0.3 / 1 / 3 / 8 / 16 / 24
T03	0.10 m	3.0 s	Accretive	1:20	1 / 3 / 8
T04	0.17 m	2.3 s	Erosive	1:15	1 / 3 / 8 / 16 / 24 / 48
T05	0.10 m	3.0 s	Accretive	1:15	1 / 3 / 8 / 16 / 24
T06	0.17 m	2.3 s	Erosive	1:10	1 / 3 / 8 / 16 / 24
T07	0.10 m	3.0 s	Accretive	1:10	1 / 3 / 8

VOP

Similar to the SANDS experiments, two wave conditions are applied for the VOP tests:

Table 2.6 Wave conditions VOP

Scheldt flume	Condition	Hs	Tp
Jonswap1	Accretive	0.10 m	3.0 s
Jonswap2	Erosive	0.17 m	2.3 s

During eight hours waves of the erosive wave condition (Jonswap2) have been generated on a profile based on an experiment carried out by J. Bosboom (2000), resulting in the initial profile (see Figure 2.3). Reference tests for both wave conditions are done and subsequently two nourishment designs are implemented. Two wave spectra are run successively; firstly, the accretive condition (Jonswap1) and secondly, after restoring the profile the erosive wave condition (Jonswap2). All tests were carried out with a water level of 0.7 m above the flume bottom.

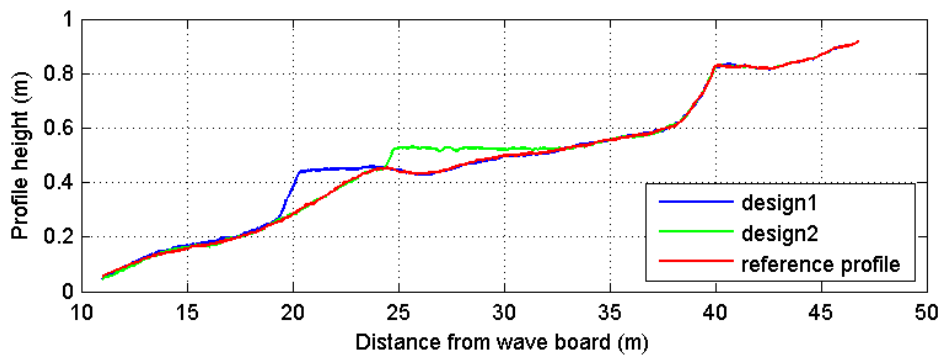


Figure 2.3 Initial profiles VOP

An overview of VOP tests is shown in Table 2.7. The duration of the accretive tests is 24 hours, the duration of the erosive tests is 16 hours.

Table 2.7 Overview of VOP tests

Test nr	Hs	Tp	Condition	Profile	Profile measurement (hrs)
T02	0.10 m	3.0 s	Accretive	Reference	1 / 3 / 8 / 16 / 24
T03	0.17 m	2.3 s	Erosive	Reference	1 / 3 / 8 / 16
T04	0.10 m	3.0 s	Accretive	Design1	1 / 3 / 8 / 16 / 24
T05	0.17 m	2.3 s	Erosive	Design1	1 / 3 / 8 / 16
T06	0.10 m	3.0 s	Accretive	Design2	1 / 3 / 8 / 16 / 24
T07	0.17 m	2.3 s	Erosive	Design2	1 / 3 / 8 / 16

2.1.3 Sediment

The sediment used for the tests in the Scheldt flume, for SANDS as well as for VOP, is Sibelco AF100 sediment and has been used for previous tests several times before. The grain size distribution is shown in Figure 2.4. D_{50} is slightly larger than 130 μm .

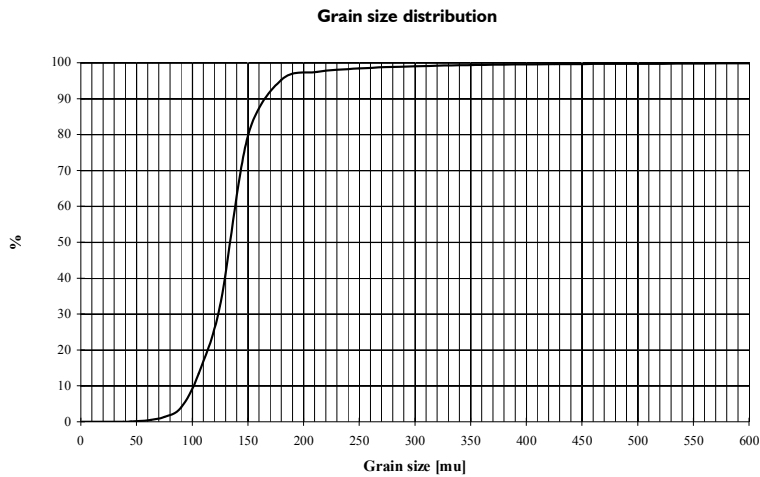


Figure 2.4 Grain size distribution of the sediment in the Scheldt flume.

2.2 Instruments including calibrations

During the tests, bed profiles, water level variations, flow velocities, sediment concentrations and sediment transport have been measured.

Figure 2.5 shows the general experimental set-up. Several instruments are attached to a carriage, which can easily roll over the flume. ASTM, ADV and EMS are connected to a computer. On the right, ten pumps suck the water containing sediment through the tubes into the buckets. Along the flume some wave gauges measure the water elevation. Instruments are described in more detail hereafter.

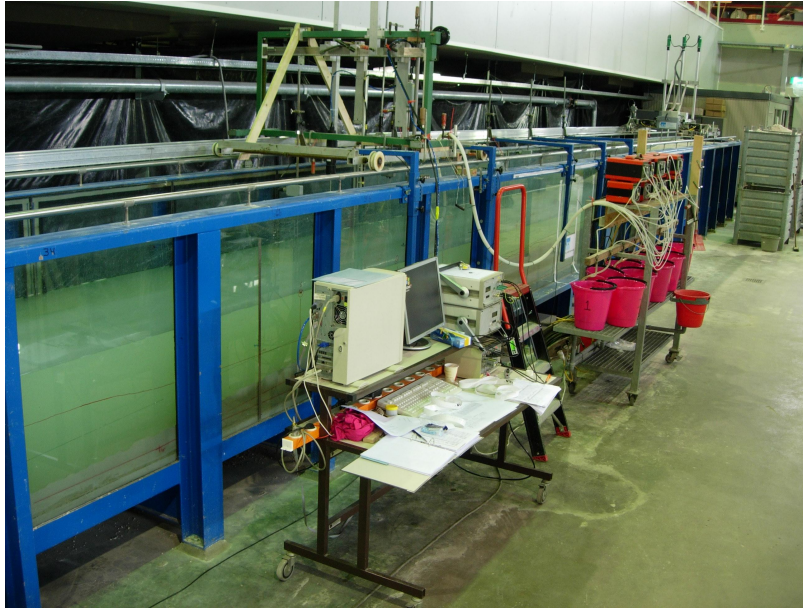


Figure 2.5 General overview tests

Bed profiler

Three probes at a mutual distance of 25 cm are constructed on a carriage that moves along the flume. The probes can move up, forward and down again. The distance between two measured points is variable. The results of the three parallel measurements give the average bed profile, which is used in the analyses.



Figure 2.6 Bed profiler with three probes

Transport Suction System (TSS)

A Transverse Suction System (TSS), developed by Bosman et al. (1987), was used to simultaneously measure time-averaged suspended-sediment concentrations at ten different heights. The mutual positions of the suction tubes are schematically indicated in Figure 2.7. The tubes, with an inner diameter of 3 mm, are connected to several pumps, which generate a velocity of approximately 1.5 m/s of the water in the nozzles of the tubes. The pumps extract water and sediment, for approximately 15 minutes. The extracted volume of water is read from the volume scale on the buckets in which the water and sediment are collected. The suspended sediment samples are flushed in a volume meter tube and this number can be converted to the concentration of sediment in the water. To derive the weight of the sediment from the measured volumes in these volumetric volumes, calibrations for different grain sizes are available. Here, the mass of the samples was determined using a calibration factor for dry mass/wet volume of 1.54 g/cm^3 , which was originally derived for sand with a median grain size of $118 \text{ }\mu\text{m}$. The suspended sediment, collected through the TSS was analysed on grain size with a Visual Accumulation Tube (VAT). For detailed information about determination and use of calibration factors concerning the transverse suction tubes, reference is made to Den Heijer (2004).

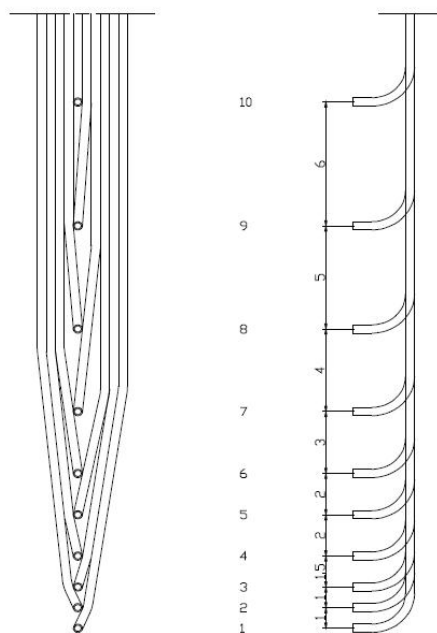


Figure 2.7 Lay-out of the suction tubes



Figure 2.8 From left to right: TSS, EMS, reference rod, WHM, ASTM, ADV

Electrical Magnetic Velocity (EMS)

This instrument is based on the principle that a conducting fluid will generate a voltage proportional to the flow velocity as it passes through the magnetic field created by the sensor.

Reference rod

A reference rod, a small rectangular piece of steel is connected to the carriage to determine the vertical positions of the instruments with respect to the sediment bed. The rod can be rotated in the direction of the flume. In this way, it can be placed on the sloping sand bed over the ripples (see Figure 2.9). Before each experiment the depth-reference rod was placed on the sediment and with a marker the position of the rod could be determined.

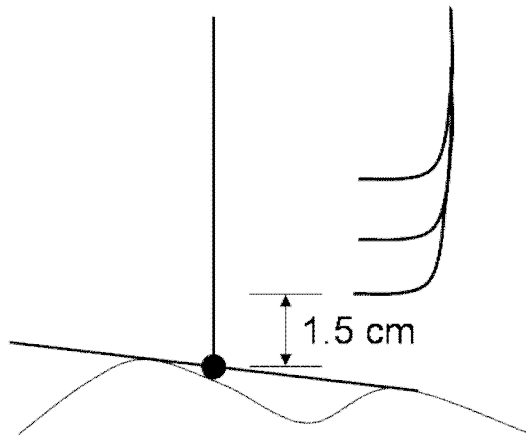


Figure 2.9 Schematisation of reference rod and positioning of TSS

By means of a reference attached to the carriage the relative position of the instruments in respect to the sediment could be adjusted. As a result, the instruments could consistently be placed at 1.5 cm above the sediment (see Figure 2.9).

Wave gauges (WHM)

Several wave gauges along the flume measure the water elevation. The free surface elevations, with respect to still water level, are recorded with resistance type twin-wire wave height meters. The output signal range from -10 to 10 V, corresponds to a water elevation measuring range of -0.25 m to 0.25 m.

Acoustic Sediment Transport Monitor (ASTM)

ASTM is an acoustic instrument for measuring the flow and the sand concentration. The Acoustic Sand Transport Monitor is based on the transmission and scattering of ultrasound waves by the suspended sand particles in the measuring volume. Using the amplitude and frequency shift of the scattered signal, the concentration and the velocity and hence the transport of the sand particles can be determined simultaneously and continuously.

Another device measuring the sediment concentration was the ASTM. The analogue output signal of the ASTM ranges from 0 to 10V for concentration. The device was calibrated for concentrations up to 3 kg/m^3 using sand with $d_{50} = 170 \text{ }\mu\text{m}$ resulting in a calibration factor of $0.391 \text{ kg/m}^3/\text{V}$. Sand concentrations up to 3.91 kg/m^3 could be measured. In the experiments the gain factor was reduced to allow for concentrations up to 25 kg/m^3 . Afterwards ASTM measurements were re-calibrated by means of the data obtained by the transverse suction system. The mean concentrations from the ASTM were divided by the initial calibration factor ($0.391 \text{ kg/m}^3/\text{V}$) leading to an output in Volts.

Table 2.8 Changes in calibration factors during the experiments

date	test nr	range	K (gain)	g/l/V
		3,91	1	0,391
4-jun-07	1-11	7,83	0,5	0,783
22-jun-07		12	0,3262	1,2
22-jun-07	12-22	16	0,2446	1,6
27-jun-07	SANDS 23-70 VOP 1-30	25	0,1565	2,5

In Figure 2.10 the concentration measured by the suction tubes in g/l is plotted against the measurements by means of the ASTM in volts. The lower concentrations are positioned relatively close to the calibration line. However, the larger concentrations deviate more and more. It can be concluded that the initial calibration factor is not valid for the concentrations larger than 6 g/l and therefore, re-calibration was necessary.

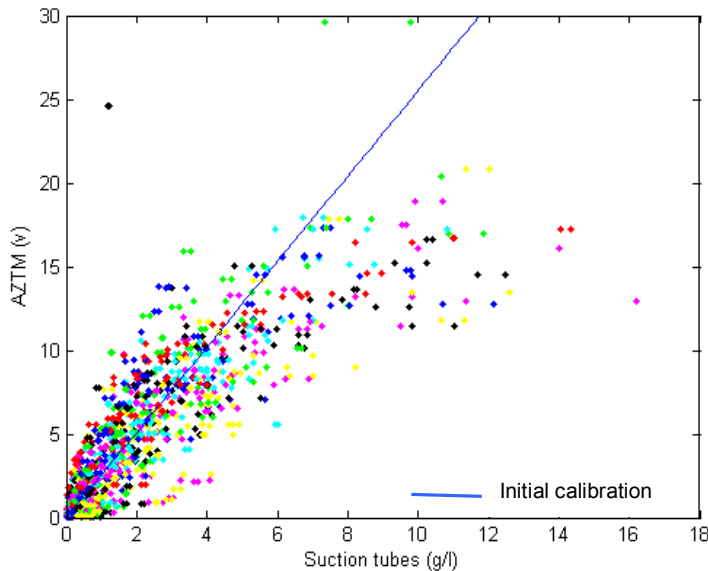


Figure 2.10 Scatter plot measured concentrations from suction tubes against ASTM output

Some points are far out of range and therefore omitted. (expnb 50 and 67)

In Figure 2.11, the data are clustered into seven divisions. The average concentration of the clusters and error bars are plotted in Figure 2.12. This error bar implies the standard deviations of the sample means. This is also referred to as the standard error of the estimate of the mean, or simply the standard error:

$$s_e = \sqrt{\frac{\sigma^2}{n}} = \sigma \sqrt{\frac{1}{n}} \tag{2.2}$$

in which,

σ is the standard deviation

n is the number of samples

Subsequently a non-linear fit was applied to acquire the adjusted calibration of the ASTM.

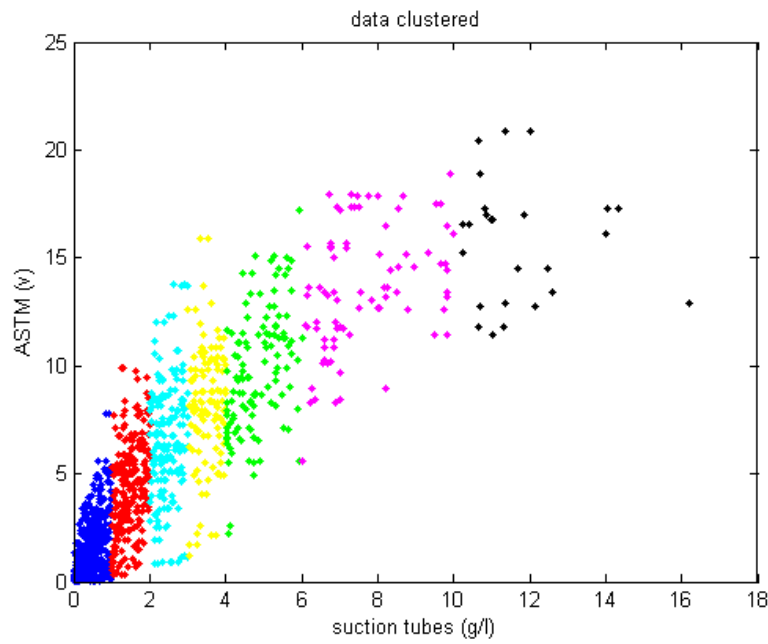


Figure 2.11 Clustering data

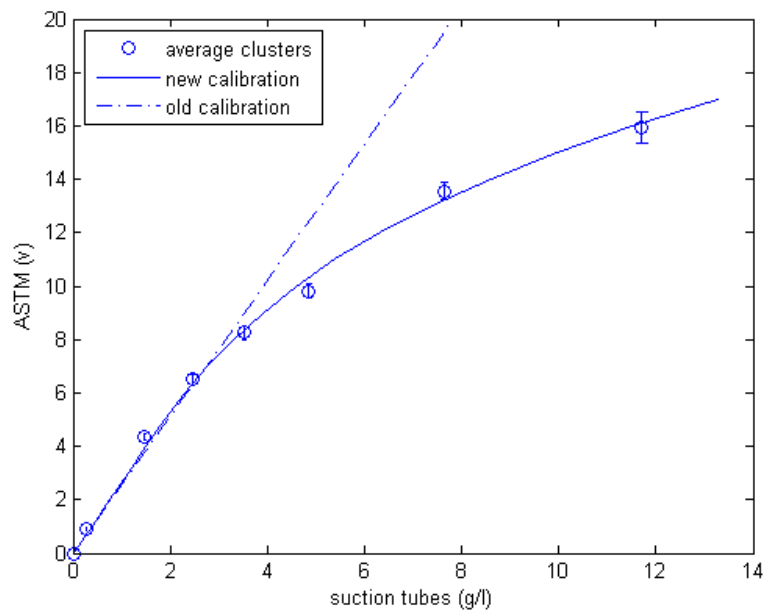


Figure 2.12 New non-linear calibration curve through average concentrations and error margins of clustered TSS data against ASTM output

Old calibration	$C_{astm} = 0.3914 * V$
New calibration	$C_{astm} = 0.0024 * V^3 - 0.0191 * V^2 + 0.4112 * V$

Acoustic Doppler Velocity (ADV)

An ADV or Vectrino measures three-dimensional flow velocities using the Doppler shift principle. It consists of a sound emitter, three sound receivers and a signal conditioning electronic module. The emitter of the instrument generates an acoustic signal that is reflected back by sound-scattering particles present in the water. These particles are assumed to move at the water velocity. The scattered sound signal is detected by the instrument receivers and used to compute the signal Doppler phase shift with which the radial flow velocity component is calculated.

Visual Accumulation Tube (VAT)

During the tests samples are taken from the sand collected by the suction tubes. The fall velocity and grain size distribution is determined by means of the Visual Accumulation Tube (VAT). The VAT consists of a settling tube with a length of about 2 m and a diameter of approximately 3 cm. The sample is released on top of the tube by means of a simple clamp device. Under the settling tube a small tube is suspended in which the deposit height can be determined as a function of time. Based on this information, the fall velocity distribution can be determined.

The method may not be very accurate due to hindered settling of the particles in the contracted section and the capillary tube (Van Rijn, 2006). In addition, the shape of the sediment particles influences its fall velocity and as a result its grain size. Therefore, samples of sieved sediments are released in the settling tube to properly calibrate the VAT.

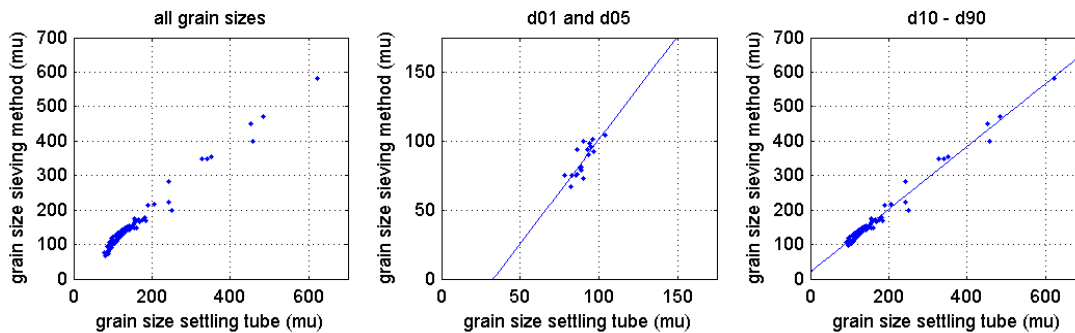


Figure 2.13 Calibration of VAT

In the scatter plot, above data of sieved samples and data acquired by VAT are shown. Grain sizes in the range 60-80 obtained by sieving are slightly smaller compared to data obtained by VAT. This could be due to the fact that small grains are exposed to cohesive forces and are easily trapped by other grains in the VAT. Two different calibrations are applied, one for D_{01} and D_{05} and one for D_{10} - D_{90} (see Figure 2.13).

For D_{01} to D_{05} the following relation has been found: $d_{\text{samples}} = 1.5 \cdot d_{\text{VAT}} - 49$

For D_{10} to D_{90} the following relation has been found: $d_{\text{samples}} = 0.91 \cdot d_{\text{VAT}} + 20$

Comparison performance of velocity measurements

Throughout the experiments, flow velocities have been measured at several heights in the vertical and at different positions along the flume by means of EMS, ASTM and ADV. Basically, the ASTM and ADV measures the horizontal velocity of the sand particles from the Doppler shift in frequency of the emitted and received acoustic signals. The EMS measures the fluid velocities.

Each measurement lasted 5 minutes. Data obtained by the EMS and ADV slightly differ from each other. A typical example is shown in Figure 2.14, in which the blue line corresponds with the data of the ASTM, the green line with the data of the EMS and the red line with the data of the ADV. Considering the first graph, the signals are obtained at 10 cm above mean bed level, positioned at deep water, with an accretive wave condition. The EMS and ADV, represented by the green and red line respectively, show a rather smooth single. The ASTM, correspondent with the blue line, gives a single in blocks due to the fact that the processor was not able to compute more than two points in one second.

The second graph shows a time series obtained on top of the bar applying an erosive wave condition. The signals of EMS and ADV show spikes because of air bubbles in the water due to wave breaking. The spikes from the ADV are more distinct than the spikes of the EMS.

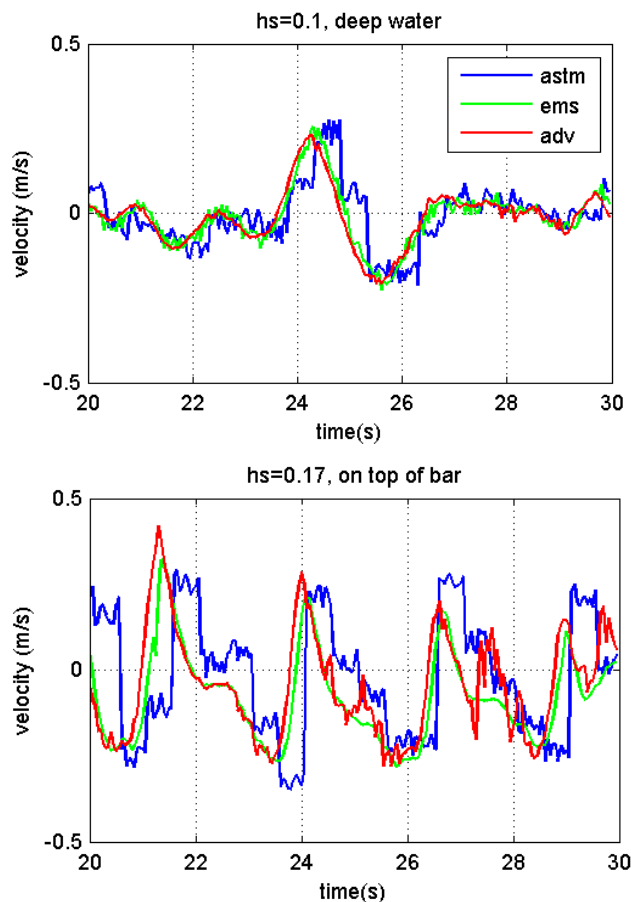


Figure 2.14 Time series of velocity measurements at 10 cm above bed level. The upper plot shows the series obtained at 19.9 m for the accretive test T04 (Design 1). The lower plot represents the series obtained at 24.9 m for the erosive test T05 (Design 1).

Velocities measured at shallow water show a significant difference in the upper measuring points (see Figure 2.15). At small water depths, the instruments are partially out of the water. Since the measurement volume of the ADV is located 4 cm below the measuring volume of the EMS, the ADV is already out of the water, whereas the EMS is still in the water. Therefore, some points measured by the ADV may not be valid. Thus, at shallow water the data obtained for the upper measurement points by the EMS are more accurate compared to the data obtained by the ADV.

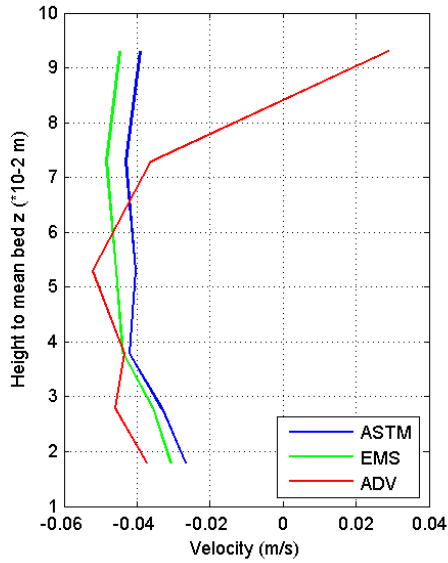


Figure 2.15 Comparison of velocity verticals measured by ASTM, EMS and ADV

2.3 Methodology of process-based measurements

During a number of subtests the carriage was placed at several cross-shore locations. The measurement period lasted around one hour at each location. The measurements were performed by following the next methodology at the beginning of the measurement period. The TSS, Vectrino, ASTM and EMS were positioned at 1.5 cm from the local depth, determined by the reference rod. This depth represents the depth at the top of ripples, if present. After five minutes of measuring an average value of the Vectrino, ASTM and EMS is taken, they are raised to the next suction tube. Five more minutes of measurements are taken before moving the Vectrino, ASTM and EMS again to the next tube. This operation is repeated 10 times to gain data of these three devices at equal depth that every tube has taken the water/sediment sample. During the measurement period of one hour, two samples by means of the TSS are taken.

Step by step the following actions are undertaken during a process-based measurement:

- Position carriage
- Set reference rod on top of ripples
- Read marker
- Put TSS at 1.5 cm above ripples
- Measure local ripple height
- Measure temperature
- EMS ADV and ASTM positioned at level of lowest suction tube
- Start five minutes measurements EMS ADV and ASTM
- Elevate EMS, ADV and ASTM
- Start another five minutes measurement EMS, ADV and ASTM
- Start TSS sample 1
- Continue five minutes measurements EMS,ADV and ASTM
- Start TSS sample 2

3 Results of SANDS experiments

3.1 Introduction

As already mentioned, tests are carried out aiming to advance mobile bed scaling laws, within the framework of project SANDS. In Section 3.2, the development of the beach profiles of the 1:10, 1:15 and 1:20 tests, for erosive condition as well as accretive condition, are discussed.

Since at this moment no data are available on the tests in Hannover and Barcelona, no comparison can be made and no extensive analysis can be done focussing on scaling laws at different scale levels. However, because the 1:10 and 1:15 tests in the Scheldt flume can be seen as distorted tests of 1:20, research can be done within one scale level, concerning distortion scale and morphological time scale. In Section 3.3, the focus is on the scale relationships within the Scheldt flume tests at WL | Delft Hydraulics.

In Section 3.4, several geometric characteristics of the beach profiles of the Scheldt flume tests with an erosive condition are studied. The features of the profiles are discussed and the profiles are made dimensionless to be able to compare with the tests carried out in Hannover and Barcelona for future research.

Analysis of wave height and water level can be found in Section 3.5. Flow velocities, sand concentrations and sediment transport are discussed respectively in Section 3.6, 3.7 and 3.8.

3.2 Beach profile development

At the start of each test, the initial profile is measured. Subsequently, the bed profile is measured after each time interval (see Table 2.5). The bed profile measurements were carried out with three probes attached to a carriage that moves from 12 meters from the wave paddle to the end of the profile. The average of the three measured profiles is assumed to be the representative coastal profile. Possible cross-flume non-uniformity has been checked and can be neglected.

Sections 3.2.1, 3.2.2 and 3.2.3 show bed profile development of all tests, the erosive tests as well as the accretive tests.

Migration of the sand bar can clearly be observed in the profile development of all tests. The bed profiles of T02, T04 and T06 are exposed to an accretive wave condition and the bed profiles of T03, T05 and T07 are subject to an erosive wave condition. The accretive wave condition makes the bar move shoreward, contrary to the erosive condition, which shifts the bar offshore. This can be explained by the occurrence of two different dominant processes.

In general, the net cross-shore sediment transport in coastal areas is a balance between landward transport by wave asymmetry and seaward transport by undertow. The term wave

asymmetry may be somewhat confusing because both horizontal wave asymmetry and vertical wave asymmetry exists. Horizontal wave asymmetry (or wave skewness) is caused by non-linear wave transformation. Linear wave theory is not applicable when the wave steepness is too large. This occurs in the nearshore or in case of extreme waves. Stokes formulated a theory which introduces a second order correction in steepness to the linear solution.

The initially symmetric, nearly sinusoidal profiles, develop into a profile characterized by a peaked wave crest and a flat trough, while propagating into shallow water. This shape is shown in Figure 3.1, originated from a first order and second order wave. As a result, a short period of high onshore-directed orbital velocities and a long period of low offshore-directed orbital velocities occur. The sediment transport is related to the velocities by a power of third and this results in an onshore-directed sediment transport.

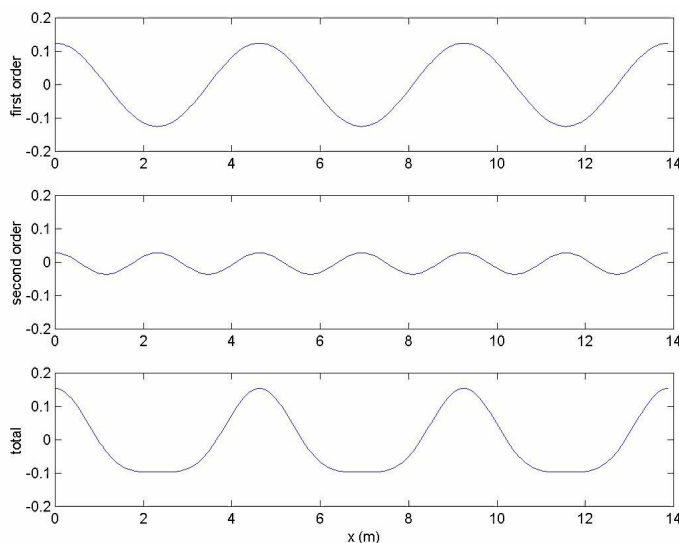


Figure 3.1 Sinusoidal waves development into waves with peaked wave crest and flat trough

Vertical wave asymmetry is characterized by a sawtooth-like wave with equal onshore and offshore-directed velocities, and dominates in the swash zone. Neglecting the effect of acceleration, they do not contribute to net onshore or offshore-directed sediment transport. The horizontal wave skewness will hereafter be referred to as wave asymmetry.

The magnitude of onshore transport by wave asymmetry and seaward transport by undertow increases with the wave height. Onshore transport by wave asymmetry dominates over seaward transport by undertow during calm wave condition ($H_s = 0.10$ m). However, the transport rates during these conditions are low. During storm conditions ($H_s = 0.17$ m), offshore transport generally exceeds onshore transport, since sediment transport by the undertow dominates the onshore transport by wave asymmetry.

Another remark can be made. In Figure 3.2, the bed profile development of SANDS test T04 is shown. In front of the active profile, at deep water, some kind of rippling can be noticed. Contrary to the VOP tests, during the SANDS tests second-order steering was turned off to be consistent with the wave generation in the Hannover and Barcelona flumes.

Because of this, spurious waves could develop in the flume resulting in the large rippling. It is assumed that the results of the tests are not affected.

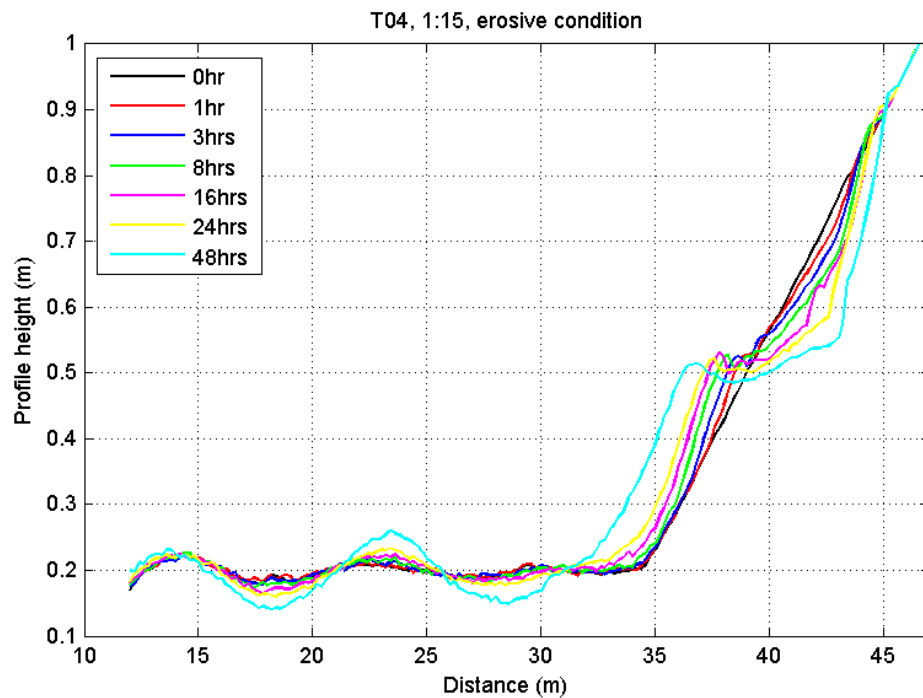


Figure 3.2 Profile development of SANDS test T04, 1:15

3.2.1 Profile 1:20

Profile development of T02 and T03 with an initial plane slope of 1:20 are shown in Figure 3.3 and in Figure 3.4. Applying an erosive condition, a small bar is formed after the first sub test. This bar migrates offshore in time. Behind the bar, a trough appears and becomes more pronounced in time. The length between trough and beach slope increases in time. The initial smooth transition to the beach slope becomes rather sharp. A swash bar appears and this bar does not move. It merely increases in height.

After 24 hours of propagating waves of the erosive condition, test T03 is started, which is subject to the accretive wave condition. The breaker bar migrates onshore and its height increases. A smaller second bar occurs between the outer breaker bar and beach slope. No changes can be observed in the profile development near the swash bar.

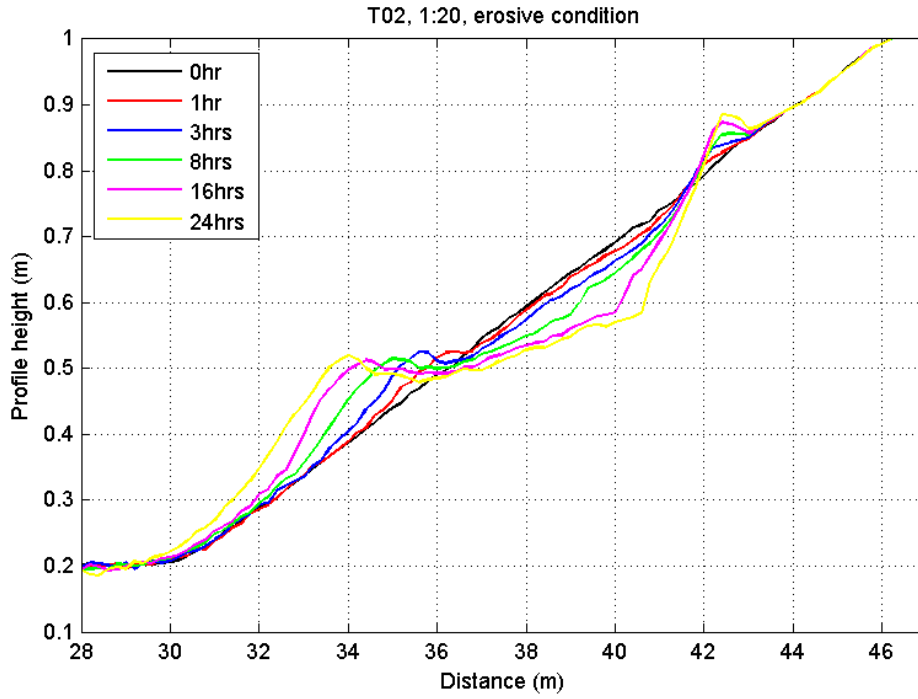


Figure 3.3 Profile development T02, 1:20, erosive condition

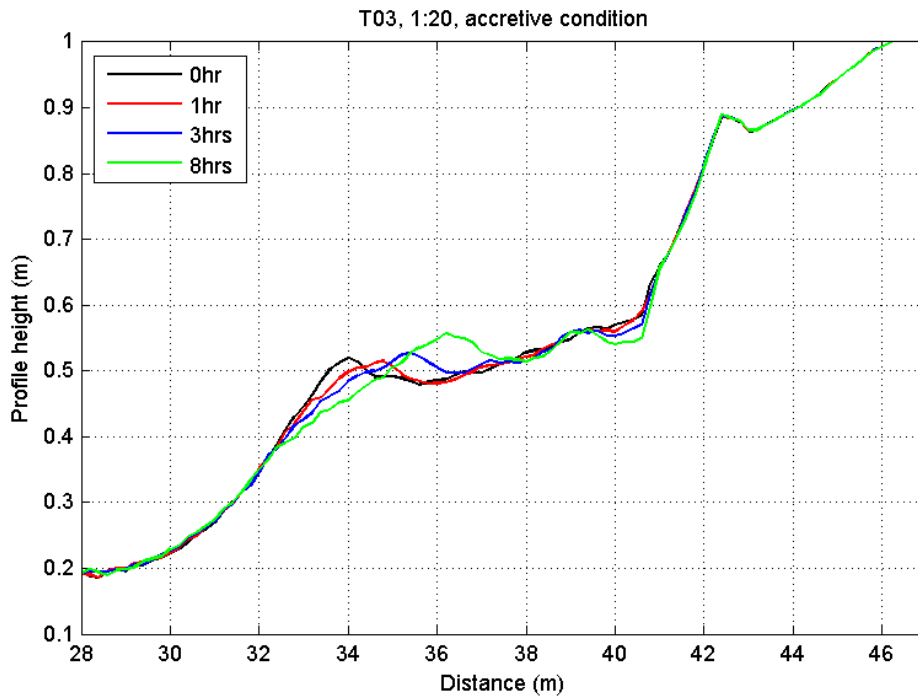


Figure 3.4 Profile development T07, 1:10, accretive condition

Dimensionless profiles T02 and T03

In Figure 3.5 and Figure 3.6, bed profiles of T02 and T03 are made dimensionless by dividing horizontal and vertical values by the offshore water depth (upper plot) and the offshore wave height (lower plot). The origin is at the intersection of the still water line (SWL) with the initial bed profile.

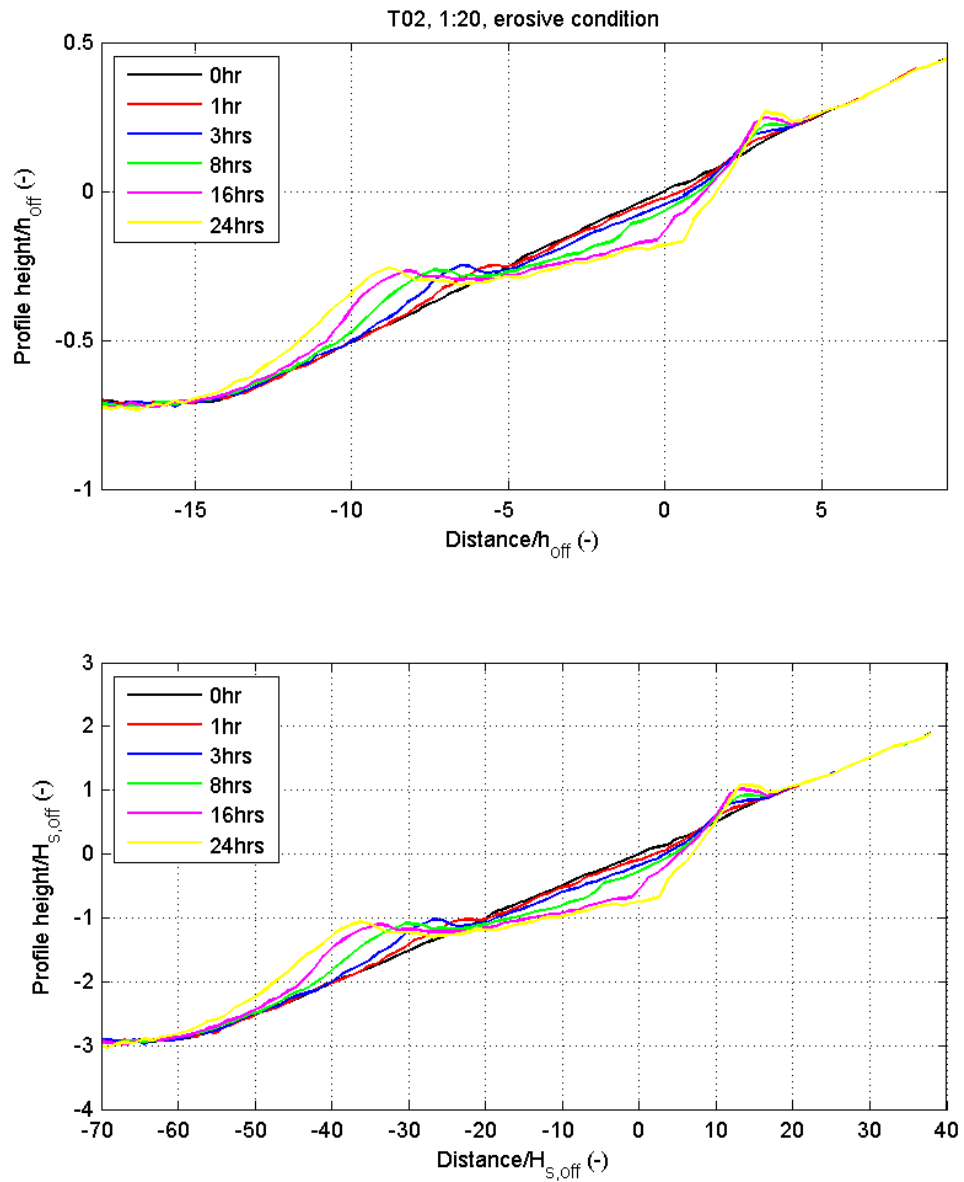


Figure 3.5 Dimensionless profiles T02

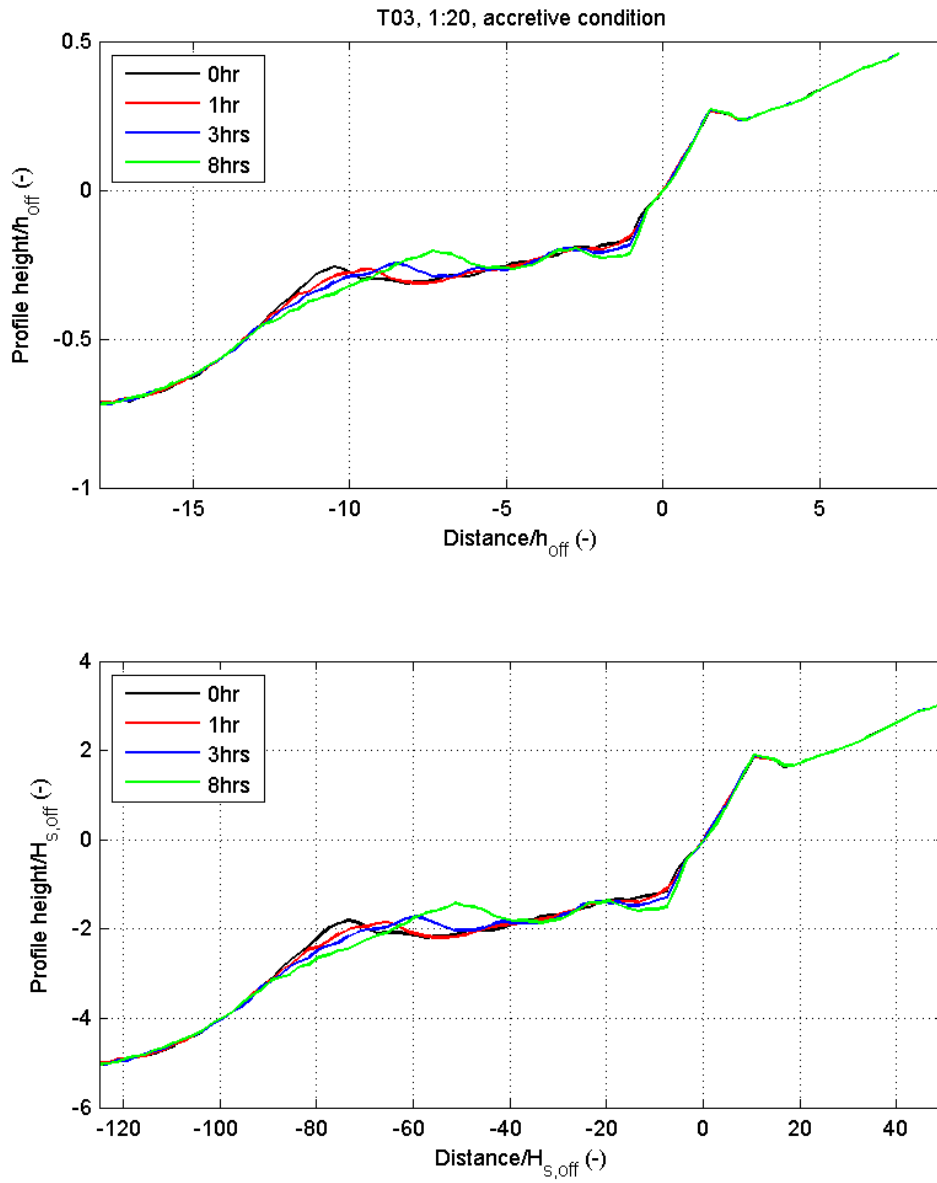


Figure 3.6 Dimensionless profiles T03

3.2.2 Profile 1:15

Profile development of T04 and T05 with an initial plane slope of 1:15 are shown in Figure 3.7 and in Figure 3.8. Applying an erosive condition, a small bar is formed after the first sub test. This bar migrates offshore in time. Behind the bar, a trough appears and becomes more pronounced in time. The length between trough and beach slope increases in time. The initial smooth transition to the beach slope becomes rather sharp. A swash bar appears and migrates landwards; its height relative to the initial bed profile does not increase.

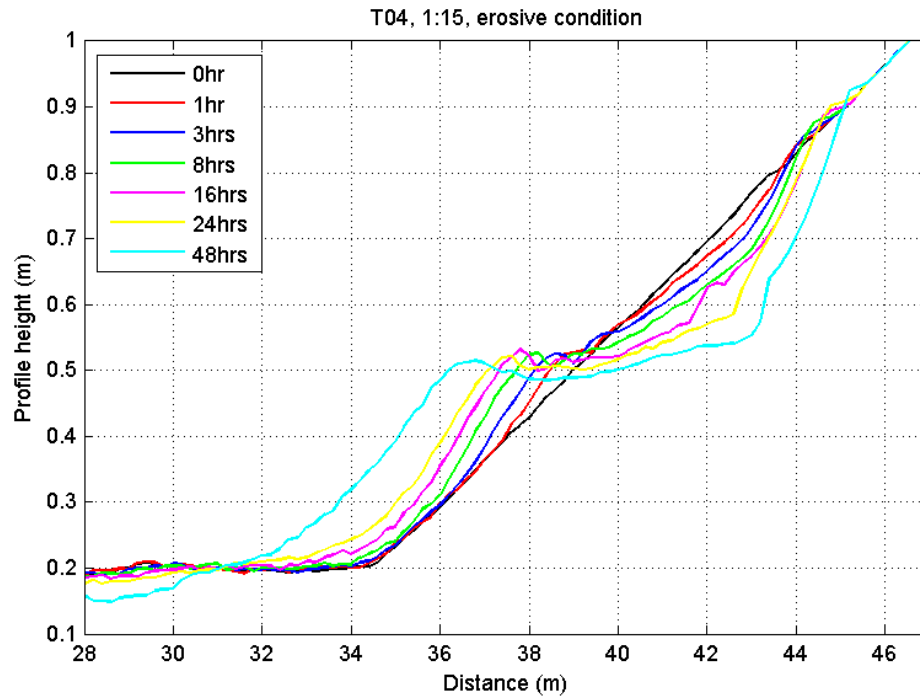


Figure 3.7 Profile development T04, 1:15, erosive condition

After 48 hours of propagating waves of the erosive condition, test T05 is started, with the accretive condition. The breaker bar migrates onshore and its height significantly increases. A smaller second bar occurs between the outer breaker bar and beach slope. Hardly any changes are observed in the profile development near the beach slope and the swash bar.

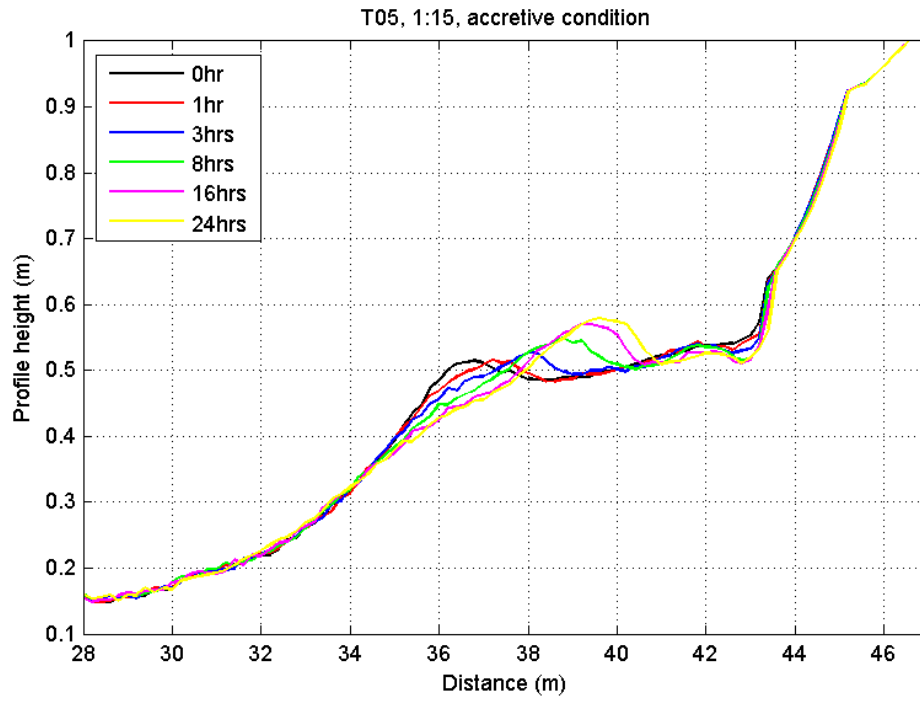


Figure 3.8 Profile development T05, 1:15, accretive condition

Dimensionless profile T04 and T05

In Figure 3.9 and Figure 3.10 profiles of T04 and T05 are made dimensionless by dividing horizontal and vertical values by the offshore water depth (upper plot) and the offshore wave height (lower plot). The origin is at the intersection of the still water line (SWL) with the initial bed profile.

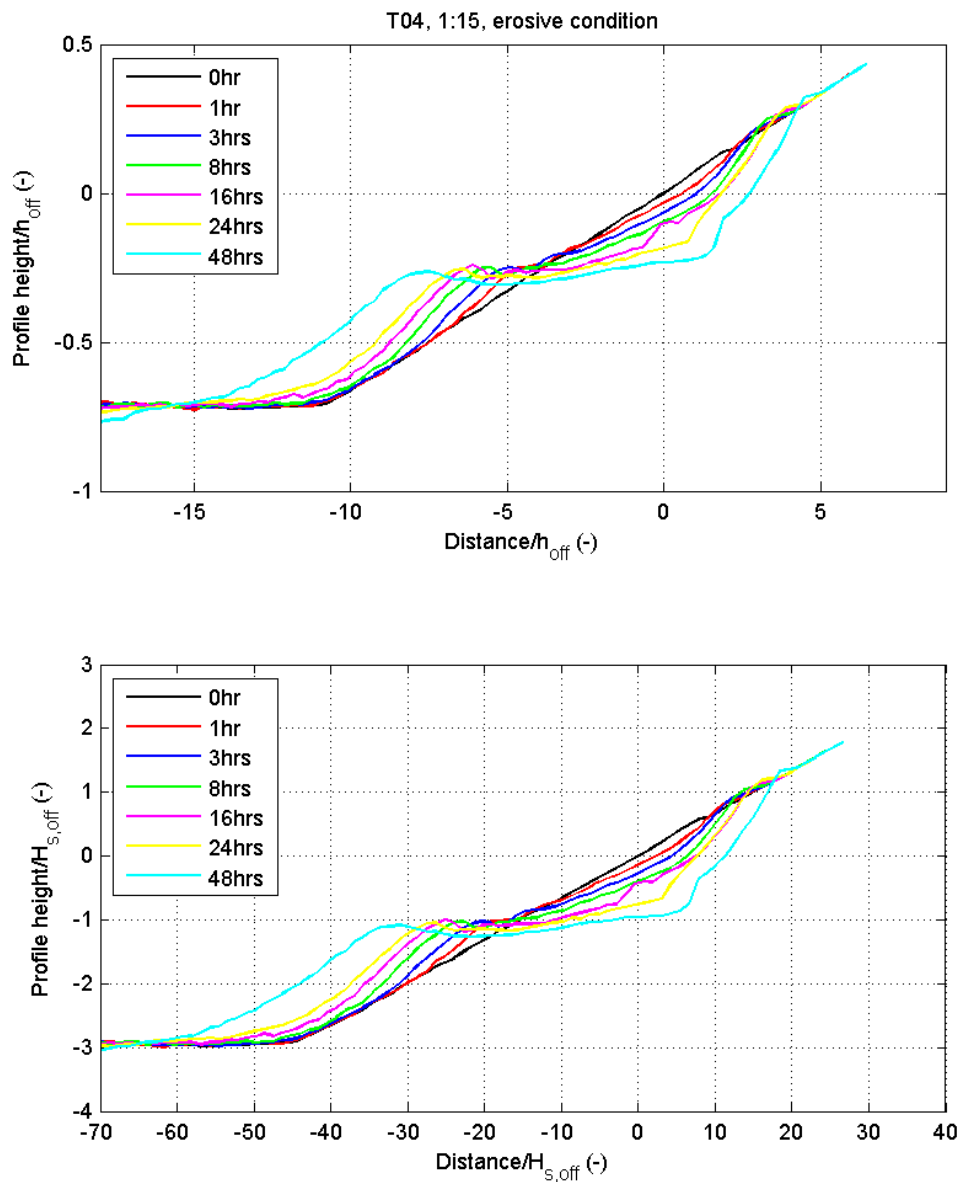


Figure 3.9 Dimensionless profiles T04

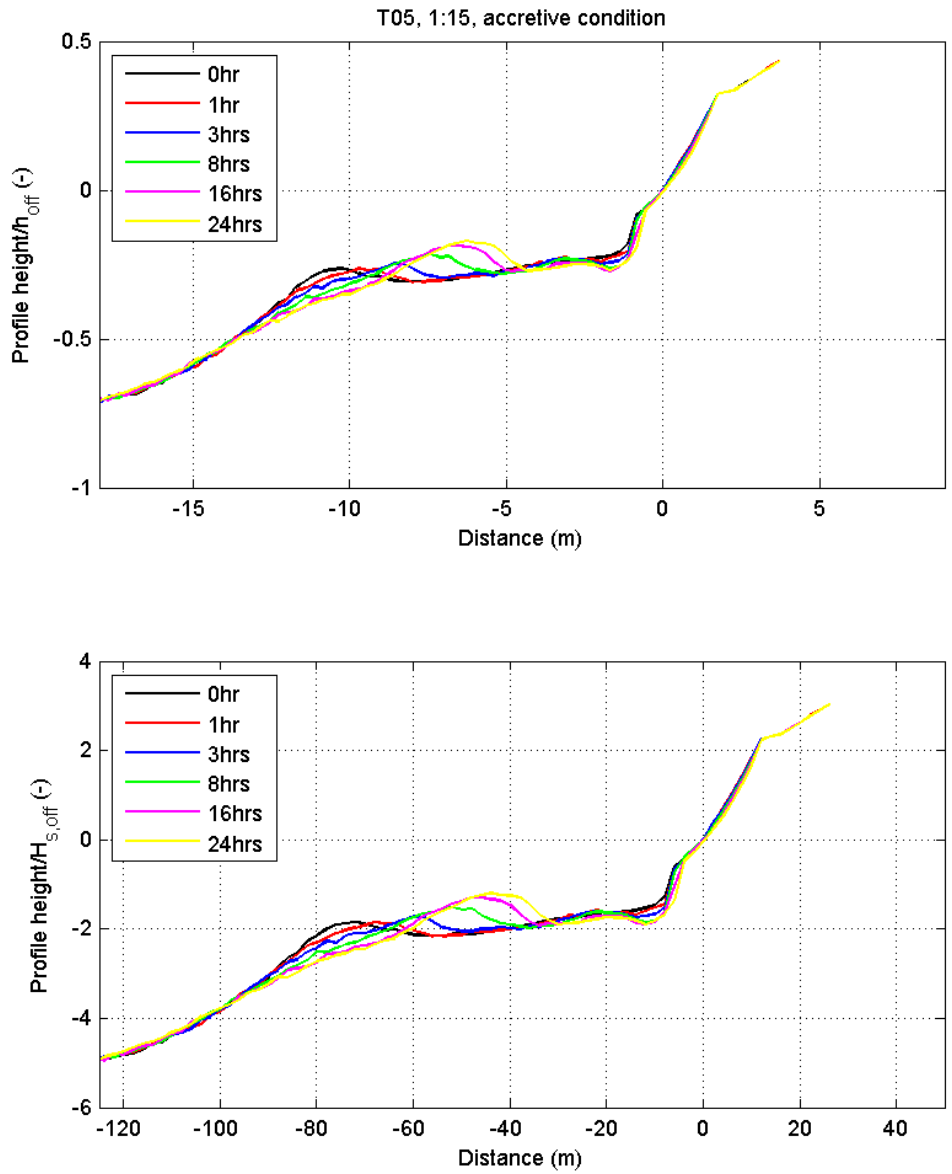


Figure 3.10 Dimensionless profiles T05

3.2.3 Profile 1:10

Profile development of T06 and T07 with an initial plane slope of 1:10 are shown in Figure 3.11 and Figure 3.12. Similar to the 1:15 and 1:20 tests, a small bar is formed after the first sub test. This bar migrates offshore in time. Behind the bar, a small trough appears and becomes more pronounced in time. The length between trough and beach slope increases. The transition from the trough to the swash bar remains rather smooth, contrary to the 1:15 and 1:20 tests, which show a slightly sharper transition. At the end of the profile, no swash bar can be observed.

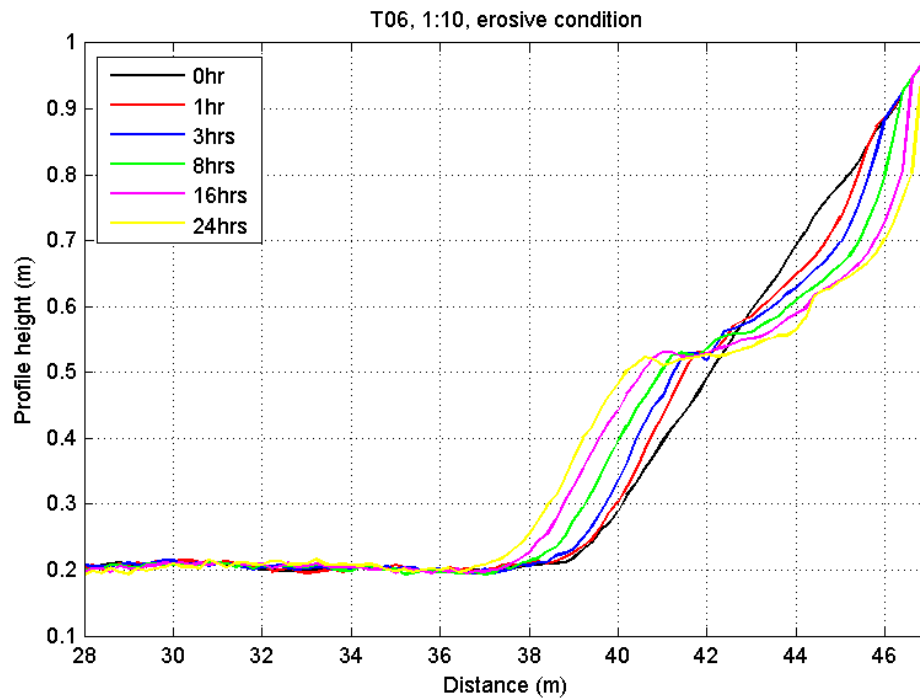


Figure 3.11 Profile development T06, 1:10, erosive condition

After 24 hours of propagating waves of the erosive condition, test T07 is started, with the accretive condition. The breaker bar migrates onshore and its height increases. A smaller second bar occurs between the outer breaker bar and beach slope. This second bar disappears after eight hours; it seems to fuse together with the beach slope. No significant changes can be observed near the beach slope and the swash bar. However, the changes in profile development are slightly bigger for T07 than for T03 and T05.

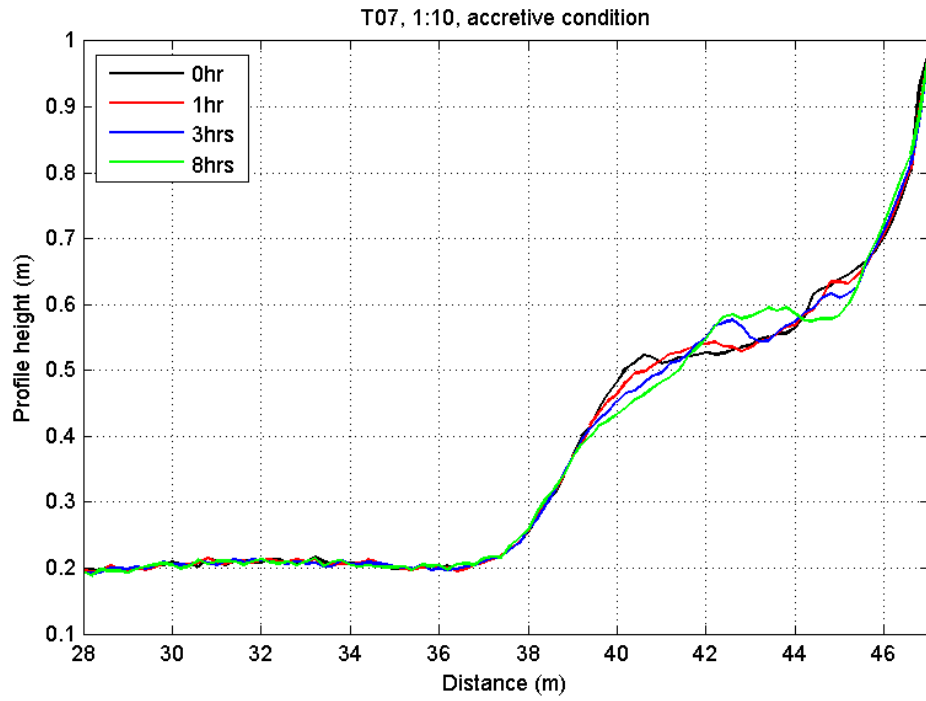


Figure 3.12 Profile development T07, 1:10, accretive condition

Dimensionless profile T06 and T07

In Figure 3.13 and Figure 3.14 profiles of T04 and T05 are made dimensionless by dividing horizontal and vertical values by the offshore water depth (upper plot) and the offshore wave height (lower plot). The origin is at the intersection of the still water line (SWL) with the initial bed profile.

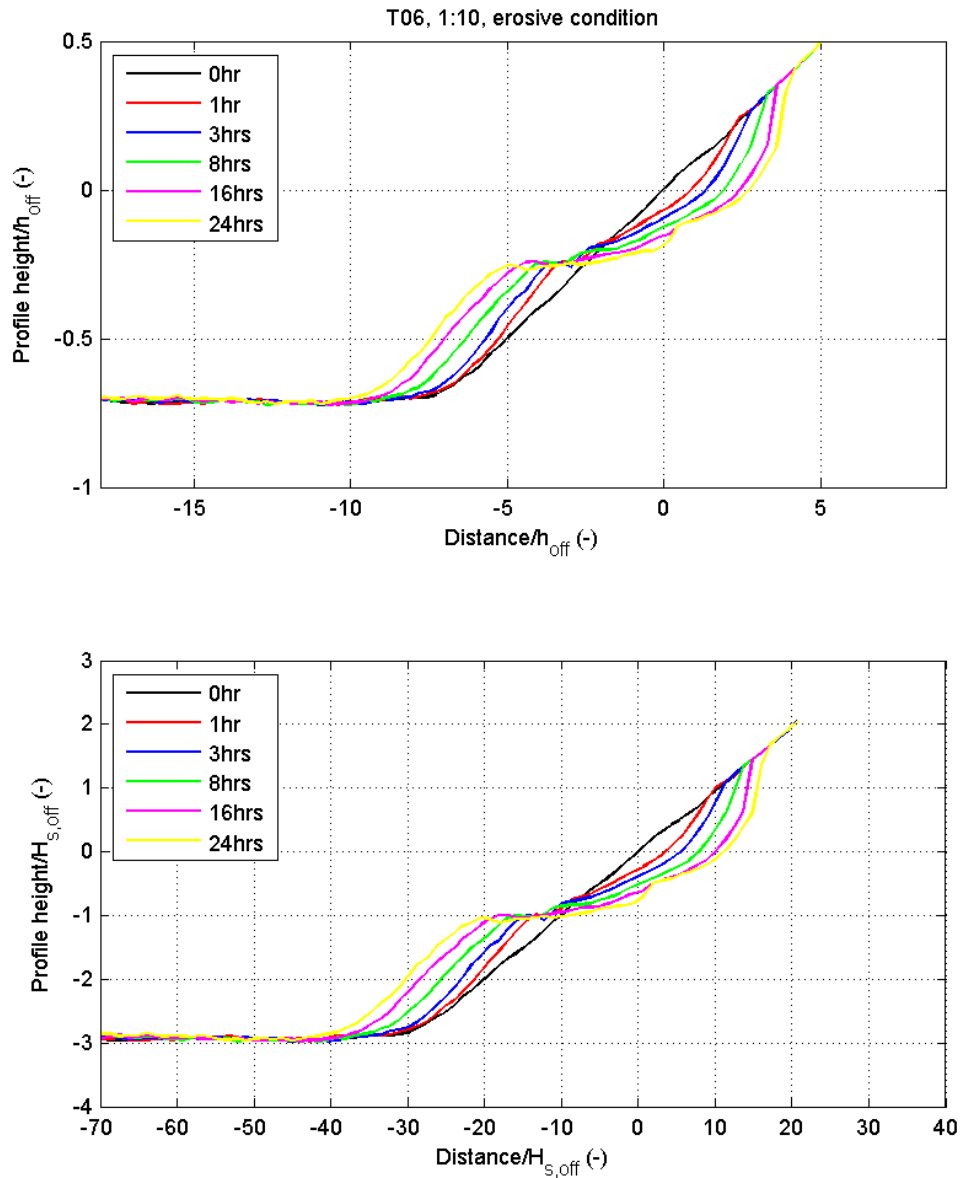


Figure 3.13 Dimensionless profiles T06

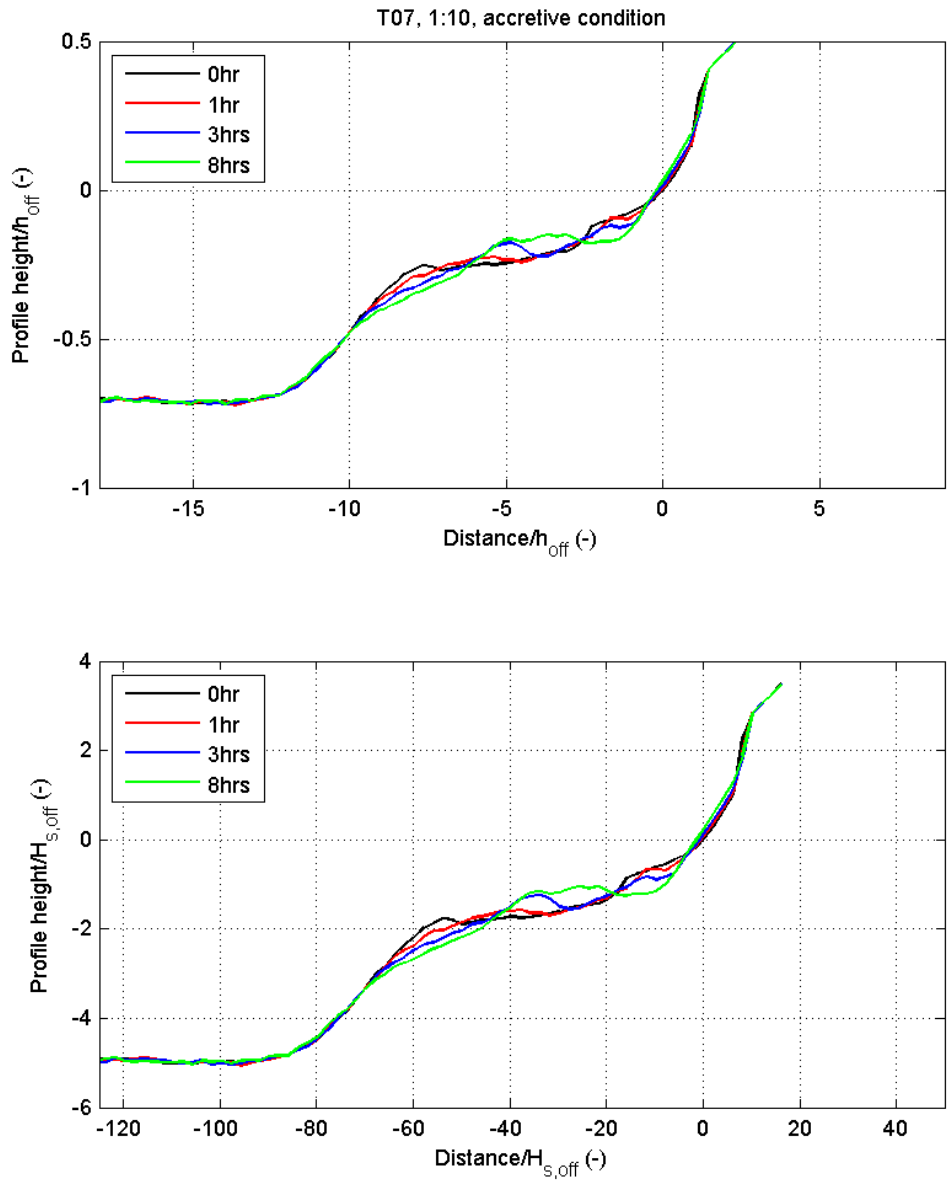


Figure 3.14 Dimensionless profiles T07

3.2.4 Development of sediment volumes

In this section, the development of the sediment volumes, are shown. The profiles are divided into three parts and for every part the development of the sediment volume in time are computed. The initial amount of sediment is subtracted and therefore, the initial sediment volume, indicated in the upper plots, start at zero.

It is remarked that the values on the axes of the volume plots for the erosive tests differ from the values on the axes for the accretive tests.

Discussion on equilibrium profile

Considering Figure 3.15 to Figure 3.20, it can be said that for the SANDS tests 1:10, 1:15 and 1:20, subject to an erosive condition as well as an accretive condition, no equilibrium profile is reached. First, the erosive tests are discussed. Even after 48 hours of propagating waves on the initial 1:15 slope, profile development is observed. Sediment transport, migration of breaker bar and extension of length (see Section 3.4) indicate a development of the profile. However, this development remains small and does not considerably change in time. It can be assumed that this process will continue until the end of the flume is reached. In addition, it may be possible that the process stops, if the decay of the wave height over the surf zone is sufficiently large, that the sediment transport due to the undertow does not dominate over the sediment transport caused by the wave asymmetry. The length between the breaker bar and the coast line should be very large, in order to be able to reduce the wave height to such an extent. Such a profile is not likely to occur in reality.

Profiles exposed to an accretive condition (see Figure 3.16, Figure 3.18 and Figure 3.20) were not able to reach an equilibrium. After 24 hours, the landward migration of the breaker bar is still visible for test 1:15 (see Figure 3.18). Contrary to the profile development of the erosive tests, it could be possible, that the profile development of the accretive tests reaches an equilibrium. The migration of the breaker bar could stagnate, because the sediment transport due to the undertow is equal to the sediment transport caused by the wave asymmetry. This, however, is not substantiated by the measured bed profiles.

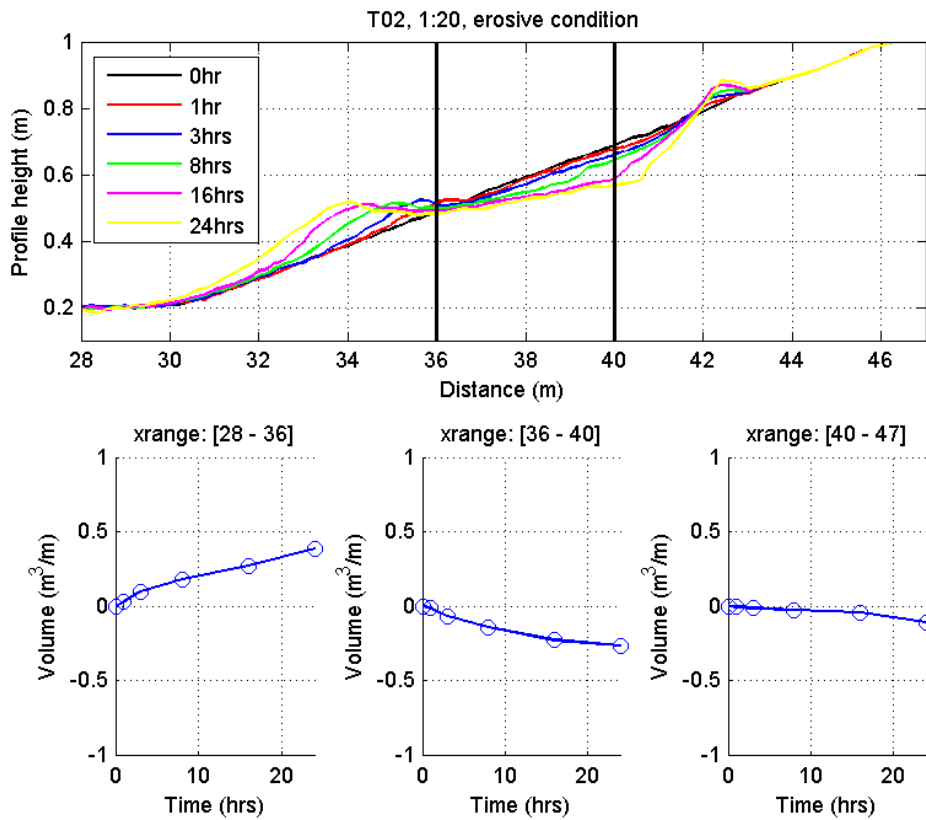


Figure 3.15 Development of erosion/deposition volumes in time, divided into three parts: 28-36, 36-40, 40-47

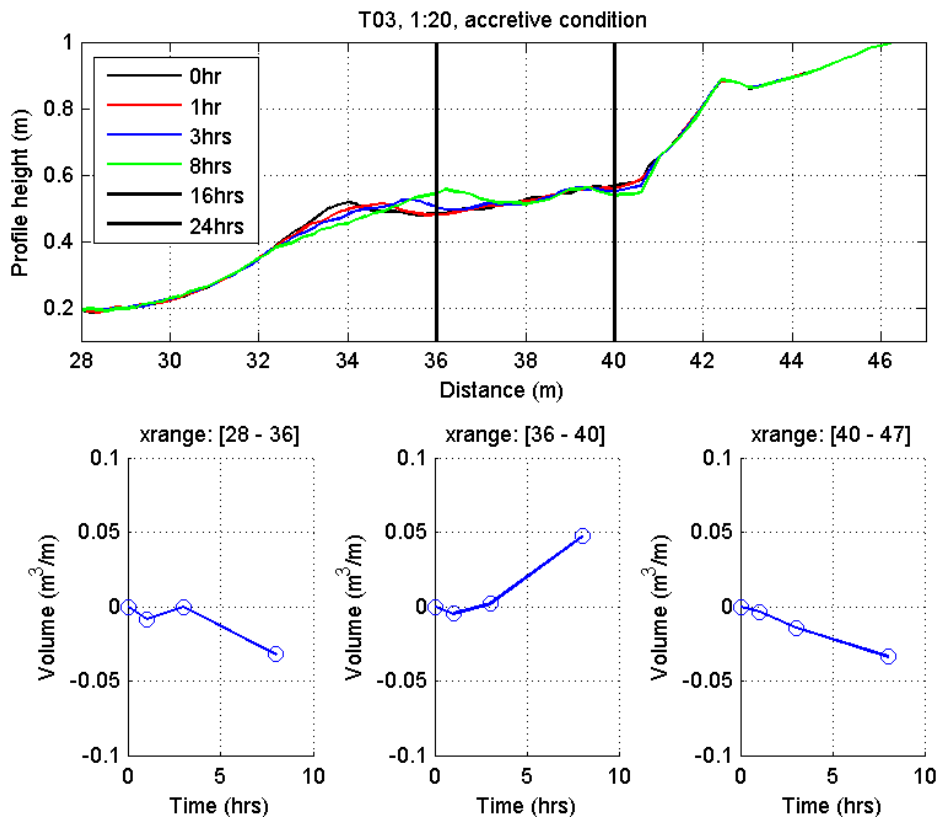


Figure 3.16 Development of erosion/deposition volumes in time, divided into three parts: 28-36, 36-40, 40-47

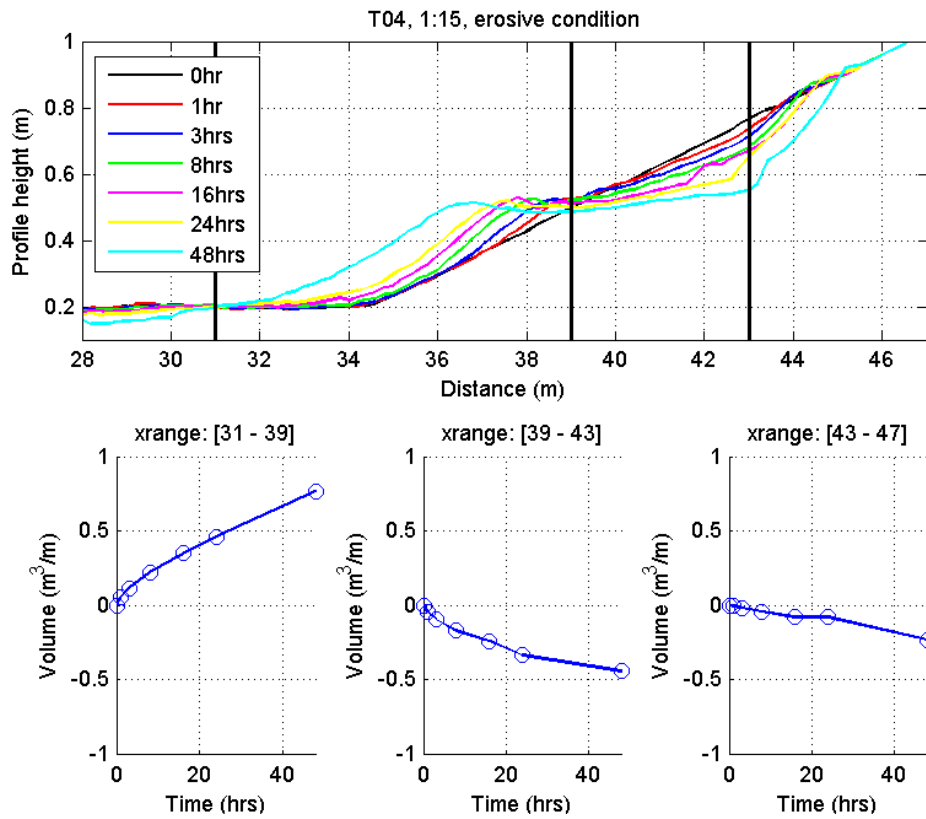


Figure 3.17 Development of erosion/deposition volumes in time, divided into three parts: 31-39, 39-43, 43-47

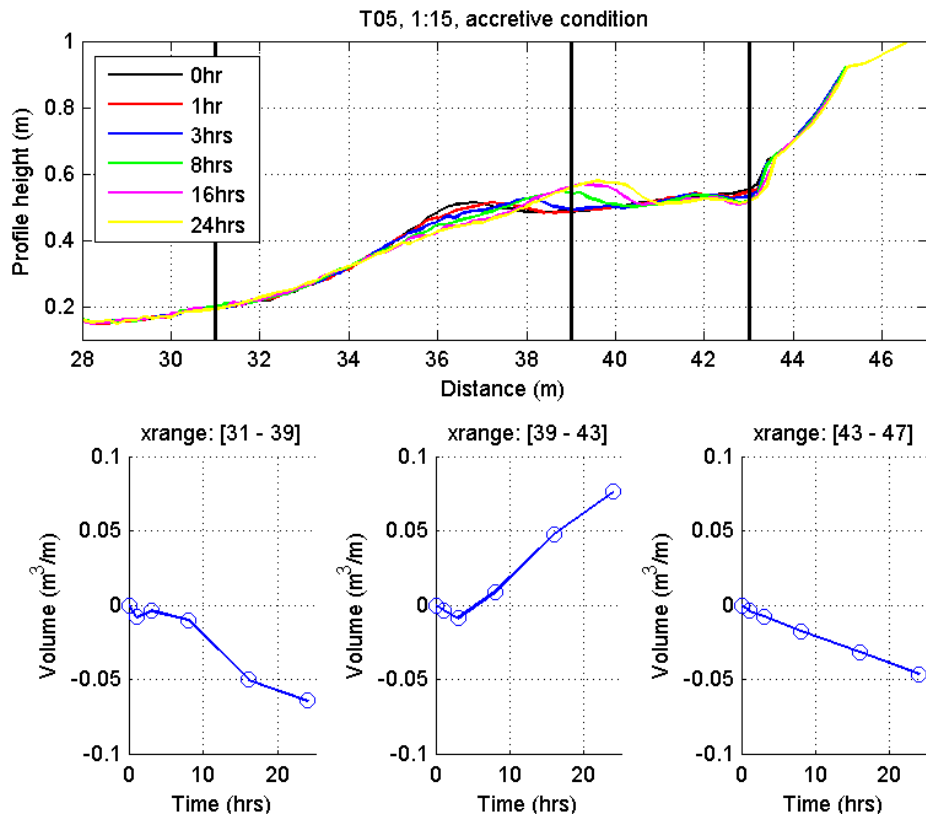


Figure 3.18 Development of erosion/deposition volumes in time, divided into three parts: 31-39, 39-43, 43-47

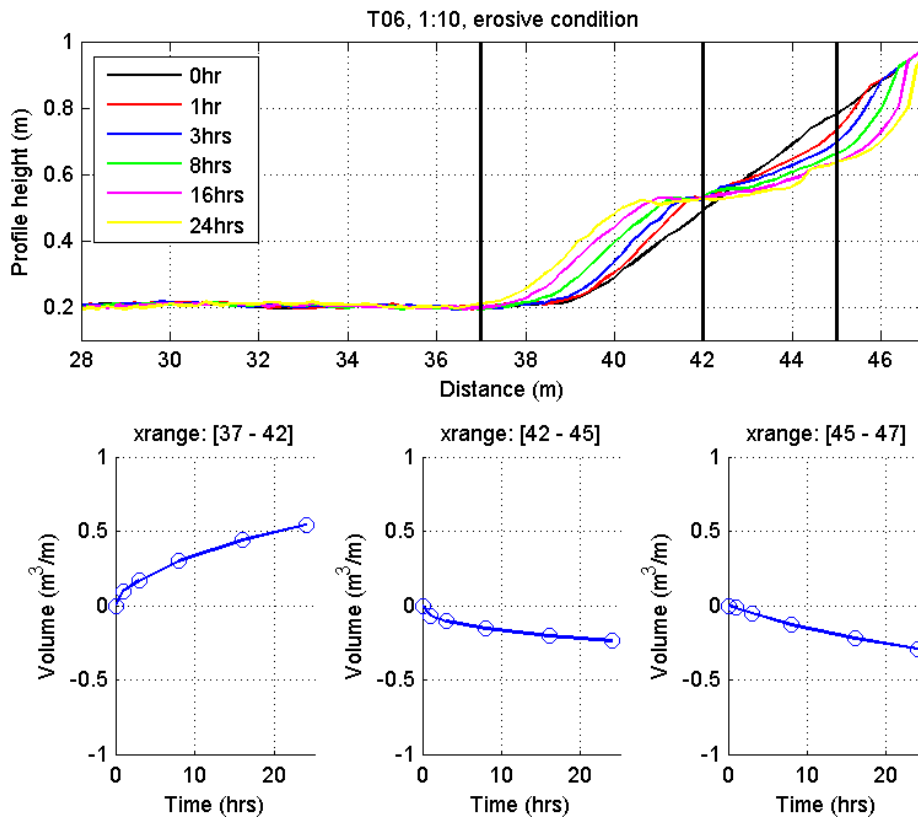


Figure 3.19 Development of erosion/deposition volumes in time, divided into three parts: 37-42, 42-45, 45-47

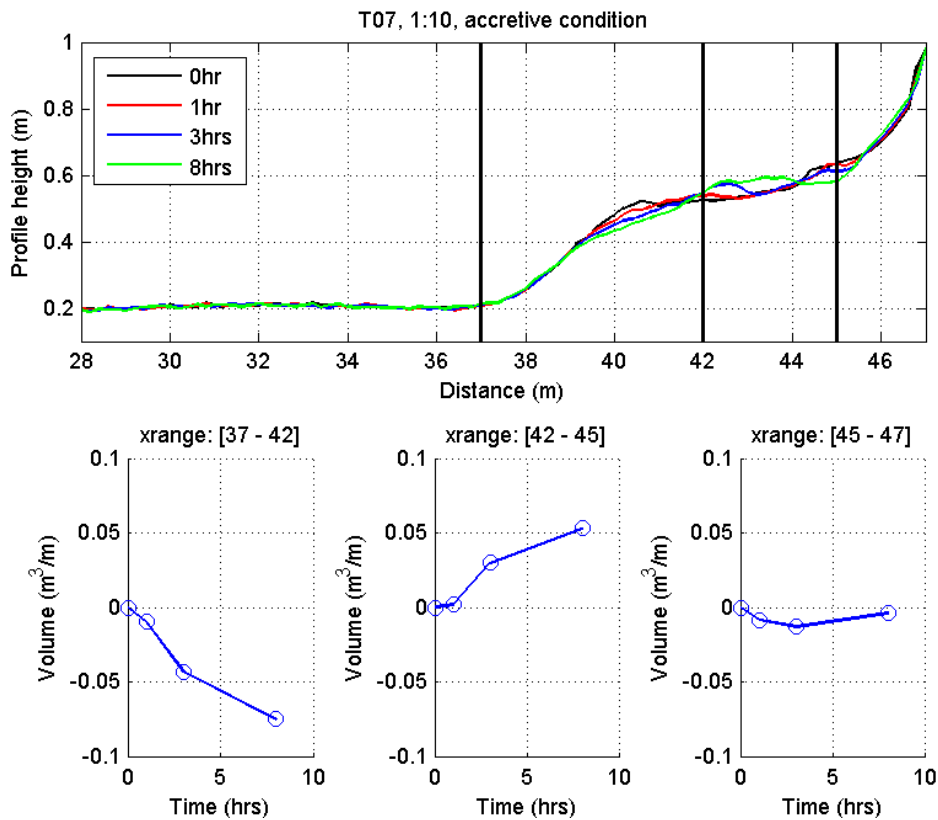


Figure 3.20 Development of erosion/deposition volumes in time, divided into three parts: 37-42, 42-45, 45-47

3.3 Analysis of morphological time scale for distorted tests

The physical model of the project SANDS consists of three different initial profiles. The bed profiles consist of plane slopes, 1 to 10, 1 to 15 and 1 to 20. Tests 1:10 and 1:15 can be seen as the distorted models of test 1:20. Test 1:20 is referred to as the prototype situation.

Distorted models are physical models in which the horizontal length scale and the vertical length scale are different. In other words, a distorted model is not geometrically similar to the prototype situation (Hughes, 1993).

Non-distorted models with the same scale in both the horizontal and vertical directions, are by far preferable. Still distorted hydraulic models may have to be used because of several reasons. A distorted model is accomplished by exaggerating the vertical scale relative to the horizontal scale. The distortion scale is expressed as n_l/n_h . The need for a distorted model may arise from (1) limitations on the available space in which to construct the model, or (2) because of a lack of control over the modelling materials and conditions.

- (1) The size of the modelling facility often limits model scales because most water bodies are relatively shallow in comparison to their plan dimensions. If the prototype area to be modelled is large, the scale reductions necessary to fit the model within the available (or economically feasible) space may be so great that vertical dimensions cannot be measured with adequate resolution, or viscous and surface tension effects become dominant. In this case, the vertical scale may be distorted relative to the horizontal scale provided that appropriate modifications are made to the remaining scale ratios.
- (2) Another reason for distorted models arises from the limitations on modelling materials and conditions.

Within the flume tests in Delft the 1:10 and 1:15 test can be seen as the distorted test of the 1:20 test. Because n_h remains one, distortion scale n_l/n_h is similar to n_l . Values of distortion scale are listed in Table 3.1.

Table 3.1 Values of distortion scales

profile	distortion scale	test
1:20	1	T02
1:15	1.33	T04
1:10	2	T06

The wave characteristics are equal for all tests, just the initial bed profiles differ. The three bed profiles are subject to the erosive wave condition.

The morphological time scale can be represented by (see Appendix A.6)

$$n_{Tm} = (n_l / n_h)^{b+1} (n_{d50})^d (n_{s-1})^e / (n_h)^{0.5-0.5a+0.5c} \quad (\text{A.26})$$

Using $n_h = 1$, $n_{d50} = 1$ and $n_{s-1} = 1$, this yields,

$$n_{Tm} = (n_t)^{b+1} = (n_t)^\beta \quad (3.1)$$

Factor β is assumed to lie between 1.5 and 3.5 (Van Rijn, 2007).

This formula can be interpreted in the following way. For instance, the beach profile 1:20 after 24 hours is similar to the beach profile 1:10 after $(24/(n_t)^\beta)$ hours.

The distortion scale of test 1:10 with respect to reference test 1:20 is 2 ($n_t/n_h = n_t = 2$). And with factor β lying between 1.5 and 3.5, $(24/(n_t)^\beta)$ becomes $(24/(2)^{1.5-3.5})$. In this example, the beach profile 1:20 after 24 hours is similar to the beach profile 1:10 after 2.1 hours - 8.5 hours.

Results of tests in the Scheldt flume are used to determine the exponent of distortion scale, β . The tests are beach erosion tests and not dune erosion tests, as Vellinga described. Therefore, it is examined whether this scale relation is valid regarding beach erosion tests.

Erosion and deposition volumes are analysed to find the exponent β . Figure 3.21 indicates the volumes A, B and C. Swash bar volume C is subtracted from D, resulting in:

Deposition volume $A = A$

Erosion volume $B = D - C$

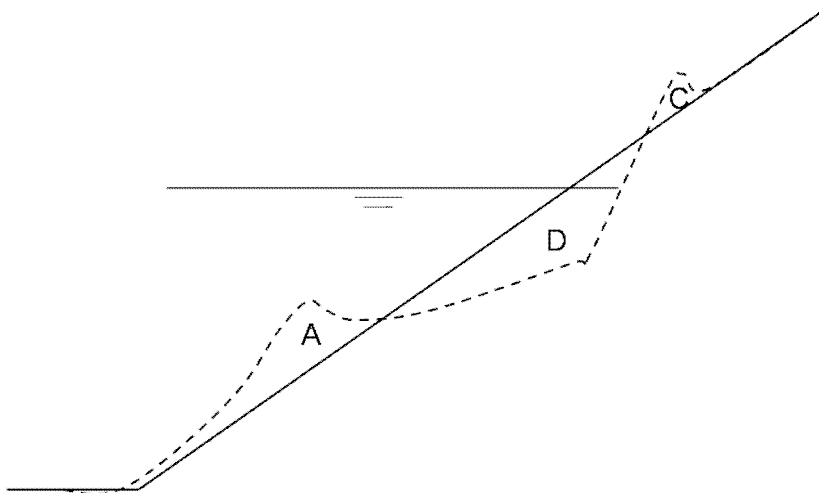


Figure 3.21 Definition of erosion and deposition volumes used for the determination of the time scale factor

The measured erosion area is converted to prototype values (test 1:20) using n_t .

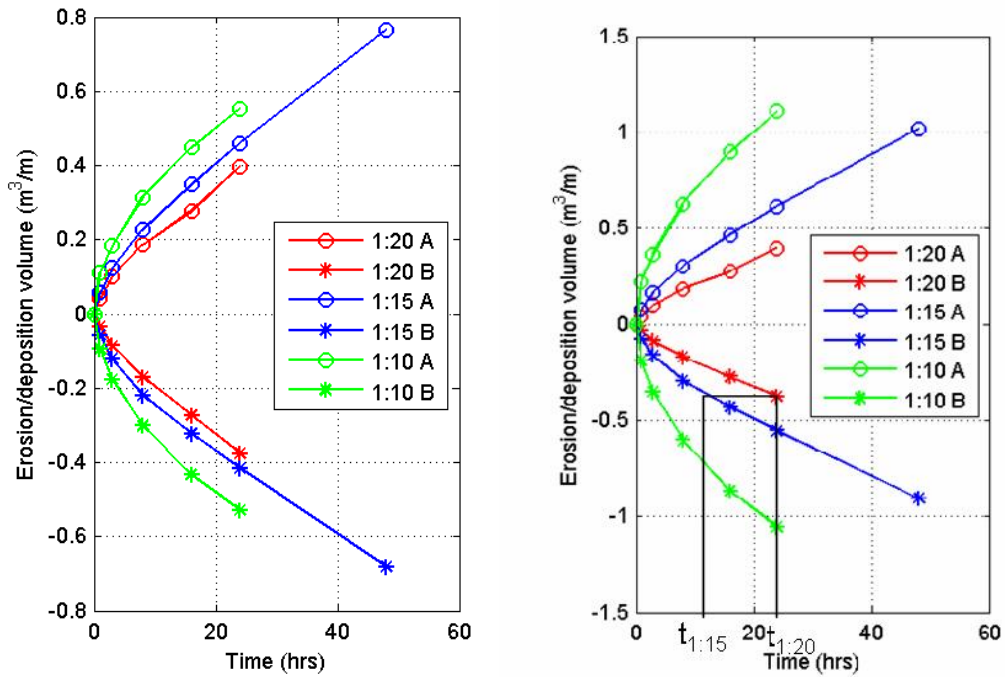


Figure 3.22 On the left measured erosion areas. On the right these are converted to prototype values.

Time scale factor as a function of erosion or deposition volume (vol) is expressed:

$$n_{T_m}(vol) = \frac{t_{1:20}}{t_{1:15}} \qquad n_{T_m}(vol) = \frac{t_{1:20}}{t_{1:10}} \qquad (3.2)$$

The right plot in Figure 3.22 shows an example of $t_{1:20}$ and $t_{1:15}$ at deposited volume 0.4 m³/m.

For erosion or deposition volume in the range of 0.1 - 0.37 m³/m, the time scale factor is presented in Figure 3.23. The time scale factor of test 1:15 is represented by the blue line and the time scale factor of test 1:10 by the green line.

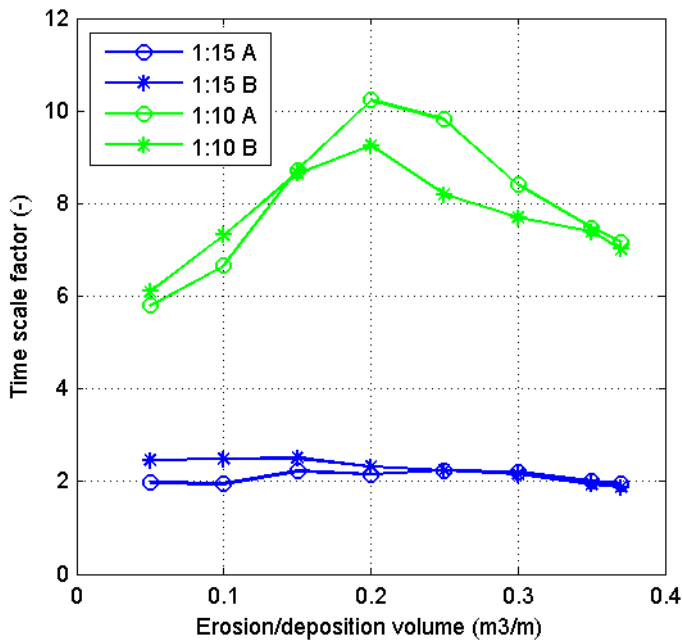


Figure 3.23 Time scale factor for tests 1:10 and 1:15

For test 1:15 a time scale factor of approximately 2-2.5 is noticeable. For test 1:10, no single value for the time scale factor can be observed. As more sediment is deposited or eroded, the time scale factor initially increases and subsequently, when 0.2 m³/m sand is eroded or deposited, decreases again. Time scale factor varies from 6 to 10, with an average of approximately 8.

Test 1:15:

$$n_{Tm} = (n_t)^{b+1} = (n_t)^\beta = 2 \tag{3.3}$$

as a result, exponent β is 2.4.

Test 1:10:

$$n_{Tm} = (n_t)^{b+1} = (n_t)^\beta = 8$$

as a result, exponent β is 3.

Time scale factor 2 for test 1:15 and time scale factor 8 for test 1:10 are applied to the volumes of prototype test 1:20. The result of the re-calculation of the erosion or deposition volumes are represented by the dashed line in Figure 3.24. These re-calculated erosion and deposition volumes of the erosive tests 1:15 and 1:10 correspond fairly well to the original erosion and deposition volumes of test 1:20.

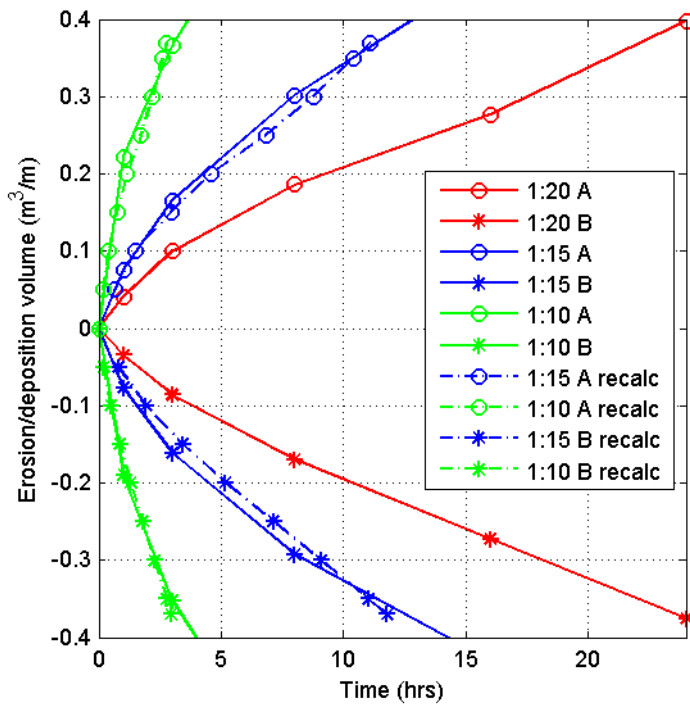


Figure 3.24 Re-calculation of the erosion and deposition volumes by means of multiplication of the values of the erosion/deposition volumes of the reference tests and the time scale factors for test 1:10

Moreover, the acquired time scale factors can be checked by analysis of the profile development of test 1:10 and 1:15 with the reference test 1:20. A time scale factor of 2 implies that profile 1:20 after 16 hours should approximately be equal to profile 1:15, translated to profile, after 8 hours (Figure 3.25). The correspondence of the two profiles is relatively good, particularly in the vicinity of the breaker bar.

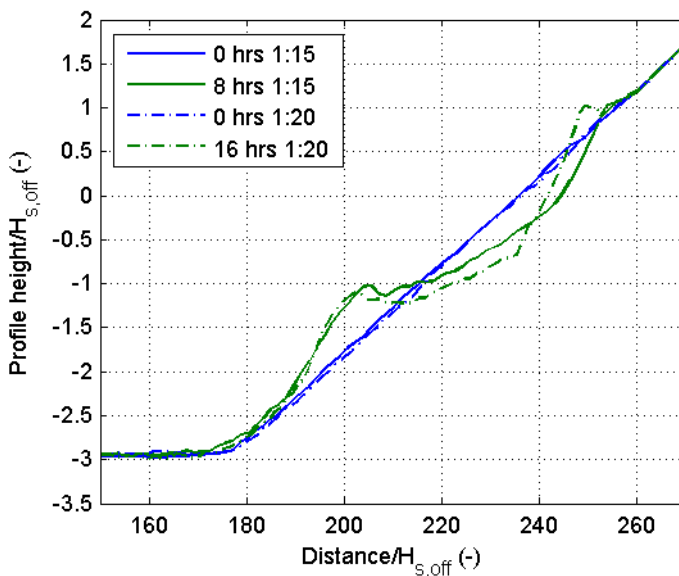


Figure 3.25 Comparison test 1:15 after 16 hours and test 1:20 after 24 hours

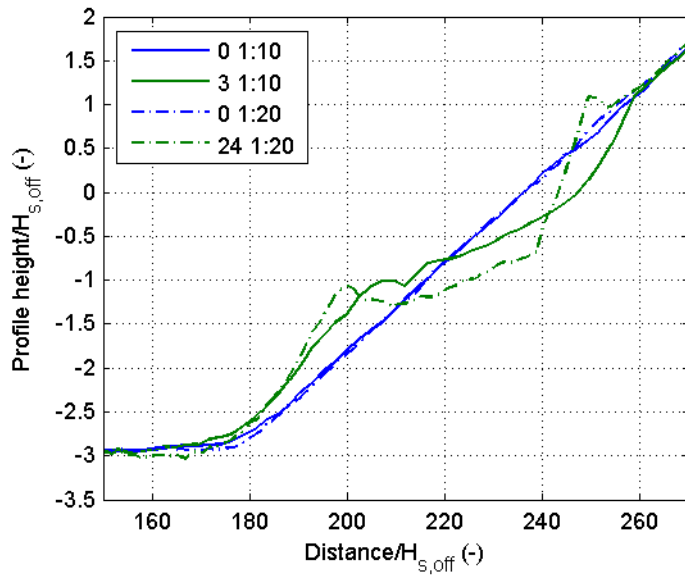


Figure 3.26 Comparison test 1:10 after 3 hours and test 1:20 after 24 hours

By means of the time scale factor for translation of test 1:10 to prototype test 1:20, test 1:10 after 3 hours should correspond with test 1:20 after 24 hours. From Figure 3.26 it can be concluded that these similarities are not that good in comparison with the prototype test 1:20 and test 1:15. However, the bulk erosion values are approximately equal.

Differences between prototype results and results of distorted tests after translation are indicated as scale effects. Large scale effects are correlated with ‘poor’ scale relations. These scale effects can be attributed to the fact that scale laws concerning the surf similarity parameter ($n_T = (n_h)^{0.5} (n_l / n_h)$) and fall velocity parameter ($n_{ws} = (n_h)^{0.5} (n_l / n_h)^{-1}$) are not lived up to.

In Figure 3.27 and Figure 3.28, the bed profile development of test 1:10 and 1:15 are scaled up to prototype. From these figures, it can be concluded that the distortion scale should be as small as possible, to prevent the generation of scale effects. Applying a distorted scale the wave breaking and wave run-up processes are overestimated, which results in overestimated erosion.

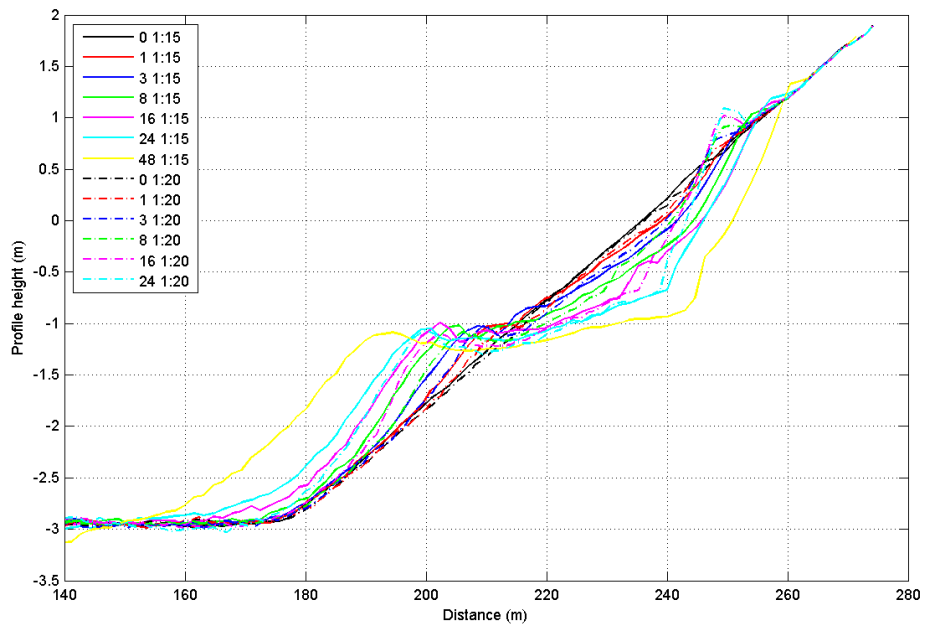


Figure 3.27 Test 1:15 scaled up to test 1:20

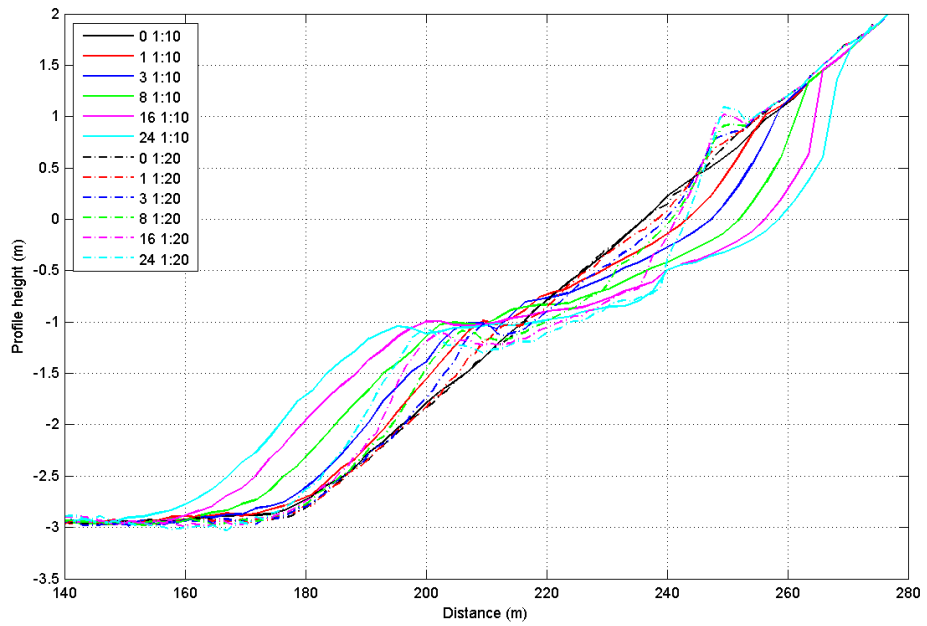


Figure 3.28 Test 1:10 scaled up to test 1:20

3.4 Geometric characteristics of beach profiles

Within the project SANDS beach profiles at three different scale levels are compared. Extensive analysis was made to define and quantify parameters describing profile change and relate these parameters to wave characteristics. Geometric parameters are made non-dimensional to be able to draw a parallel between tests at all scale levels.

The development of beach profiles starting with an initial even slope of 1:10, 1:15 and 1:20 are shown in Section 3.2. Some characteristics of the evolution of the profiles due to erosive waves are summarized below.

Definition of parameters are presented to allow for comparison of bed profile evolution between the different scaled experiments. The profile is expressed in dimensionless numbers by dividing the horizontal and vertical length by the offshore water depth and the offshore wave height. Offshore water depth and offshore wave height are meant to be the values close to the wave paddle.

Table 3.2 Dimensionless profiles by division with offshore water depth and wave height

Dimensionless by	Height
offshore water depth	0.5 m
offshore wave height	0.17 m

The intersection of the SWL and the initial profile is adopted as the zero-axis.

Quantification of beach profile development is done by comparison of the coordinates of distinct features on the three profiles. These features are indicated in Figure 3.29 and listed in Table 3.3.

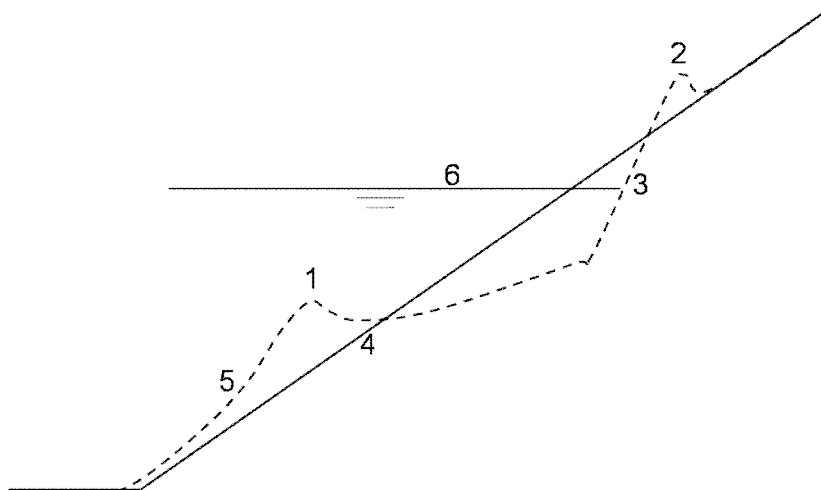


Figure 3.29 Distinct features of beach profile

Table 3.3 Feature numbers 1-6

Feature number	Description
1	top of breaker bar
2	top of swash bar
3	beach slope
4	bottom of trough
5	outer slope breaker bar
6	still water line

The test T02 with an initial slope of 1:20 has been selected as the prototype profile. Profiles of 1:15 and 1:10 are compared to this prototype profile. In Section 3.2, all profiles are represented in a dimensionless form by dividing horizontal and vertical length by offshore wave height or water depth. In Appendix B prototype profile and respectively profile 1:10 and 1:15 are plotted on top of each other, where the top of the breaker bar and the intersection of still water level and profile are used as reference points. In this way, insight is given into several features analysed in more detail in Section 3.4.1 through Section 3.4.4. These characteristics are divided into three categories:

- Vertical positions
- Horizontal positions
- Slopes

3.4.1 Vertical positions

Four vertical positions are considered: the height of the breaker bar (h_{bar}), trough (h_{trough}), swash bar ($h_{swashbar}$) and depth of maximum erosion point ($h_{max,eros}$). Three parameters are non-dimensionally expressed with respect to the Still Water Level (Figure 3.30). Height of maximum erosion point is the distance between the initial plane profile and profile after a subtest.

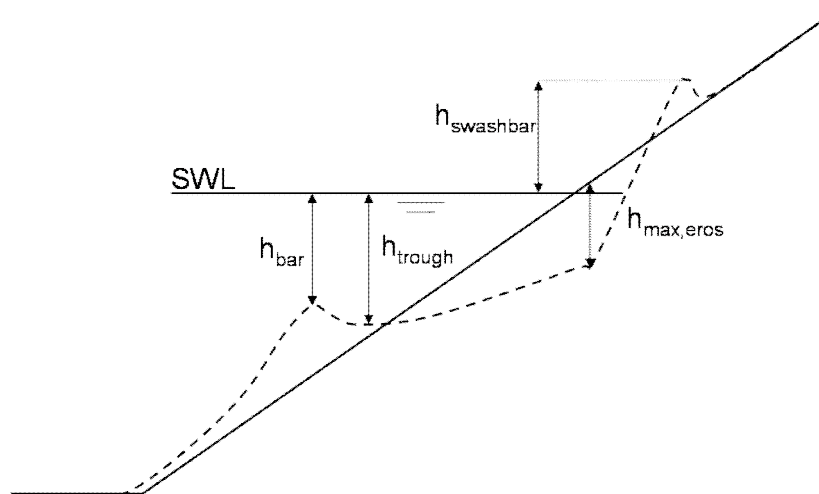


Figure 3.30 Definition of geometric vertical parameters

Bar height

The development of the height of the bar in time is given in Figure 3.31.

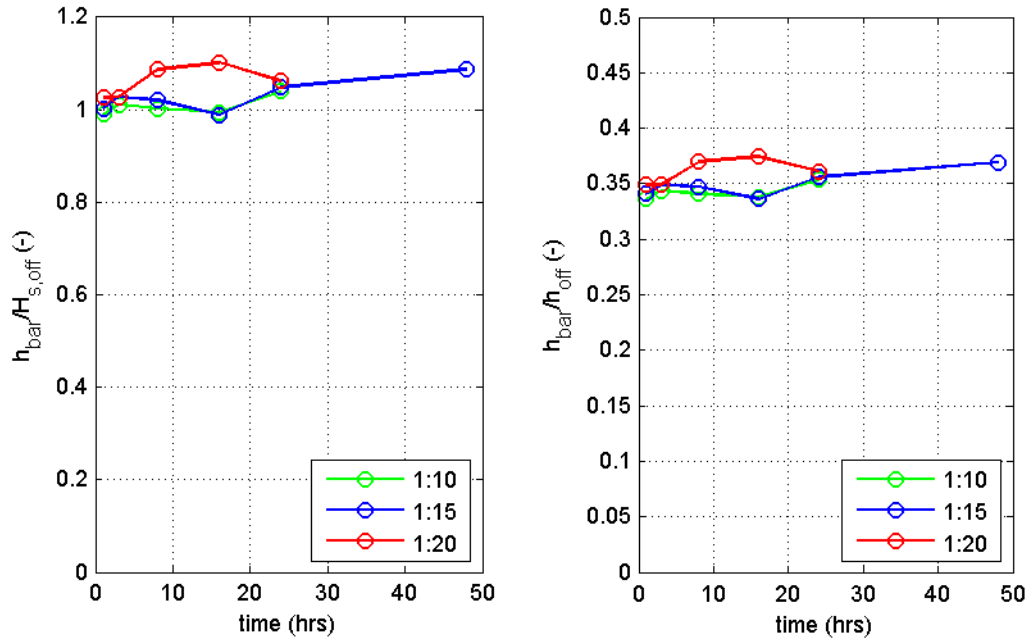


Figure 3.31 Evolution of bar height in time

The distance from SWL to the top of the bar (h_{bar}) does not underceed 1 and this can be seen as the upper limit of the breaker bar height. The following relation can be found:

$$\min(h_{bar}) = H_{s,offshore} \tag{3.4}$$

Trough height

The trough is the lowest point between the breaker bar and swash bar. Definition of the trough height, relative to the SWL is given in Figure 3.2. After 24 hours, the values of the trough height of test 1:15 and test 1:20 are more or less equal. The trough height increases in time; no equilibrium value can be found.

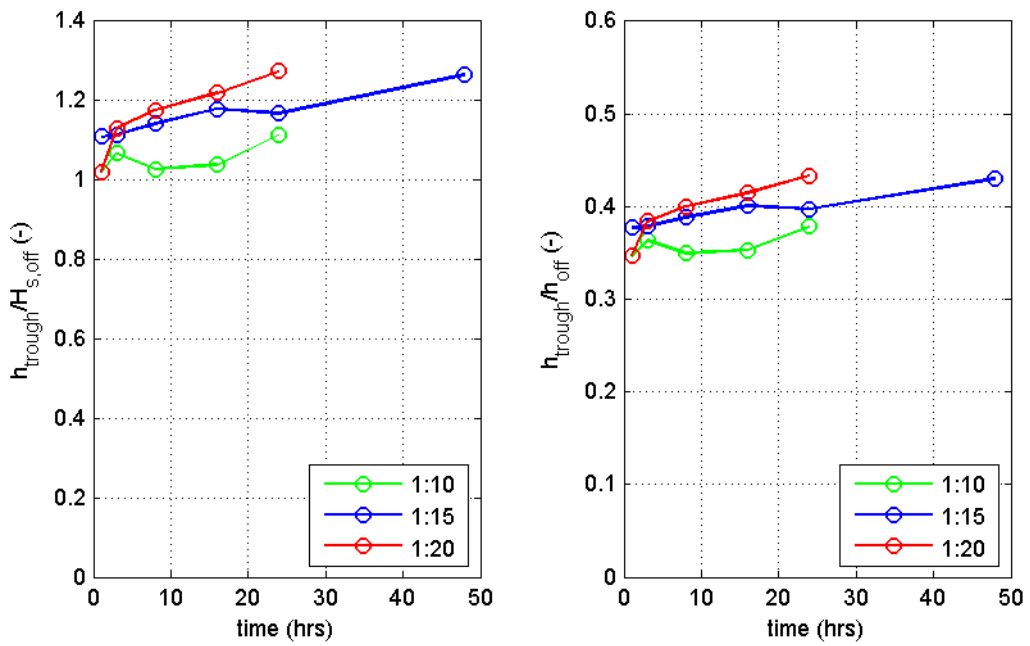


Figure 3.32 Evolution of trough height in time

Swash bar height

A swash bar can only be noticed for tests 1:20 and 1:15. For that reason, test 1:10 is absent in this analysis. Definition of the swash bar height, relative to the SWL is given in Figure 3.2. Swash bar of test 1:15 is positioned higher up in the profile. The development of the height of the swash bar is similar for both tests.

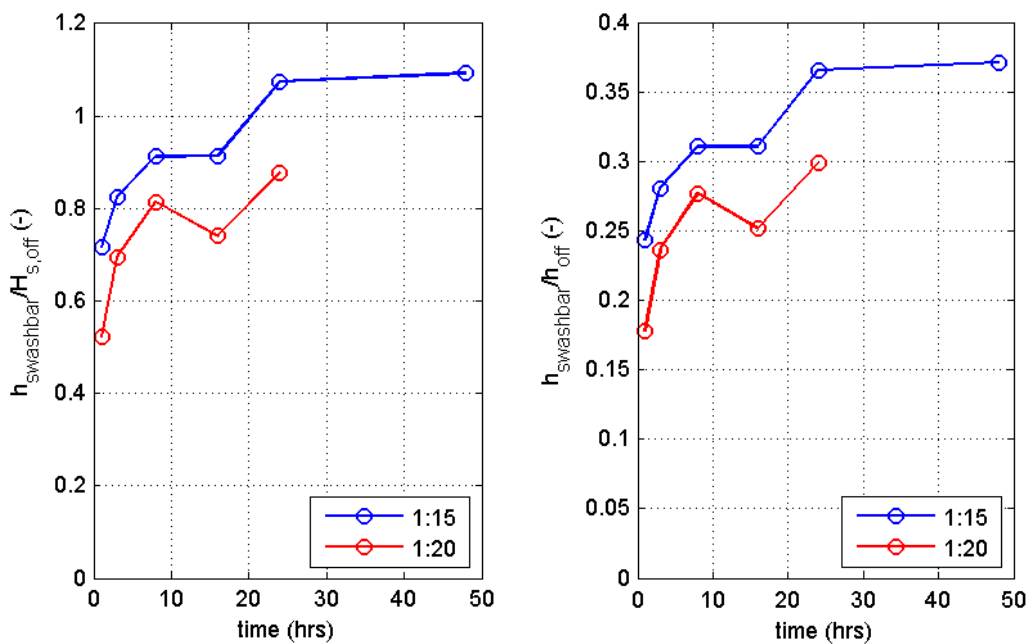


Figure 3.33 Evolution of swash bar height

Height of maximum erosion point

Height of maximum erosion point is indicated in Figure 3.30. All tests show a similar trend. Height of maximum erosion point keeps growing in time, but the process slows down in time.

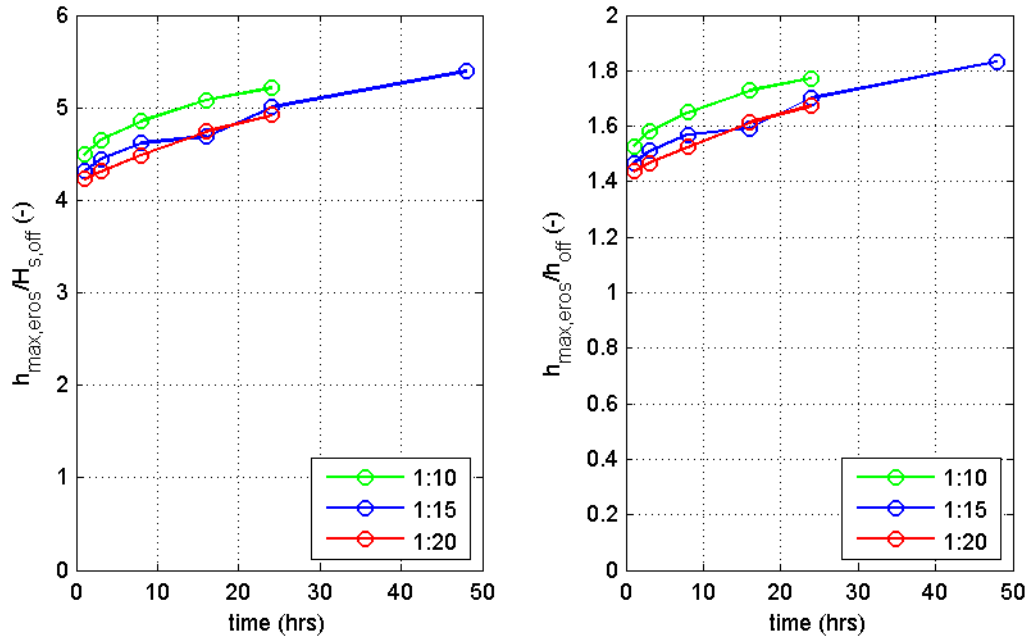


Figure 3.34 Evolution of maximum erosion point in time

3.4.2 Horizontal positions

Three horizontal positions are considered relative to the intersection of the SWL and the initial bed profile. In Figure 3.35, the position of the top of the breaker bar (L_{bar}), swash bar ($L_{swashbar}$), and trough (L_{trough}) are indicated. In addition, a fourth horizontal distance is formulated; the length of the surf zone ($L_{surfzone}$) is defined as the distance from the top of the breaker bar to the intersection of the SWL and the measured profile after every subtest.

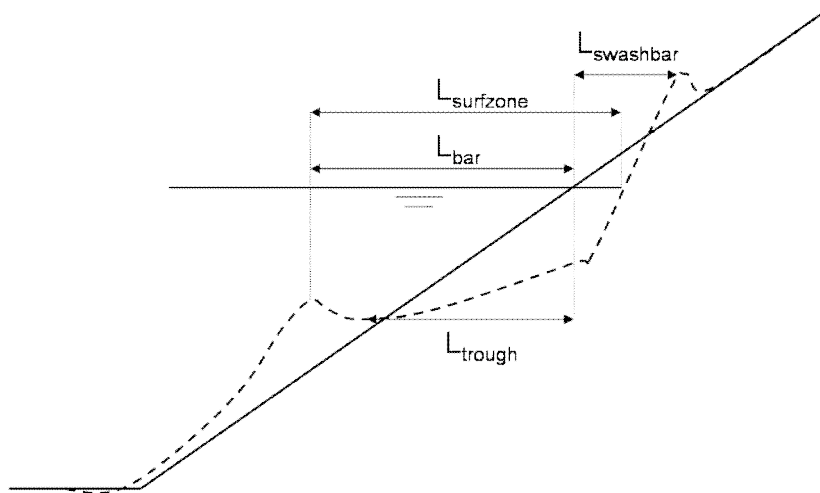


Figure 3.35 Definition of geometric horizontal parameters

Bar length

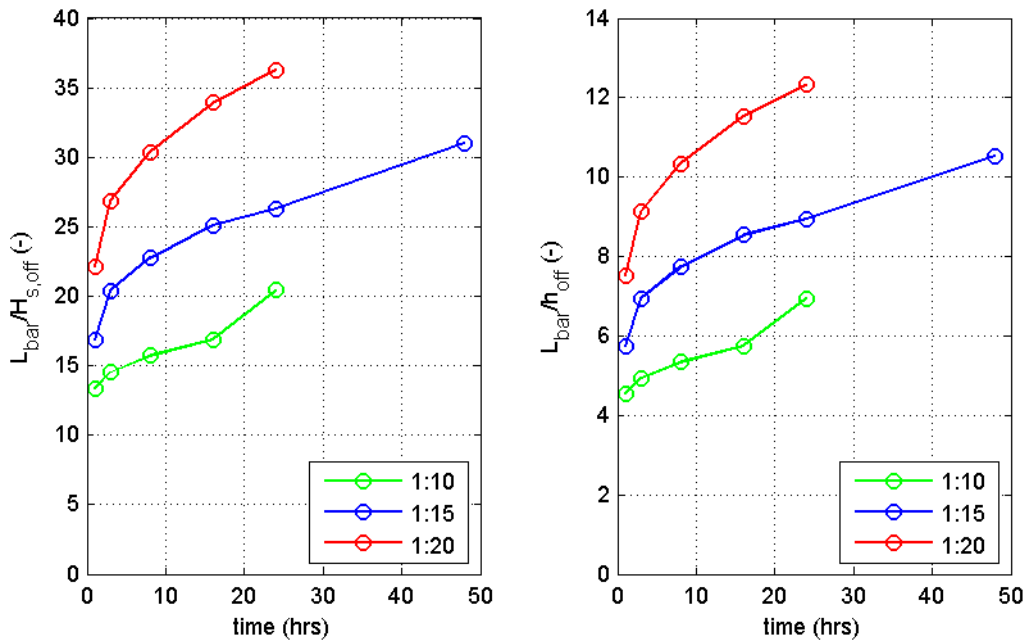


Figure 3.36 Evolution of bar length in time

The evolution of the bar length, the length between top breaker bar and intersection of SWL and initial profile, is displayed in Figure 3.36. At first, a rapid increase in bar length is visible. For tests 1:15 and 1:20, it can be said that this process slows down in time and turns into a linear process.

Trough length

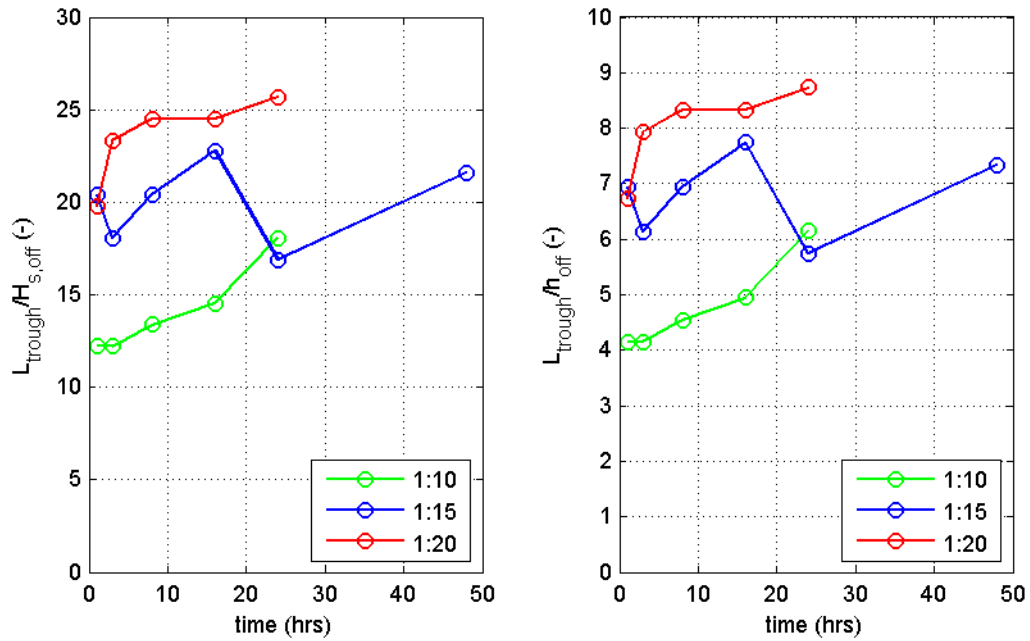


Figure 3.37 Evolution of trough length in time

Lowest point between breaker bar and swash bar up to intersection of initial profile and SWL is defined as the trough length (see Figure 3.35). Test 1:10 shows an increasing trough length, whereas in case of test 1:20 and 1:15 the trough length remains more or less the same.

Swash bar length

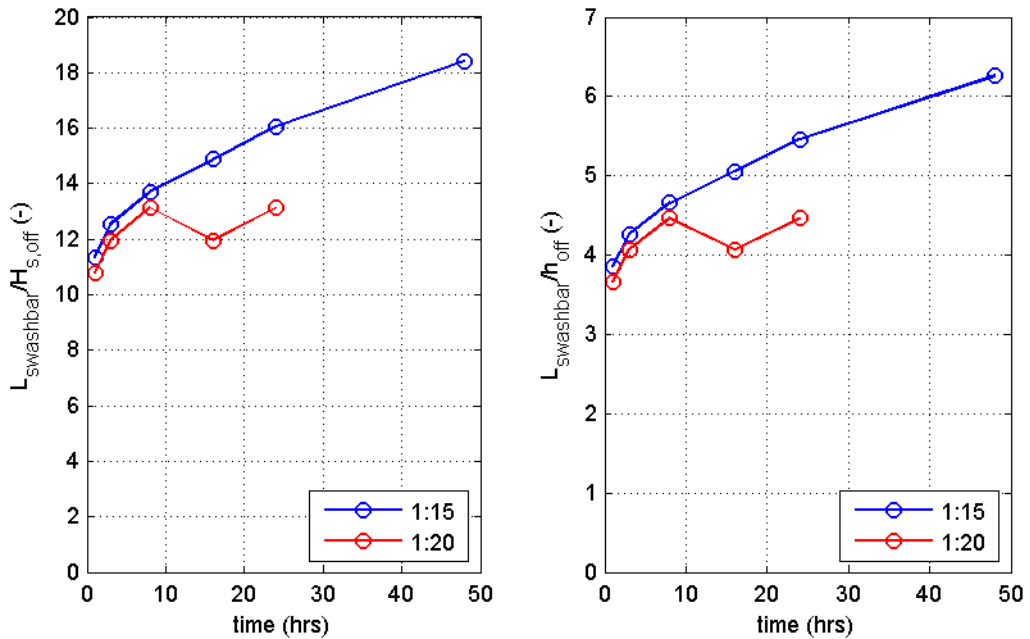


Figure 3.38 Evolution of swash bar length in time

Schematisation of the swash bar length ($L_{swashbar}$) implies the distance from the top of the swash bar to the intersection of the SWL and the initial profile. For test 1:10, no swash bar can be seen. From Figure 3.38, it can be noticed that the swash bar length of 1:20 is limited to 13. It seems to be stabilizing. After 48 hours, swash bar of test 1:15 is still moving landwards.

Length surf zone

The length of the surf zone ($L_{surfzone}$) is defined as the distance from the top of the breaker bar to the intersection of the SWL and the bed profile after each subtest (see Figure 3.35). Additionally, in order to gain insight into the development of the profile length in time, extension of the surf zone is described in the following way.

$$extension_{surfzone} = \frac{L_{profile2} - L_{profile1}}{t_2 - t_1} \tag{3.5}$$

The length of the surf zone increases very rapidly at the start of the test. Figure 3.39 shows a fastest extension of the bed profile for test 1:20. Test 1:15 has a slightly smaller incident growth, whereas test 1:10 has an initial growth, approximately half of test 1:20. Furthermore, it can be seen that the length of the surf zone of test 1:20 after 24 hours is equal to the length of the surf zone of test 1:15 after 48 hours.

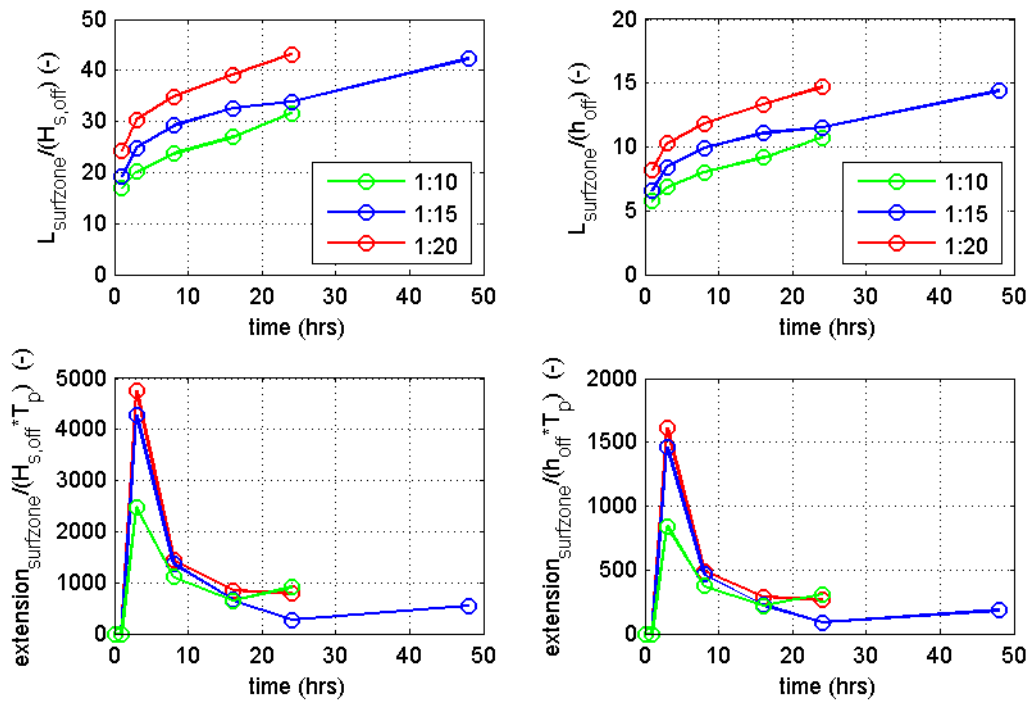


Figure 3.39 Evolution of length of the surf zone in time

3.4.3 Slopes

In Figure 3.40, the slope of the bar and the slope of the beach are illustrated.

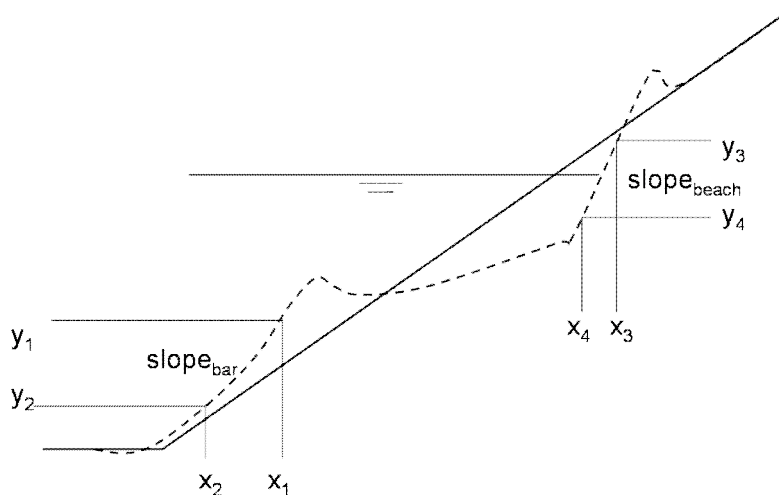


Figure 3.40 Definition of geometric slope parameters

Outer slope of breaker bar

The slope seawards of the bar is defined as indicated in Figure 3.40:

$$slope_{bar} = \frac{y_1 - y_2}{x_1 - x_2} \tag{3.6}$$

where,

$y_1 = 1.5 * H_{s,offshore}$ above offshore bed level

$y_2 = 0.5 * H_{s,offshore}$ beneath SWL

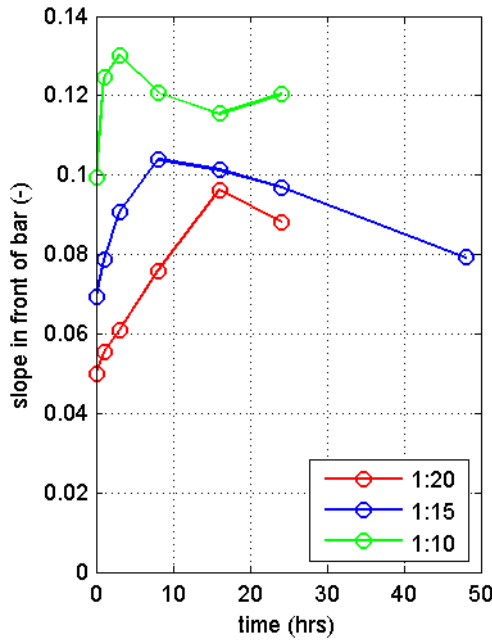


Figure 3.41 Evolution of slope of breaker bar in time

Test 1:15 and 1:20 show good resemblance with respect to the evolution of the outer slope of the breaker bar. Figure 3.41 illustrates a steeper slope for test 1:10.

Beach slope

The slope of the beach is defined as indicated in Figure 3.40:

$$slope_{beach} = \frac{y_3 - y_4}{x_3 - x_4} \tag{3.7}$$

where,

$y_3 = 0.5 * H_{s,offshore}$ above SWL

$y_4 = 0.5 * H_{s,offshore}$ beneath SWL

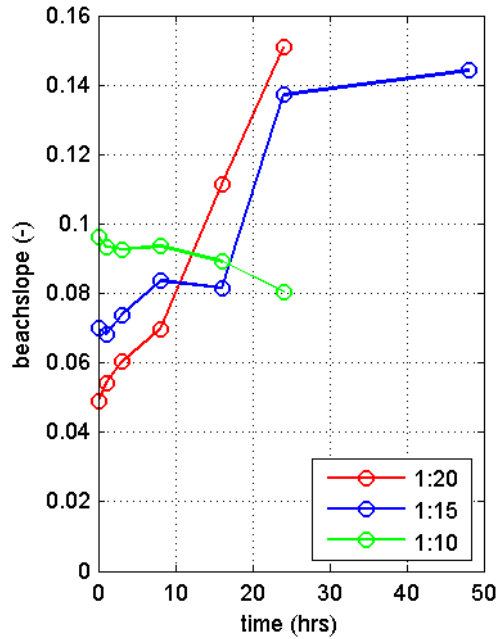


Figure 3.42 Evolution of beach slope in time

Beach slope development of tests 1:20 and 1:15 are almost equal. At the end of these tests, a slope of approximately 1:7 is noticeable. Test 1:20 attains a beach slope of 1:7 first. For test 1:15 it takes more time to reach this value. Slope development of test 1:10 does not resemble 1:20 or 1:15.

Bar migration

Migration of the bar is outlined in Figure 3.43 and equation (3.8).

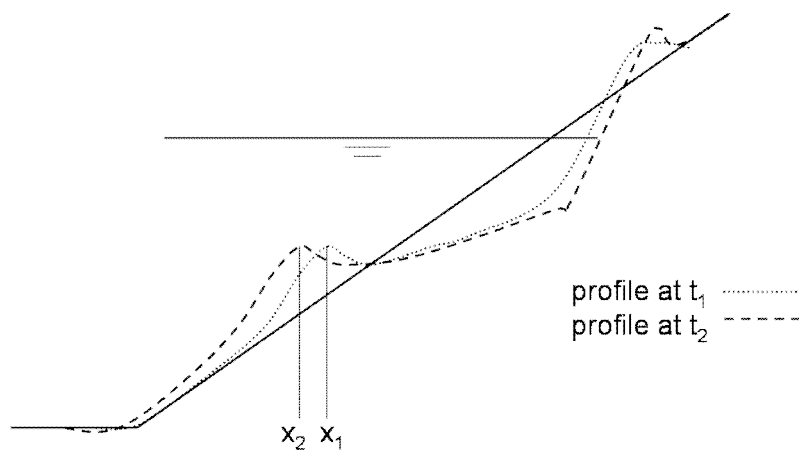


Figure 3.43 Definition of bar migration

$$migration_{bar} = \frac{x_1 - x_2}{t_1 - t_2} \tag{3.8}$$

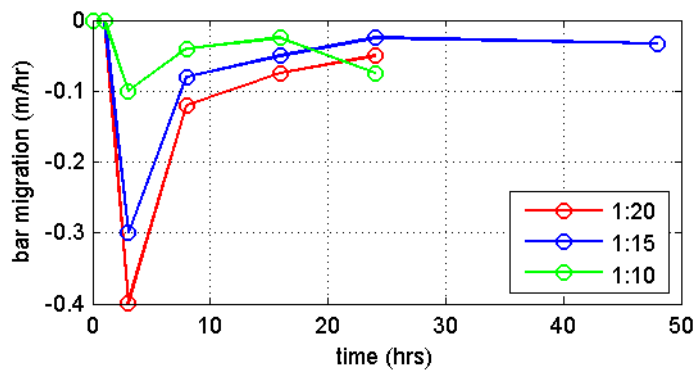


Figure 3.44 Migration breaker bar in time

Considering Figure 3.44, a large initial migration is noticed for all tests. Subsequent intervals show a rapid decrease in offshore bar movement. At the end of the tests, they more or less seem to go to a single value.

3.4.4 Erosion and deposition volumes

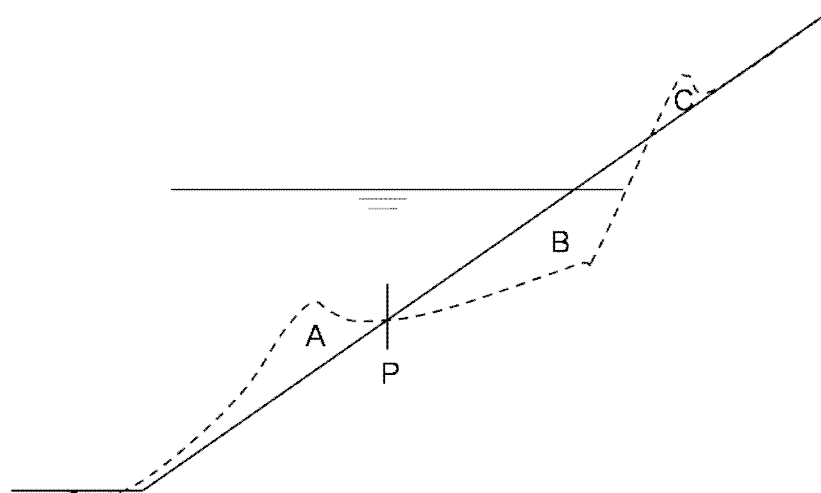


Figure 3.45 Definition of erosion and deposition volumes

In Figure 3.45 and Table 3.4, definitions of three erosion and deposition volumes (A, B and C) are presented. Volumes are expressed in dimensionless numbers by division with $(H_{s,off})^2$.

Table 3.4 Definition of erosion and deposition volumes

Erosion/deposition volume	Description
A	Deposited breaker bar volume
B	Eroded beach volume
C	Deposited swash bar

Regarding Figure 3.46, it can be concluded that the swash bar volume is very small and does not grow in time. It stabilises rapidly. The other two volumes, on the other hand, do not reach a fixed value: erosion and deposition volumes A and B continue growing in time.

After 24 hours, test 1:10 is exposed to most erosion and deposition. Test 1:20 is subject to least erosion. Test 1:15 show values in between test 1:10 and 1:20. Even after 48 hours, erosion and deposition development is still proceeding.

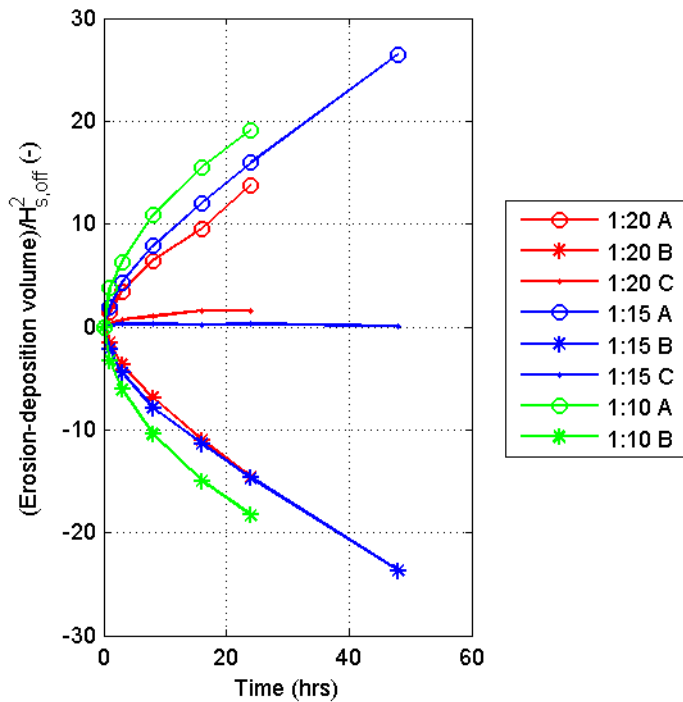


Figure 3.46 Evolution of erosion and deposition volumes in time

Total sediment transport

Elaborating on the deposition volumes (A) found in the previous Section, the time-averaged sediment transport passing the intersection P on the profile is derived from:

$$sedtransport_p = \frac{\Delta volume_{deposition}}{\Delta time} \tag{3.9}$$

As a result, evolution of sediment transport is exhibited in Figure 3.47 . At the beginning of the test, a relatively large transport is observed for all tests. The figure presents a significant difference between the three tests. Test 1:10 shows an initial sediment transport twice as high compared to test 1:15 and even a bigger difference is visible in comparison with test 1:20.

After 16 hours, all transports are reduced and seem to be more or less equal. It does not, however, result in a zero sediment transport. After 24 hours and 48 hours the process is still going on.

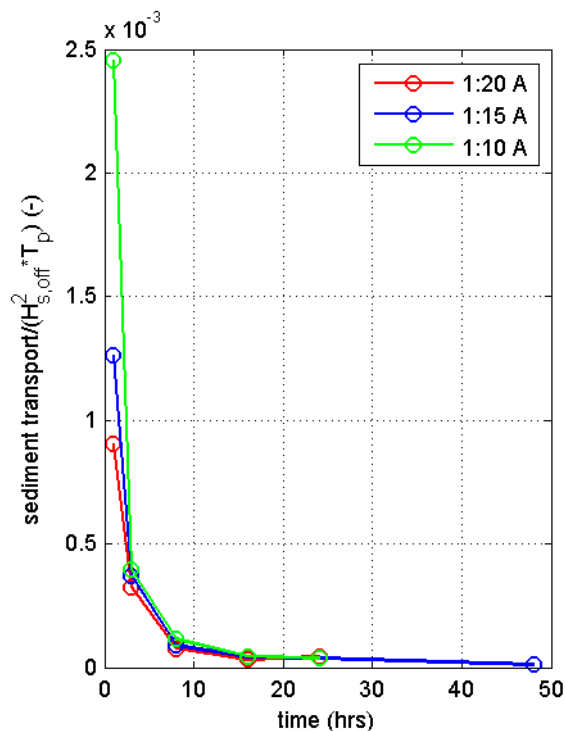


Figure 3.47 Evolution of sediment transport in time

3.4.5 Conclusions on bed profile development

Through detailed analysis of the geometric characteristics of beach profiles in Section 3.4 some conclusions can be drawn with respect to the profile development.

Analysis of beach slope, slope of outer bar, length of the surf zone, bar height, trough height and bar height show similar values for test 1:20 after 24 hours and 1:15 after 48 hours. Figure 3.48 and Figure 3.49 confirms this. Just the height of the swash bar differs. This implies that, after a certain period, the initial profile is not of importance in the profile development.

From that moment on, it can be expected that the profile development will be more or less equal. As a result, a time scale factor can not be applied in the infinity, because this value will amount to one in time.

For test 1:10 such great similarities with prototype test 1:20 can not be found. Although comparable sediment transports with respect to test 1:20 and test 1:15 are found at the end of the test, little similarity between beach profiles is displayed. Especially higher up in the profile deviations are significant; no swash bar can be found and the beach slope considerably differs (see Figure 3.50 and Figure 3.51). It can be expected that at a certain moment in time, the bed profile will be more or less equal to the bed profile of test 1:20. However, it is not evident, when this will be about to happen. It can be assumed that it will

take more than profile 1:15 to 'catch up' with test 1:20, because the initial profile of test 1:10 is more out of equilibrium than the initial profile of test 1:15.

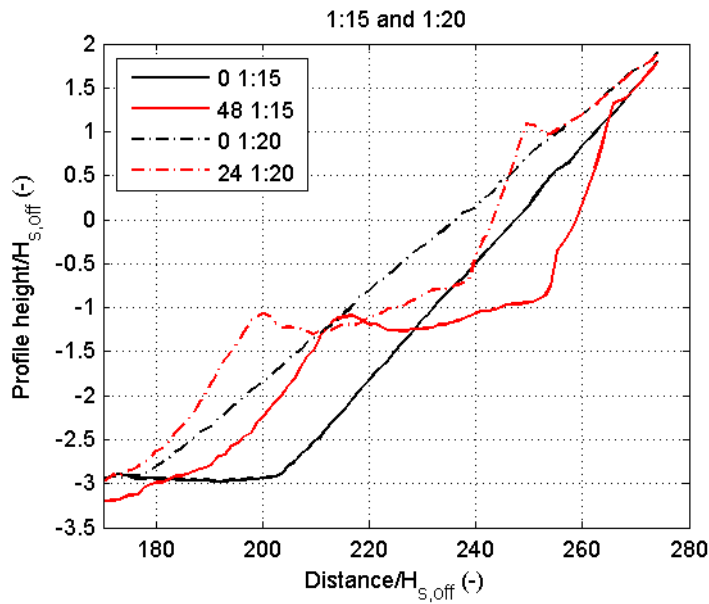


Figure 3.48 Comparison profiles of test 1:20 after 24 hours and test 1:15 after 48 hours

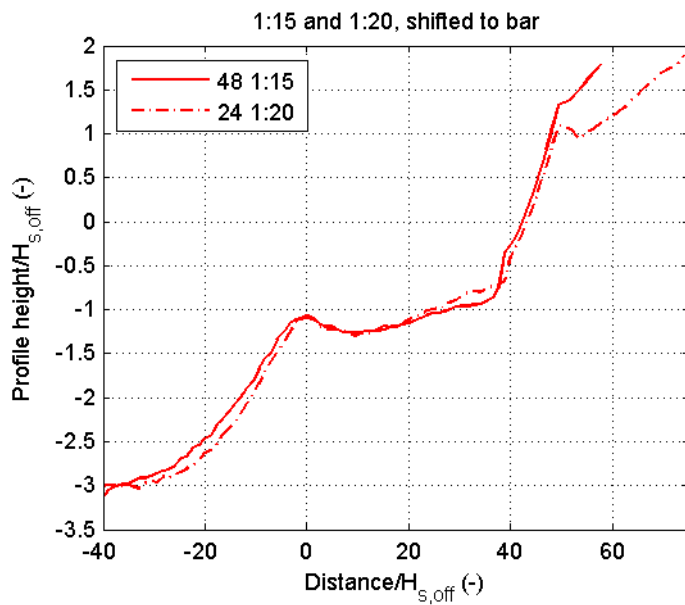


Figure 3.49 Profiles shifted on top of each other with reference to top of bar

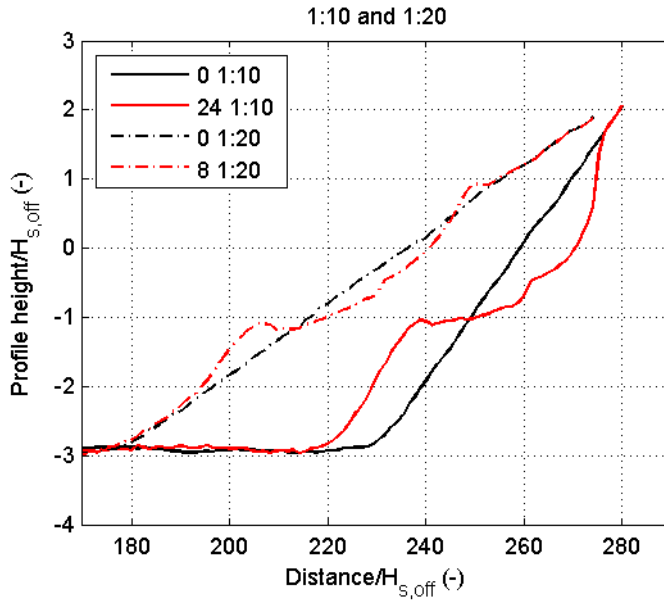


Figure 3.50 Comparison profiles of test 1:20 after 8 hours and test 1:10 after 24 hours

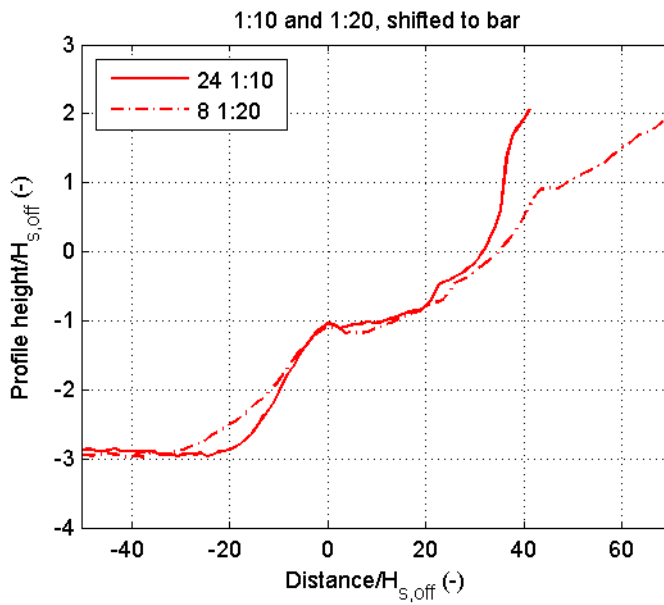


Figure 3.51 Profiles shifted on top of each other with reference to top of bar

3.5 Wave height and water level

The water level variation over the flume was measured consequently at several fixed cross-shore locations. For each interval within each test, a separate surface elevation signal is obtained. Three wave height meters, that determine the incident wave characteristics, were positioned close together near the wave board. For detailed information on the location of the other gauges is referred to Data report flume experiments SANDS (2007).

The wave time series run on the profile consists of 500 waves. These wave time series are run consecutively. Wave characteristics are obtained for the entire interval as well as for a period of 500 waves. In Figure 3.52, Figure 3.53 and Figure 3.54 wave height variation and water level variation along the flume are shown for the erosive tests, T02, T04 and T06. The wave characteristics are derived from the first 500 waves run on the profile after every bed profile measurement. Near the wave board, variations are limited; however, as waves propagate along the flume, deviations in time are visible due to bottom changes.

Due to shoaling, initially a slightly increasing wave height can be observed. Propagating further, the wave height decays, as a result of energy dissipation due to bottom friction and breaking of waves. In Figure 3.52, Figure 3.53 and Figure 3.54, the point of wave breaking is more or less above the breaker bar. Because of the offshore migration of the breaker bar, the point of wave breaking also shifts seawards.

The wave height measured closest to the coastal zone slightly increases in time. An opposite behaviour can be observed for the water level set-up. During the first subtest, the highest water level set-up was measured closest to the coastal zone. Subsequently, during the next subtests, a decrease in set-up in time is shown.

At the end of all tests, the wave heights measured closest to the coastal zone are more or less equal, 10 cm.

Waves exert a net time-averaged force on the fluid mass. This force is the net result of horizontal gradients in total mean momentum fluxes as induced by waves. The total mean momentum fluxes are referred to as the radiation stresses (Hulscher et al., 2002). This momentum flux consists of a component associated with the horizontal water velocity and a component associated with the water pressure. The principal component of the radiation stress is defined as the mean value of the total momentum flux in the water column in the presence of waves minus its value in the absence of waves:

$$S_{xx} = \frac{1}{T} \int_0^T \int_0^{h+\xi} (p + \rho u^2) dz dt - \int_0^{h+\xi} p_0 dz$$

in which,

S_{xx} is the radiation stress

T is the wave period

h is the water depth in the situation without waves

ξ is the mean water level variations

p_0 is the hydrostatic pressure

p is the pressure
 u is the flow velocity

Wave set-up is the elevation of the mean water level caused by wave-action. A strongly decreasing wave height (energy dissipation due to wave breaking) results in a gradient in the cross-shore directed radiation stress. Wave set-up balances the gradient in the cross-shore directed radiation stress.

$$\frac{d\eta}{dx} = -\frac{1}{\rho g d} \frac{dS_{xx}}{dx} \quad (3.10)$$

in which η is de water level set-up.

Similarly, in shoaling areas, just outside the surf zone, the wave height increases. An increase in wave height results in an increase in radiation stress. This leads to a decrease in water level: a set-down.

Considering test T02, as the point of wave breaking moves seaward in time, the position, where the wave set-up starts, also shifts seaward. For T04 and T06, this relation is not very evident.

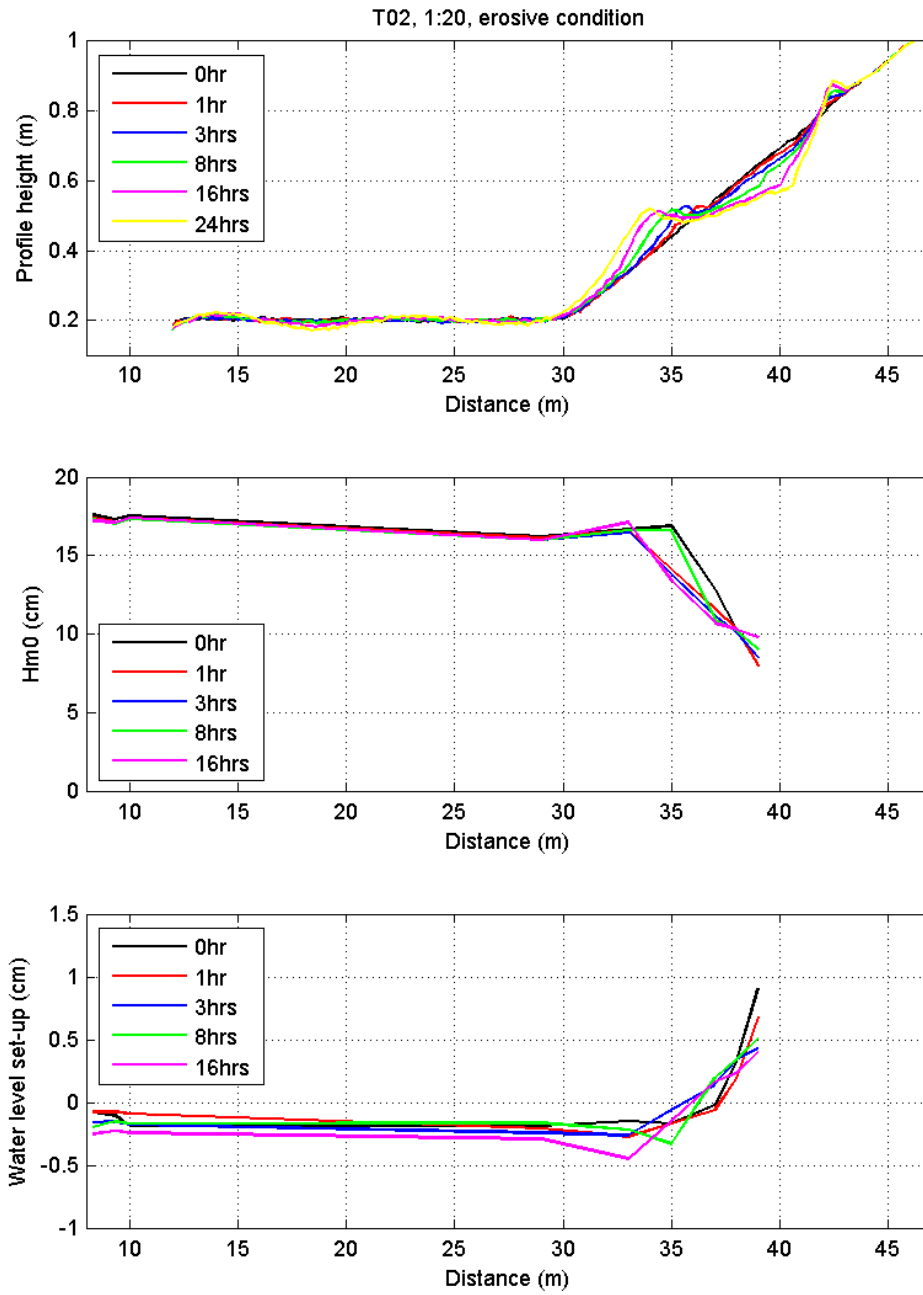


Figure 3.52 Wave height and water level variation along the flume, T02 (1:20), erosive condition

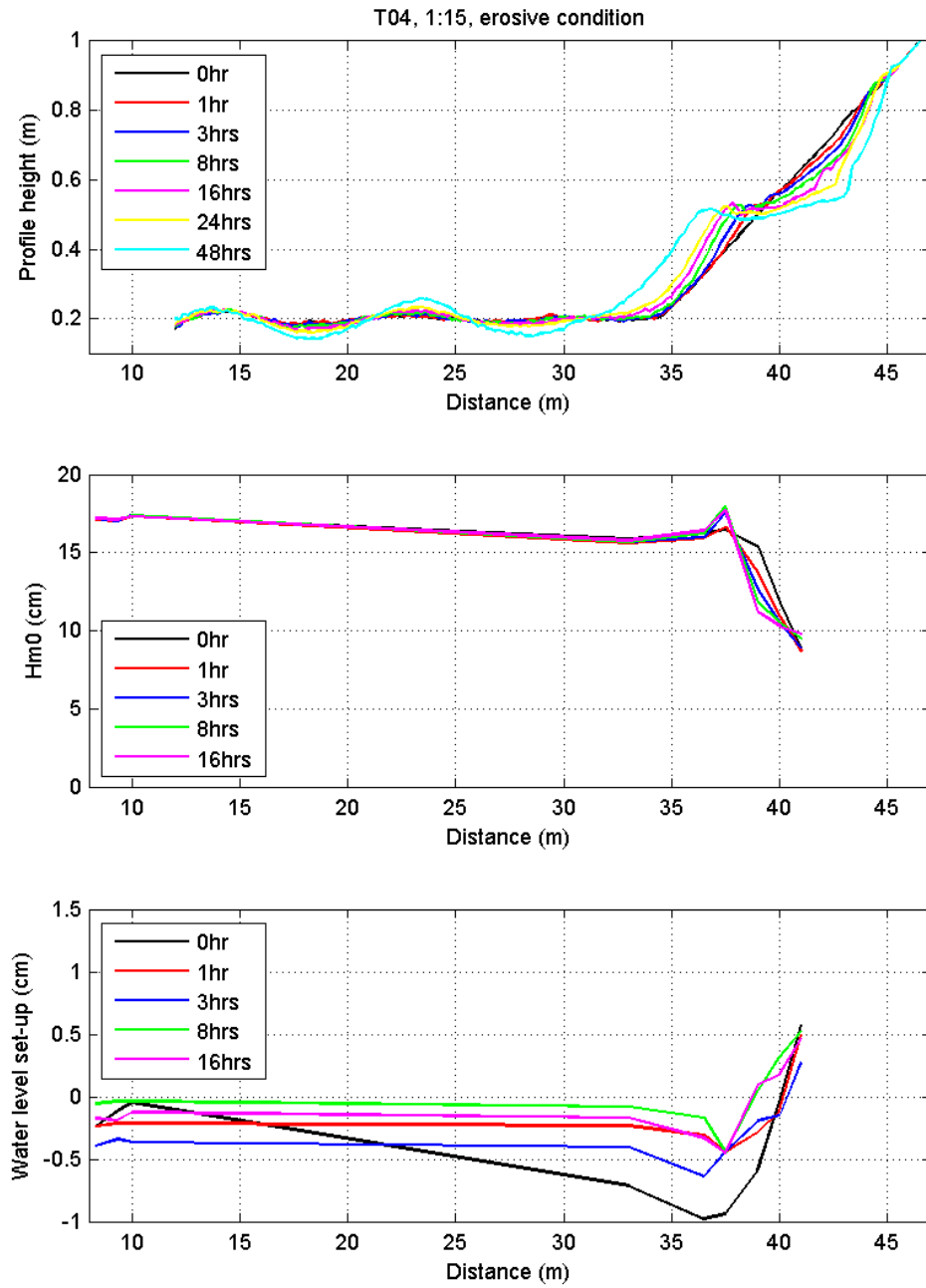


Figure 3.53 Wave height and water level variation along the flume, T04 (1:15), erosive condition

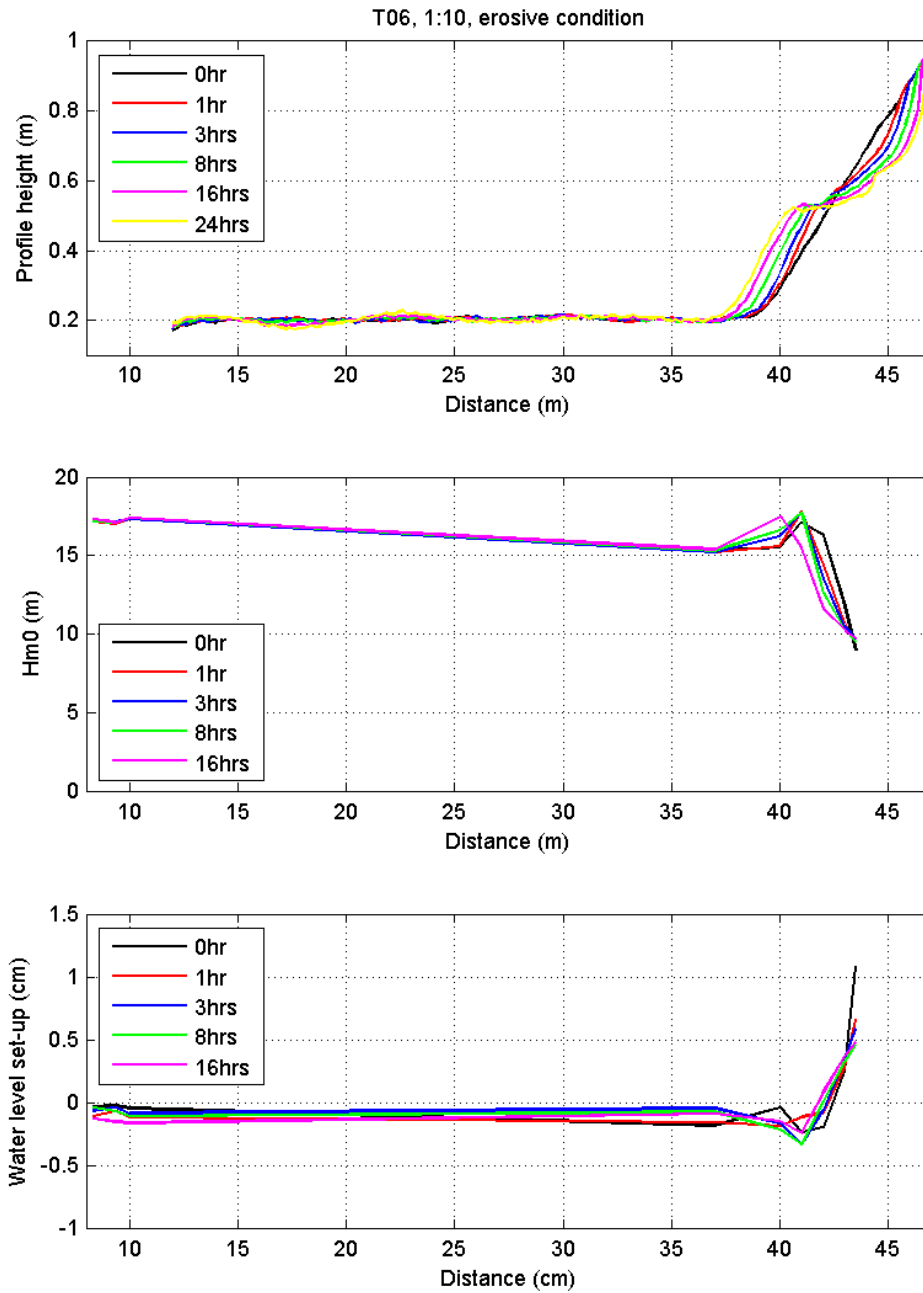


Figure 3.54 Wave height and water level variation along the flume, T06 (1:10), erosive condition

3.6 Flow velocities

During the experiments undertow flow velocities were measured with the measurement carriage construction (see Section 2.2) at different cross-shore locations. For this analysis, data obtained by the EMS are used.

Three mechanisms are responsible for three different velocity profiles (Hulscher et al., 2002).

- The breaking of waves leads to a decreasing radiation stress and an increasing wave set-up. This wave set-up generates an offshore directed return flow
- The onshore-directed mass flux M or Stokes drift as generated by non-breaking waves have to be compensated by a return flow
- Within the wave bottom boundary layer, bottom friction dominates the flow. Here, the linear wave theory is no longer applicable and an additional mean stress is generated by the interaction of horizontal and vertical orbital velocities. This stress leads to an onshore directed mean flow, also indicated as boundary layer streaming.

The total mean velocity profile under waves has a shape as shown in Figure 3.55.

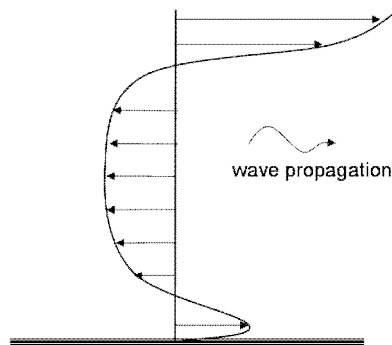


Figure 3.55 The shape of the total mean velocity profile under waves

The plots in Figure 3.56 show the measured velocity verticals of the erosive test T04 (1:15) at 35.6 m, 36.6 m, 37.1 m, 37.8 m, 38.4 m, 39.4 m and 40.8 m from the wave paddle. At these positions, two experiments were carried out consecutively, except at 39.4 m, where three experiments were done. All experiments were executed between 24 hours and 48 hours. In the upper plot, all velocity profiles are presented with the corresponding bed profile measurement at 24 hours. In the lower plots, the velocity verticals are shown separately.

The experiments at 37.1 m were carried out twice; the first experiment at 25 hours (represented by the solid line) and the second experiment at 47 hours (represented by the dashed line). It can clearly be seen that the velocity verticals obtained at these points in time considerably differ from each other. The flow velocities after 25 hours are much larger compared to the flow velocities after 47 hours. These differences can be attributed to the fact that the bed profile changes as the experiments are taken along the flume.

The plots in Figure 3.57 show the measured velocity verticals of the accretive test T05 (1:15) at 36.6 m, 38.1 m, 38.7 m, 39.3 m, 40.6 m, 42 m and 43 m from the wave paddle. Tests at 38.7 m, 39.3 m and 38.1 m (represented by the red line) were carried out between 8 hours and 16 hours, whereas tests at 40.6 m, 42 m, 43 m and 36.6 m, correspond with the blue line, were carried out between 16 hours and 24 hours.

In a similar way, the plots in Figure 3.58 show the measured velocity verticals of the erosive test T06 (1:10) at 39.0 m, 40.4 m, 41.25 m, 41.75 m, 42.5 m and 43.4 m from the wave paddle. Tests at 41.25 m, 41.75 m and 40.4 m, represented by the red line, were carried out between 8 hours and 16 hours, whereas tests at 42.5 m, 43.4 m and 39 m, correspondent with the blue line, were carried out between 16 hours and 24 hours.

The measured velocities of the erosive tests (T04 and T06) show consistently larger values than the velocities of the accretive tests (T05). The shape of the velocity verticals is not as curved as based on the theory might be expected. Practically all verticals show a more upright shape instead of a curved shape.

At every position, two velocity verticals are derived. The mean of the differences of the verticals is computed and the mean of the measured velocities. Division of these two values result in a relative error for the measurements of 12%.

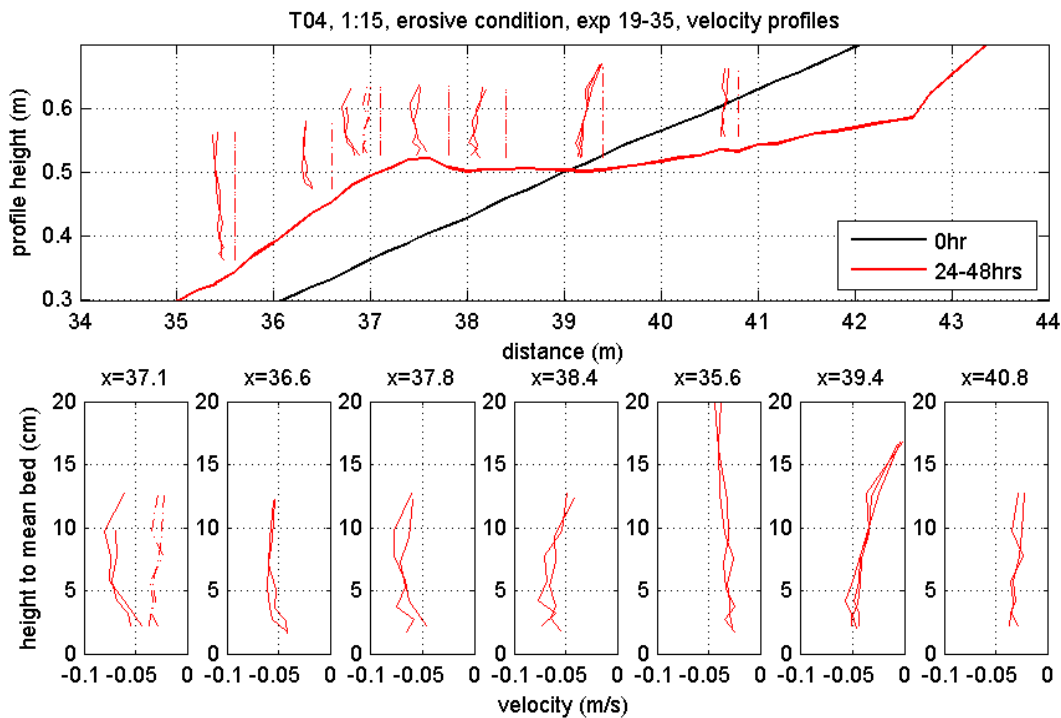


Figure 3.56 Flow velocity verticals for erosive test T04, experiment 19-35

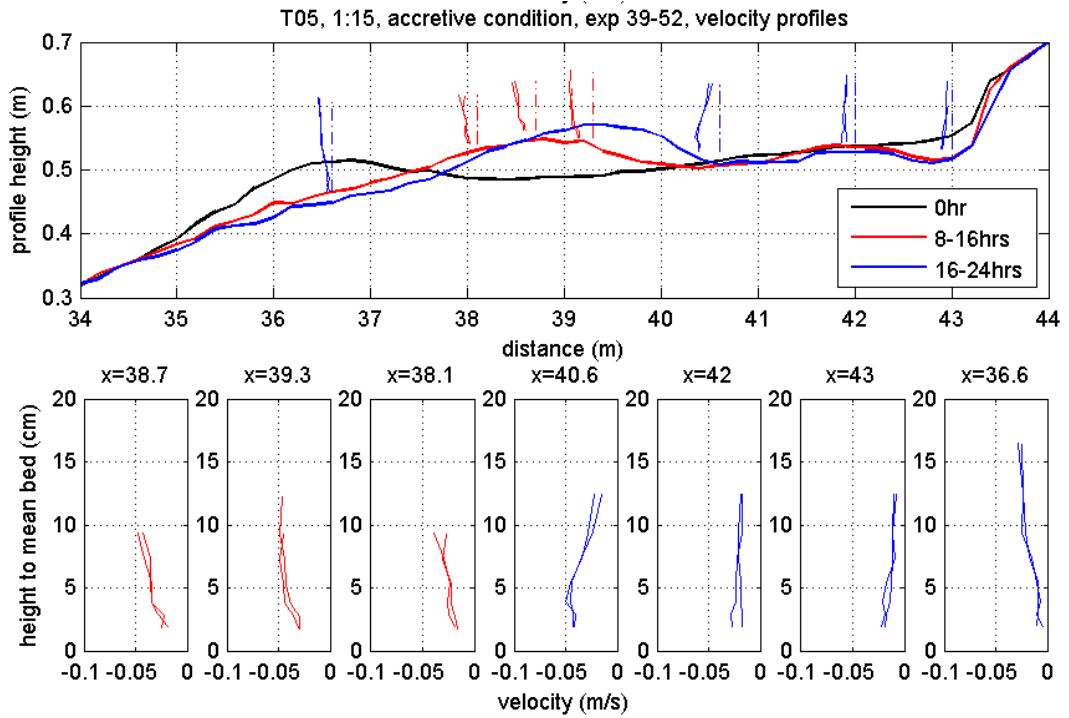


Figure 3.57 Flow velocity verticals for accretive test T05, experiment 39-52

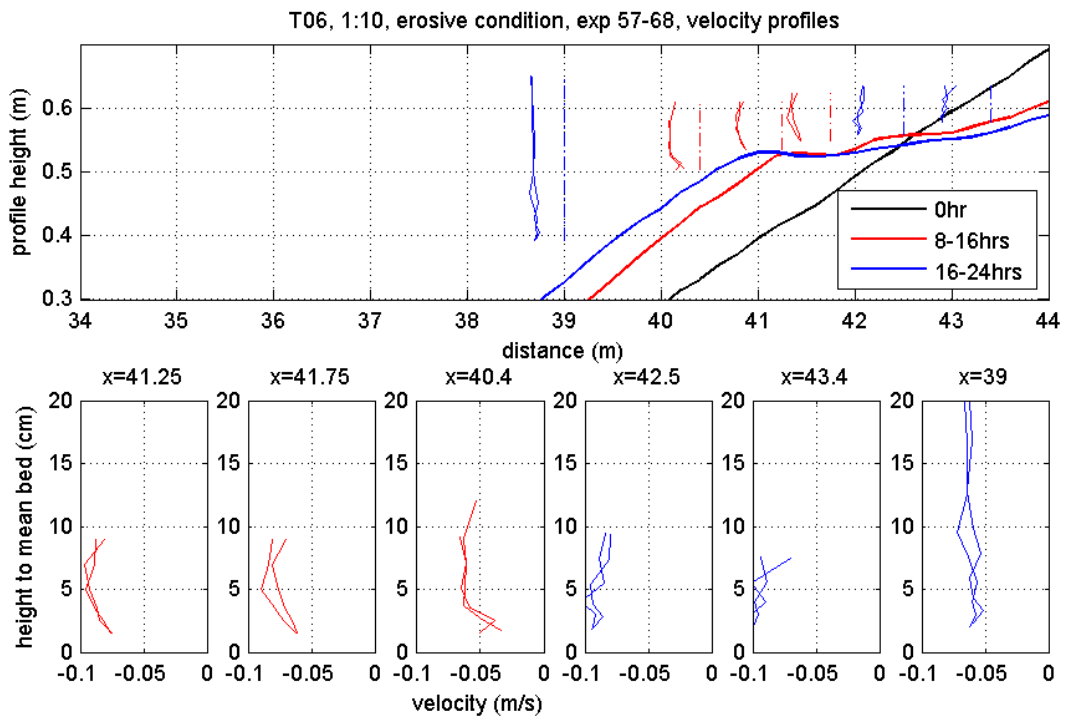


Figure 3.58 Flow velocity verticals for erosive test T06, experiment 57-68

Depth-averaged velocities

To be able to obtain better insight in the behaviour of the flow velocities, all measured velocity verticals are integrated over depth. The method used for this integration is based on a procedure described by Van Rijn (1991) and its description can be found in Appendix C.

Based on the higher waves of T04 and T06, larger undertow velocities are expected with respect to T05. This can indeed be observed in Figure 3.59, Figure 3.60 and Figure 3.61.

The depth-averaged velocities of T04 lay in a range of approximately -0.07 m/s to -0.03 m/s. Figure 3.59 shows a higher flow velocity at the position of the breaker bar and a lower flow velocity just shoreward and seawards of the breaker bar. Furthermore, at 37.1 m, a large difference can be found between the experiment carried out at the beginning of the tests (the highest value) and the experiment carried out at the end (the smallest value).

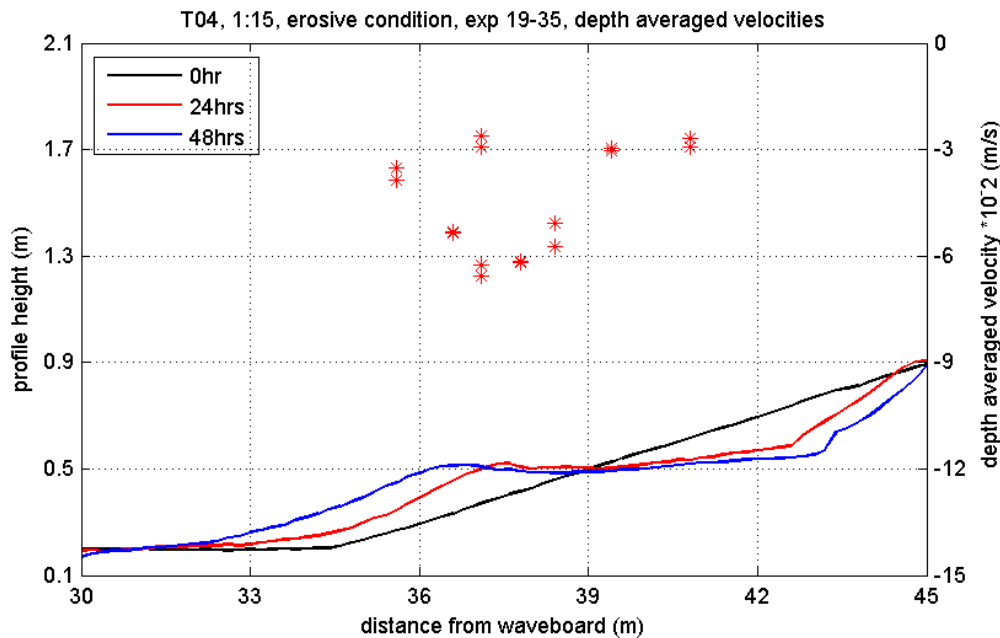


Figure 3.59 Depth-averaged velocities of erosive test T04, experiment 19-35

The depth-averaged velocities of T05 (see Figure 3.60) are smaller than the velocities of T04 and lay in a range of approximately -0.05 m/s to -0.01 m/s. Again, the highest depth-averaged velocity is measured at the position of the breaker bar.

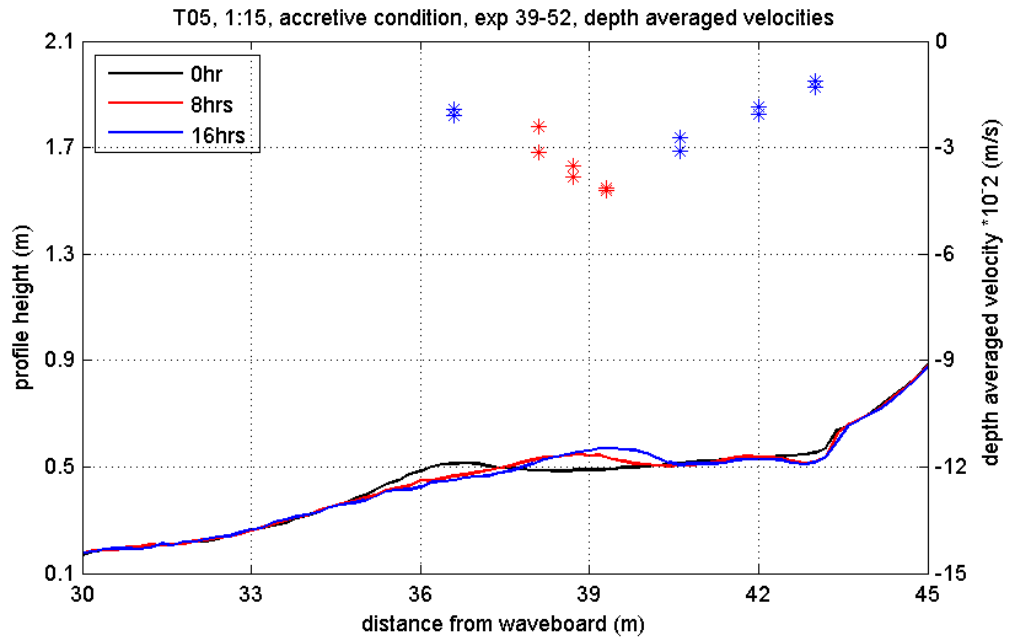


Figure 3.60 Depth-averaged velocities of accretive test T05, experiment 39-52

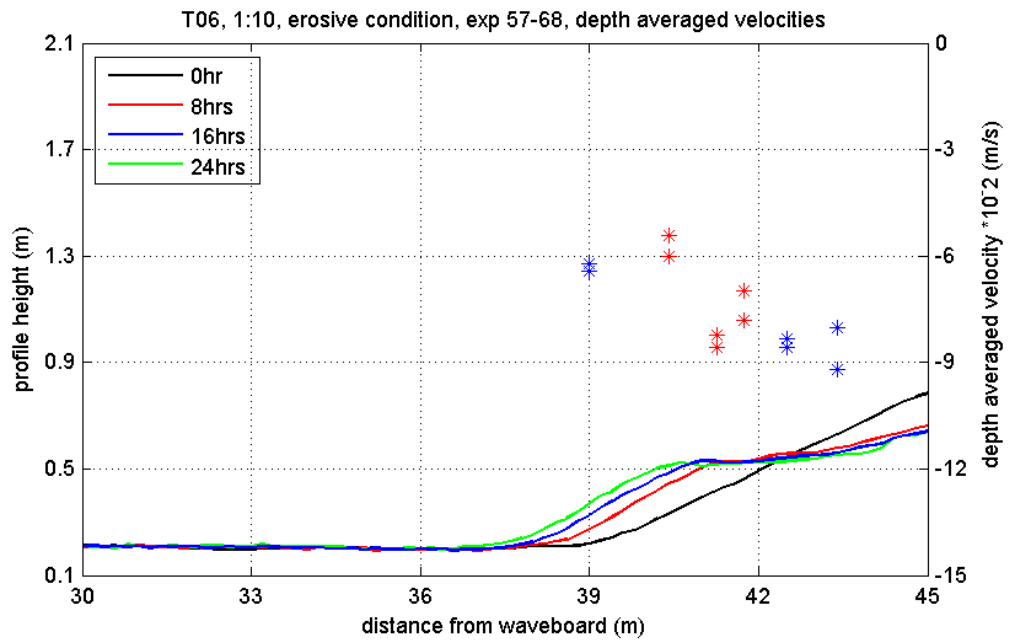


Figure 3.61 Depth-averaged velocities of erosive test T06, experiment 57-68

The depth-averaged velocities of T06, ranging from approximately -0.09 m/s to -0.05 m/s (see Figure 3.61) are much bigger compared to the velocities of T04 as well as T05. Towards the coastline, an increasing depth-averaged flow velocity can be observed.

Variance density spectra and velocity moments

The time series of the EMS, closest to the bed level, are analysed by means of a variance density spectra. The one-dimensional variance density spectrum shows how the variance of the oscillatory velocities is distributed over the frequencies of the wave components (Holthuijsen, 2007).

From Figure 3.62, Figure 3.63 and Figure 3.64, it can be seen that the initial wave spectrum at 21 m shows a large peak at approximately 0.45 Hz for the erosive tests (T04 and T06) and 0.3 Hz for the accretive test, T05. This can be expected, since these values correspond to the wave period of the erosive tests 2.3 seconds, and the wave period of the accretive tests 3 seconds.

Another phenomenon can be observed from the figures: the spectra are changing as the distance from the shore line to the measurement point decreases. The initial large peak, corresponding to the wave period, decreases and at the lower frequencies a new peak occur. The initial peak is referred to as the short wave group (blue line) and the new peak represents the long waves (red line).

According to a rule of thumb, every seventh wave is a high wave. In a system of waves two characteristic time-scales exist: the individual waves and the wave groups. On the time-scale of individual waves, a sinusoidal fluctuation of the water level and the velocity field can be observed. On the time-scale of the wave groups, the amplitude of these fluctuations vary slowly (Roelvink, 1993). The long waves travel with the wave groups and they may be released as free waves, if the wave groups force them to change rapidly due to breaking in the surf zone.

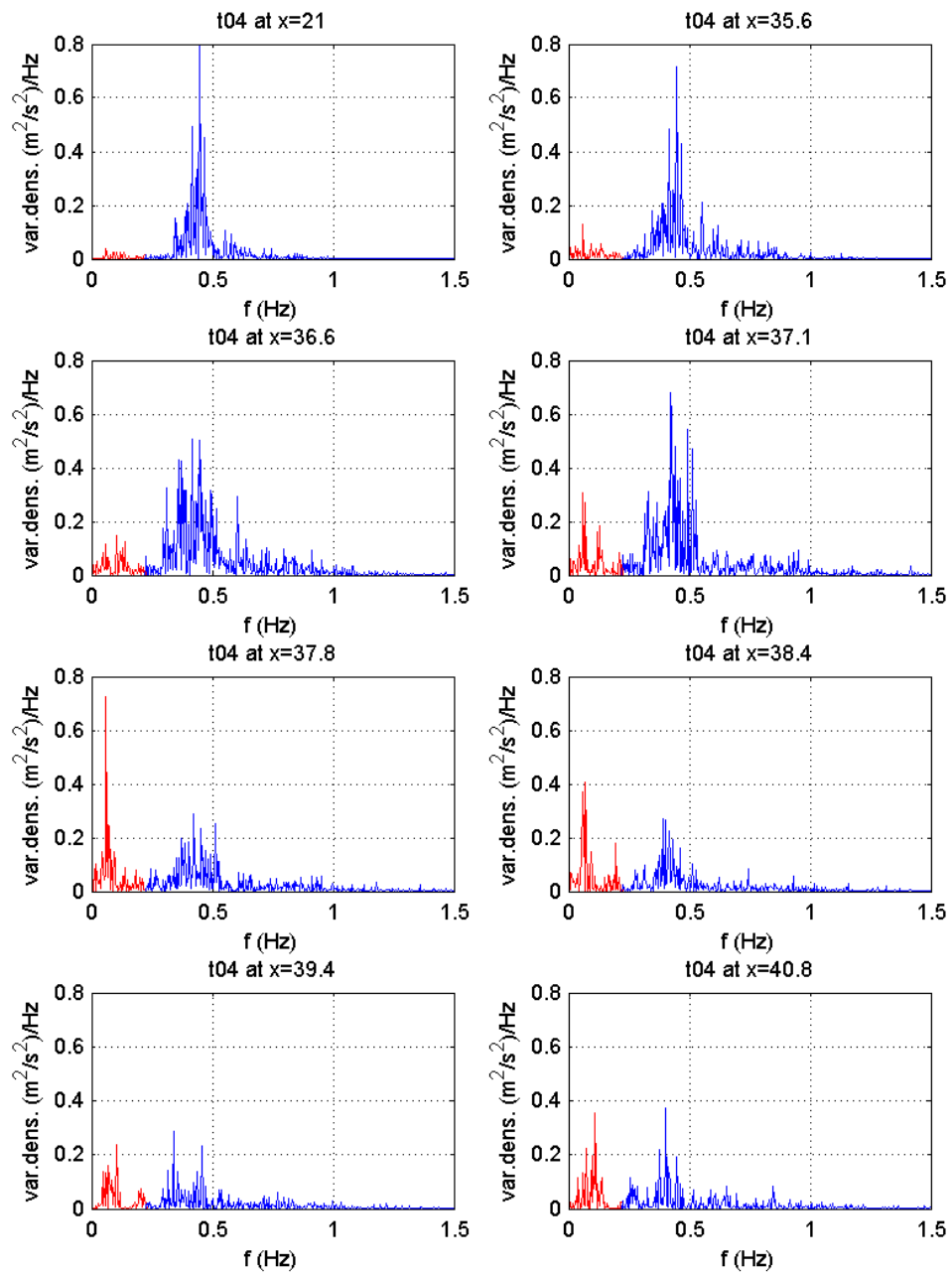


Figure 3.62 Development of the variance density spectrum of T04, subject to an erosive condition. The long waves are represented by the blue line, the short waves by the red line.

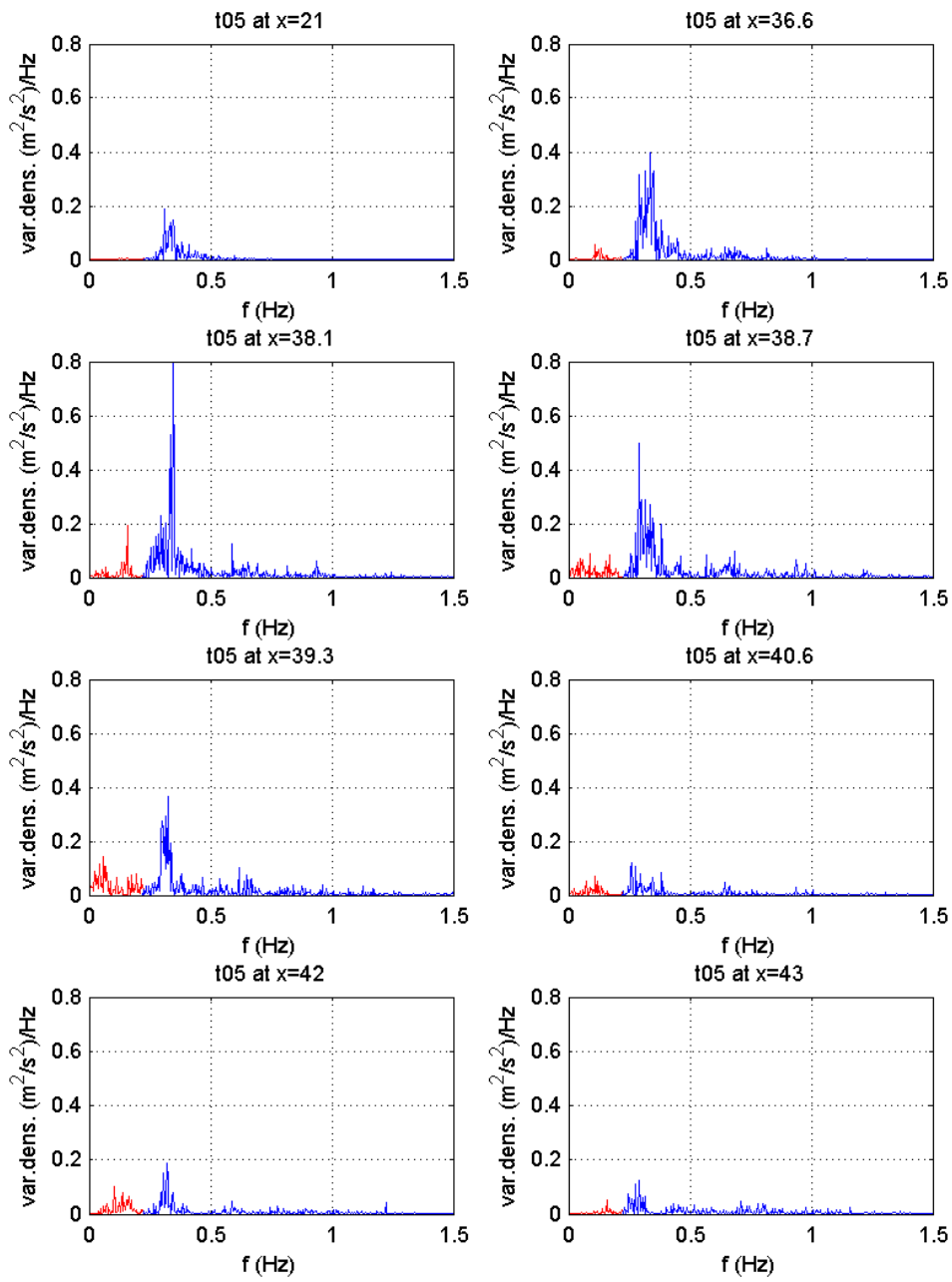


Figure 3.63 Development of the variance density spectrum of T05, subject to an accretive condition. The long waves are represented by the blue line, the short waves by the red line.

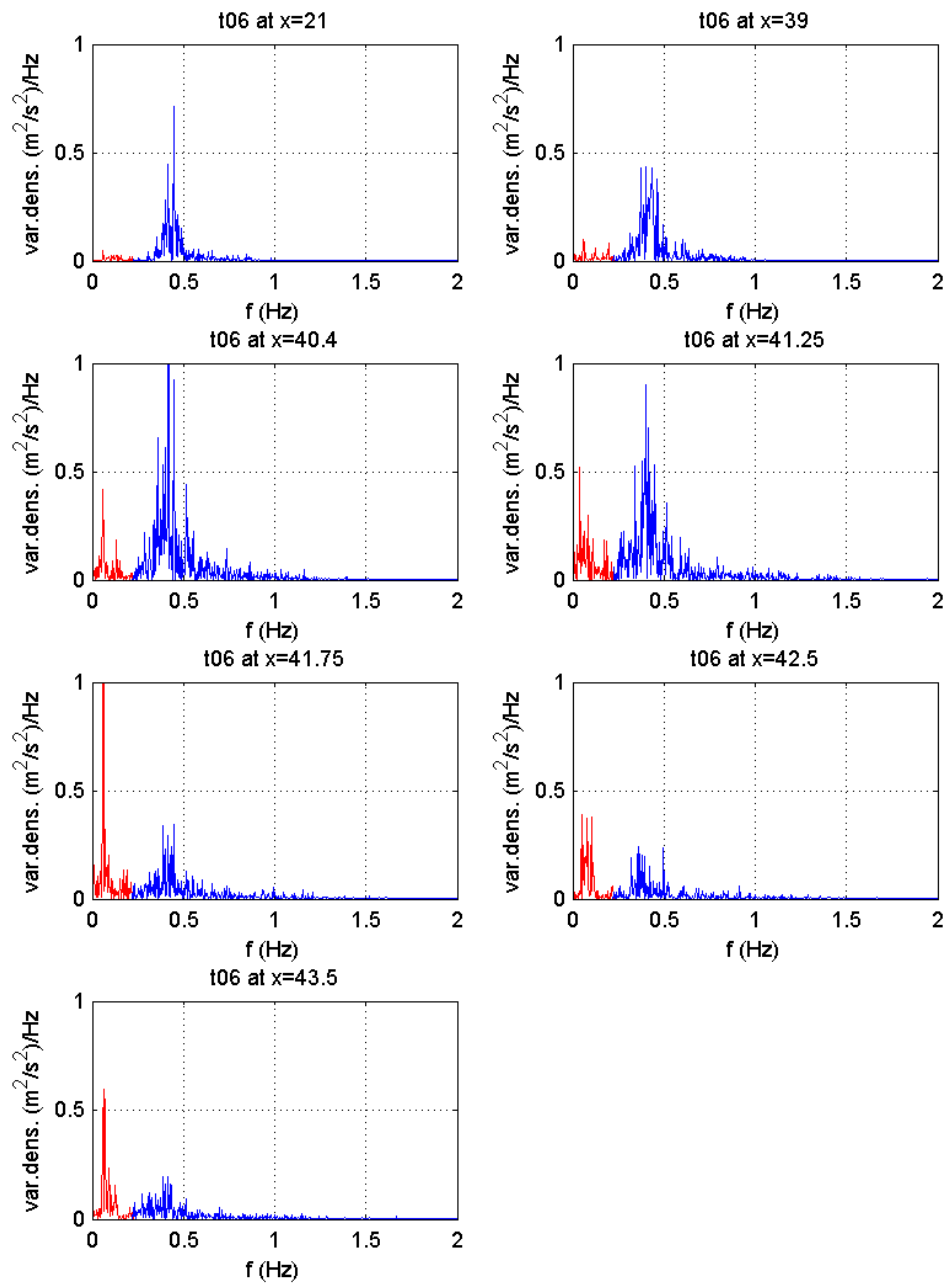


Figure 3.64 Development of the variance density spectrum of T06, subject to an erosive condition. The long waves are represented by the blue line, the short waves by the red line.

According to Roelvink and Stive (1989), on the time scale ranging from that of the wave groups to that of the individual waves, it is useful to subdivide the total oscillatory part of the near bottom flow into a component varying on the time scale of the wave groups, u_L , and a component varying on the time scale of the individual waves, u_s , so the total time-varying flow component is given as

$$\tilde{u} = u_s + u_L \tag{3.11}$$

Assuming $u_L \ll u_s$ and u_s to be uncorrelated to $|u_L|^2$ and $|u_L|^3$, we can evaluate the contributions to the third order velocity moments with:

$$\langle \tilde{u} |\tilde{u}|^2 \rangle = \langle u_s |u_s|^2 \rangle + 3 \langle u_L |u_s|^2 \rangle \quad (3.12)$$

In which the two components are referred to as (Van Dongeren et al, 2006)

$$\begin{aligned} guss &= \langle u_s |u_s|^2 \rangle \\ guls &= 3 \langle u_L |u_s|^2 \rangle \end{aligned} \quad (3.13)$$

And where u_s is the short wave velocity corresponding to the blue part of the spectra in Figure 3.62 up to Figure 3.64, u_L is the long wave velocity corresponding to the red part of the spectra. In the formulae $\langle \rangle$ denotes a long-term averaging.

In Figure 3.65, the development of the *guss* and *guls* along the profile is shown. In addition, the *guss* and *guls* are summed to be able to compare with the third order velocity, computed without separating the time series into long and short wave velocities.

The third order velocity moment can be related to the bed load transport. The skewness, indicative for the third order velocity moments, is characteristic for asymmetry in the wave profile, with systematically larger peaks and shallower troughs. A positive skewness implies a landward bed load transport.

It can be seen that the black and green line agree fairly well. The *guss*, the red line, show positive values, whereas the *guls* show negative values. Thus, the short wave velocity (i.e. *guss*) contributes to a landwards transport, whereas the long wave velocity (i.e. *guls*) contributes to a seawards transport.

In the middle plot, the accretive test T05 give much smaller values of the *guss* and *guls* in comparison to the erosive tests T04 and T06. The values of the total third order velocities of the accretive test T05 are in the same order as the values of the erosive tests T04 and T06. It can be noticed that the black line shows positive values except for T06. Here, the *guls* dominates the *guss*.

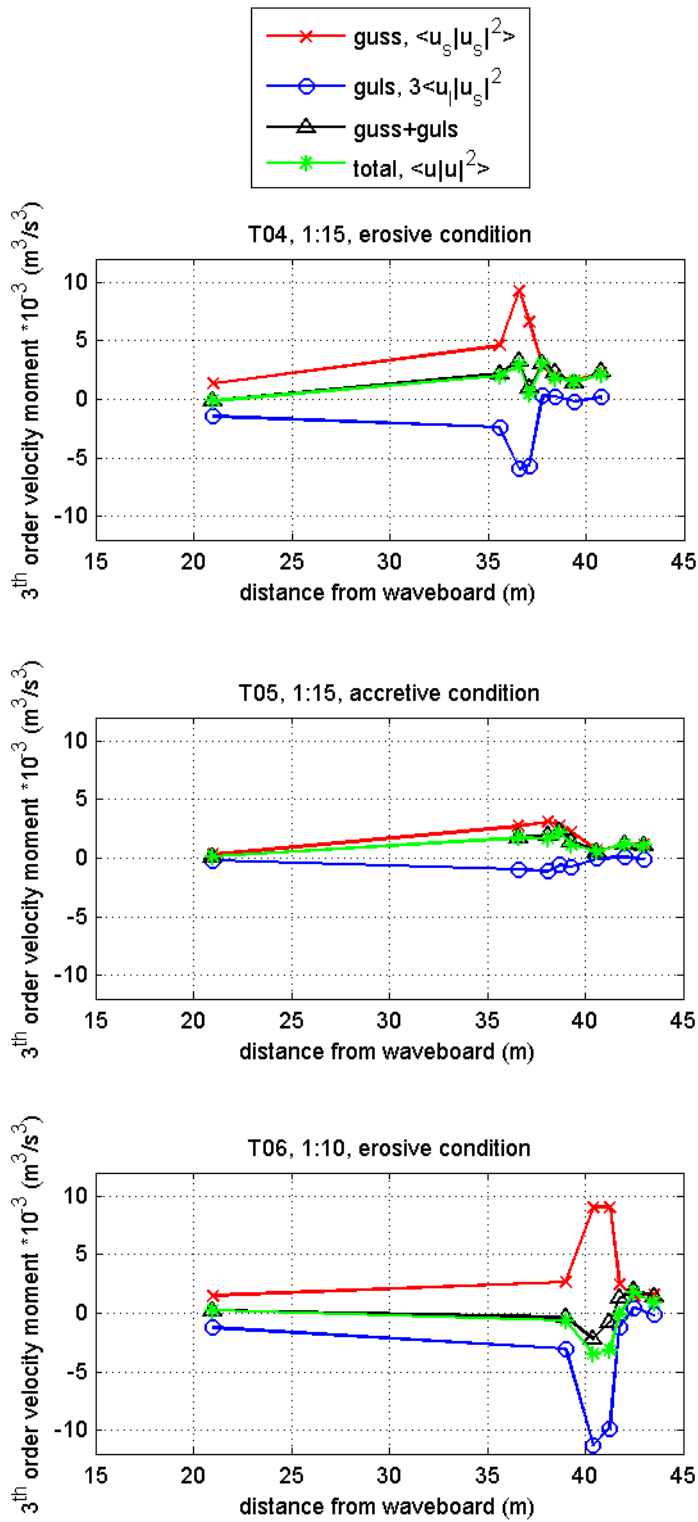


Figure 3.65 Third order velocity moments of T04, T05 and T06 along the profile, separated in the contribution of the short wave velocities (guss) and the contribution of the long wave velocities (guls).

3.7 Concentrations

The concentrations obtained by the suction tubes are shown in Figure 3.66, Figure 3.67 and Figure 3.68. During one experiment, two concentration verticals are taken by means of the transverse suction system. The verticals shown in the figures are the averaged verticals of these two measurements.

The plots in Figure 3.66 show the measured concentration verticals of the erosive test T04 (1:15) at 35.6 m, 36.6 m, 37.1 m, 37.8 m, 38.4 m, 39.4 m and 40.8 m from the wave paddle. At these positions, two experiments were carried out consecutively, except at 39.4 m, where three experiments were done. All experiments were carried out between 24 hours and 48 hours. In the upper plot, all concentration profiles are presented with the corresponding bed profile measurement at 24 hours. In the lower plots, the concentration verticals are shown separately.

The experiments at 37.1 m were carried out twice; the first experiment at 25 hours (represented by the solid line) and the second experiment at 47 hours (represented by the dashed line). The concentration verticals obtained at these points in time are quite similar.

The plots in Figure 3.67 show the measured concentration verticals of the accretive test T05 (1:15) at 36.6 m, 38.1 m, 38.7 m, 39.3 m, 40.6 m, 42 m and 43 m from the wave paddle. Tests at 38.7 m, 39.3 m and 38.1 m (represented by the red line) were carried out between 8 hours and 16 hours, whereas tests at 40.6 m, 42 m, 43 m and 36.6 m, correspond with the blue line, were carried out between 16 hours and 24 hours.

In a similar way, the plots in Figure 3.68 show the measured concentration verticals of the erosive test T06 (1:10) at 39.0 m, 40.4 m, 41.25 m, 41.75 m, 42.5 m and 43.4 m from the wave paddle. Tests at 41.25 m, 41.75 m and 40.4 m, represented by the red line, were carried out between 8 hours and 16 hours, whereas tests at 42.5 m, 43.4 m and 39 m, correspondent with the blue line, were carried out between 16 hours and 24 hours.

The differences between the two measurements taken during one experiment are computed to obtain a measure for the error. The mean of the differences are divided by the mean of the concentration values, resulting in a relative error of 27.4%.

Generally, it can be stated that the concentrations are larger in the vicinity of the breaker bar. Closer to the coastline, smaller values of the sediment concentrations are found.

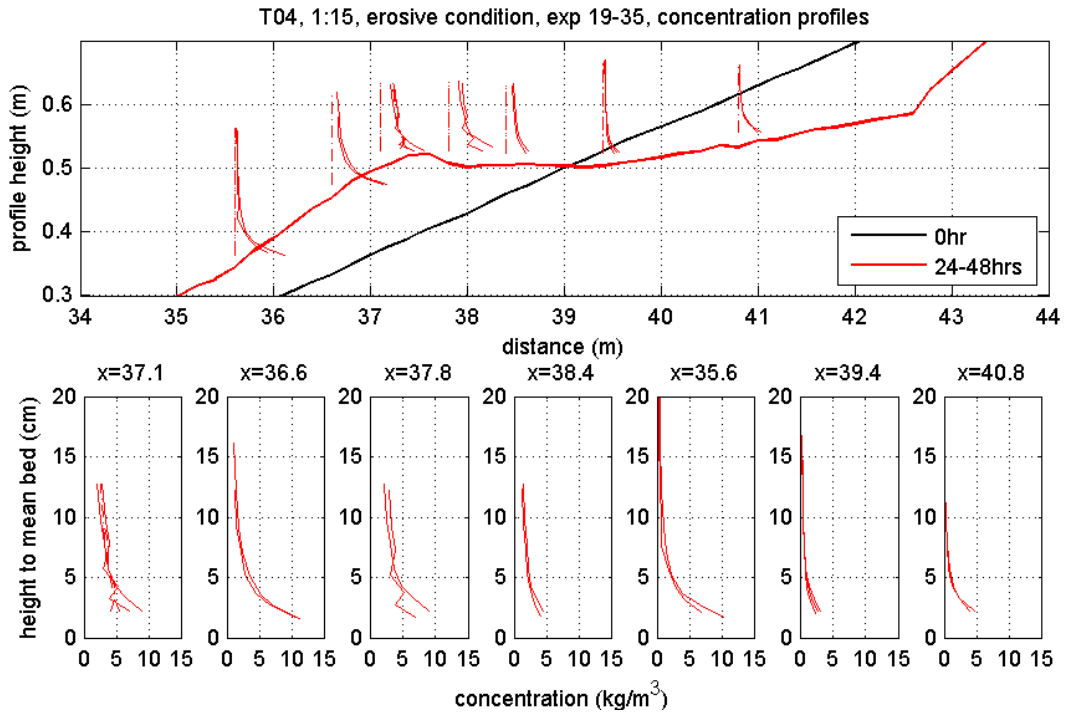


Figure 3.66 Concentration verticals for erosive test T04, experiment 19-35

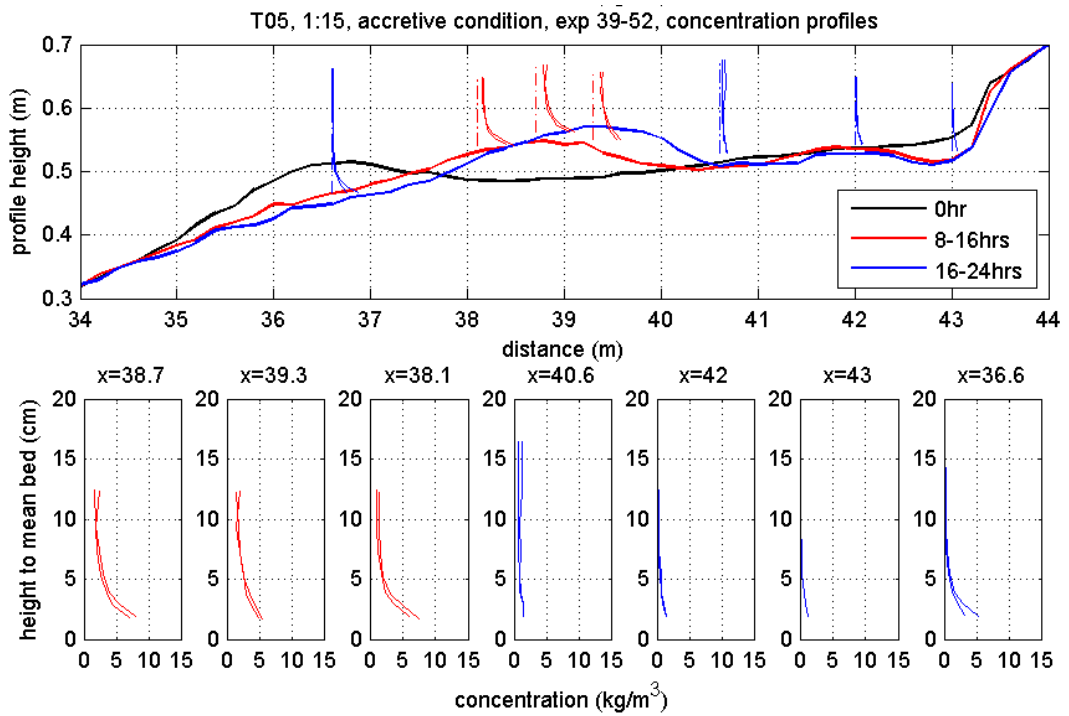


Figure 3.67 Concentration verticals for accretive test T05, experiment 39-52

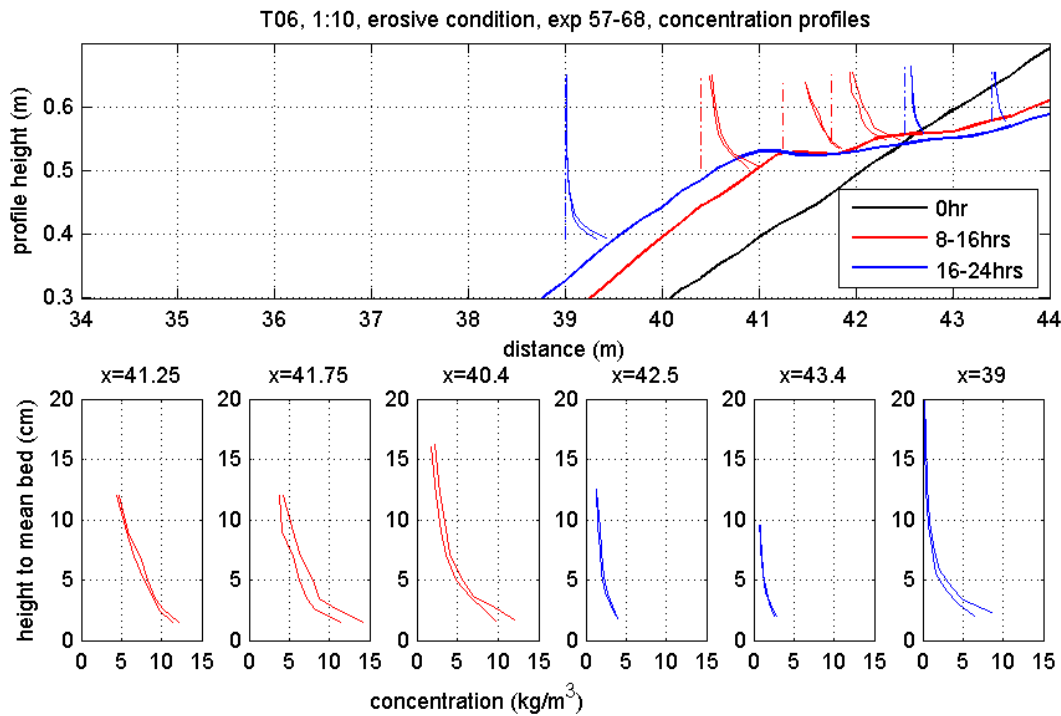


Figure 3.68 Concentration verticals for erosive test T06, experiment 57-68

3.8 Sediment transport

Sediment transports are computed by multiplying the sediment concentration verticals and the flow velocity verticals. In addition, the sediment transports are derived from the measured bed level change.

3.8.1 Sediment transport derived from verticals

The sediment transport is derived from velocity and concentration profiles applying the integral method according to Van Rijn (1991, Appendix C). This method gives the total suspended load transport between the bed and the water surface by fitting a distribution to the measured velocity and concentration profiles. Three different methods are applied to derive the concentration vertical. As an example, concentration verticals and velocity verticals of experiment number 27 (T04 at position $x = 35.6$) are given in Figure 3.69. As a result, three verticals for the sediment transport are derived.

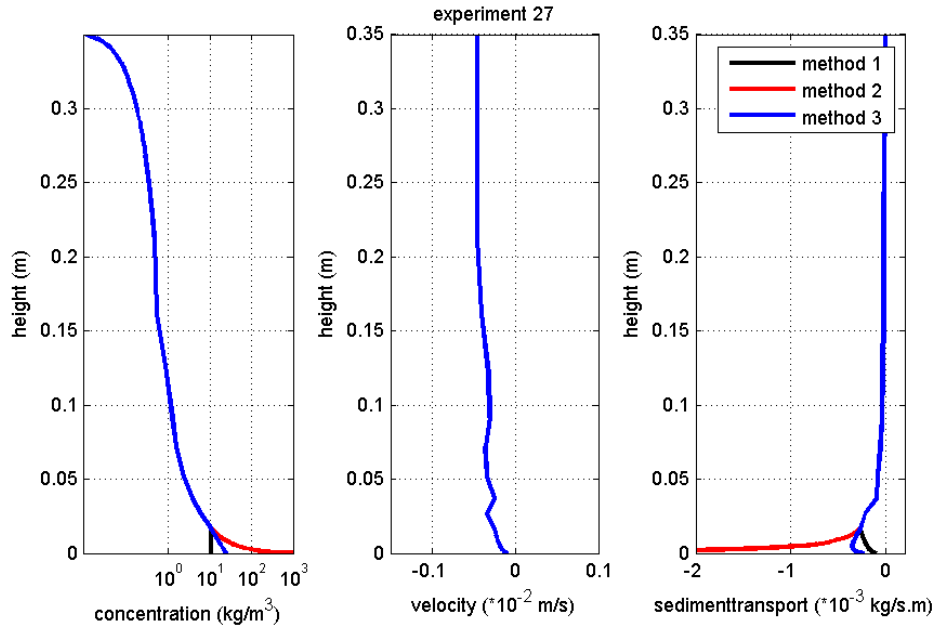


Figure 3.69 On the left, the concentration vertical of experiment 27, T04, at x = 35.6 is shown for three different interpolation methods. The concentration vertical is multiplied by the velocity vertical (second plot) resulting in the sediment transport.

The different methods result in three different values of the total suspended sediment transport. These values are shown in Figure 3.70. Method 1 and Method 3 are quite similar. Method 2, on the other hand, deviates considerably and is, therefore, omitted in the computation of the sediment transport. The average of Method 1 and Method 3 is considered.

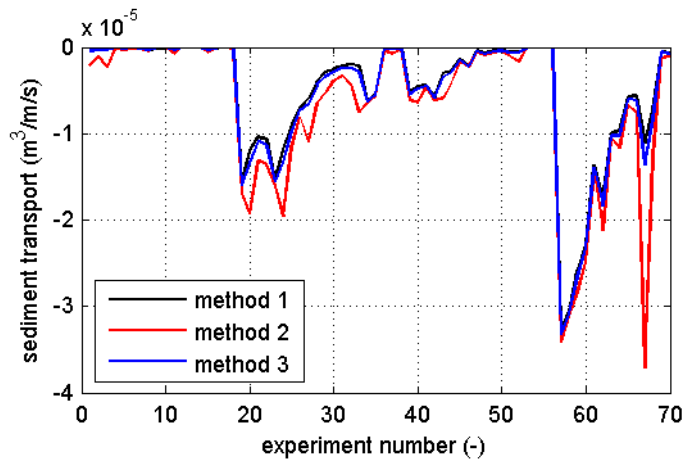


Figure 3.70 Sediment transport using three different methods for all SANDS experiments

Standard deviation of the mean values of Method 1 and Method 3 is $7.43 \cdot 10^{-6} \text{ m}^3/\text{m/s}$.

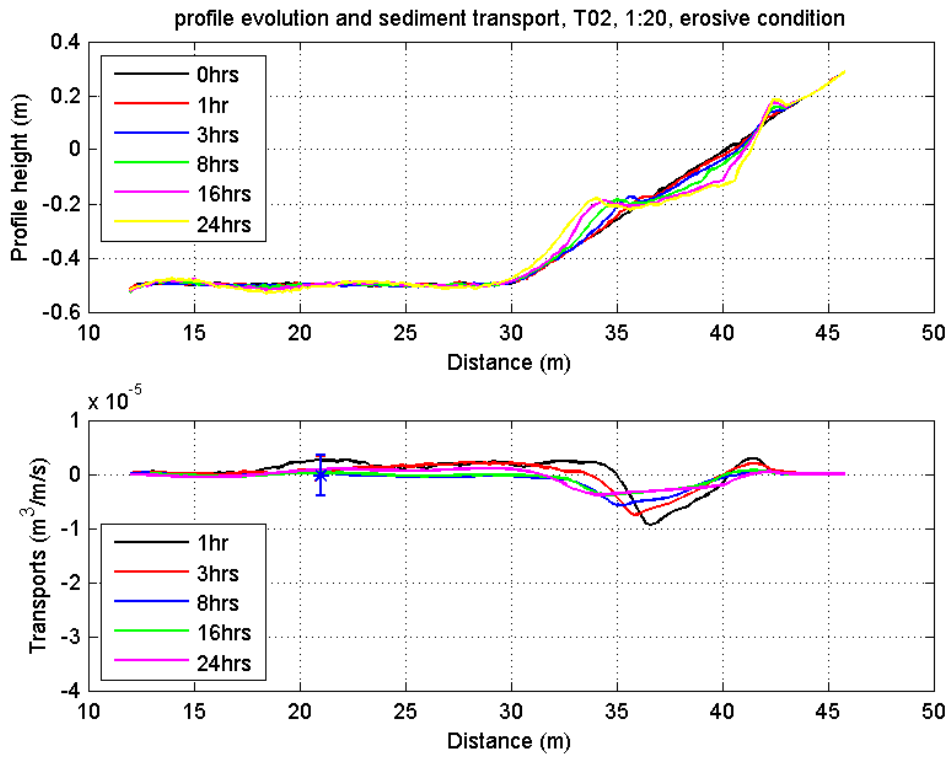


Figure 3.71 Profile evolution and sediment transport of test 1:20

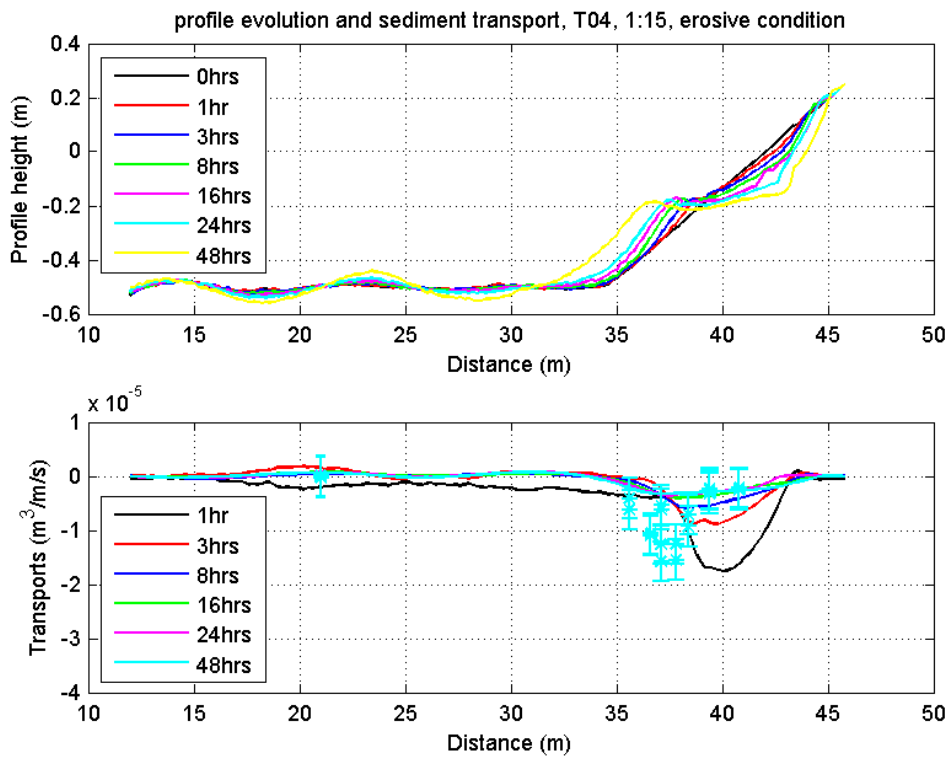


Figure 3.72 Profile evolution and sediment transport of test 1:15

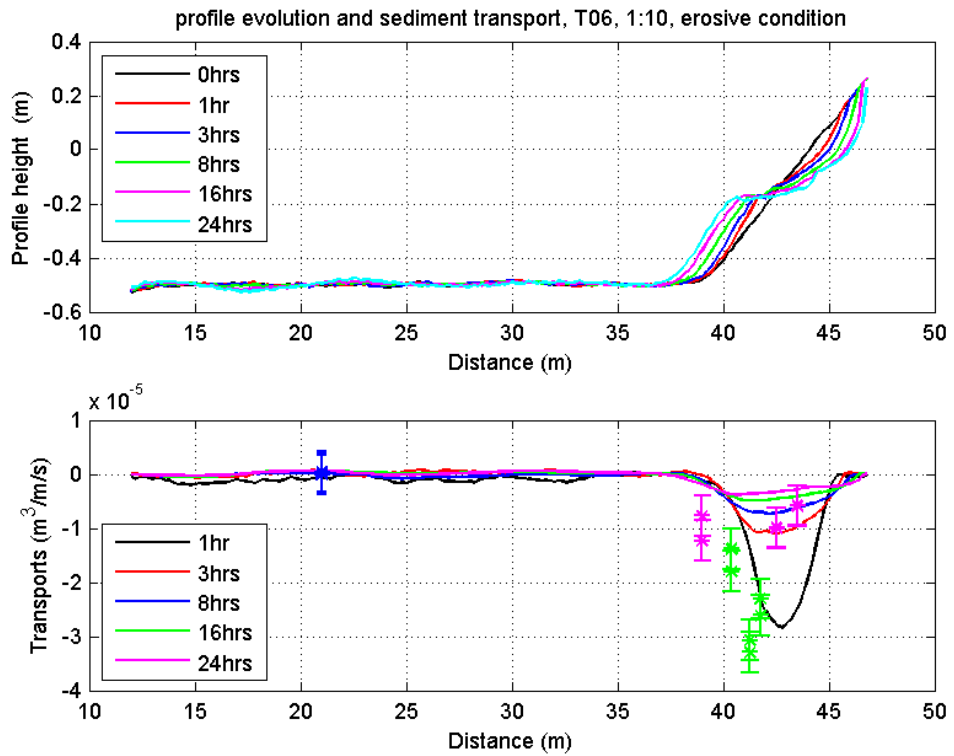


Figure 3.73 Profile evolution and sediment transport of test 1:10

3.8.2 Sediment transport derived from bed level change

Besides the estimation of the sediment transport from the verticals, a mean sediment transport is derived from the change in bed level between the different subtests. The mean sediment transport over the entire profile is calculated from the bed level change according to:

$$S = \int_0^{end} \frac{dz}{dt} dx \tag{3.14}$$

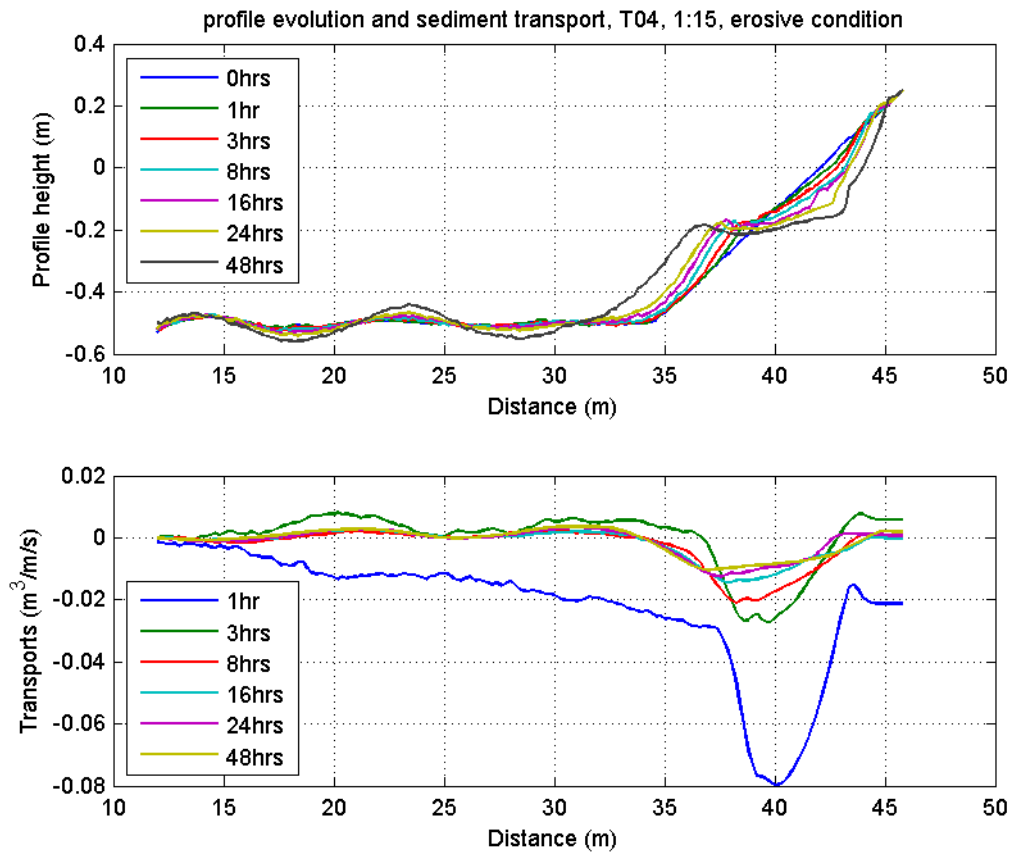


Figure 3.74 Sediment transport derived from changes in bed level for T04

A zero transport at the beginning and at the end of the profile is assumed. In Figure 3.74, a non-closing sediment balance is shown for T04. Particularly after the first subtest, represented by the blue line in the lower plot, the sediment transport balance is deviating more and more. A justification of the non-closing sediment balance could be variation of the bed profile in lateral direction along the flume. In the Delta flume this phenomenon has frequently been observed. However, after checking the cross-flume profiles, a curvature was not noticeable.

Another reason for the non-closing sediment balance could be the occurrence of ripples. The first profile measurement after restoration does not contain ripples, the second one does. Perhaps, the probes are not able to accurately measure the bed level in the presence of ripples. This could be the reason why the sediment balance is not perfectly closed. Succeeding subtests show more acceptable closing sediment balances.

Erosion and sedimentation volumes indicate a small loss or gain of sediment along the entire profile. Assuming a zero transport at the beginning and at the end of the profile, this volume should be zero. This difference is evenly distributed over the profile between the beginning of the profile and point of no bed level change. As a result, the sediment balance is nearly closed. (see Figure 3.75).

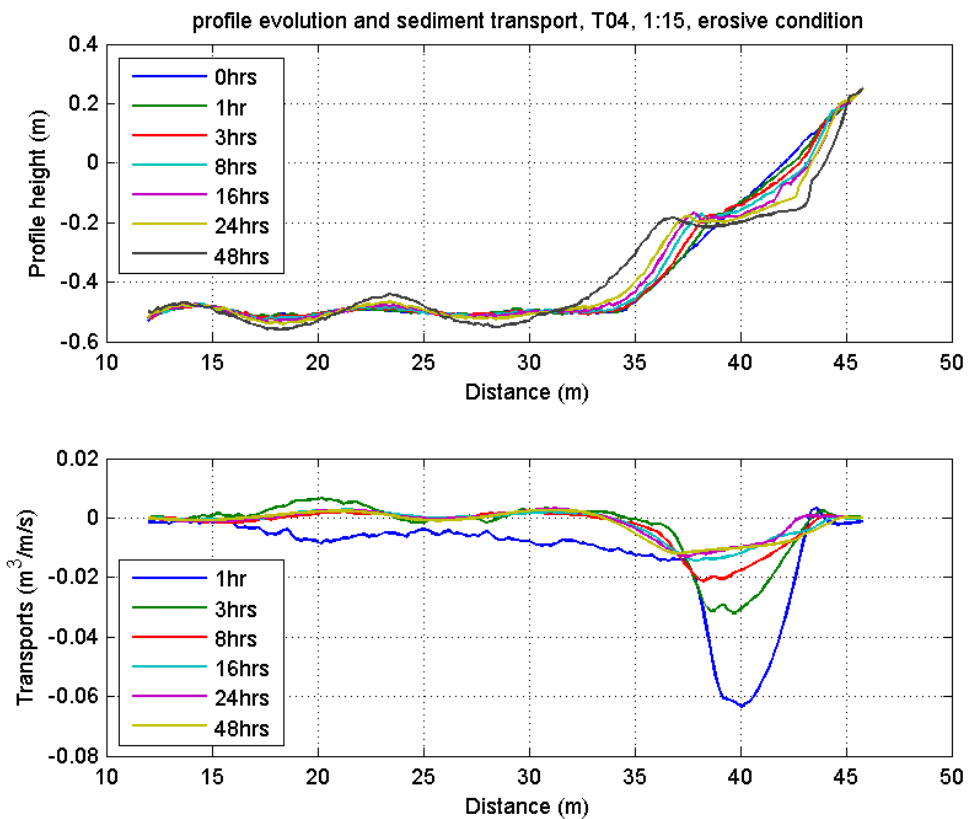


Figure 3.75 Corrected sediment transport

3.8.3 Comparison of results

Sediment transports along the flume are derived from bed level change as explained in Section 3.8.1. The values of the sediment transport derived from the velocity and concentration verticals are plotted in the same colour as the corresponding sediment balance derived from bed level change. The dots represent the results of integration of the sediment transport vertical. The solid lines give the mean sediment transports as derived from the change in bed level in the different subtests. It is remarked that the solid lines represent the mean transports over an entire interval between two successive bed profile measurements. The dots represent mean transports only over a certain interval (related to shallow water frame measurements). This may lead to a small overestimation or underestimation of the mean values, dependent on the moment of measurement.

Initial sediment transport for the three erosive tests considerably differs at the start of the test. The first interval shows a large peak, highest for test 1:10, and during subsequent intervals sediment transport is decreasing. In the last interval, all tests show a similar maximum sediment transport of approximately $0.015 \text{ m}^3/\text{m/s}$.

The values of the sediment transport derived from the velocity and concentration verticals are plotted with an error bar. For T04 (see Figure 3.72) and T06 (see Figure 3.73), it is stressed that differences between the two methods are significant. This could be due to the

fact that the sediment transport derived from the verticals are obtained during approximately one hour, whereas the sediment balance covers the total interval between the bed profile measurements.

In addition, the differences between the two methods can be explained by the fact that sediment transport derived from the bed level change includes all physical processes which play a role during the model tests (e.g. also wave-induced transports). Sediment transports derived from the verticals are in this respect limited. The method of integration has its influence as well.

4 Analysis of shoreface nourishments (VOP)

4.1 Introduction

Previously, in Section 2.1.2, the set-up of the VOP experiments was presented. This chapter aims at establishing and quantifying the dominant physical processes that are affected by the presence of a shoreface nourishment.

The position of a shoreface nourishment in the profile is considered an important design parameter (Walstra et al, 2006). The effect of a shoreface nourishment on the bed profile development largely depends on its position in the profile. Therefore, two nourishment designs are tested: one design positioned seawards of the breaker bar and one located higher up on the coastal profile. The high nourishment design is located on top of the original breaker bar and covers the trough.

Another important design parameter is the nourishment volume. The lower limit of a nourishment volume is considered $350 \text{ m}^3/\text{m}$, based on existing nourishments. In this study, this parameter is not dealt with. The two nourishment designs have identical volumes, which amounts to $400 \text{ m}^3/\text{m}$ on prototype scale.

The red line in Figure 4.1 represents the reference profile. On top of this profile, the two nourishment designs are visible; one design positioned seawards of the breaker bar, the blue line, and one located higher up on the coastal profile, the green line.

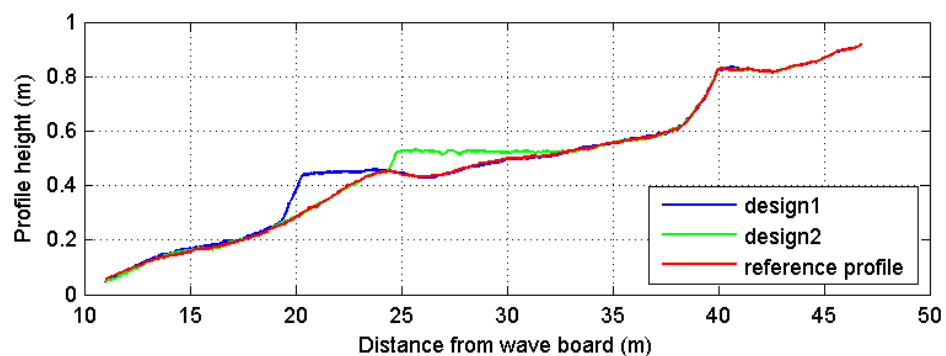


Figure 4.1 The reference profile (red line) with the two nourishment designs (blue and green line)

The performance of the nourishment designs are tested in the Scheldt flume. The three different initial bed profiles are exposed to two wave conditions; an averaged wave condition and a storm wave condition, also referred to as the accretive wave condition and the erosive wave condition. Three bed profiles and two wave conditions result in six tests. A detailed overview of the tests is given in Table 2.7. During these tests, at fixed intervals, the bed profile is measured to be able to determine to what extent the presence of a nourishment affects the morphology. In addition, process-based measurements are carried out. The data on sediment concentration, flow velocities and wave height are analysed to be able to quantify the physical processes that are affected by the presence of a shoreface nourishment.

The results of the tests with the two nourishment designs are compared to the results obtained for the reference tests. The effects of the two shoreface nourishment designs on the morphology are analysed in more detail in Section 4.2. In Section 4.3, detailed comparisons are made between the results for the nourishment designs and the reference profile using the process-based measurements. As a result, an overview of the dominant processes, which are affected by the presence of a shoreface nourishment, is presented in Section 4.5.

4.2 Bed profile development

In Figure 4.2 to Figure 4.3, the beach profile development of the reference tests and the tests with the two nourishment designs are shown. When the bed profile is subject to the erosive wave condition, an offshore migrating breaker bar develops, whereas the profile exposed to an accretive wave condition shows a landward migration of the breaker bar. This can be explained by the net cross-shore sediment transport, which is a balance between landward transport caused by wave-asymmetry and seaward transport caused by undertow. This process is described in more detail in Section 3.2.

First, the accretive tests are discussed (Figure 4.2). The height of the breaker bar of the reference tests and of the test with Nourishment Design 1 increase. At the end of these two tests, the heights of the breaker bar are more or less the same, 0.5 m. The breaker bar of the test with Nourishment Design 2 does hardly change. Its height is larger than the reference test and test with Nourishment Design 1. An explanation could be that the initial bed profile of Nourishment Design 2 is closer to an equilibrium profile compared to the other tests.

For the reference test and the test with Nourishment Design 1, the morphological changes around the coastal zone are alike. The beach slope retreats and just in front of the beach, sand is eroded up to $x = 32$ m. The retreat of the beach slope of the test with Nourishment Design 2 is significantly smaller. In addition, sand is eroded only up to $x = 36$ m. For all tests, a small swash bar is visible.

Secondly, the erosive tests are dealt with (Figure 4.3). For the reference tests and the tests with Nourishment Design 1, an increasing height of the breaker bar can be observed, whereas the height of the breaker bar of the test with Nourishment Design 2 decreases. The height of the nourishment tests are equal, 0.5 m. The height of the reference tests is somewhat smaller, 0.47 m. The breaker bar of the reference test and the test with Nourishment Design 2 is clearly migrating offshore. The position of the breaker bar of Nourishment Design 1, however, remains more or less the same. It even seems to move a bit shoreward.

The morphological changes of the erosive tests resemble the changes of the accretive tests. Again, the test with Nourishment Design 2 shows less erosion around the coastal zone.

At first sight, the nourishment positioned higher in the profile is most effective.

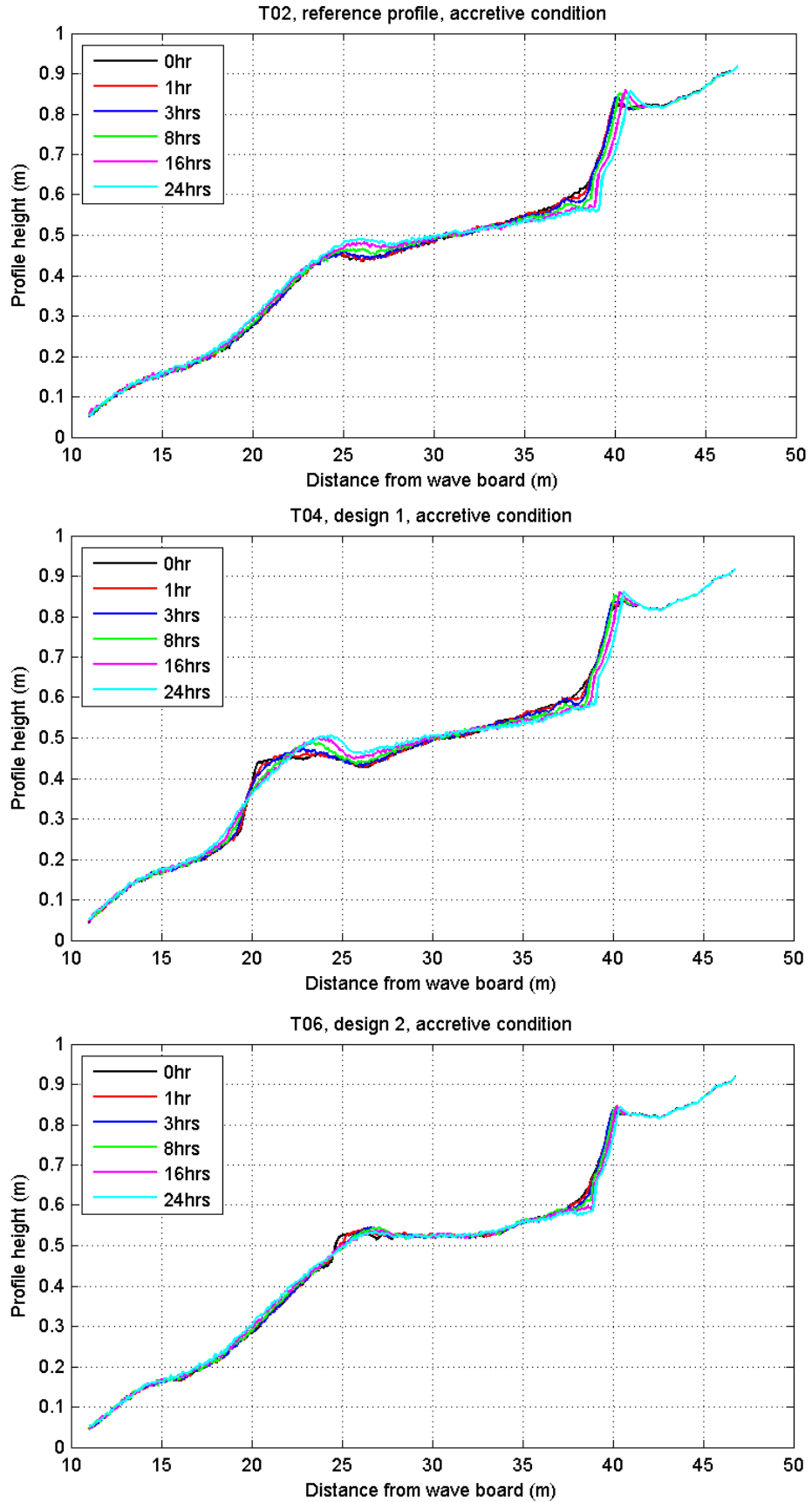


Figure 4.2 Beach profile development of T02, T04 and T06, the accretive tests

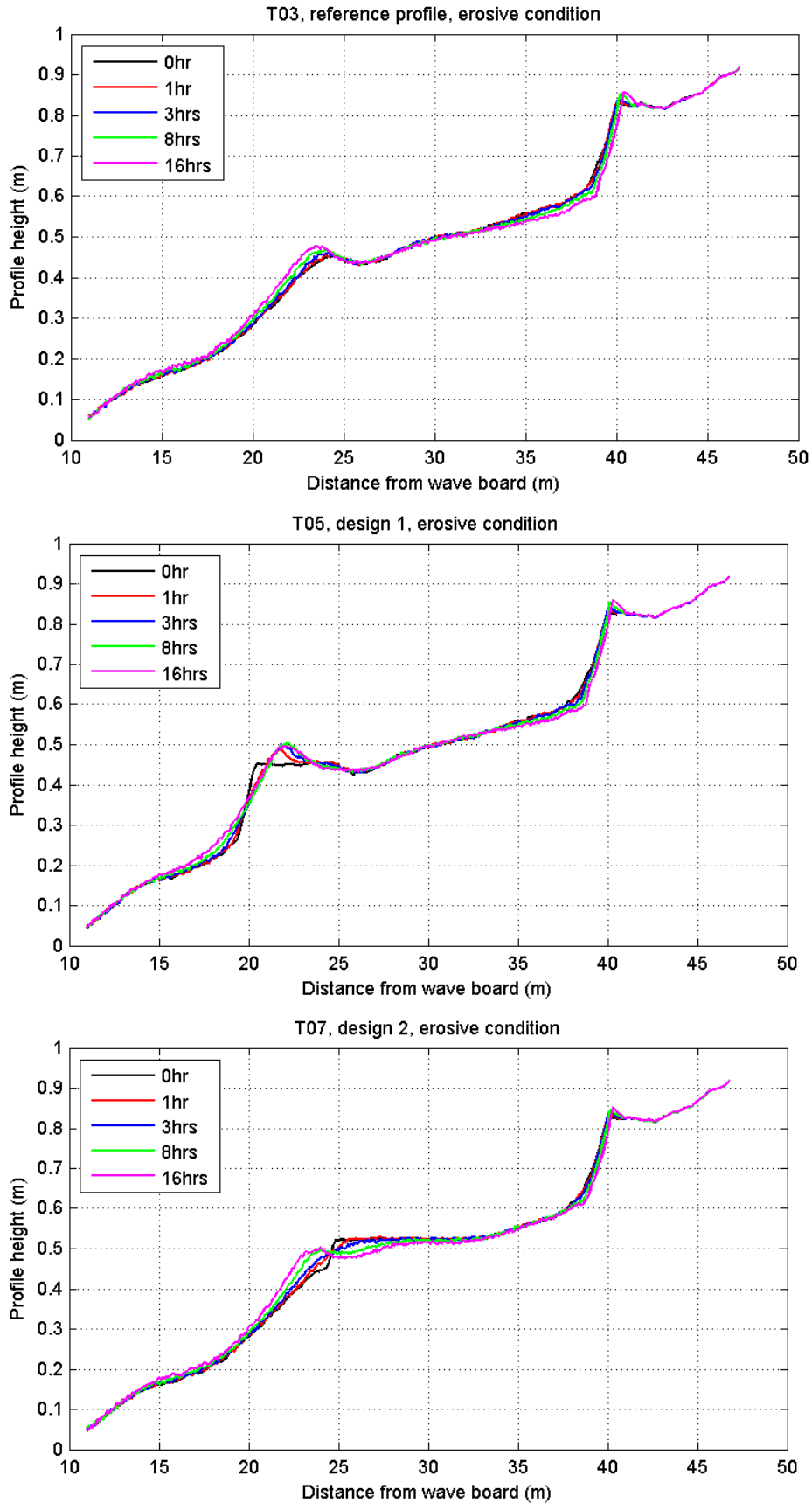


Figure 4.3 Beach profile development of T03, T05 and T07, the erosive tests

4.2.1 Effect of nourishment designs

In this section, the effects of the low and high nourishment on the morphology are discussed in more detail.

First, the bathymetry of the tests with a nourishment design is compared to the bathymetry of the reference tests. The bed profile measurements of the reference tests are subtracted from the bed profile measurements of the accretive tests as well as the erosive tests at equal time intervals (see Figure 4.4). In this way, insight is obtained into the position of the additional sand volume, i.e. the nourishment, in time.

The black line is the start position of the nourishment design. During the first intervals, the nourishment rapidly changes. In the last interval, changes in the position of the nourishment designs are still visible. However, keeping in mind the duration of the last interval (eight hours) compared to the duration of the first interval (one hour), the rate of change considerably decreases.

For both nourishment tests, the sand volume remains in the active zone. However, a clear distinction between the development of the two nourishment designs can be seen (see Figure 4.4). The sand volume of Design 2 does not entirely remain in the vicinity of the breaker bar, as can be noticed for Design 1. At the end of the tests, a large part of the sand volume of Nourishment Design 2 can be found higher up in the profile, in the range from 35 m to 40 m, in comparison with Design 1, where the volume remains in the vicinity of the breaker bar.

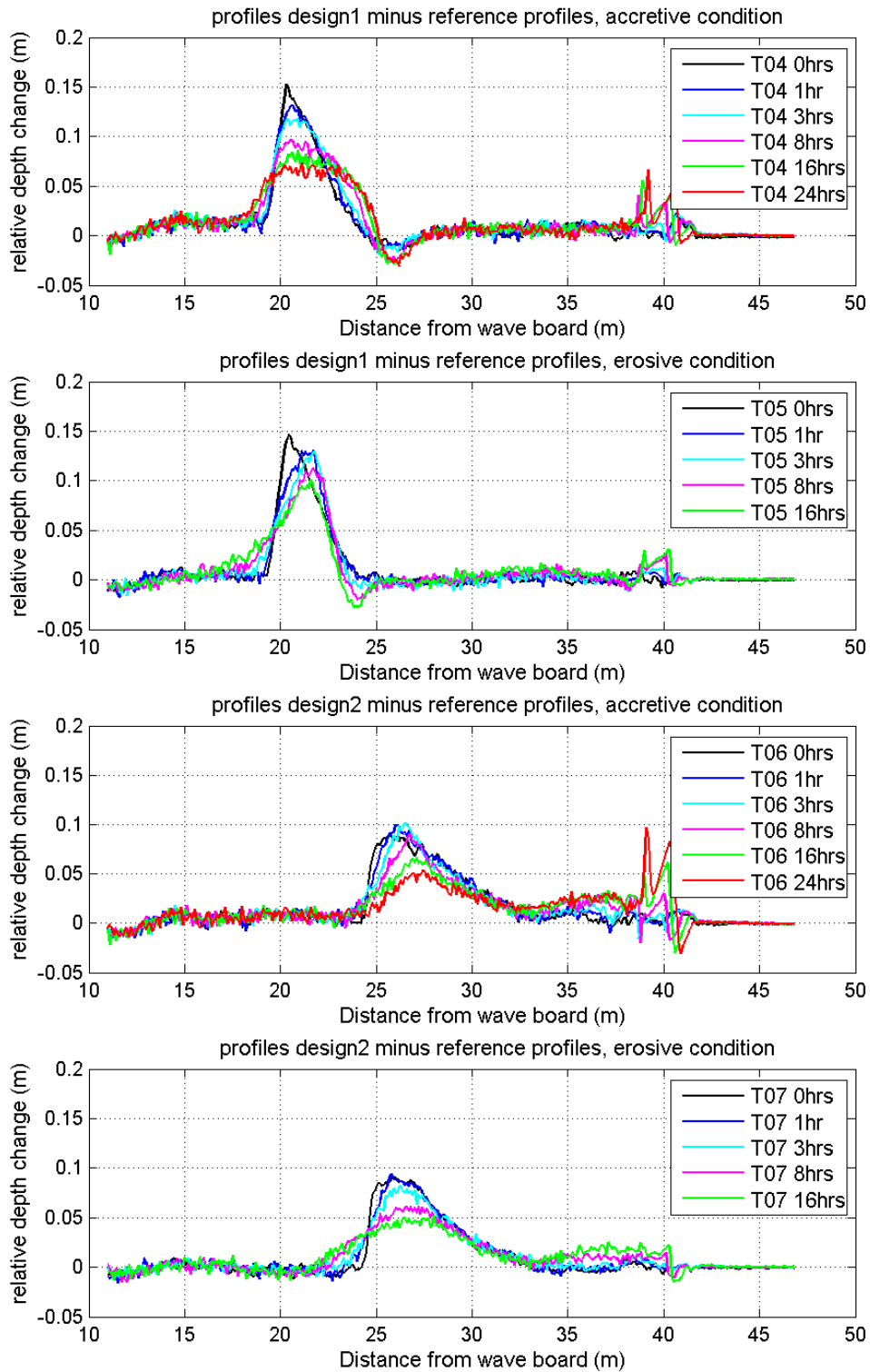


Figure 4.4 Differences between reference bed profile development and development of nourishment design profiles

Secondly, to be able to quantify the effect of the two nourishment designs, the erosion volumes are determined for the upper part of the profile of all tests. The upper part of the profile ranges from 32 m up to 47.7 m, defined as the coastal zone. Figure 4.5 shows the erosion volumes of the accretive tests and Figure 4.6 shows the erosion volumes of the erosive tests. The reference test is represented by the red line, the test with Nourishment Design 1 by the blue line and the test with Nourishment Design 2 by the green line.

It can clearly be observed that both designs positively affect the bed profile development. The reference test is subject to the largest erosion, 0.3 m³/m for the accretive test and approximately 0.2 m³/m for the erosive test. Due to the implementation of Design 1, less sand has been eroded: 0.25 m³/m for the accretive test and 0.12 m³/m for the erosive test. Tests with Nourishment Design 2 show even lower erosion rates: 0.12 m³/m for the accretive test and 0.08 m³/m for the erosive test. It can be concluded that the shoreline is mostly sheltered by Design 2. The presence of the high nourishment results in lower erosion rates near the shoreline compared to the presence of the low nourishment.

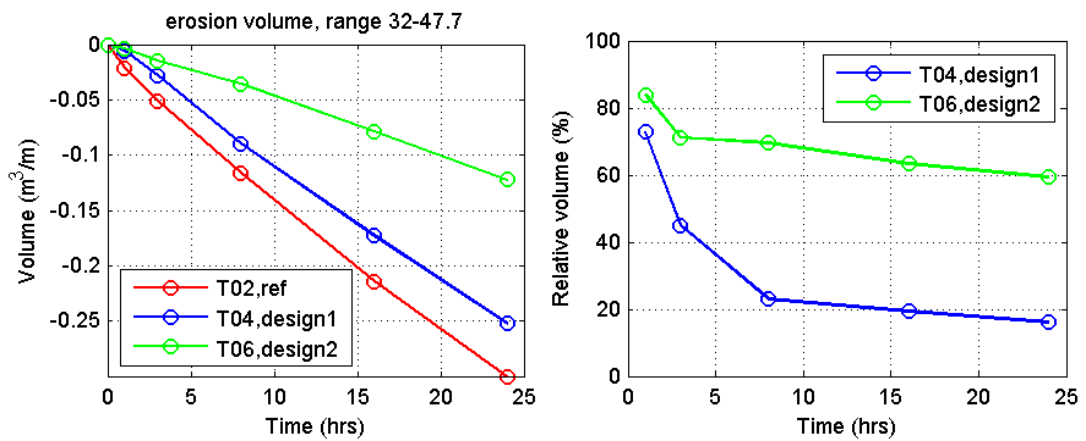


Figure 4.5 On the left, erosion volume of the accretive tests, T02, T04 and T06 in the range from 32 m-47.7 m. On the right, development of the sand volume, relative to the reference test.

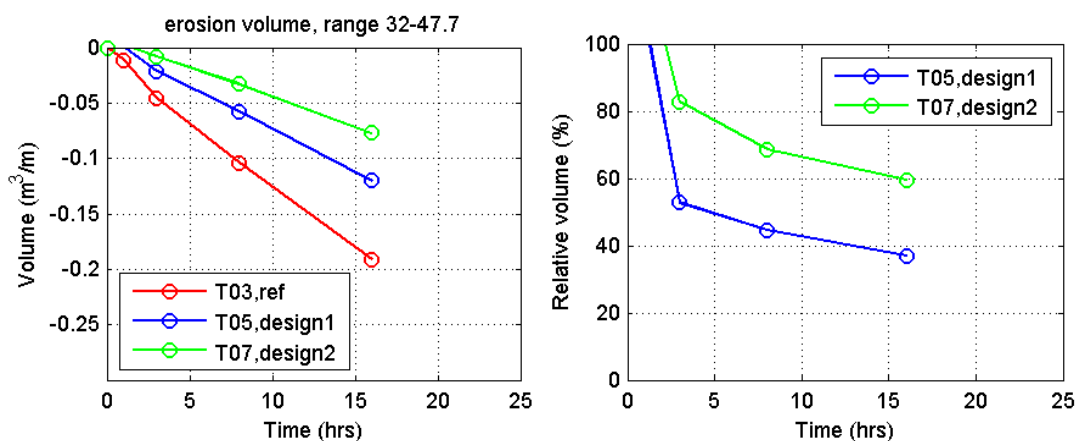


Figure 4.6 On the left, erosion volume of the erosive tests, T03, T05 and T07 in the range from 32 m -47.7 m. On the right, development of the sand volume, relative to the reference test.

To obtain better insight into the effects of the nourishments on the bed profile development, the relative increase of sand volume in the coastal zone is shown in the right plots of Figure 4.5 and Figure 4.6. Nourishment Design 1 leads to a relative increase of sand volume, 20% for the accretive condition and 40% for the erosive condition. Nourishment Design 2, however, results in the largest relative increase of sand volume, 60% for both wave conditions.

The effects of the nourishment designs are determined by the erosion volumes after 16 hours for the erosive tests and the erosion volumes after 24 hours for the accretive tests. Considering all tests after 16 hours, it is expected that for the erosive tests, the loss of volume of sand around the swash zone is larger in comparison with the accretive tests. However, an opposite behaviour can be observed: around the swash zone, the accretive tests show a slightly bigger loss of sediment compared to the erosive tests.

This could be justified by the way the initial profile is created. During eight hours, the bed profile based on an experiment carried out by J. Bosboom (2000) was subject to the erosive wave condition, resulting in the initial reference profile. This profile is used for the erosive test, as well as the accretive test. In this way, the initial profile of the accretive test is more 'out of equilibrium' compared to the erosive test. This could be a reason for the relatively large loss of sediment for the accretive tests.

4.3 Analysis of effects nourishment designs

Nourishment Design 2 was found to most positively affect the bed profile development. In order to gain insight into the efficiency of the shoreface nourishment designs, research is done to the changes in the physical processes due to the presence of a shoreface nourishment. The process-based measurements are used in this study.

The following effects are expected to occur as a consequence of the placement of a shoreface nourishment (Van Duin and Wiersma, 2002). Large waves break at the seaward side of the shoreface nourishment. Remaining shoaling waves generate onshore transport due to wave asymmetry over the nourishment area. The smaller waves in the lee-side generate less stirring of the sediment and the wave-induced return flow (cross-shore currents) reduces. This results in an increase of the onshore sediment transport and a reduction of the offshore sediment transport. Both effects lead to an enhanced onshore transport behind the shoreface nourishment area.

The following hypotheses are tested:

Addition of a shoreface nourishment to the reference profile results in

- a decrease in wave height
- an increase in wave asymmetry
- a decrease in the wave-induced return flow
- a decrease in sediment concentration
- a decrease in sediment transport landwards of the nourishment area.

4.3.1 Wave height

A number of wave characteristics were computed from the raw time series, directly after each test. The integration interval for these characteristics was chosen from 10 minutes to 40 minutes after the start of each test. In this analysis, the significant wave height, represented by H_{m0} , is used.

For the intervals of the accretive tests, T02, T04 and T06, the wave height decay over the profile are shown in Figure 4.7. Figure 4.8 shows the wave height variation of the erosive tests T03, T05 and T07.

For all tests, at approximately 20 m – 23 m, due to shoaling, initially, a slightly increasing wave height is visible. Propagating further, waves decay over the bar, as a result of energy dissipation due to bottom friction and breaking of waves, can clearly be observed. The point of wave breaking of T04 and T05, is located slightly more offshore in comparison with the reference tests. T06 and T07, however, have a slightly more landward positioned point of wave breaking with respect to the reference tests. This can be explained by the differences in the position of the breaker bar. The breaker bar of the tests with Nourishment Design 1 is located slightly more offshore compared to the reference test, whereas the breaker bar of the tests with Nourishment Design 2 is located slightly more landward compared to the reference tests.

Another remark can be made: the wave height decay of T06 and T07, tests with Nourishment Design 2, is considerably larger than the wave height decay of the reference tests and the tests with Nourishment Design 1. In the vicinity of the beach slope, at $x=35$, the reference tests and tests with Design 1 show a wave height of 8.5 cm, in case of an accretive condition. For the accretive test of Design 2 (T06), a wave height of 7.3 cm can be found. Concerning the erosive tests, the wave height of approximately 10 cm is observed for T03 and T05, whereas T07 shows the lowest wave height, ranging from 8 cm to 9 cm.

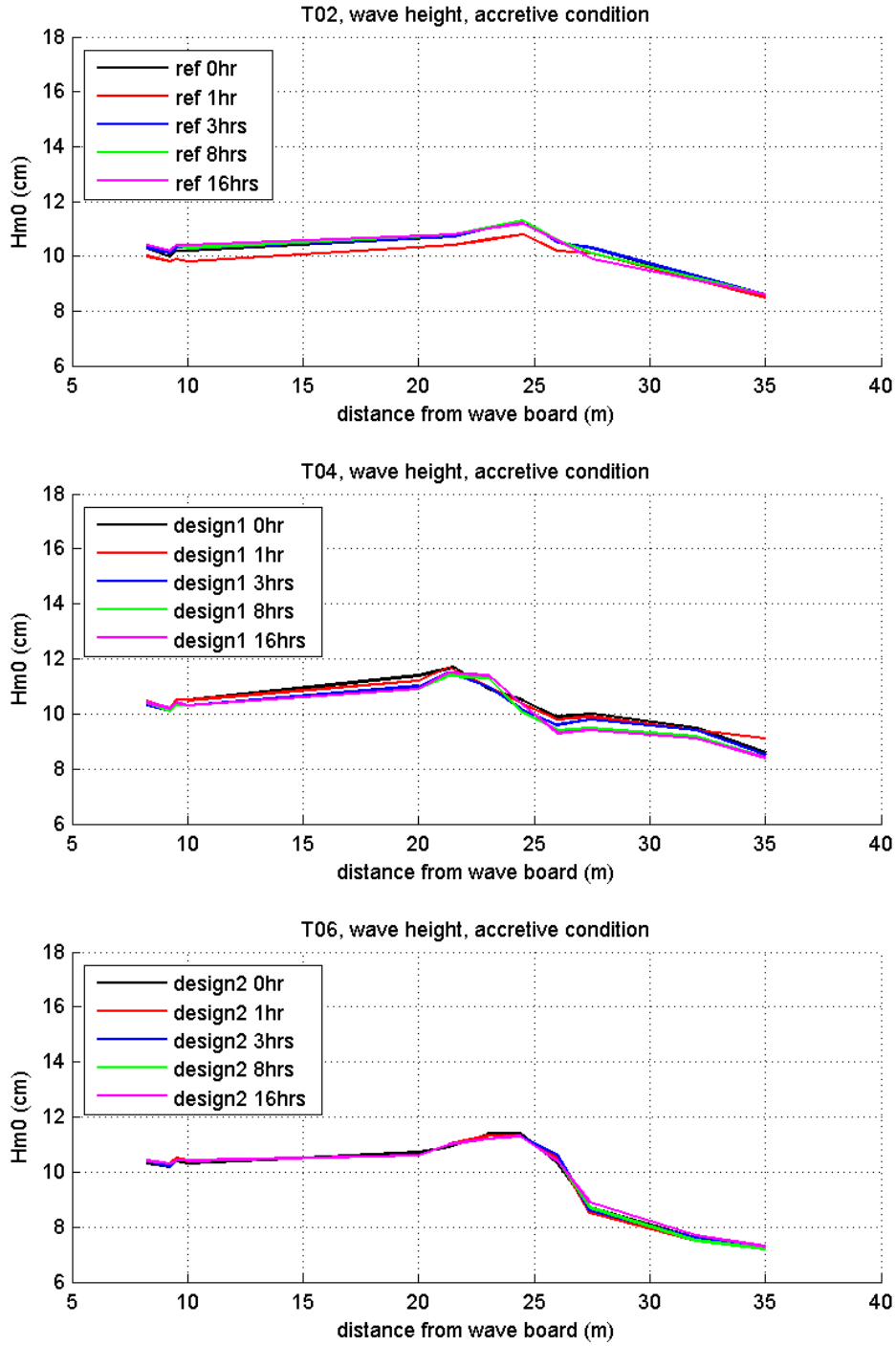


Figure 4.7 Wave height variation along the flume for the accretive tests (T02, T04 and T06)

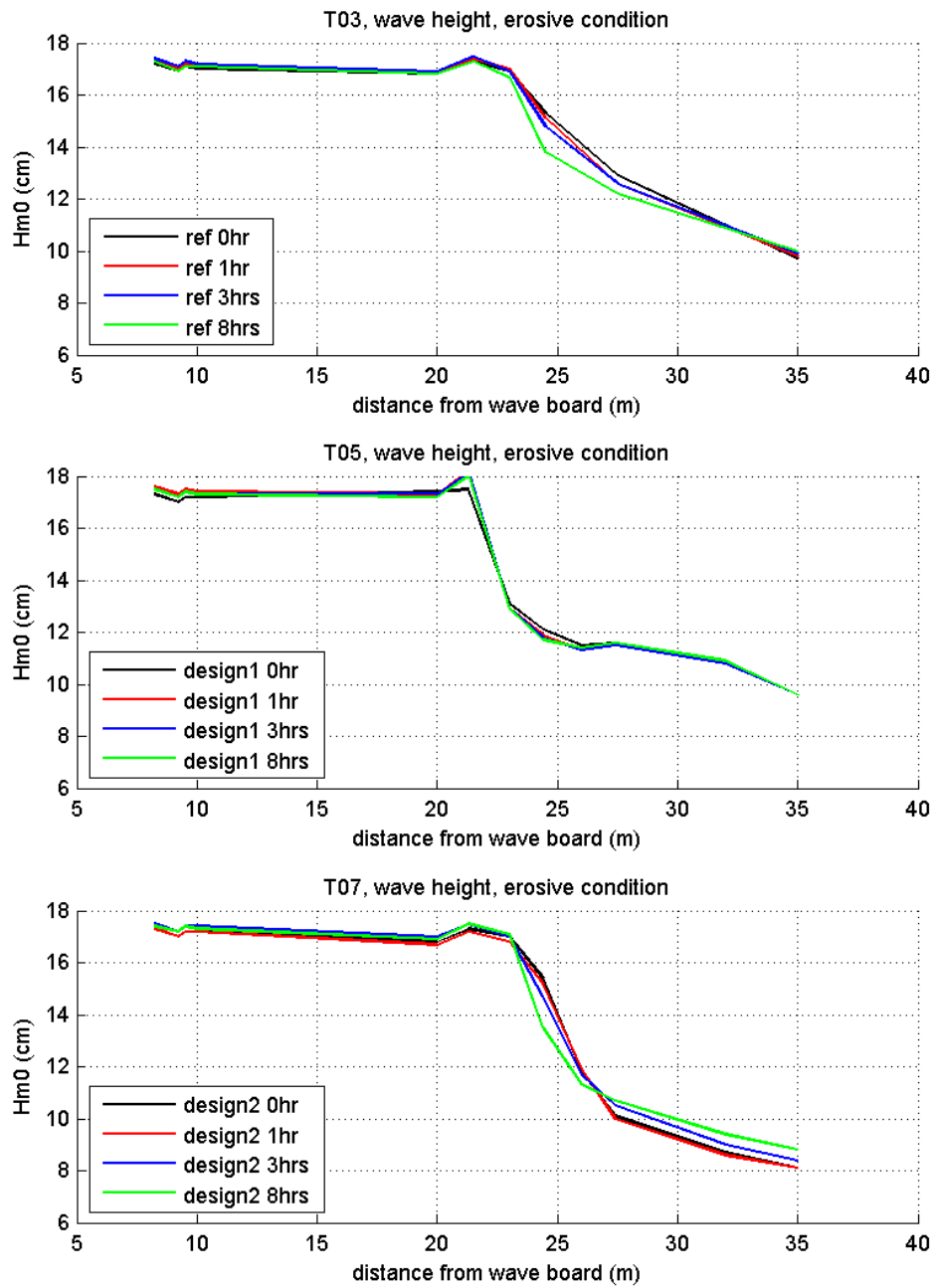


Figure 4.8 Wave height variation along the flume for the erosive tests (T03, T05 and T07)

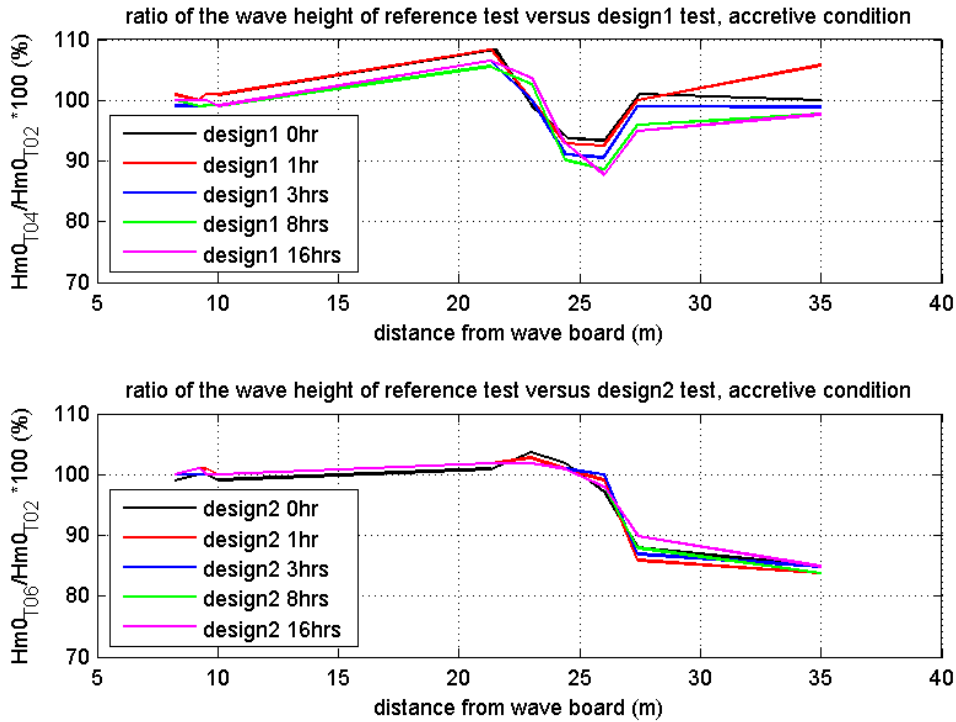


Figure 4.9 The upper plot shows the ratio between the wave height of T04 (Nourishment Design 1 test) and T02 (reference test) for the accretive condition. The lower plot shows the ratio between the wave height of T06 (Nourishment Design 2 test) and T02 for the accretive condition.

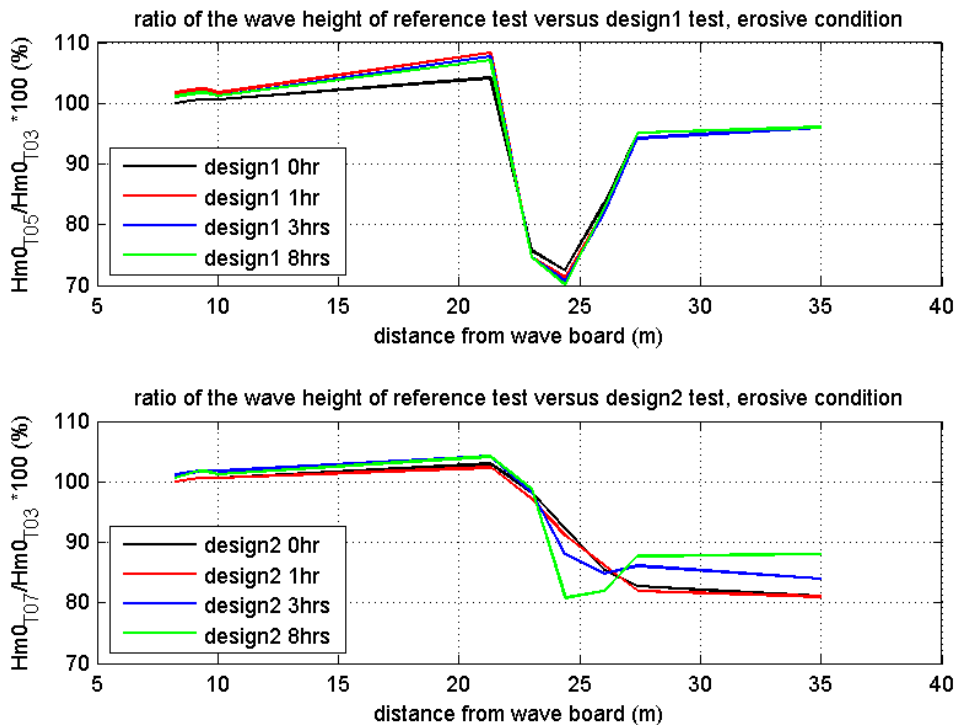


Figure 4.10 The upper plot shows the ratio between the wave height of T05 (Nourishment Design 1 test) and T03 (reference test) for the erosive condition. The lower plot shows the ratio between the wave height of T07 (Nourishment Design 2 test) and T03 for the erosive condition.

In Figure 4.9 and Figure 4.10, the ratios between the wave heights of the nourishment design tests and the wave heights of the reference tests are shown for the accretive condition and the erosive condition respectively. The upper plots in Figure 4.9 and Figure 4.10 show the effect of the Nourishment Design 1 on the wave height development along the flume and the lower plots show the effect of the Nourishment Design 2 on the wave height development along the flume.

These figures support the conclusions drawn from Figure 4.7 and Figure 4.8. It can be seen that the wave height decreases significantly more in case of implementation of Nourishment Design 2. The ratio between the wave height of the Nourishment Design 1 tests and the reference tests is 95%-105%, whereas the ratio between the wave height of the Nourishment Design 2 and the reference tests varies between 80% and 90%.

It is remarkable that, initially, the wave height of the accretive test with Nourishment Design 1 decreases to 90% of the wave height of the accretive reference test. Closer to the shoreline, where the ratio amounts to 100%, the effect of the nourishment on the wave height seems negligible. In a similar way, the wave height of the erosive tests with Nourishment Design 1 is discussed. First, the wave height increases due to shoaling. Subsequently the wave height of the erosive tests with Nourishment Design 1 reduces to 70% of the wave height of the reference test. And then, propagating further, the wave height relatively increases again to 95% of the wave height of the reference test.

The wave height decay of the tests with Nourishment Design 2 shows a different behaviour. Due to breaking, the wave height decreases to 80-90% of the wave height of the reference test. Contrary to the tests with Nourishment Design 1, it does not increase again.

This large difference in wave height decay between the two designs can be explained by the shape of the nourishment volume (see Figure 4.1). The height of Nourishment Design 1 is equal to the height of the breaker bar of the reference test. The waves break slightly more offshore, but the height of the waves that pass the breaker zone and enter the surf zone is similar to the height of the waves in the reference tests. Nourishment Design 2, on the other hand, is located higher up in the profile. Its height is positioned approximately 7 cm above the breaker bar of the reference test. This implies that also smaller waves already break at $x = 25$ m, whereas in case of the reference test, these waves do not break until they pass approximately $x = 33$ m.

The hypothesis that the addition of a shoreface nourishment to the reference profile results in a decrease in wave height, is substantiated.

4.3.2 Flow velocities and velocity moments

The process-based measurements described in Section 2.2 are carried out at five positions along the flume. These positions are equal for all tests enabling comparison between the nourishment design tests and the reference tests. In Figure 4.11, the positions are indicated: from left to right, 19.9 m, 22.9 m, 24.9 m, 28.9 m and 34.3 m. In this section, the flow velocities, depth-averaged velocities, variance density spectra and the velocity moments are discussed.

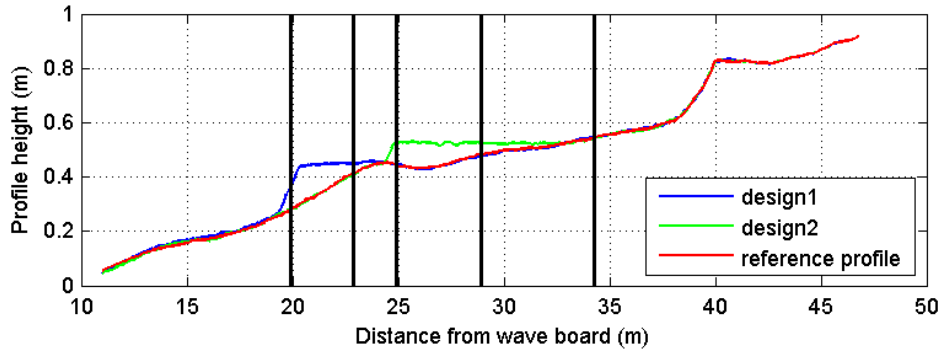


Figure 4.11 Overview of positions of process-based measurements

Flow velocities

During the experiments undertow flow velocities were measured with the measurement carriage construction (see Section 2.2) at five cross-shore locations, indicated in Figure 4.11. Initially, data obtained by the EMS are used.

The plots in Figure 4.12 show the measured velocity verticals at 19.9 m, 22.9 m, 24.9 m, 28.9 m and 34.3 m from the wave paddle for the reference tests and the tests with the two nourishment designs. On the left, the tests with an accretive wave condition (T02, T04 and T06) are shown and on the right, the velocity verticals with an erosive wave condition (T03, T05, T07) can be found.

Comparison of the verticals of the nourishment designs and the reference tests leads to the following comments. At 19.9 m, it could be expected that all flow velocity verticals of the erosive tests are more or less equal. For the erosive tests with Nourishment Design 2, the flow velocities are considerably smaller than the reference test and test with Nourishment Design 1. This does not account for the experiment at 24.9 m. It can be assumed that the data obtained by the EMS for the erosive test with Nourishment Design 2 are not correct. This can be attributed to the intermediate calibration of the EMS. It is presumed that the water in the flume was still moving, while the EMS was calibrated.

The flow velocities are also obtained by the ASTM. In **Error! Reference source not found.**, these data are shown.

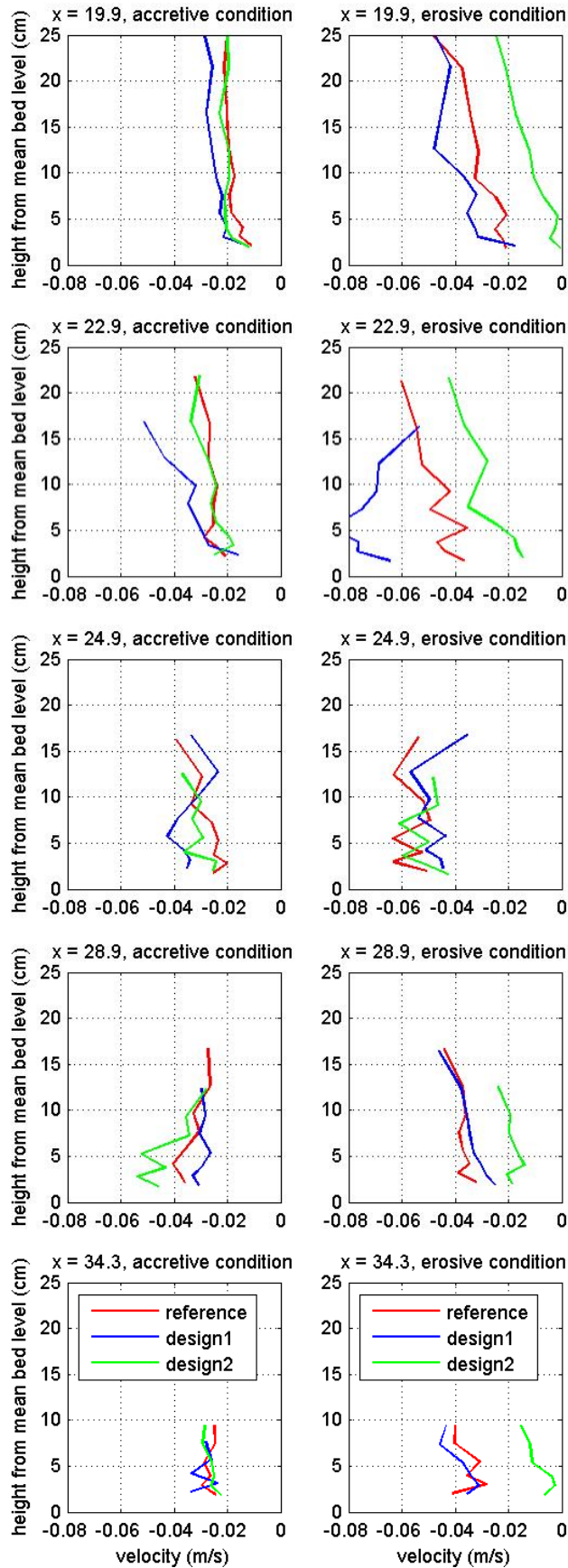


Figure 4.12 On the left, the undertow of the accretive tests, on the right, the erosive tests measured by the EMS

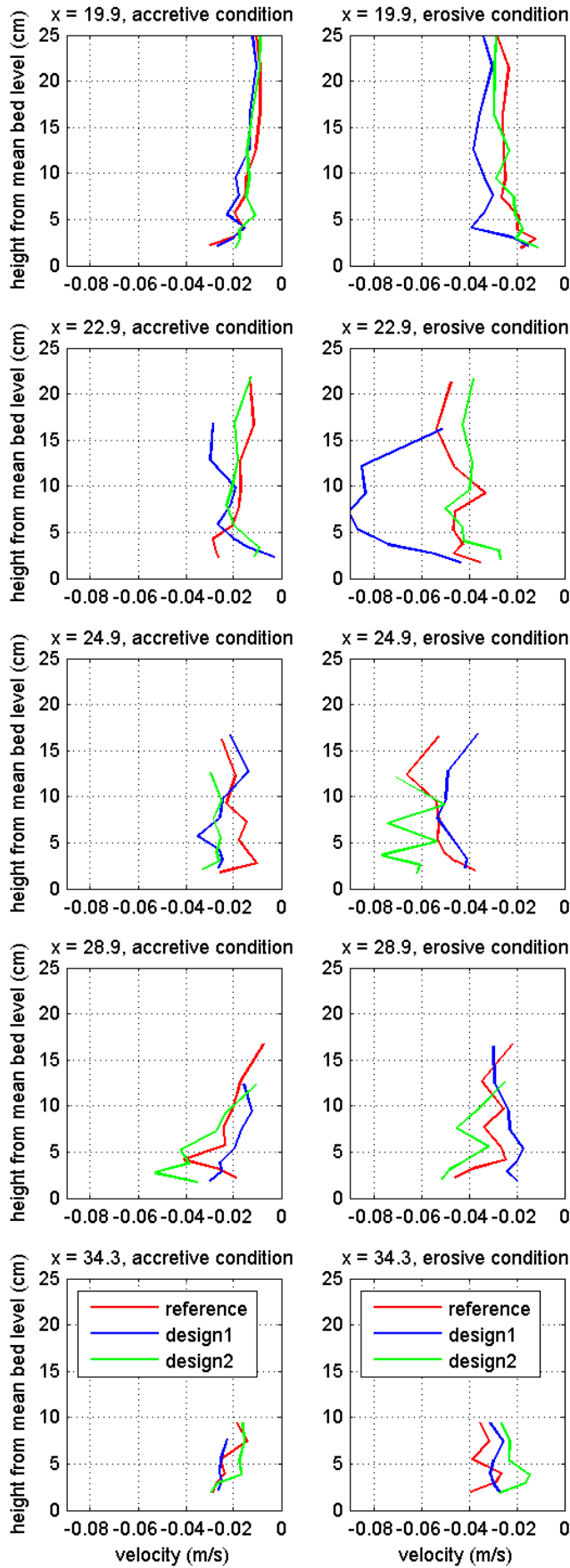


Figure 4.13 On the left, the undertow of the accretive tests, on the right, the erosive tests measured by the ASTM

At 22.9 m, a large difference can be observed between the erosive test with Nourishment Design 1 with the reference test and test with Nourishment Design 2. The flow velocities of the test with Nourishment Design 1 are considerably larger. For this test, waves break slightly more offshore. The large decrease in wave height due to wave breaking results in a large set-up, which in its turn leads to increased flow velocities. For the other tests, i.e. the reference test and the test with Nourishment Design 2, waves break slightly more onshore.

Depth-averaged velocities

To be able to obtain better insight in the behaviour of the flow velocities, all measured velocity verticals are integrated over depth. The method used for this integration is based on a procedure described by Van Rijn (1991, Appendix C).

Error! Reference source not found. shows the depth-averaged velocities of all tests. In the upper plot the tests with an accretive condition (T02, T04 and T06) and in the lower plot the tests with an erosive condition (T03, T05 and T07) can be observed.

Figure 4.15 shows the ratios between the depth-averaged velocities of the tests with a nourishment design and the reference tests. The upper plot gives the ratios of the tests with an accretive condition, the lower plot the ratios of the tests with an erosive condition. Based on the higher waves of the erosive tests T03, T05 and T07, larger undertow velocities are expected with respect to the accretive tests, T02, T04 and T06. This can indeed be observed in the lower plot of **Error! Reference source not found.**

The depth-averaged velocities of all tests lay in a range of approximately -0.07 m/s to -0.01 m/s. For the accretive tests and the erosive tests, the plots shows a higher flow velocity at the location of the shoreface nourishment area. Landwards of the shoreface nourishment area, the flow velocity considerably decreases. For the erosive tests with a nourishment design close to the coastline, at 34.3 m, the flow velocities are smaller compared to the reference test.

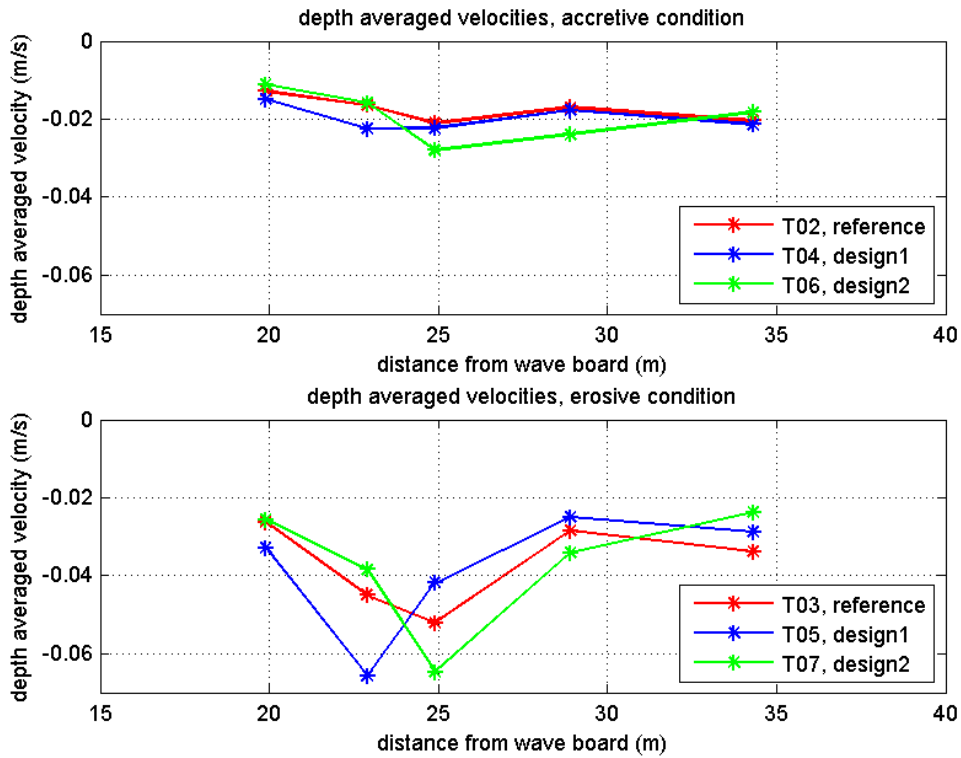


Figure 4.14 Depth-averaged velocities for all tests for the ASTM. The upper plot shows data for the accretive condition, the lower plot for the erosive condition.

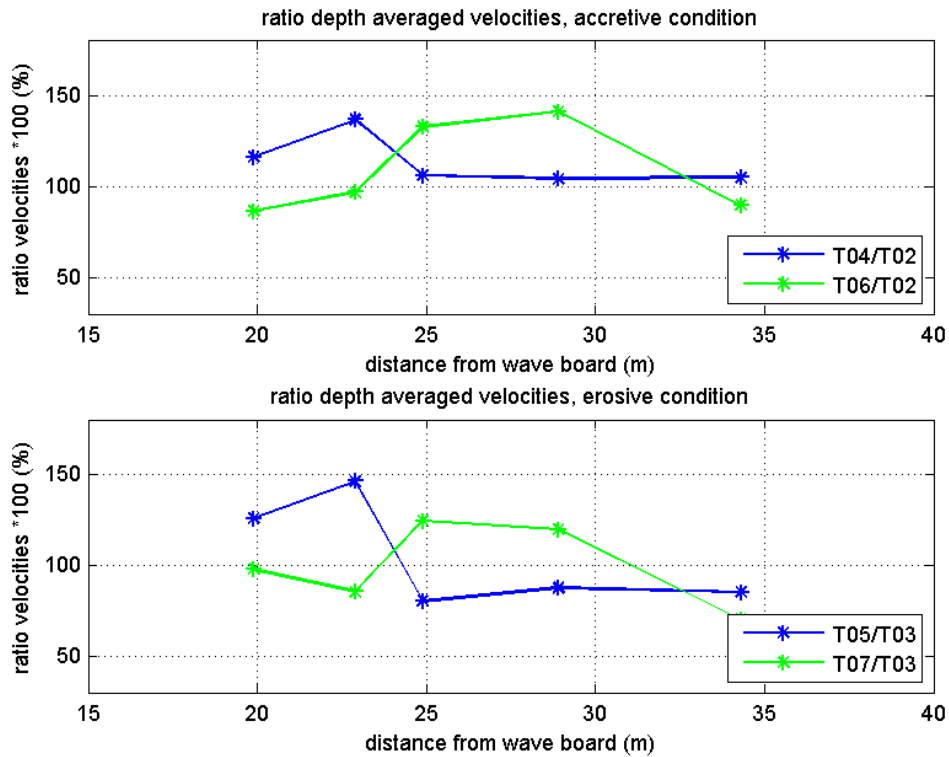


Figure 4.15 Ratio between depth-averaged velocities of nourishment design tests and the reference tests

Another way to derive the depth-averaged flow velocities is by means of the mass flux. The wave-induced mass fluxes have been estimated using Phillips (1977)

$$M_f = \frac{E}{c}, \tag{4.1}$$

in which,

M_f is the total wave-induced mass-flux in kg/m/s

E is the total energy density for a surface wave in kg/s²

c is the velocity of propagation in m/s

The flow velocity can be derived from,

$$u = \frac{M_f}{\rho h} = \frac{E}{\rho h c} = \frac{1}{8} \frac{\rho g H^2}{\rho h \sqrt{gh}} \tag{4.2}$$

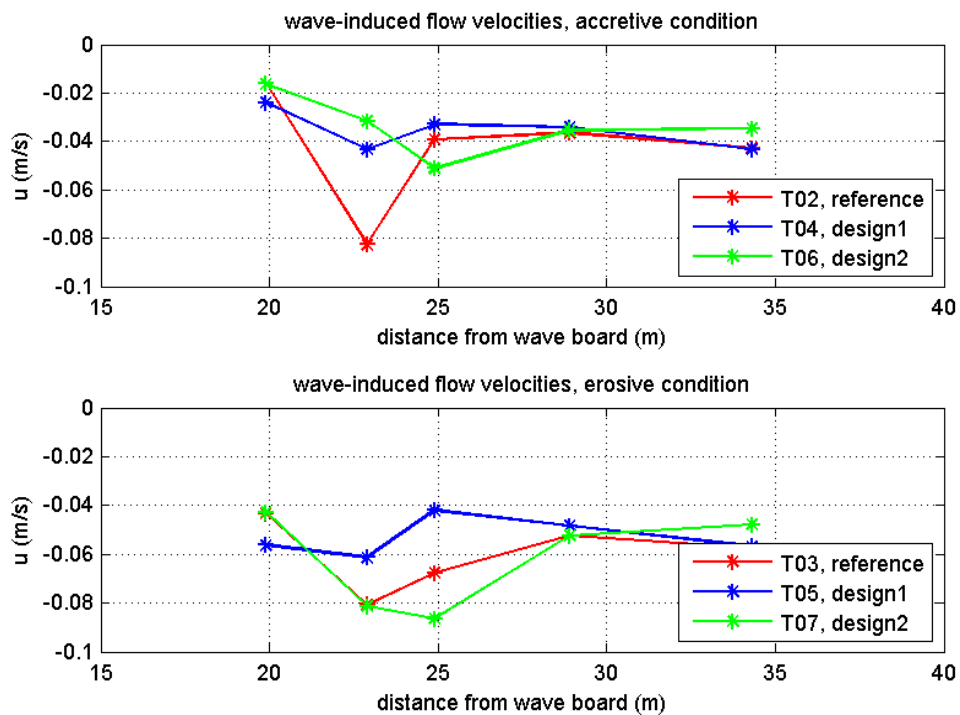


Figure 4.16 Wave-induced flow velocities derived from the wave mass flux (Phillips, 1977). The upper plot shows data for the accretive condition, the lower plot for the erosive condition.

In Figure 4.16, the wave-induced flow velocities derived from the mass flux are shown. All wave-induced flow velocities of the nourishment design tests are smaller or equal to the velocities of the reference tests, except for the velocities of the accretive and erosive test with Nourishment Design 2 at $x = 24.9$ m and the test with Nourishment Design 1 at $x = 19.9$ m.

In addition, it can be observed that close to the coastline at 34.4 m the flow velocities of the tests with Nourishment Design 2 are smaller compared to the flow velocities of the reference tests and the tests with Nourishment Design 1. A decrease in wave-induced flow velocity results in a decrease in offshore sediment transport, leading to less erosion in the coastal zone.

The analysis of the flow velocities and the depth-averaged flow velocities partially substantiates the hypothesis of a decrease of the flow velocity shoreward of the shoreface nourishment as a result of the shoreface nourishment area (lee effect). For the erosive tests, the flow velocities shoreward of the shoreface nourishment are significantly reduced. However, this is not very evident for the accretive tests.

Variance density spectra and velocity moments

The time series of the EMS, closest to the bed level, are analysed by means of a variance density spectra. The one-dimensional variance density spectrum shows how the variance of the oscillatory velocities is distributed over the frequencies of the wave components (Holthuijsen, 2007). The ASTM data are not used, because the blockiness of the signal does not contribute to reliable velocity moments.

From Figure 4.17, Figure 4.18 and Figure 4.19, it can be seen that the initial wave spectrum at 21 m shows a large peak at approximately 0.3 Hz for the accretive tests (T02, T04 and T06) and 0.45 Hz for the erosive tests (T03, T05 and T07). This can be expected, since these values correspond to the wave period of the erosive tests 2.3 seconds and the wave period of the accretive tests 3 seconds.

Another phenomenon can be observed from the figures: the spectra are changing as the distance from the shoreline to the measurement point decreases. The initial large peak, corresponding to the wave period, decreases and at the lower frequencies a rather small peak occurs. The initial peak is referred to as the short wave group (blue line) and the new small peak represents the long waves (red line). In Section 3.6, the release of free waves are discussed in more detail.

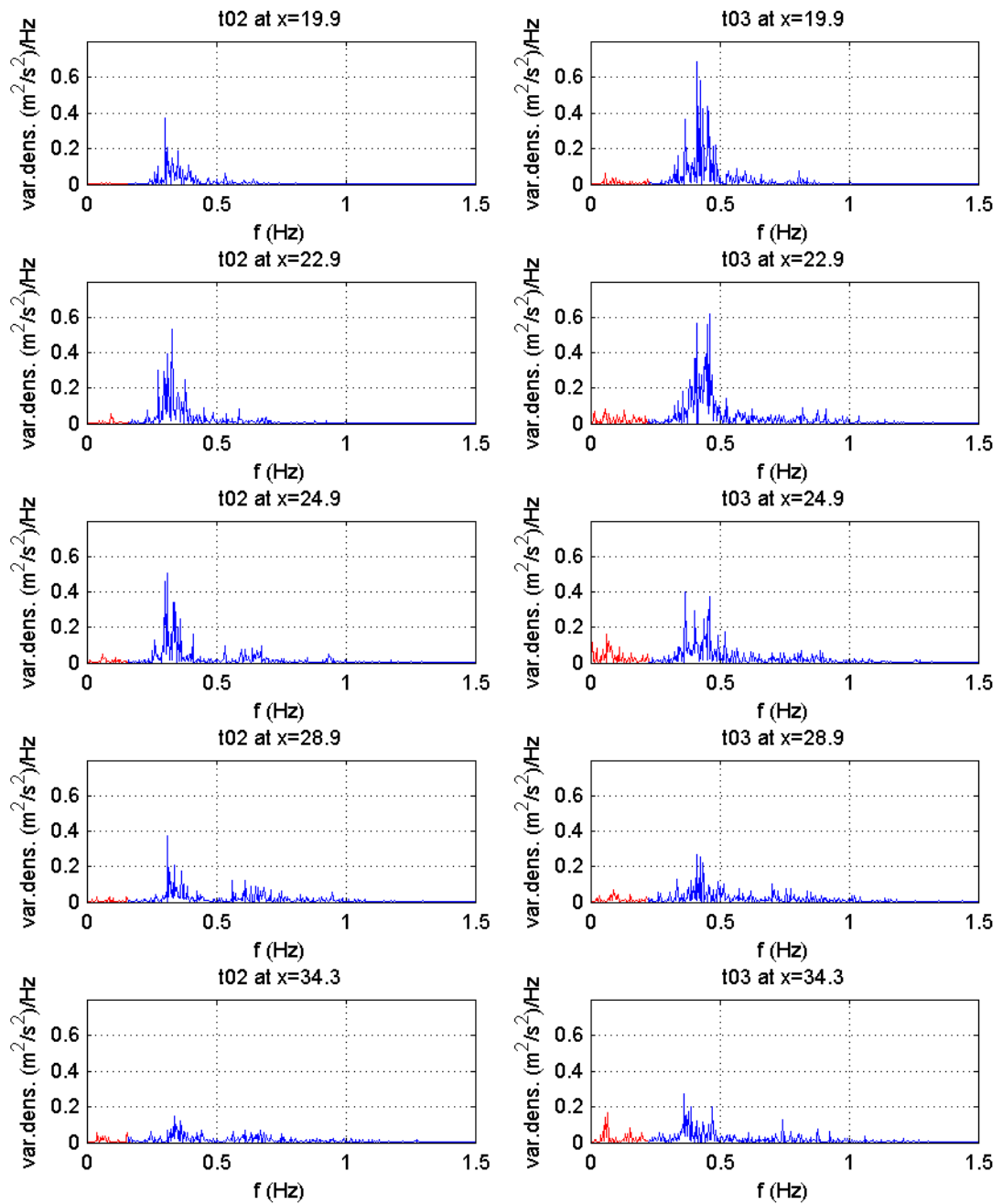


Figure 4.17 Development of the variance density spectrum of T02 and T03, the reference tests. On the left, the accretive test T02 is shown. On the right, the erosive test T03 is shown. The long wave velocities are represented by the red line, the short wave velocities by the blue line.

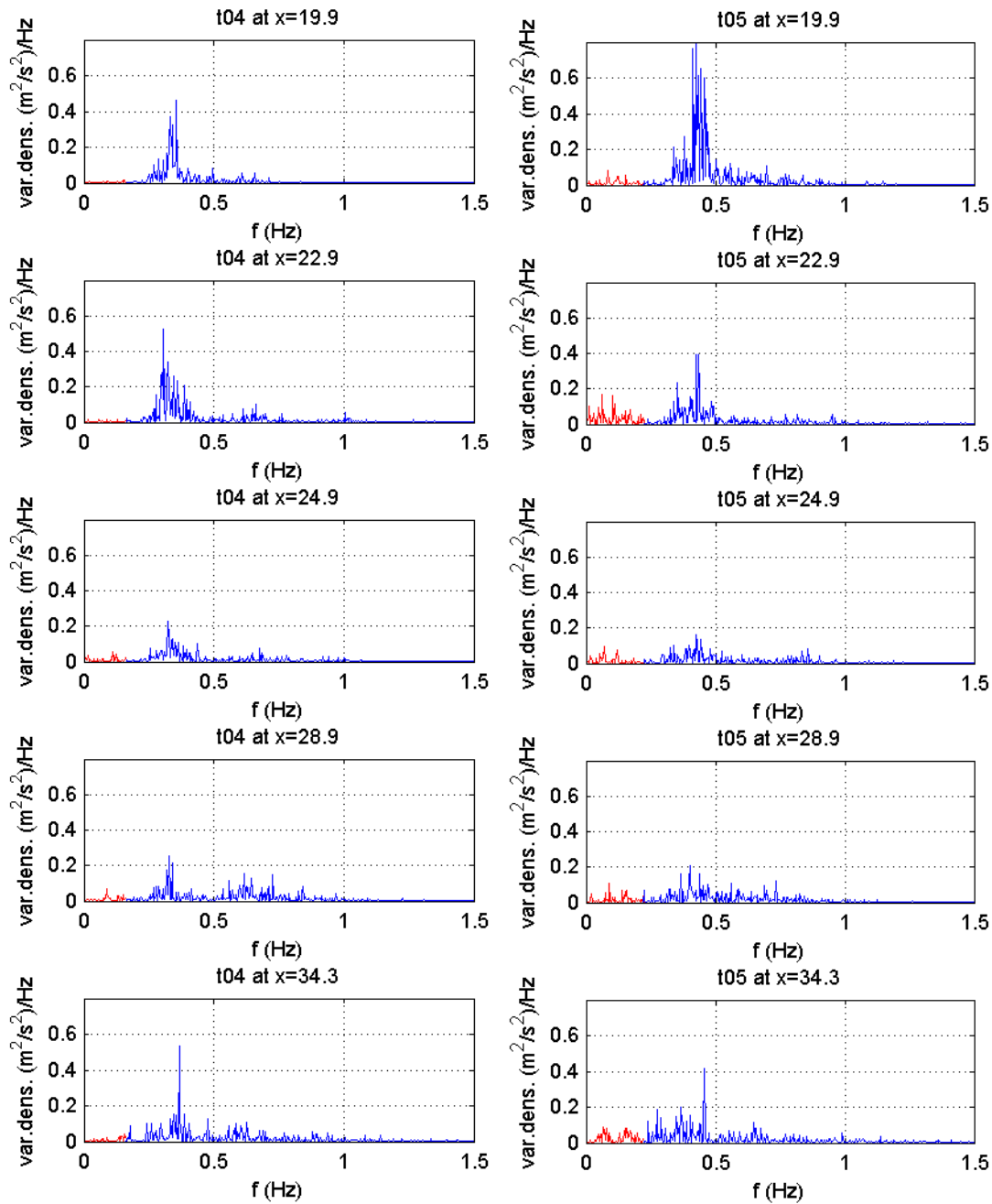


Figure 4.18 Development of the variance density spectrum of T04 and T05, the tests with Design 1. On the left, the accretive test T04 is shown. On the right, the erosive test T05 is shown. The long wave velocities are represented by the red line, the short wave velocities by the blue line.

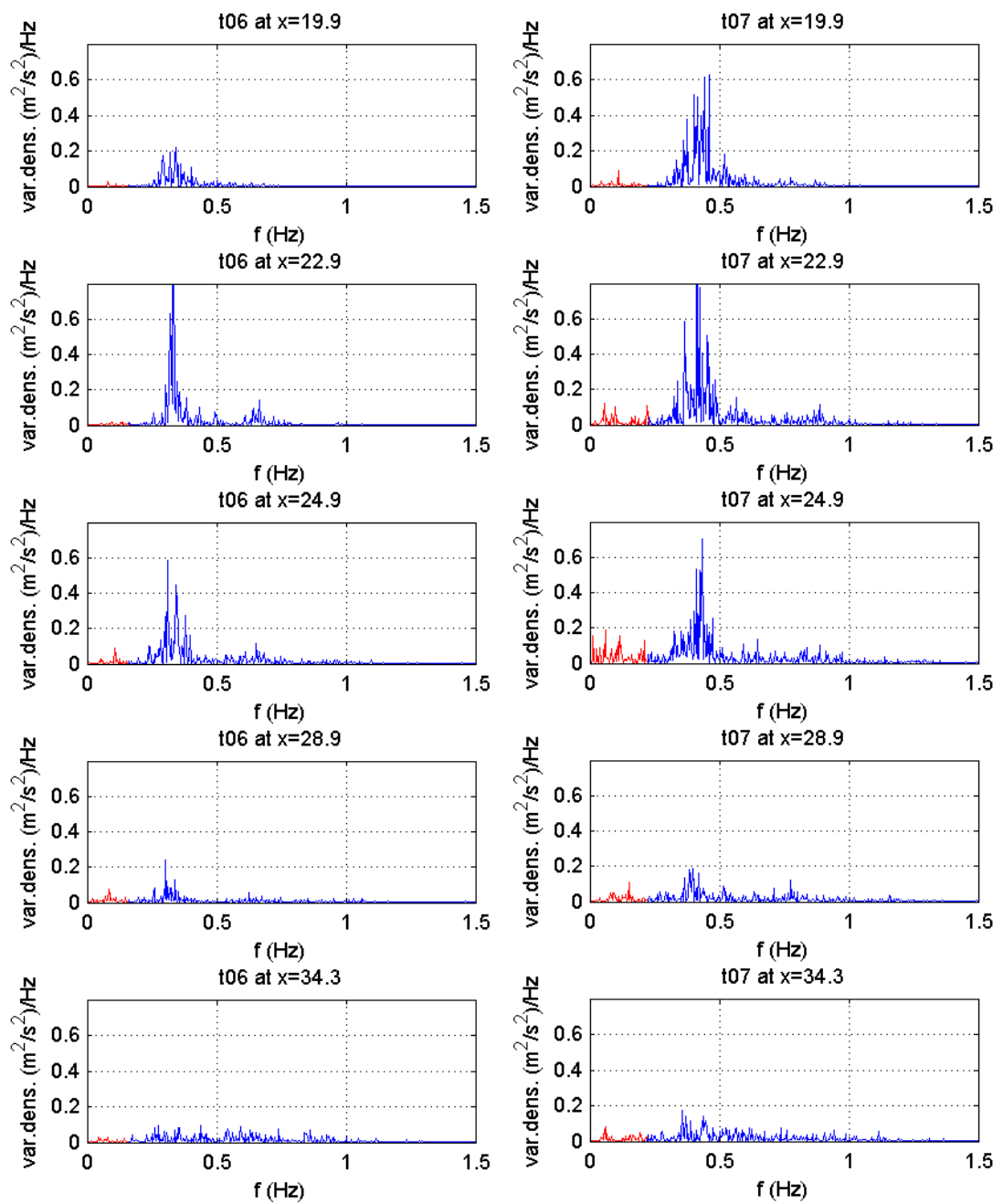


Figure 4.19 Development of the variance density spectrum of T06 and T07, the tests with Design 2. On the left, the accretive test T06 is shown. On the right, the erosive test T07 is shown. The long wave velocities are represented by the red line, the short wave velocities by the blue line.

The time series of the wave velocities are separated in long and short waves in order to analyse the contributions to the third order velocity moments. For discussion on the third order velocity moments and its components *guss* and *guls*, is referred to Section 0. The third order velocity moment is indicated as:

$$\langle \tilde{u} |\tilde{u}|^2 \rangle = \langle u_s |u_s|^2 \rangle + 3 \langle u_L |u_s|^2 \rangle \quad (4.3)$$

In which the two components are referred to as (Roelvink et al):

$$\begin{aligned} guss &= \langle u_s |u_s|^2 \rangle \\ guls &= 3 \langle u_L |u_s|^2 \rangle \end{aligned} \quad (4.4)$$

In Figure 4.20, the development of the *guss* and *guls* along the profile is shown. In addition, the *guss* and *guls* are summed to be able to compare with the third order velocity, computed without separating the time series into long and short wave velocities.

The third order velocity moment can be related to the bed load transport. The skewness, indicative for the third order velocity moments, is characteristic for asymmetry in the wave profile, with systematically larger peaks and shallower troughs. A positive skewness implies a landward bed load transport.

It can be seen that the black and green line agree fairly well. The *guss*, the red line, show positive values, whereas the *guls* show negative values or values close to zero. Thus, the short wave velocity (i.e. *guss*) contributes to a landwards transport, whereas the long wave velocity (i.e. *guls*) contributes to a seawards transport.

For the erosive condition, on top of the high nourishment, the third-order velocity moment are significantly larger than the other two tests. The third order velocity moments close to the coastline are more or less the same. In order to obtain better insight in the effects of the nourishments on the third order velocity moments, the ratios between the results of the tests with nourishment and the results of the reference tests are computed (see Figure 4.21). In this plot, again, the third order velocity moments close to the coastline are more or less the same.

It can be remarked, that close to the coastline, although the third order velocity moments are more or less equal, the wave asymmetries are not equal. This is also related to the wave height. For the reference test, a higher wave height was found in comparison with the nourishment tests. The presence of a shoreface nourishment results in a decrease in wave height. To obtain an equal third order velocity moments for a smaller and a higher wave, the smaller wave must be more asymmetrical.

Therefore, it can be concluded that the hypothesis that the presence of a shoreface nourishment results in an increase in wave asymmetry shoreward of the nourishment, can be substantiated.

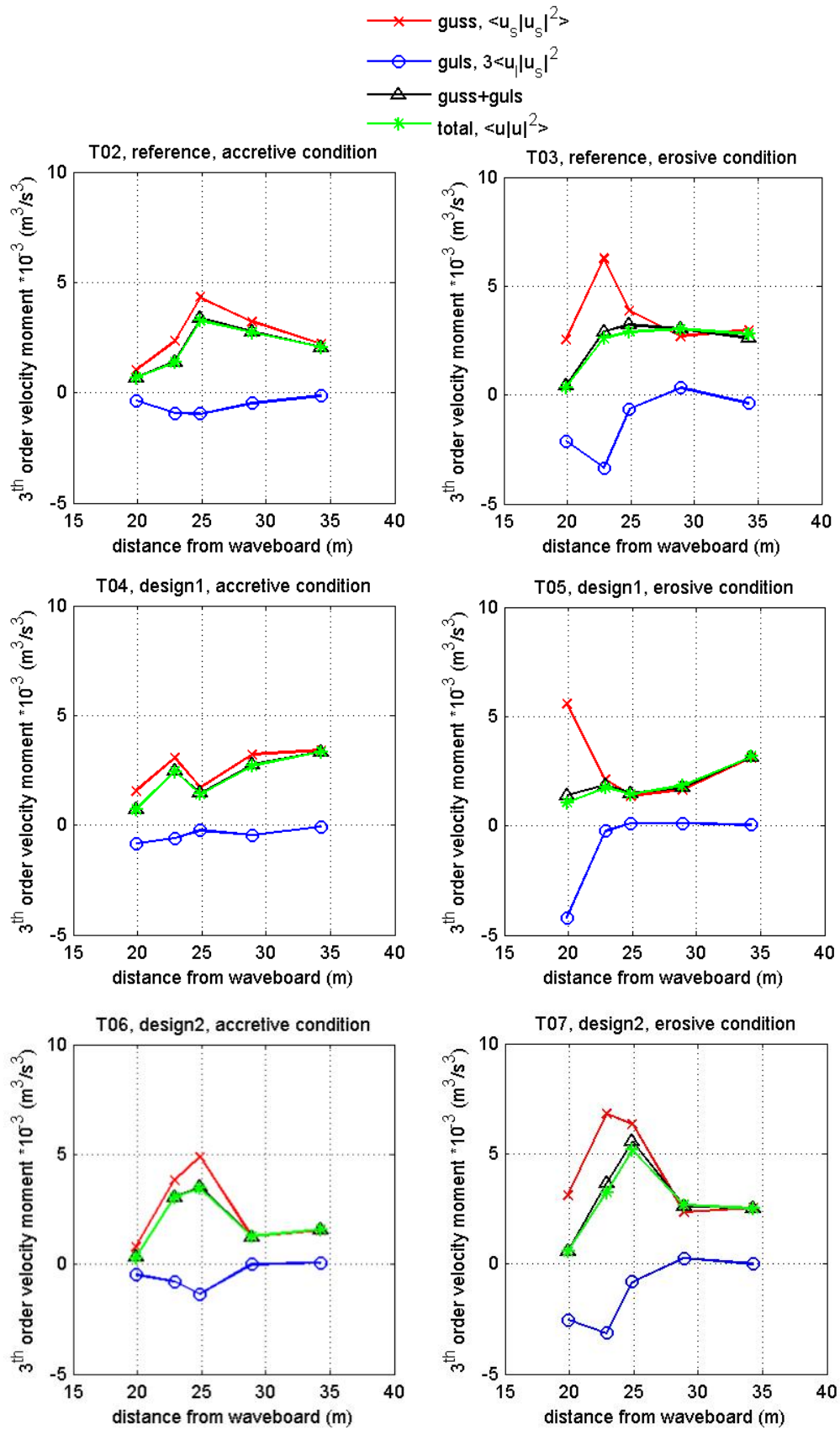


Figure 4.20 Third order velocity moments along the profile, separated in the contribution of the short wave velocities (guss) and the contribution of the long wave velocities (guls). On the left, the accretive tests are shown and on the right, the erosive tests.

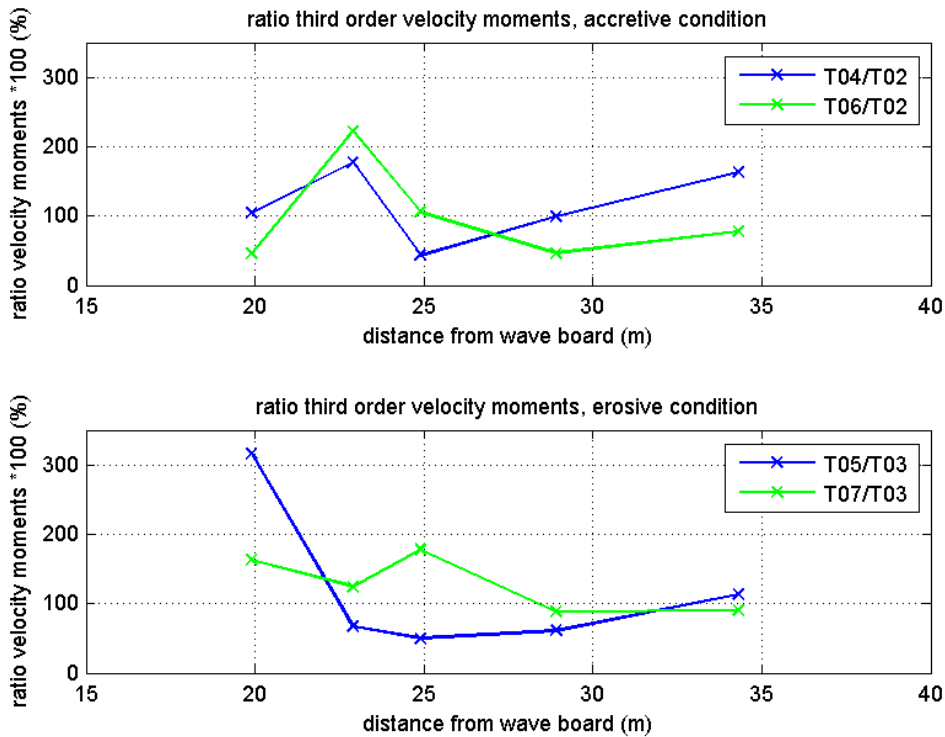


Figure 4.21 The upper plot shows the ratios between the accretive tests with a nourishment design and the reference tests. The lower plot shows the ratios between the erosive tests with a nourishment design and the reference tests.

4.3.3 Concentrations

In this section, the sediment concentration verticals, obtained from the transverse suction system, are analysed in more detail. Similar to the velocity verticals, the concentration verticals of the accretive tests are plotted on the left and the verticals of the erosive tests on the right. Equal measurement positions, i.e. 19.9 m, 22.9 m, 24.9 m, 28.9 m and 34.3 m, are plotted side by side.

Generally, it can be stated that the concentrations of the erosive tests are larger than the concentrations of the accretive tests. At 19.9 m, the concentration verticals of the accretive tests as well as the erosive tests are more or less identical. This can be expected, because at this position, the nourishment designs are not able to affect the concentration.

The erosive tests at 22.9 m and 24.9 m show significant smaller values for Design 1. At these locations, the concentrations of the reference test and test of Design 2 are roughly the same.

Landwards of the nourishment area, a decrease in sediment concentration was expected. It is remarkable that at $x = 28.9$ m, a slightly smaller sediment concentration can be observed for the tests with a nourishment compared to the reference test, whereas closer to the coastline, the opposite occurs. At this point, $x = 34.3$ m, the concentrations of the reference test are smaller than the concentrations of the tests with a nourishment design. This was not

foreseen; it was expected that, due to a decrease in wave height, smaller waves generate less stirring of the sediment, resulting in a decrease in sediment concentration.

These large differences at the bottom of the bed profile can be attributed to the way the sediment concentrations are derived. A transverse suction system, developed by Bosman et al. (1987), is used to measure timeaveraged suspended-sediment concentrations at a height equal to the measuring volume of the EMS, ADV and ASTM. A disadvantage of the method is the laborious sample-handling. The tubes, with an inner diameter of 3 mm, are each connected to a pump. The pump generates a velocity of the water in the nozzle of the suction tube of 1.2 m/s. The pumps extract water and sediment for about 30 minutes, producing about two 10-litre buckets of water and sediment. The extracted volume of water is read from the volume scale on the buckets in which the water and sediment are collected. The suspended sediment samples are flushed in a volume meter tube. Many operations are needed to derive the sediment concentration by means of the transverse suction system.

Research by R.L. Koomans (2000) found that, similar to the findings of Bosman et al. (1987), a statistical uncertainty in the suspended-sediment concentrations of 30% (relative) can be expected, when the transverse suction system is used.

In addition, analysis of the sediment concentration verticals obtained by the transverse suction system for the project SANDS, resulted in a relative error of 27.6%. This is more or less similar to the findings of Bosman et al. (1987) and Koomans (2000).

This could be a reason that no evident conclusions can be drawn with respect to the influence of the presence of a nourishment on the sediment concentration. Hence, considering the sediment concentrations obtained by the suction tubes, the hypothesis, that the addition of a shoreface nourishment to the reference profile results in a decrease in sediment concentration landwards of the nourishment area, can not be substantiated.

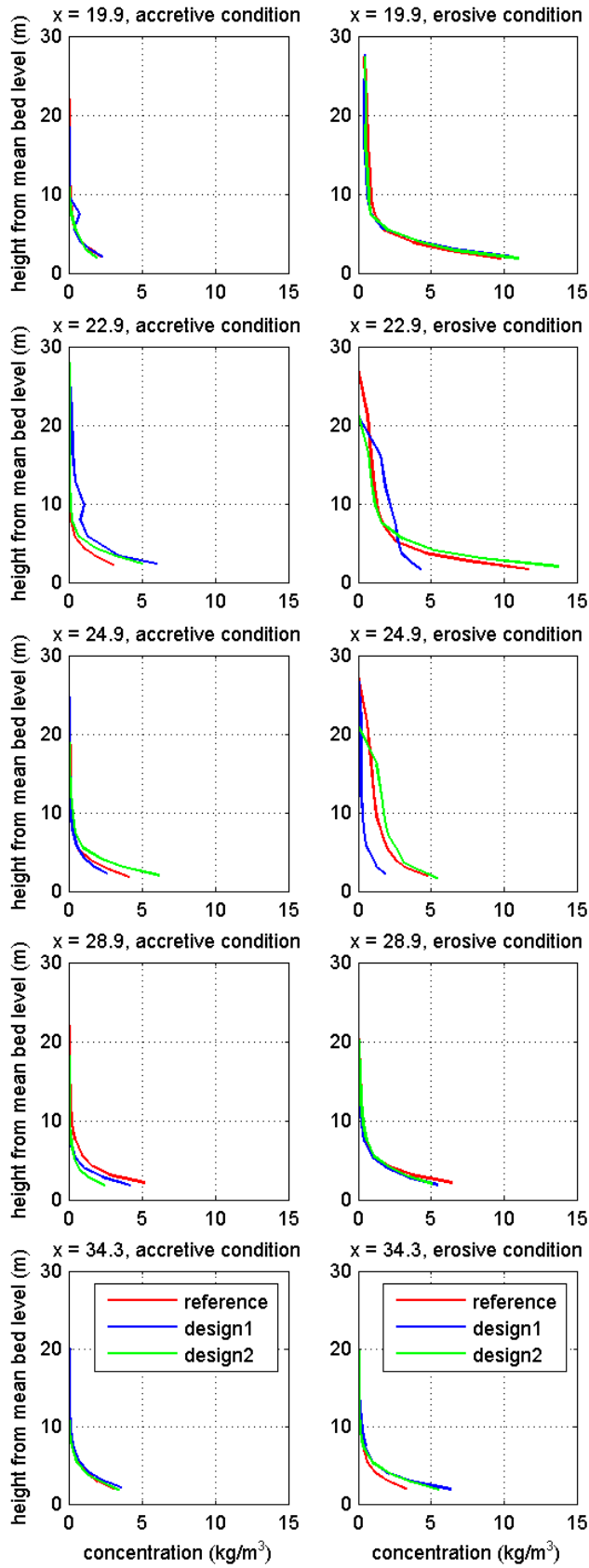


Figure 4.22 On the left, the concentration verticals of the accretive tests, on the right the erosive tests

4.3.4 Sediment transport

Sediment transport is derived from velocity and concentration profiles applying the integral method according to Van Rijn (1991). This method gives the total suspended load transport between the bed and the water surface by fitting a distribution to the measured velocity and concentration profiles.

As already mentioned in Section 3.8.1, three different methods result in three different values of the suspended sediment transport. These values are shown in Figure 4.23. Method 1 and Method 3 are quite similar. Method 2, on the other hand, deviates considerably and is, therefore, omitted in the computation of the sediment transport. The average of Method 1 and Method 3 is used in the analysis. Appendix C extensively describes the three methods of integration.

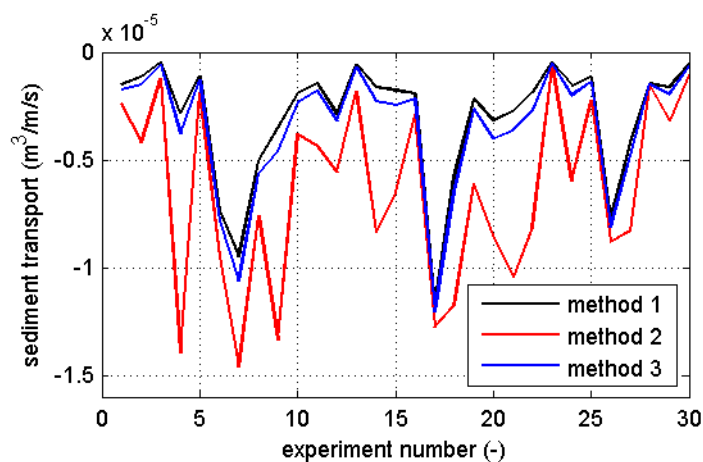


Figure 4.23 Sediment transport using three different methods for all VOP experiments

Standard deviation of the mean values of Method 1 and Method 2 is $2.87 \cdot 10^{-6} \text{ m}^3/\text{m/s}$.

In addition, sediment transports along the flume are derived from bed level change as explained in Section 3.8.2. In Figure 4.24 and Figure 4.25, the values of the sediment transport derived from the velocity and concentration verticals are plotted in the same colour as the corresponding sediment balance derived from bed level change. The dots represent the results of integration of the sediment transport vertical. The solid lines give the mean sediment transports as derived from the change in bed level in the different subtests. The solid lines represent the mean transports over an entire interval between two successive bed profile measurements. The dots represent mean transports only over a certain interval (related to shallow water frame measurements). This may lead to a small overestimation or underestimation of the mean values, dependent on the moment of measurement.

The values of the sediment transport derived from the velocity and concentration verticals are plotted with an error bar. It can be seen that the values of the sediment transport derived from the verticals correspond fairly well with the values derived from the bed level change. Merely, T03 and T05 show different values at the locations 19.9 m and 22.9 m.

This could be due to the fact that the sediment transport derived from the verticals are obtained during approximately one hour, whereas the sediment balance covers the total interval between two bed profile measurements.

In addition, the differences between the two methods can be explained by the fact that sediment transport derived from the bed level change includes all physical processes, which play a role during the model tests (e.g. also wave-induced transports). Sediment transports derived from the verticals are limited in this respect. The method of integration has its influence as well.

The upper plot in Figure 4.24 shows negative values for the sediment transport, with the exception of the coastline. Negative sediment transport corresponds with an offshore sediment transport, positive sediment transport with a landwards transport. It can be seen that, initially, T04 and T06 show landward sediment transport in the vicinity of the nourishment. In the following intervals, this gradually dampens, resulting in a sediment balance similar to the balance of the reference test. However, it can be seen that the sediment transport of T04 at the leeside of the nourishment design is somewhat smaller relative to the sediment transport of T02. This is even more distinct for T06, where the sediment transport in the last interval is less than half of the sediment transport of T02.

The values of the sediment transport of the erosive tests (see Figure 4.25) are in the same order as the sediment transport of the accretive tests. It was expected that the erosive tests would show larger sediment transports. This can be explained, as mentioned before in Section 4.2.1, by the fact that the initial profile is generated by waves of the erosive wave condition.

Conclusions can be drawn for the erosive tests, which are quite similar to the accretive tests. At the leeside of Nourishment Design 1, slightly lower sediment transports can be observed in comparison to the reference test. Implementation of Nourishment Design 2 results in even smaller sediment transports.

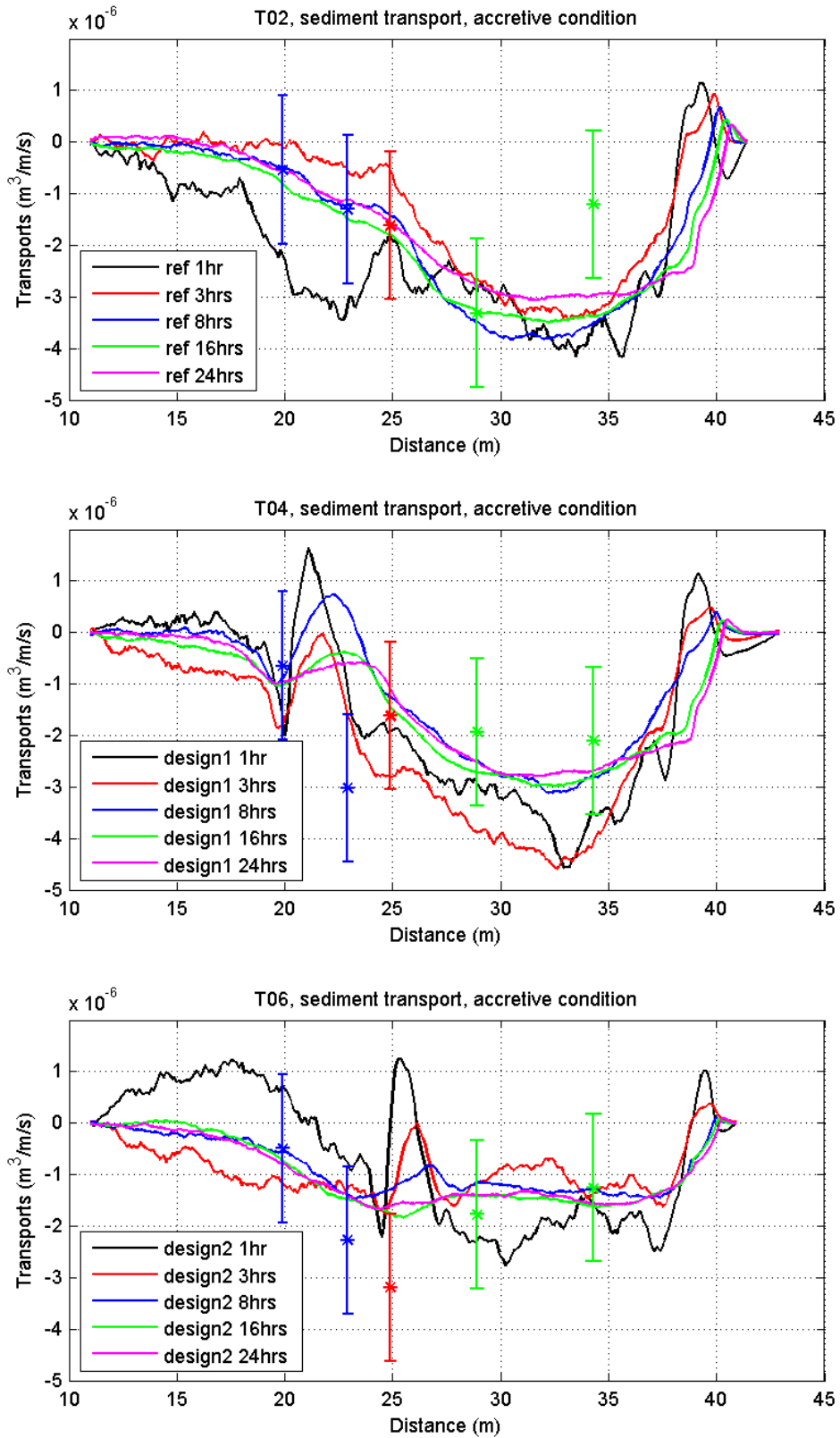


Figure 4.24 Sediment transports (derived from velocity and concentration verticals and derived from bed level change) for the accretive tests T02, T04 and T06

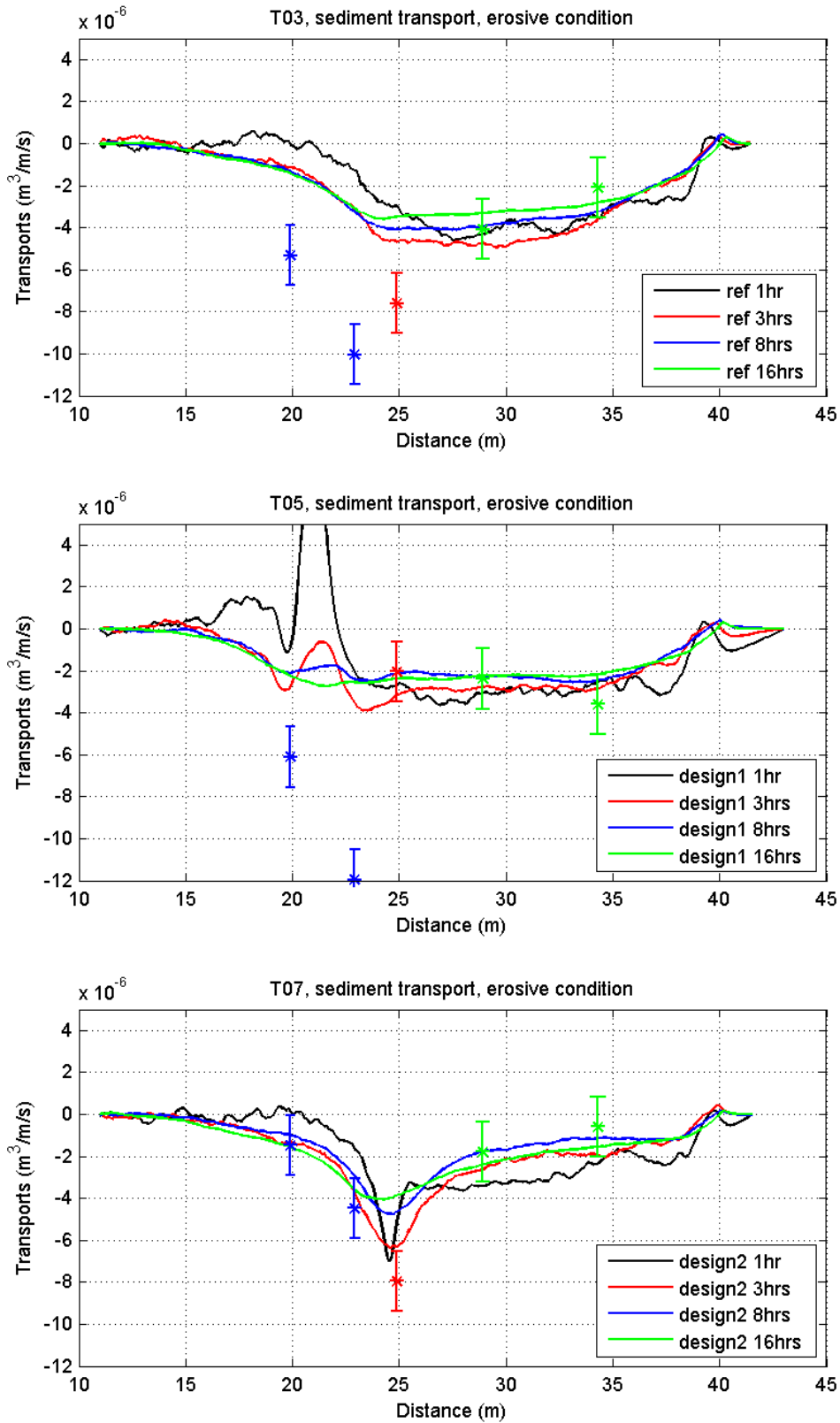


Figure 4.25 Sediment transport (derived from velocity and concentration verticals and derived from bed level change) for the erosive tests T03, T05 and T07

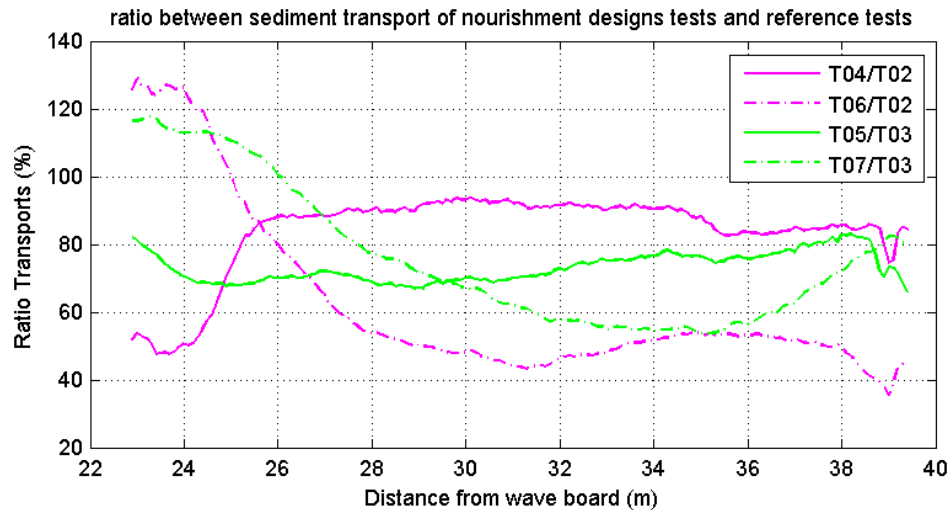


Figure 4.26 Ratio between sediment transport of nourishment design tests and the reference tests. Ratio of test with Design 1 and the reference test (solid lines). Ratio of test with Design 2 and the reference tests (dotted lines).

In Figure 4.26, the ratios between the sediment transport of the nourishment design tests and the sediment transport of the reference tests are shown for the accretive condition and the erosive condition. The pink and green lines correspond with the sediment transports in the last interval in Figure 4.24 and Figure 4.25. The solid lines represent the ratios of the transports of the tests with Nourishment Design 1 and the dotted lines represent the ratios of the transport of the tests with Nourishment Design 2.

This figure supports the conclusions drawn from Figure 4.24 and Figure 4.25. In this ratio analysis the area of interest is limited from 28 m to 38 m. It can be noticed that the ratio between the sediment transport of the tests with Nourishment Design 1 and the sediment transport of the reference tests varies between 70% and 90%. The ratio between the wave height of Nourishment Design 2 and reference tests shows much larger values: 45% - 80%.

The hypothesis, that addition of a shoreface nourishment to the reference profile results in a decrease in sediment transport landwards of the nourishment area, can be substantiated.

4.4 Sediment characteristics

After completion of the reference tests and completion of the tests with Nourishment Design 1, samples of bed sediments are taken at different positions along the flume. The cross-shore distribution of sediments is determined by sieving these samples. As an example, sieved samples of T03 (Figure 4.27) are discussed. The plot shows that coarser material settles in the swash zone. The black line is clearly deviating from the other lines; in particular, D_{90} is significantly bigger. Far offshore, the sediments are finer, resulting in the grey line.

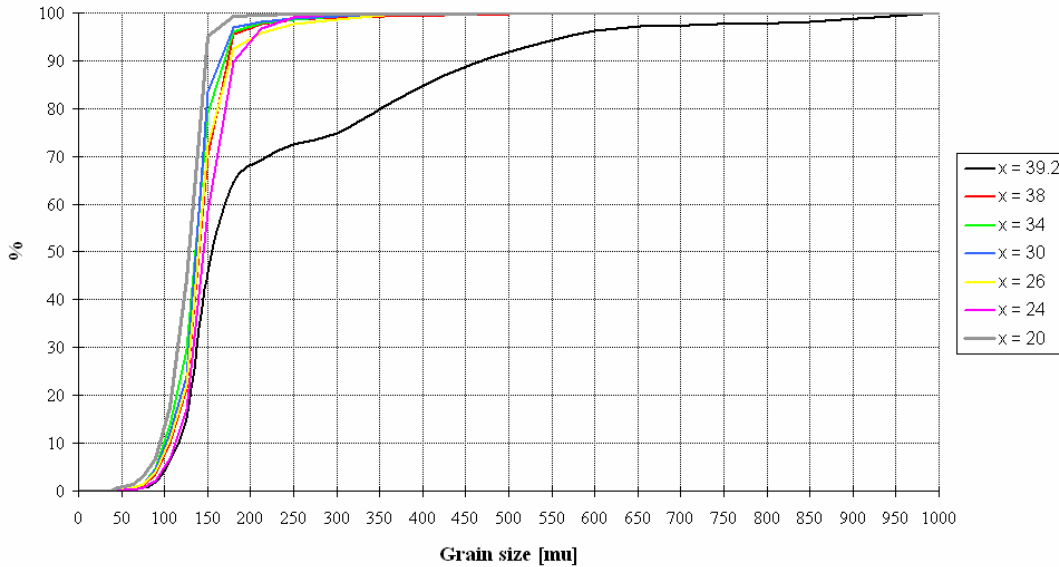


Figure 4.27 Cross-shore distribution of sediments of T03, reference test subject to an erosive condition

In Figure 4.28, bottom profiles are plotted with corresponding grain size distributions. D_{10} , D_{50} and D_{90} imply the grain sizes at which respectively 10%, 50% and 90% of a sample are finer. Once again, it is clearly visible that D_{90} in the swash zone (at $x = 39$) is much bigger compared to all other sample positions along the flume.

In the lower plot, remaining distributions are given in more detail. A remark can be made: on top of the breaker bar of the profiles of T02, T03, T04 and of the test T05 coarser grain size is present compared to neighbouring grain size distributions. A justification for this phenomenon can be the relatively large wave impact on top of the bar. Because of the highly turbulent area, small particles are not able to settle and remain in suspension or settle somewhere else along the profile. Therefore, a slightly coarser grain size can be found on top of the breaker bar.

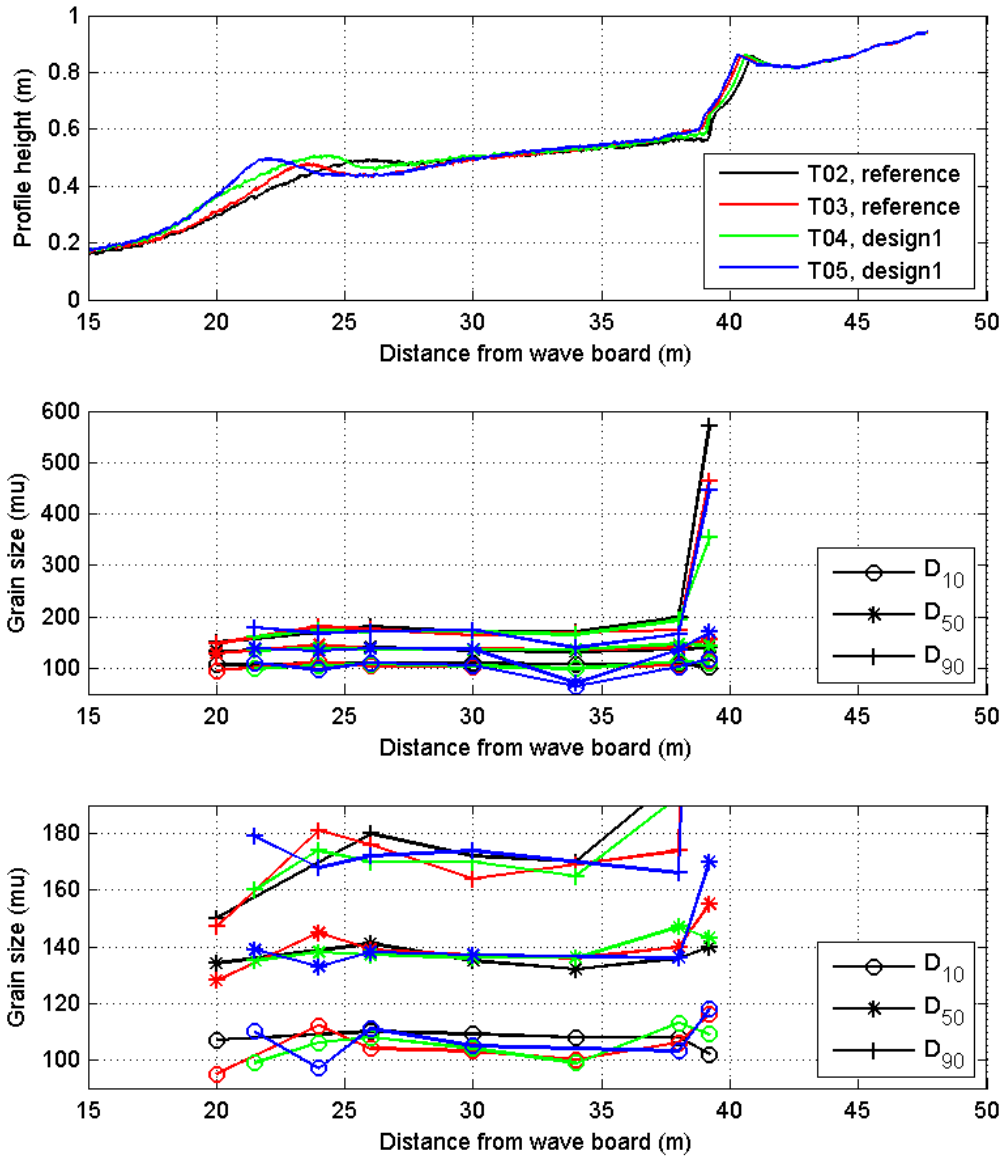


Figure 4.28 Upper plot shows last profile measurements of VOP test T02 up to T05, lower plots indicate distribution of D_{10} , D_{50} and D_{90} along the profile.

4.5 Conclusions

The low Nourishment Design 1, as well as the high Nourishment Design 2, positively affect the bed profile development. Nourishment Design 1 leads to a relative increase of sand volume, 20% for the accretive condition and 40% for the erosive condition. Nourishment Design 2, however, results in the largest relative increase of sand volume, 60% for both wave conditions. It can be concluded that the high nourishment is most effective.

Testing of the hypotheses, stated in Section 4.3, results in an overview of the dominant physical processes that are affected by the nourishment.

The wave height decreases significantly in case of implementation of Nourishment Design 2. Close to the coastline, the ratio between the wave height of the Nourishment Design 1 tests and the reference tests is 95-105%, whereas the ratio between the wave height of the Nourishment Design 2 and the reference tests varies between 80% and 90%.

- The hypothesis that the addition of a shoreface nourishment to the reference profile results in a decrease in wave height is substantiated.

For the erosive wave condition, the flow velocities at the leeside of Nourishment Design 1 and Design 2 are significantly smaller compared to the reference test. This relation is not clear for the accretive tests.

- The hypothesis that the addition of a shoreface nourishment to the reference profile results in a decrease in wave-induced return flow is partially substantiated.

It can be remarked, that close to the coastline, although the third order velocity moments are more or less equal, the wave asymmetries are not equal. This is also related to the wave height. For the reference test, a higher wave height was found in comparison with the nourishment tests. The presence of a shoreface nourishment results in a decrease in wave height. To obtain an equal third order velocity moments for a smaller and a higher wave, the smaller wave must be more asymmetrical.

- The hypothesis that the addition of a shoreface nourishment to the reference profile results in an increase in wave asymmetry is substantiated.

Generally, it can be stated that the concentrations of the erosive tests are larger than the concentrations of the accretive tests. However, considering the measured concentration verticals, it can not be concluded that the sediment concentration is affected by the implementation of the nourishment.

- The hypothesis that the addition of a shoreface nourishment to the reference profile results in a decrease in sediment concentration is not substantiated.

Landwards of the nourishment, the ratio between the sediment transport of the tests with Nourishment Design 1 and the sediment transport of the reference tests varies between 70% and 90%. The ratio between the wave height of Nourishment Design 2 and reference tests shows much larger values: 45% - 80%.

- The hypothesis that the addition of a shoreface nourishment to the reference profile results in a decrease in sediment transport is substantiated.

It can be concluded that the presence of a shoreface nourishment significantly affect the wave height, the wave-induced return flow, wave asymmetry and the sediment transport, whereas the presence of shoreface nourishment does not have a clear relation with the sediment concentration. The implementation of a nourishment results in a decrease in wave height, a decrease in wave-induced return flow, an increase in wave asymmetry and a decrease in sediment transport. Furthermore, these processes are strongly connected. A reduced wave height leads to a reduced return flow, which in its turn leads to a reduced sediment transport.

The presence of a shoreface nourishment has a combined relative effect. On one hand, the shoreward sediment transport is reduced due to the decreased wave-induced return flow. On the other hand, the landward sediment transport is increased because of an increased wave asymmetry.

The presence of the high nourishment and the low nourishment both positively affect the bed profile development. The high nourishment, however, is far more effective than the low nourishment. An important aspect in the design of a nourishment seems to be the height of the nourishment. This can be explained by the fact that, due to the presence of the high nourishment, also smaller waves are not able to pass the breaker zone and break already on top of the nourishment instead of closer to the coastline.

Analysis of the samples of the bed sediments taken at different positions along the flume, showed that on top of the breaker bar of the profiles of the reference tests and tests with the low nourishment, a slightly coarser grain size is present compared to the grain size adjacent to the breaker bar.

5 Comparison UNIBEST-TC and test results

5.1 Introduction

In this chapter, the UNIBEST-TC model is applied to simulate the physical model tests focussing on the physical processes involved in implementation of a shoreface nourishment. The effects of the shoreface nourishments are analysed in a similar way as in Section 4.3.

The computational set-up is described in Section 5.2 and the calibration procedure in Section 5.3.

In Section 5.4, the modelled and measured wave heights, flow velocities, sediment concentrations and sediment transports are discussed. Furthermore, the bed profile development according to UNIBEST-TC and the measured bed profile development are compared.

5.2 Computational set-up

This section describes the UNIBEST-TC model. UNIBEST-TC stands for UNIFORM Beach Sediment Transport – Time dependent Cross-shore. For this study version 2.04 is used.

The model can be divided into five sub models. The scheme in Figure 5.5 shows how these sub models interact with each other. In one time step UNIBEST TC computes first the local wave height according to wave height decay model ENDEC (Battjes and Janssen, 1978). From the local wave height, the orbital velocity and mean current are computed. Subsequently separate transport formulations are used for bed load transport and suspended transport. Finally, bottom changes are computed using a sediment mass balance equation, resulting in a new profile, which is used in the next time step.

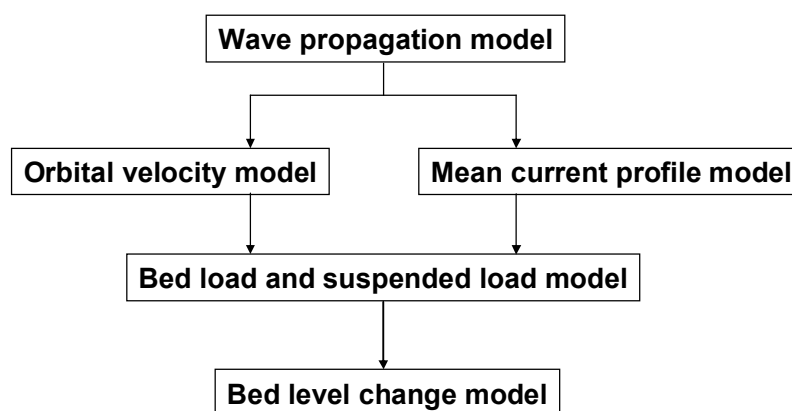


Figure 5.1 Set-up of model UNIBEST-TC

The model requires an initial profile, grain sizes and offshore boundary conditions.

For a short description of the sub-models is referred to Appendix D, for a more complete description and background of the model is referred to Bosboom et al. (2000).

5.2.1 Input

To make a proper comparison between UNIBEST-TC and the physical model tests it is necessary to generate model input which represents as good as possible the actual situation in the flume. Assuming a certain grid for each test an initial profile can be generated based on the profile measurements. With these cross-shore profiles, simulations have been carried out.

Table 5.1 gives an overview of the default run parameters and the chosen values. The parameters that differ from default are described below.

Table 5.1 Run parameters

Run Parameter	Symbol	Description	Default value	Chosen value	Unit
'DT'	dt	Time step	2.0	0.01	days
'NT'	Nt	Number of time steps	5	66/100	-
'USTRA'		User defined transport rate at the last computational grid point	0	0	m ³ /h
'JFR'		Frequency of output (JFR = 10 means once per 10 time steps)	1	1	-
'IBOD'		Morphodynamic switch	1	1	-
'ALFAC'	α	Wave breaking parameter for use in dissipation formulation according to Battjes & Janssen (1978)	1.0	1	-
'GAMMA'	γ	Wave breaking parameter to determine maximum local wave height	0.00	0.00	-
'BETD'		Roller parameter according to Nairn et al. (1990), expressing the steepness of the wave front	0.1	0.1	-
'FWEE'	f_w	Friction factor for wave dissipation due to bottom friction. The default value is obtained from Delta Flume experiments	0.01	0.01	-
'K_IJL'		Breaker delay switch	1	1	-
'TANPHI1'		Internal friction angle at location XF1; computed bed load transport rates are corrected for the local bottom slope, as a function of the local angle of internal friction ϕ	0.03	0.15	-

'TANPHI2'		Internal friction angle at location XF2	0.10	0.6	-
'XF1'		Reference location for TANPHI1 (most seaward)	500.0	15	m
'XF2'		Reference location for TANPHI2 (most shoreward)	1200.0	22	m
'D50'	D ₅₀	grain size of bed material	0.20*10 ⁻³	130	m
'D90'	D ₉₀	grain size of bed material	0.30*10 ⁻³	160	m
'DSS'		D ₅₀ of suspended sediment	0.17*10 ⁻³	100	m
'DVAR'		Cross-shore varying grain size switch: linearly varying sediment sizes cross-shore, according to the diameter multiplication factors FDIA# at reference depths HDIA#	0	0	-
'FCVISC'	α _w	Viscosity coefficient of vertical velocity profile	0.1	0.1	-
'RKVAL'		Friction factor for mean current computation	0.01	0.02	m
'DIEPV'		Referene depth for tidal velocity	5.0	5.0	m
'REMLG'		Layer over which the sediment transport is reduced to zero in case of a fixed bed	0.10	0.10	m
'RC'		Current related roughness for sediment transport computation, the default value is obtained from Delta flume experiments	0.01	0.06	m
'RW'		Wave related roughness for sediment transport computation, the default value equals RC	0.01	0.06	m
'TEMP'		Temperature of the water	10.0	10.0	°C
'SALIN'		Salinity of the water	0.0	0.0	‰
'C_R'		Correlation coefficient between wave envelope and bound long waves; varies from -C_R at deep water up to +C_R at the shore line	0.25	0.25	-
'FLAM'		Number of wave lengths over which weighted depth is integrated.	2	0.5	-

5.3 Calibration procedure

Calibration of UNIBEST-TC is a calibration of its sub-models, described in Appendix D. First, the hydrodynamic modules (waves and flow) are calibrated followed by the morphological modules (sand transport and bottom changes).

In order to estimate the degree of interrelation between the measured and modelled results, the correlation coefficient is introduced. The correlation coefficient implies the ratio of the covariance of two variables to the product of their standard deviations (Davis, 2002):

$$r_{ab} = \frac{\text{COV}_{ab}}{S_a S_b} \quad (4.5)$$

A correlation of +1 indicates a perfect direct relationship between the two variables. A correlation greater than 0.8 is generally described as strong, whereas a correlation less than 0.5 is generally described as weak.

5.3.1 Calibration of wave model

The breaker index GAMMA is set to the default value according to Battjes and Stive (1985):

$$\gamma = 0.5 + 0.4 \tanh(33s_0) \quad (4.6)$$

The strongest correlation between the measured and modelled wave height is found with a FLAM value of 0.5 (see Figure 5.2). Application of these settings result in a considerably strong correlation coefficient of 0.99.

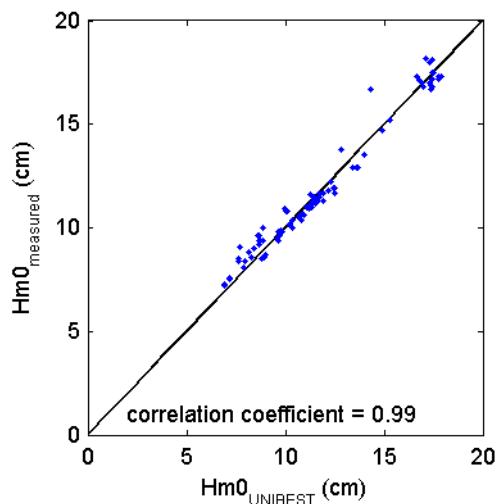


Figure 5.2 Scatter plot modelled wave height versus measured wave height

5.3.2 Calibration of flow model

The correlation between the measured velocities and the velocities obtained by UNIBEST-TC is strongest when the parameter FCVISC is set on default value, 0.01, and FACDF on 1. Applying these settings, the correlation coefficient is 0.80. For the flow velocities, this correlation coefficient is considered relatively high.

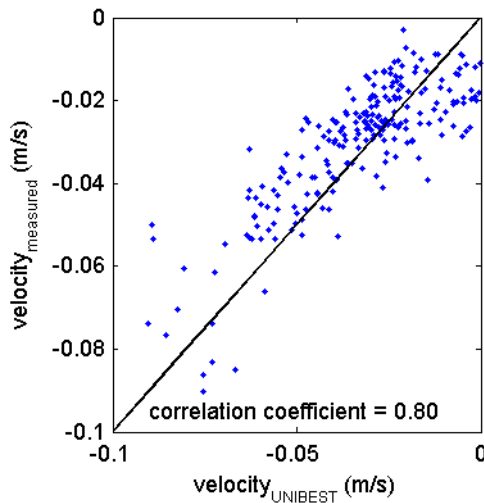


Figure 5.3 Scatter plot modelled velocities versus measured velocities

5.3.3 Calibration of concentrations

The current and wave-related roughness heights (RC and RW) are both set on 0.07 m. This value is relatively high. Lower values of the roughness parameters results in very small concentrations or even concentrations equal to zero.

By increasing the roughness parameter, the Chezy coefficient is lowered, leading to an increase in bed shear stress and in concentration.

The correlation between the measured and the modelled values is very strong. In Figure 5.4, it can be seen that UNIBEST-TC can not properly simulate the high concentrations measured in the flume.

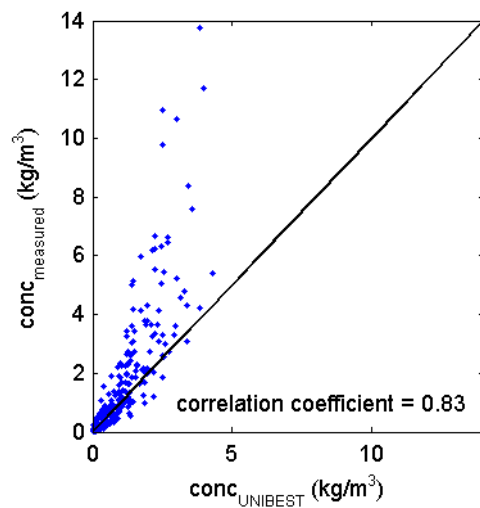


Figure 5.4 Scatter plot modelled concentrations versus measured concentrations

5.4 Comparison UNIBEST-TC and physical model tests

5.4.1 Wave height

In Figure 5.5, the modelled wave height is represented by the solid lines. The measured wave height corresponds with the dotted lines. In the upper plot the accretive tests are shown and in the lower plot the erosive tests are shown. It can clearly be seen that the modelled wave height development along the flume is very similar to the measured wave height development. This could be expected from the high correlation coefficient found between the measured and modelled wave heights. This coefficient amounts to 0.99 (see 5.4.1).

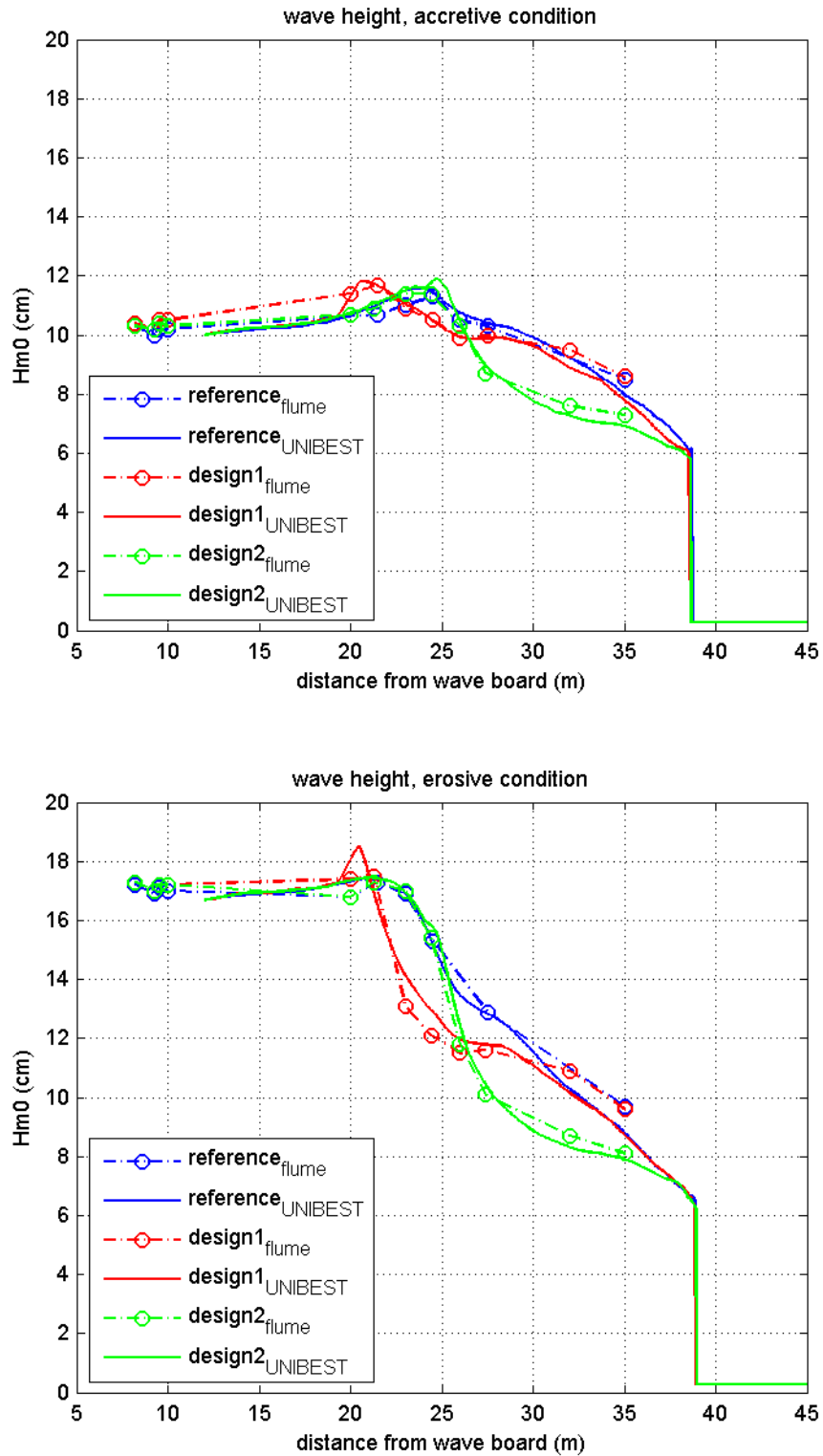


Figure 5.5 Measured (dotted lines) and modelled (solid lines) wave height development. The upper plot shows the accretive tests, the lower plot the erosive tests.

5.4.2 Flow velocities

In Figure 5.6, the modelled flow velocities are represented by the solid lines. The measured flow velocities correspond with the dotted lines. The left plots show the accretive tests and the right plots show the erosive tests. The tests, carried out at equal positions, are plotted side by side.

At some points, the modelled flow velocities correspond fairly well with the measured velocities. This accounts for the velocity verticals of the erosive tests at 19.9 m and 22.9 m and the velocity verticals of the accretive tests at 24.9 m.

However, at other points, the modelled flow velocities considerably differs from the measured flow velocities. This is applicable for the velocity verticals of the erosive tests at 24.9 m and 28.9 m. Here, the flow velocities of the test with Nourishment Design 2 are considerably over estimated, which suggests an over estimation of the sediment transport around these locations; hence, just shoreward of the breaker bar.

The correlation coefficient found for the flow velocities amounts to 0.7. (see 5.4.2).

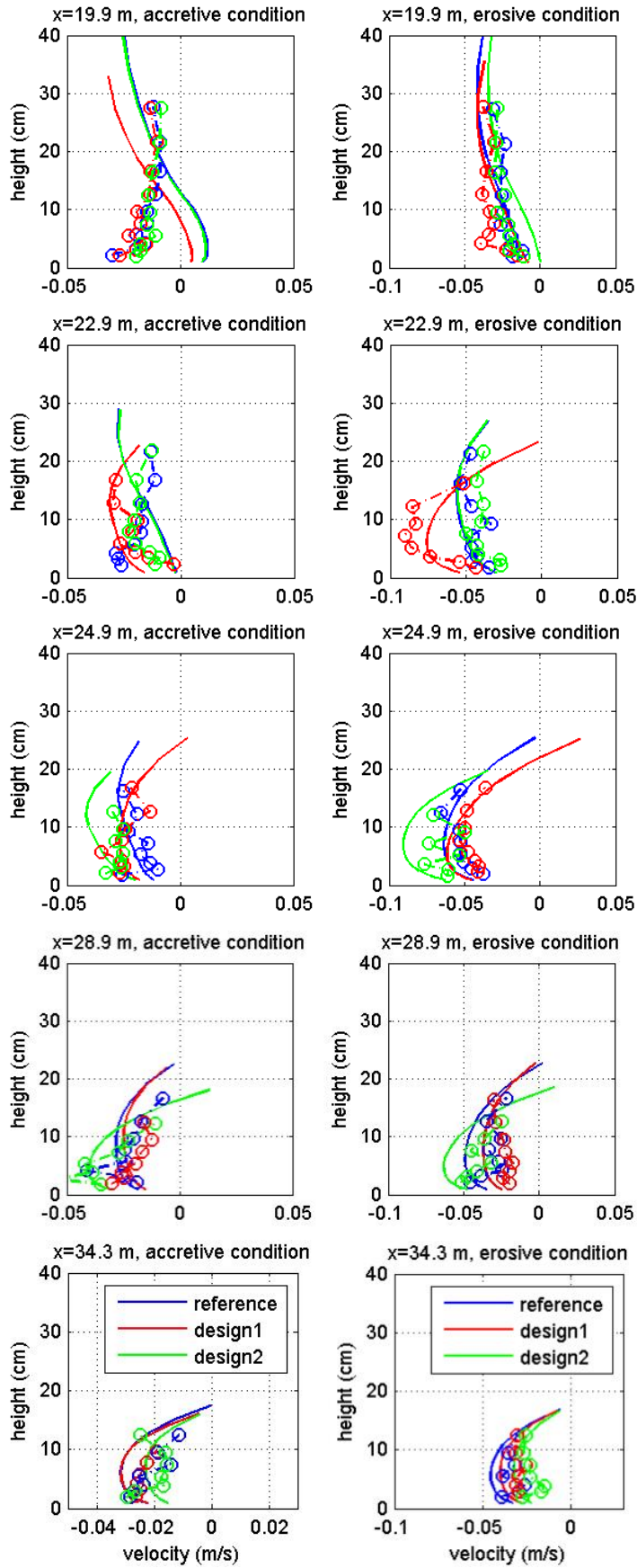


Figure 5.6 Measured (dotted lines) and modelled (solid lines) flow velocities

5.4.3 Concentrations

The sediment concentrations obtained by the transverse suction system are compared to the modelled concentrations. The correlation coefficient between the measured and modelled concentrations was found to be 0.83. The correlation is very strong.

In Figure 5.7, the modelled sediment concentrations are represented by the solid lines. The measured sediment concentrations correspond with the dotted lines. The left plots show the accretive tests and the right plots show the erosive tests. The tests, carried out at equal positions, are plotted side by side.

The modelled sediment concentrations corresponds fairly well with the measured sediment concentrations. Especially in the upper measuring points, they are very much alike. However, close to the bottom, the modelled sediment concentrations are considerably underestimated. This accounts for all tests.

This under estimation of the sediment concentrations close to the bottom could have a large effect on the sediment transports. This will be analysed in Section 5.4.4.

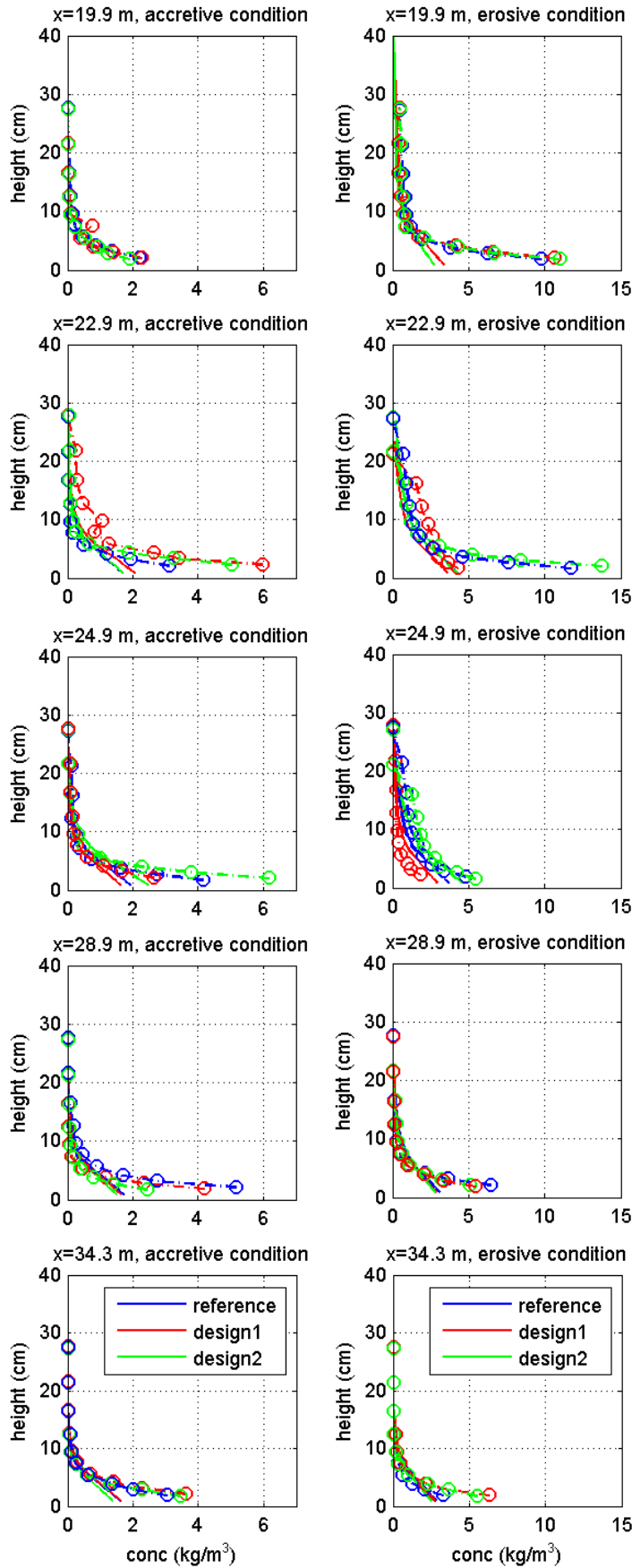


Figure 5.7 Measured (dotted lines) and modelled (solid lines) sediment concentrations.

5.4.4 Sediment transport

In Figure 5.8 and Figure 5.9, the modelled sediment transports are represented by the solid lines. The measured sediment transport corresponds with the dotted lines and are derived from bed level change. Figure 5.8 shows the accretive tests and Figure 5.9 shows the erosive tests.

UNIBEST-TC largely underestimates the sediment transport, especially for the accretive tests. In addition, onshore sediment transport is observed in the surf zone, whereas offshore sediment transport is measured.

This could be explained by the underestimation of the sediment concentrations. It was observed that close to the bottom the concentrations are largely underestimated. Close to the bottom, the flow velocities are relatively large and directed offshore. As a result, a considerable underestimation of the offshore directed sediment transport occurs.

Another explanation for the underestimation of the sediment transport, is an overestimation of the landward transport by wave asymmetry.

For the erosive tests, the relative position of the peaks of the transports are quite good. They should be positioned somewhat more onshore.

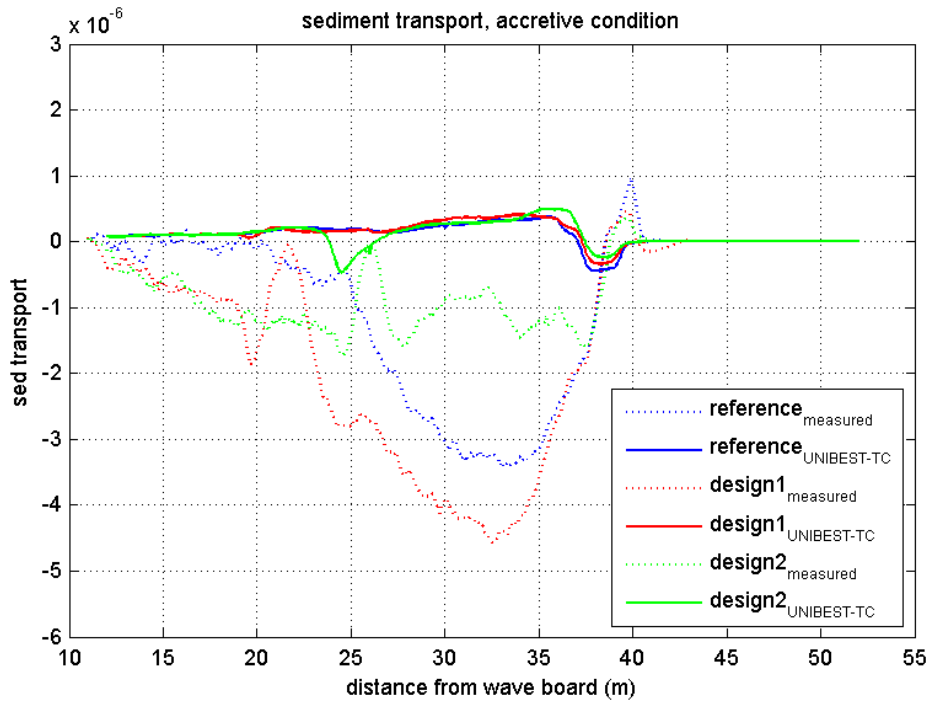


Figure 5.8 Measured (dotted lines) and modelled (solid lines) sediment transports for the accretive tests

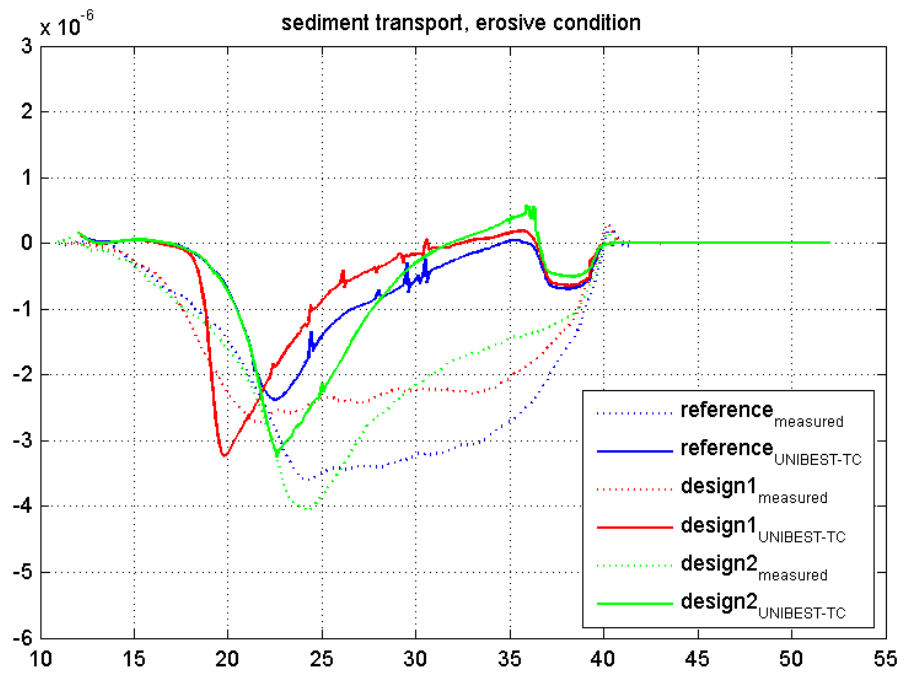


Figure 5.9 Measured (dotted lines) and modelled (solid lines) sediment transports for the erosive tests

5.4.5 Bed profile development VOP

In Figure 5.10 and Figure 5.11, the modelled and measured bed profile development is shown. The black line represents the initial profile. The blue line is the measured profile at the end of the test, whereas the red line is the modelled profile at the end of the test.

Figure 5.10 shows the accretive tests and Figure 5.11 shows the erosive tests. As already discussed in Section 5.4.4, the onshore directed sediment transports are overestimated. Near the shoreline, less sediment has been eroded compared to the measured tests. Just before $x = 38$ m, even accretion is observed. The height of the modelled breaker bar is much smaller compared to the measured breaker bar. This accounts for the erosive tests as well as the accretive tests.

It could be possible that, although the bed profile development isn't simulated properly, the measured effects of the presence of a shoreface nourishment could be similar to the modelled effects. Therefore, the erosion volumes in the range from 32 m to 47 m are computed (see Table 5.2).

For the erosive condition, the erosion volume is smaller for the tests with Nourishment Design 1 and Nourishment Design 2 compared to the erosion volume of the reference test. Regarding the modelled erosion volumes, Nourishment Design 2 is most effective, as was found with the measured data. The accretive tests, however, show a different behaviour. Design 2 has the smallest deposition volume, whereas Design 1 has the largest deposition volume. It can be said that the erosion/deposition volumes are not properly simulated by UNIBEST-TC.

Table 5.2 Erosion/deposition volumes

accretive test	erosion/deposition volume (m^3/m)	erosive test	erosion/deposition volume (m^3/m)
T02	+ 0.0435	T03	- 0.0252
T04	+ 0.0518	T04	- 0.0042
T06	+ 0.0419	T05	+ 0.0014

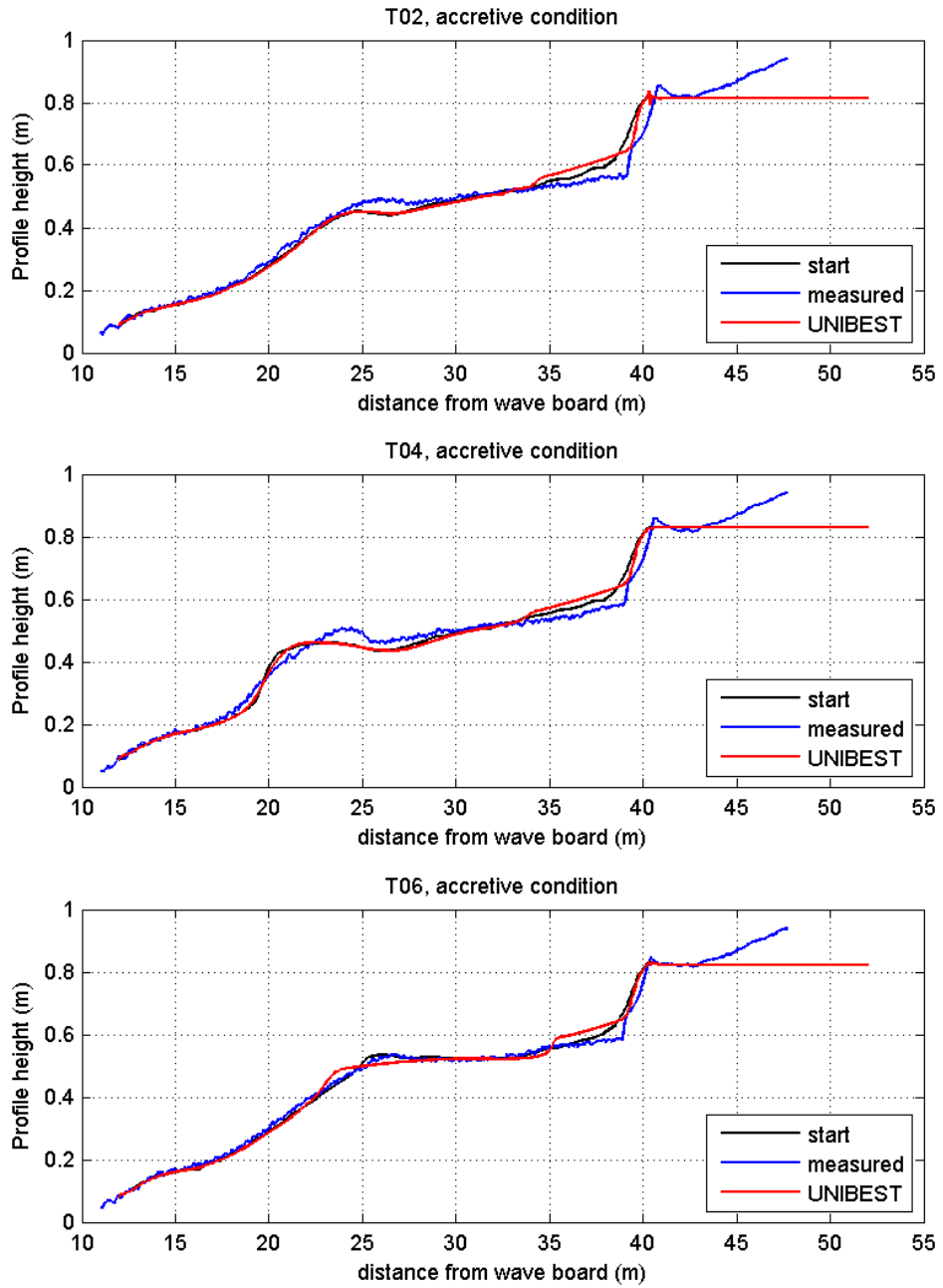


Figure 5.10 Measured (blue line) and modelled (red line) bed profile development for the accretive tests

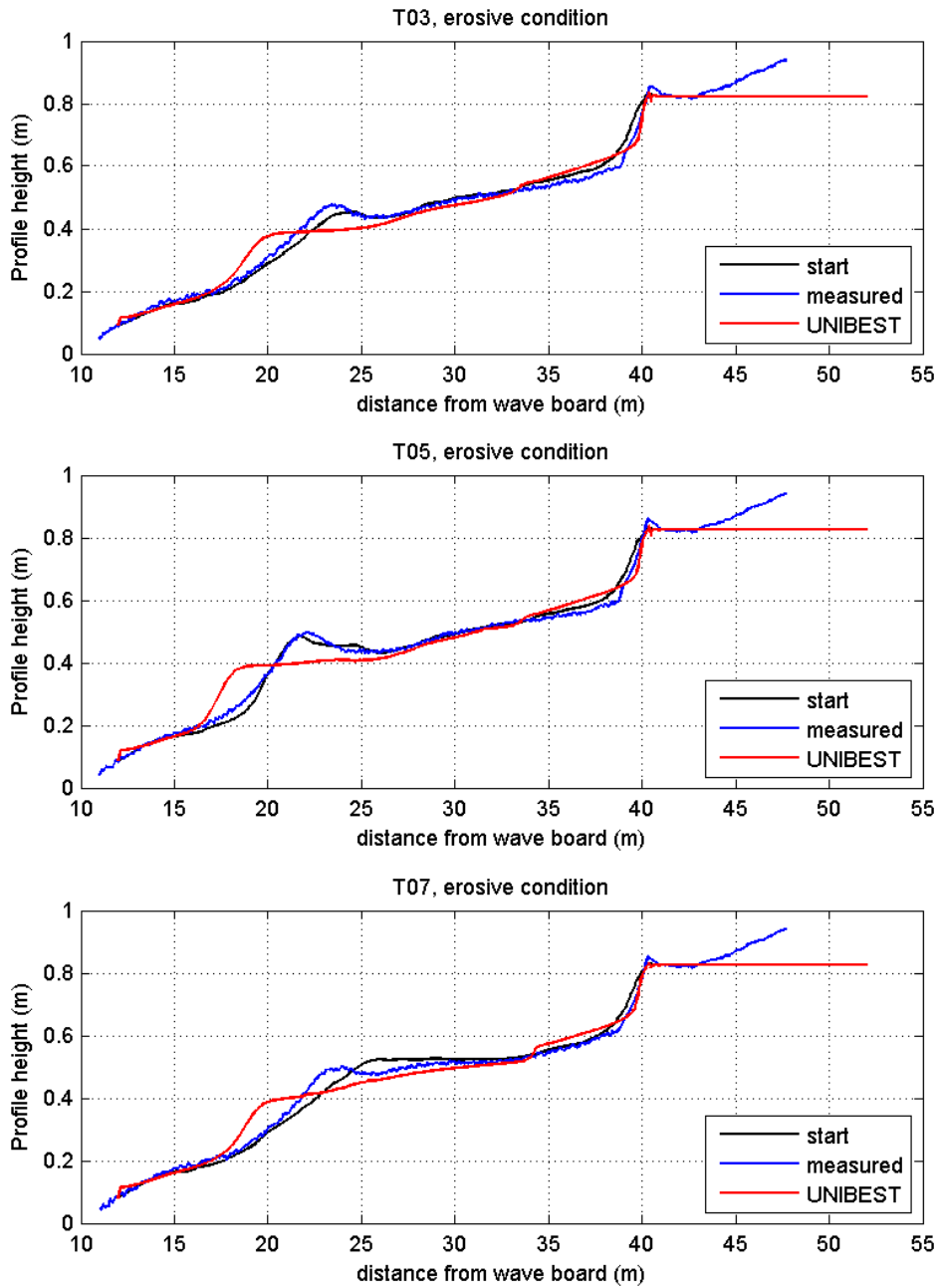


Figure 5.11 Measured (blue line) and modelled (red line) bed profile development for the erosive tests

5.4.6 Bed profile development SANDS

The measured bed profile development of the project SANDS is compared to the modelled bed profile development. The settings are equal to the settings used for VOP. The grid size of SANDS test 1:10 was decreased. Still, for this test, using a grid size of 0.02 m close to the coastline, UNIBEST-TC is not able to properly simulate the bed profile development.

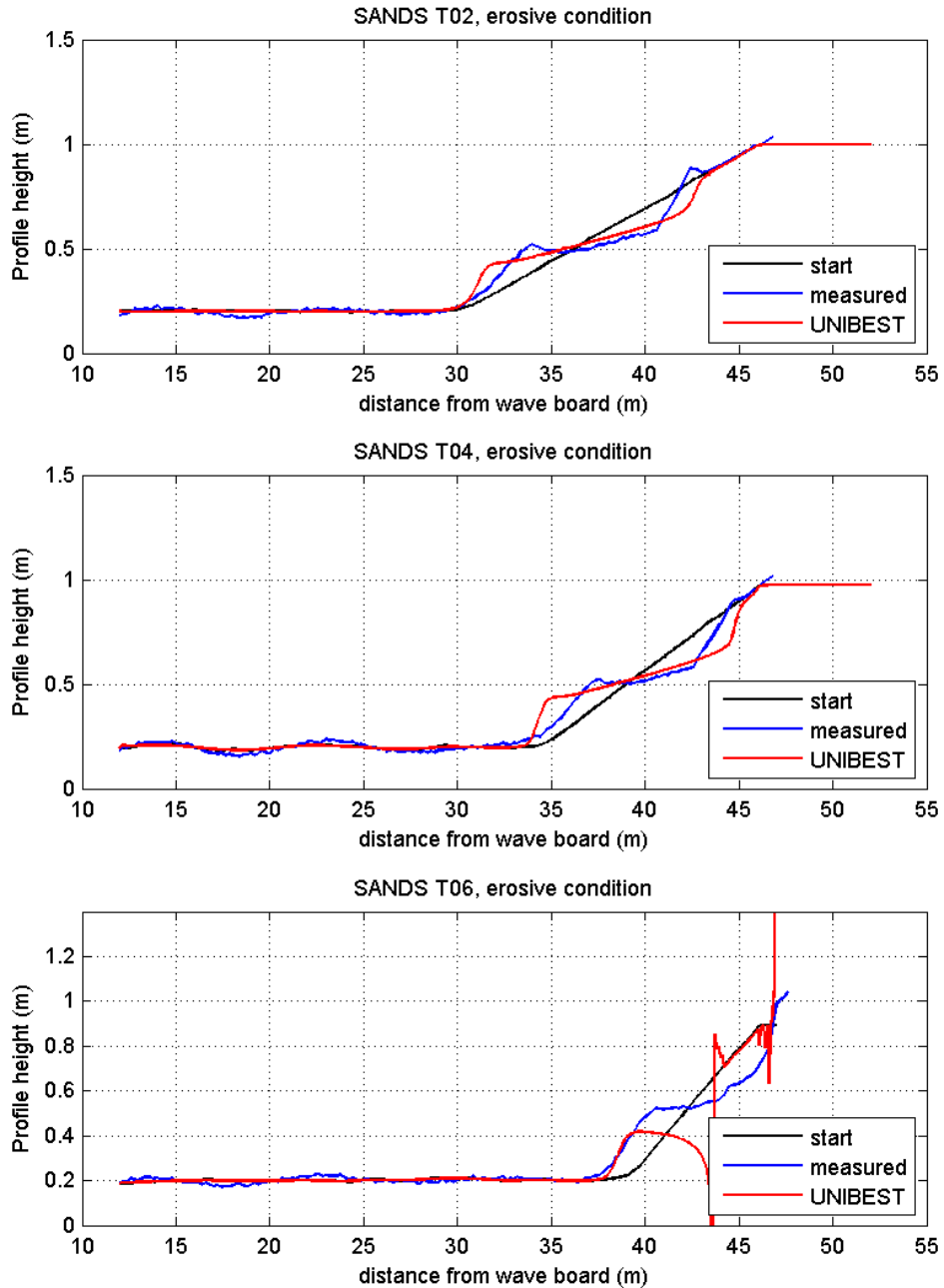


Figure 5.12 Measured (blue line) and modelled (red line) bed profile development for the erosive SANDS tests

6 Conclusions & recommendations

In this chapter, the main conclusions of this study are summarised. Subsequently, also some recommendations for further research are proposed.

6.1 Conclusions

6.1.1 Results of SANDS experiments

Beach profile development

The bed profiles exposed to an accretive wave condition show a shoreward migration of the breaker bar, whereas the bed profiles subject to an erosive wave condition show an offshore migration of the breaker bar. The net cross-shore sediment transport in coastal areas is a balance between landward transport by wave asymmetry and seaward transport by undertow. In case of a landward migration, the transport by wave asymmetry is dominant, whereas the seaward transport by undertow dominates when the bed profile is subject to an erosive condition.

Analysis of the development of sediment volumes in time indicates that no equilibrium profile is reached. Even after 48 hours of propagating erosive waves on the initial 1:15 slope, the bed profile changes. It may be possible that the process stops, if the decay of the wave height over the surf zone is sufficiently large, that the sediment transport due to the undertow does not dominate over the sediment transport caused by wave asymmetry. The length between the breaker bar and the coastline should be very large, in order to be able to reduce the wave height to such an extent. Such a profile is not likely to occur. Profiles exposed to an accretive condition, did not reach an equilibrium either. Contrary to the profile development of the erosive tests, it could be possible, that the profile development of the accretive tests reaches an equilibrium. This is not substantiated by the measured bed profiles.

Morphological time scale for distorted tests

Distorted models are physical models in which the horizontal length scale and the vertical length scale are different. Non-distorted models with the same scale in both the horizontal and vertical directions, are by far preferable. Still distorted hydraulic models may have to be used because of limitations on the available space in which to construct the model, or because of a lack of control over the modelling materials and conditions. The distortion scale is expressed as n_l/n_h .

The morphological time scale can be represented by

$$n_{Tm} = (n_l / n_h)^{b+1} (n_{d50})^d (n_{s-1})^e / (n_h)^{0.5-0.5a+0.5c}$$

Using $n_h = 1$, $n_{d50} = 1$ and $n_{s-1} = 1$, this yields,

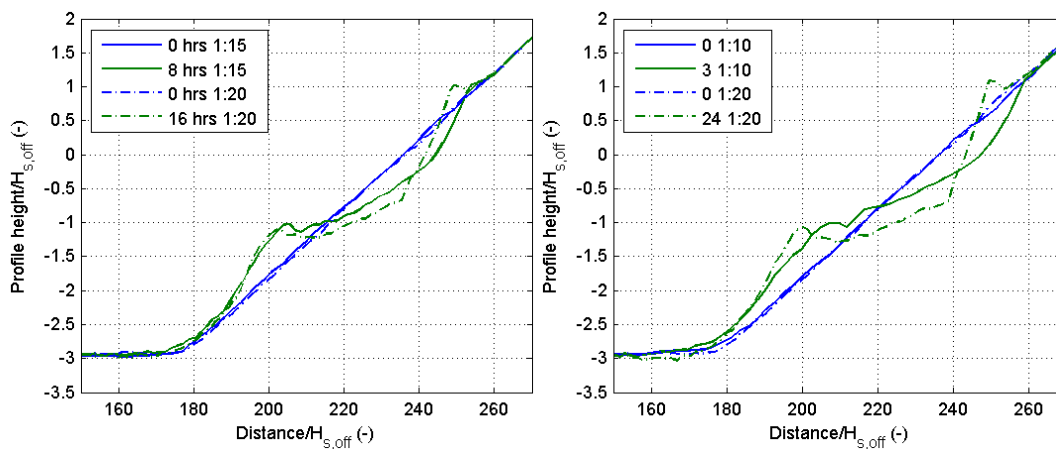
$$n_{Tm} = (n_t)^{b+1} = (n_t)^\beta$$

Factor β is assumed to lie between 1.5 and 3.5 (Van Rijn, 2007). Erosion and deposition volumes are analysed to find the exponent β . The morphological time scale factor of test 1:15 is approximately 2-2.5. For test 1:10, no single value for the time scale factor can be observed. As more sediment is deposited or eroded, the time scale factor initially increases and subsequently decreases again. The time scale factor varies from 6 to 10, with an average of approximately 8.

The tests do not have equal time scale factors. The exponents β of 2.4 for test 1:15 and 3 for test 1:10 both lie between 1.5 and 3.5, as Van Rijn predicted.

Time scale factors 8 for test 1:10 and 2 for test 1:15 are applied to the volumes of prototype test 1:20. The re-calculated erosion and deposition volumes of the erosive tests 1:10 and 1:15 correspond fairly well to the original erosion and deposition volumes of test 1:20.

The obtained time scale factors are checked by analysis of the profile development of test 1:10 and 1:15 with the reference test 1:20. A time scale factor of 2 implies that profile 1:20 after 16 hours should approximately be equal to profile 1:15, translated to profile 1:20, after 8 hours. The correspondence of the two profiles is relatively good, particularly in the vicinity of the breaker bar.



By means of the time scale factor for translation of test 1:10 to prototype test 1:20, test 1:10 after 3 hours should correspond with test 1:20 after 24 hours. It can be concluded that these similarities are not that good in comparison with the prototype test 1:20 and test 1:15. However, the bulk erosion values are approximately equal. For test 1:10 no swashbar is present.

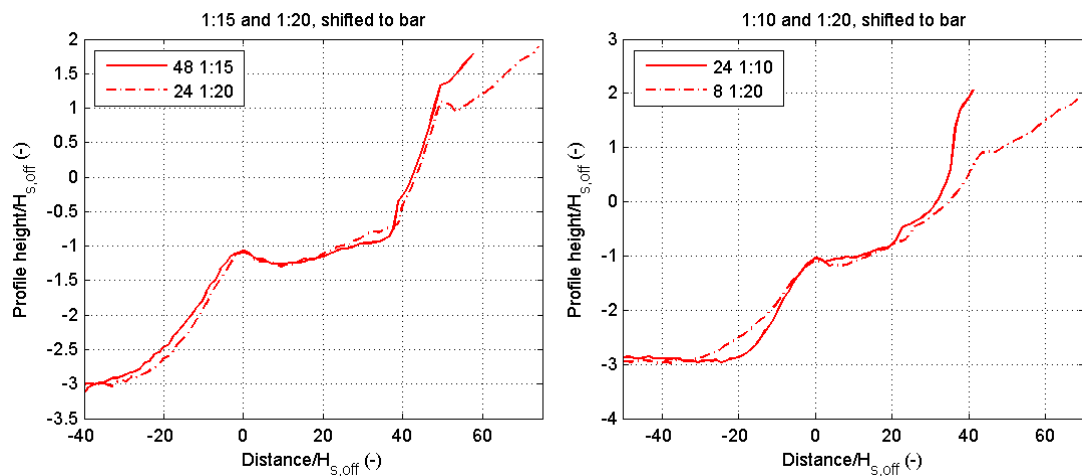
The distortion scale should be as small as possible, to prevent the generation of scale effects. Applying a distorted scale the wave breaking and wave run-up processes are overestimated, which results in overestimated erosion around the swash zone. The scale effects can be attributed to the fact that scale laws like the surf similarity parameter ($n_r = (n_h)^{0.5} (n_t / n_h)$) and fall velocity parameter ($n_{ws} = (n_h)^{0.5} (n_t / n_h)^{-1}$) are not lived up to.

Geometric characteristics

Extensive analysis is done to define and quantify parameters describing profile change. Geometric parameters are made non-dimensional to be able to draw a parallel between tests at all scale levels.

Analysis of beach slope, slope of outer bar, length of the surf zone, bar height, trough height and bar height show similar values for test 1:20 after 24 hours and 1:15 after 48 hours. Just the height of the swash bar differs. This implies that, after a certain period, the initial profile is not of importance in the profile development. From that moment on, it can be expected that the profile development will be more or less equal. As a result, a time scale factor can not be applied in the infinity, because this value will amount to one in time.

For test 1:10 such great similarities with prototype test 1:20 can not be found. Although comparable sediment transports with respect to test 1:20 and test 1:15 are found at the end of the test, little similarity between beach profiles is displayed. Especially higher up in the profile, deviations are significant; no swash bar can be found and the beach slope considerably differs. It can be expected that at a certain moment in time, the bed profile will be more or less equal to the bed profile of test 1:20. However, it is not evident, when this will be about to happen. It can be assumed that it will take more time for profile 1:10 than profile 1:15 to 'catch up' with test 1:20, because the initial profile of test 1:10 is more out of equilibrium compared to the initial profile of test 1:15.



To be able to compare the results of the three flume tests, it is recommended that the data of Hannover and Barcelona are analysed in a similar way as the data obtained in the Scheldt flume are analysed.

Results VOP experiments

Effect of nourishment designs

To obtain better insight into the effects of the nourishments on the bed profile development, the relative increase of sand volume in the coastal zone, defined as the range from 32 m from the wave board to the end of the profile, is computed. The low Nourishment Design 1, leads to a relative increase of sand volume, 20% for the accretive condition and 40% for the

erosive condition. The high Nourishment Design 2, however, results in the largest relative increase of sand volume, 60% for both wave conditions.

Effect of the presence of a shoreface nourishment on physical processes

The following effects are expected to occur as a consequence of the placement of a shoreface nourishment (Van Duin and Wiersma, 2002). Large waves break at the seaward side of the shoreface nourishment. Remaining shoaling waves generate onshore transport due to wave asymmetry over the nourishment area. The smaller waves in the leeside generate less stirring of the sediment and the wave-induced return flow (cross-shore currents) reduces. This results in an increase of the onshore sediment transport and a reduction of the offshore sediment transport. Both effects lead to an enhanced onshore transport behind the shoreface nourishment area.

Analysis of the data indicates that the presence of a shoreface nourishment significantly affects the wave height, the wave-induced return flow, the wave asymmetry and the sediment transport, whereas the presence of a shoreface nourishment does not have a clear relation with the sediment concentration. The physical processes that are affected by the presence of the nourishment are strongly connected. A reduced wave height leads to a reduced return flow, which in its turn leads to a reduced sediment transport.

The presence of a shoreface nourishment has a combined relative effect. On one hand, the shoreward sediment transport is reduced due to the decreased wave-induced return flow. On the other hand, the landward sediment transport is increased because of an increased wave asymmetry.

The presence of the high nourishment and the low nourishment both positively affect the bed profile development. The high nourishment, however, is far more effective than the low nourishment. An important aspect in the design of a nourishment seems to be the height of the nourishment. This can be explained by the fact that, due to the presence of the high nourishment, also smaller waves are not able to pass the breaker zone and break already on top of the nourishment instead of closer to the coastline.

Sediment characteristics

Analysis of the samples of the bed sediments taken at different positions along the flume, showed that on top of the breaker bar of the profiles of the reference tests and tests with the low nourishment, a slightly more coarse grain size is present compared to the grain size adjacent to the breaker bar.

6.1.2 Analysis of shoreface nourishments (VOP)

Effect of nourishment designs

To obtain better insight into the effects of the nourishments on the bed profile development, the relative increase of sand volume in the coastal zone, defined as the range from 32 m from the wave board to the end of the profile, is computed. The low Nourishment Design 1, leads to a relative increase of sand volume, 20% for the accretive condition and 40% for the erosive condition. The high Nourishment Design 2, however, results in the largest relative increase of sand volume, 60% for both wave conditions.

Effect of the presence of a shoreface nourishment on physical processes

The following effects are expected to occur as a consequence of the placement of a shoreface nourishment (Van Duin and Wiersma, 2002). Large waves break at the seaward side of the shoreface nourishment. Remaining shoaling waves generate onshore transport due to wave asymmetry over the nourishment area. The smaller waves in the leeside generate less stirring of the sediment and the wave-induced return flow (cross-shore currents) reduces. This results in an increase of the onshore sediment transport and a reduction of the offshore sediment transport. Both effects lead to an enhanced onshore transport behind the shoreface nourishment area.

Analysis of the data indicates that the presence of a shoreface nourishment significantly affects the wave height, the wave-induced return flow, the wave asymmetry and the sediment transport, whereas the presence of a shoreface nourishment does not have a clear relation with the sediment concentration. The physical processes that are affected by the presence of the nourishment are strongly connected. A reduced wave height leads to a reduced return flow, which in its turn leads to a reduced sediment transport.

The presence of a shoreface nourishment has a combined relative effect. On one hand, the shoreward sediment transport is reduced due to the decreased wave-induced return flow. On the other hand, the landward sediment transport is increased because of an increased wave asymmetry.

The presence of the high nourishment and the low nourishment both positively affect the bed profile development. The high nourishment, however, is far more effective than the low nourishment. An important aspect in the design of a nourishment seems to be the height of the nourishment. This can be explained by the fact that, due to the presence of the high nourishment, also smaller waves are not able to pass the breaker zone and break already on top of the nourishment instead of closer to the coastline.

Sediment characteristics

Analysis of the samples of the bed sediments taken at different positions along the flume, showed that on top of the breaker bar of the profiles of the reference tests and tests with the low nourishment, a slightly more coarse grain size is present compared to the grain size adjacent to the breaker bar.

6.1.3 Comparison UNIBEST-TC and physical model tests

The correlation coefficients between the measured and modelled flow velocities, wave heights and sediment concentrations are considerably high. However, the sediment transports are not simulated properly. The differences between the measured bed profile development with and without a shoreface nourishment are not comparable with the differences between the modelled bed profile development. Modelled sediment transports are significantly underestimated. This could be due to the fact that the tests are simulated on a very small (flume)scale.

6.2 Recommendations

Instruments

The ASTM gives a signal in blocks due to the fact that the processor was not able to compute more than two points in one second. It is recommended to adjust the software to obtain more accurate flow velocities and sediment concentrations.

SANDS

To be able to compare the results of the three flume tests, it is recommended that the data of Hannover and Barcelona are analysed in a similar way the data obtained in the Scheldt flume are analysed. The geometric characteristics have to be made dimensionless by division with the offshore significant wave height and the offshore water depth.

VOP

Based on this study to the effects of the presence of shoreface nourishment on the physical processes and bathymetry, it is recommended to implement the shoreface nourishment higher up the profile. Other aspects of the implementation of a high shoreface nourishment should be studied, like the impact of the presence of a high shoreface nourishment on the ecology.

Although the correlation coefficients between the modelled and measured concentrations, flow velocities and sediment concentrations are considerably high, additional modelling efforts are required, particularly for the sediment transport simulations. It is recommended to upscale the measured data and simulate this in UNIBEST-TC.

Study the effect of oblique waves versus perpendicular waves. This research was limited to studying the effect of perpendicular waves. In reality, wave directions vary.

7 References

- Battjes, J.A., 2006. Short waves combined lecture notes of DUT (2001) and IHE (1984), July 2006.
- Bosboom, J., Aarninkhof, S.G.J., Reniers, A.J.H.M., Roelvink, J.A. and Walstra, D.J.R., 1997. UNIBEST-TC 2.0. Overview of model formulations. Delft Hydraulics report H2305.42
- Bosman, J.J., E.T.J.M. van der Velden, C.H. Hulsbergen, 1987, Sediment concentration measurement by transverse suction. *Coastal Eng.*, 11: 353-370.
- Davis, J.C. (2002), *Statistics and data analysis in geology* – 3rd edition.
- Dongerren, A. van, I. Wenneker, J.A. Roelvink, A. Rusdin, 2006, A Boussinesq-type wave driver for a morphodynamical model, *Coastal Engineering*
- Hamm, L., Capobianco, M., Dette, H. H., Lechuga, A., Spanhoff, R. & Stive, M. J. F. (2002). A summary of European experience with shore nourishment. *Coastal engineering*, 47(2), 237-264, issn. 0378-3839.
- Heijer, C. den, 2005. Effect of wave period on dune erosion. M.Sc. Thesis, Delft University of Technology.
- Heijer, C. den, 2004. Concentratie meting door dwarse afzuiging. WL|Delft Hydraulics internal report H4265, March 2004.
- Hughes, S.A., 1993, *Physical models and laboratory techniques in coastal engineering*, Advanced Series on Ocean Engineering, Vol. 7. World Scientific, London, 1993, ISBN 981-02-1540-1, xv + 568 pp.
- Hulscher, S.J.M.H., J.S. Ribberink, M.A.F. Knaapen, (2002), *Marine Dynamics II*, lecture notes
- Koomans, R.L. and J. Bosboom (2000). Laboratory experiments on sediment dynamics and density gradation: Part I, time-averaged measurements.
- Koomans, R.L., 2000, *Sand in motion: Effects of density and grain size*. Rijksuniversiteit Groningen: Groningen, The Netherlands. ISBN 90-367-1338-2. 210 pp
- Phillips, O. M. (1977), *The Dynamics of the Upper Ocean*, 2nd ed., 336 pp., Cambridge Univ. Press, New York.
- Roelvink, J. A., and M. J. F. Stive (1989), Bar-generating cross-shore flow mechanisms on a beach, *J. Geophys. Res.*, 94(C4), 4785–4800.
- Roelvink, J.A., 1993. Surf beat and its effect on cross-shore profiles. Ph. D. Thesis, Delft University of Technology.
- Roelvink J.A. and M.J.F. Stive, 1989. Bar-generating cross-shore flow mechanisms on a beach. *J. Geophys. Res.*, Vol. 94, no. C4, pp. 4785-4800.
- Steezel, H.J., 1996. Schaalrelaties, Nadere analyse schaalrelaties dwarstransport via formulering pragmatisch transportmodel, WL|Delft Hydraulics report H2167, June 1996.

- Van Duin, M.J.P. and N.R. Wiersma, 2002. Evaluation of the Egmond shoreface nourishment, Part 1: Data analysis. WL | Delft Hydraulics report Z3054 / Z3148, June 2002.
- Van Duin, M. J. P., N.R. Wiersma, D.J.R. Walstra, L.C. Van Rijn, M.J.F. Stive, 2004. Nourishing the shoreface: observations and hindcasting of the Egmond case, The Netherlands. *Coast. Eng.* (in Press).
- Van Leeuwen, S.M., N. Dodd, D. Calvete, A. Falqués. Linear evolution of a shoreface nourishment, *Coast. Eng.*, 54(5), 417-431 (2007).
- Van Rijn, L. C. (2006). "Manual sediment transport measurements." *Rep.*, WL|Delft Hydraulics, Delft, The Netherlands.
- Van Rijn, L.C. and D.J.R. Walstra, 2004. Analysis and modelling of shoreface nourishments, September 2004.
- Vellinga, P., 1986. Beach and dune erosion during storm surges. Ph.D. Thesis, WL | Delft Hydraulics, Publication No.327.
- Walstra, D.J.R. and H.J. Steetzel, 2003. Description of improvements in the UNIBEST-TC model. Upgrade of UNIBEST-TC Version 2.04 to 2.10. WL | Delft Hydraulics report Z3412.
- Walstra, D.J.R., A. Cohen, S. Aarninkhof, M. van Koningsveld, *Onderwatersuppleties, Ontwerprichtlijnen*, WL|Delft Hydraulics report, RIKZ Rijkswaterstaat
- Wiersma, N.R., 2002. Evaluation of the Egmond shoreface nourishment, Part 2: Validation morphological model UNIBEST-TC. WL|Delft Hydraulics report Z3054/Z3148, June 2002

A SANDS, overview of scaling laws

A.1 Froude number

The Froude number expresses the relative influence of inertial and gravity forces and is given by the square root of the ratio of inertial to gravity forces:

$$\sqrt{\frac{\rho L^2 U^2}{\rho L^3 g}} = \frac{U}{\sqrt{gL}} \quad (\text{A.1})$$

where,

ρ is the density of the fluid in kg/m^3

g is the gravitational acceleration in m/s^2

L is the characteristic length in m

U is the

Requiring that the Froude number is the same in the model as in the prototype:

$$\left(\frac{U}{\sqrt{gL}}\right)_p = \left(\frac{U}{\sqrt{gL}}\right)_m \quad (\text{A.2})$$

leads to

$$\frac{U_p}{U_m} = \sqrt{\left(\frac{g_p}{g_m}\right)\left(\frac{L_p}{L_m}\right)} \quad (\text{A.3})$$

Expressing in terms of scale ratios:

$$\frac{n_v}{\sqrt{n_g n_L}} = 1 \quad (\text{A.4})$$

A.2 Reynolds number

Reynolds number gives the relative importance of the inertial force on a fluid particle to the viscous force on the particle.

$$\frac{(\text{inertial force})}{(\text{viscous force})} = \frac{\rho L^2 V^2}{\mu VL} = \frac{\rho LV}{\mu} \quad (\text{A.5})$$

where,

V is the mean fluid velocity in m/s
 L is the characteristic length in m
 μ is the (absolute) dynamic fluid viscosity in Pa*s or kg/m/s

For a reproduction of a geometrically similar flow field the Reynolds number should have the same value in the model and in prototype.

In terms of scale ratios:

$$\frac{n_v n_L n_\rho}{n_\mu} = 1 \quad (\text{A.6})$$

It is often sufficient that the flow is turbulent in the laboratory model, which is satisfied if the Reynolds' number is larger than about 1000.

A.3 Dynamic similarity number

According to Vellinga (1986) dynamics of water motion under oscillatory waves can reasonably well be described by the linear wave theory:

$$\frac{du}{dt} = \frac{g\pi H}{L} \frac{\cosh\{2\pi(d-y)/L\}}{\cosh\{2\pi d/L\}} \sin(2\pi x/L - 2\pi t/T) \quad (\text{A.7})$$

$$\frac{dv}{dt} = \frac{-g\pi H}{L} \frac{\sinh\{2\pi(d-y)/L\}}{\sinh\{2\pi d/L\}} \cos(2\pi x/L - 2\pi t/T) \quad (\text{A.8})$$

Dynamic similarity requirement:

$$n\left(\frac{du}{dt}\right) = n\left(\frac{dv}{dt}\right) = 1 \quad (\text{A.9})$$

leading to,

$$n\left(\frac{g\pi H}{L}\right) = 1 \quad \text{so } n_H = n_L \quad (\text{A.10})$$

$$n\left(\frac{2\pi d}{L}\right) = 1 \quad \text{so } n_d = n_L$$

$$n\left(\frac{2\pi x}{L}\right) = 1 \quad \text{so } n_x = n_L$$

$$n\left(\frac{2\pi t}{T}\right) = 1 \quad \text{so } n_t = n_T$$

Parameters in (A.10) are not independent in wave motion. They are related by the dispersion relation:

$$\left(\frac{2\pi}{T}\right)^2 = \left(\frac{2\pi g}{L}\right) \tanh 2\pi d / L \quad (\text{A.11})$$

Together with $n_d = n_L$ resulting in

$$n_L = (n_T)^2 = n_d \quad (\text{A.12})$$

Recapitulating, the Froude scale for wave motion yields:

$$n_u = n_T = (n_L)^{0.5} = (n_H)^{0.5} = (n_h)^{0.5} \quad (\text{A.13})$$

A.4 Surf similarity number

For steeper slopes the linear wave theory does not give an adequate description of reality since the slope influences the type of wave breaking and as a result the hydraulic forces. A surf similarity parameter for the schematisation of wave breaking characteristics has been derived by Battjes (1974):

$$\xi = \frac{\tan \theta}{\sqrt{H_0 / L_0}} \quad (\text{A.14})$$

where,

$\tan \theta$ is the local bed slope (-)

H_0 is the offshore wave height in m

L_0 is the offshore wave length in m

Accurate presentation of wave breaking yields:

$$n_\xi = 1 ,$$

leading to

$$n_h / n_l = (n_H / n_L)^{0.5} \quad (\text{A.15})$$

Applying Froude scaling, it follows that

$$n_T = (n_h^{0.5})(n_l / n_h) \quad (\text{A.16})$$

When the wave period is scaled according to equation (A.13), equation (A.16) is not valid. This implies that in a distorted model it is not possible to maintain the geometrical, kinematical and dynamical characteristics of the breaking waves simultaneously: there will always be a scale effect. Scale effects are differences between the prototype and model response that arise from the inability to simulate all relevant forces in the model at the proper scale dictated by the scaling criteria (Hughes, 1993).

A.5 Fall velocity parameter

Kemp and Plinston (2006), Noda (1972), Dalrymple and Thompson (1976) and Gourlay (1980) have found that the slope of the beach profile is related to the dimensionless fall velocity parameter,

$$\frac{H}{w_s T} \quad (\text{A.17})$$

where,

H is the wave breaker height in m

w_s is the sediment fall velocity in m/s

T is the wave period in s

$$n_H = n_{ws} n_T \quad (\text{A.18})$$

Combined with equation (A.16), this results in:

$$n_{ws} = (n_h)^{0.5} (n_t / n_h)^{-1} \quad (\text{A.19})$$

For sediments from 0.1 to 0.5 mm n_{ws} is equal to n_{d50} .

A.6 Suspended transport

Vellinga (1986) has derived scale relations for sediment transport processes for dune erosion. A morphological time scale is introduced.

The suspended sand concentration is assumed to be almost constant over depth at the dune foot and it is assumed to be proportional to:

$$c \approx \frac{(U)^a (SL)^b}{(T)^c (d_{50})^d (s-1)^e} \quad (\text{A.20})$$

where

U is the peak orbital velocity in m/s

SL is the bed slope

T is the wave period in s

D_{50} is the median sediment size of bed material in m

s is the relative density ($=\rho_s - \rho_w$)

From basic sediment research in laboratory flumes it is known that approximately (Van Rijn, 1993, 2006):

$$c \approx U^3, c \approx 1/(T)^{1to2}, c \approx 1/(d_{50})^{1to2}, c \approx 1/(s-1) \quad (\text{A.21})$$

The effects of bed slope on the concentration is less well known, but it is assumed that c increases with increasing bed slope:

$$c \approx (SL)^{0.5 \text{ to } 2}$$

Summarizing:

$$a = 2 \text{ to } 3,$$

$$b = 0.5 \text{ to } 2,$$

$$c = 1 \text{ to } 2$$

$$e = 1$$

Using Froude scaling and $n_{SL} = n_h / n_l$, this yields:

$$n_c = (n_h)^{0.5a-0.5c} (n_{d50})^{-d} (n_{s-1})^{-e} (n_l / n_h)^{-b} \quad (\text{A.22})$$

Sediment transport processes are represented by:

$$q_s = huc \text{ and } q_s = A_e / T_m \quad (\text{A.23})$$

in which,

A_e is the dune erosion area in m^2

T_m is the time scale to erode the dune face in s

Suspended transport scale can be represented by:

$$n_{qs} = (n_h)^{1.5+0.5a-0.5c} (n_{d50})^{-d} (n_{s-1})^{-e} (n_l / n_h)^{-b} \quad (\text{A.24})$$

and by:

$$n_{qs} = (n_l / n_h) (n_h)^2 / (n_{Tm}) \quad (\text{A.25})$$

These formula can be combined, resulting in:

$$n_{Tm} = (n_l / n_h)^{b+1} (n_{d50})^d (n_{s-1})^e / (n_h)^{0.5-0.5a+0.5c} \quad (\text{A.26})$$

B SANDS, shifted bed profiles

Prototype profile and, respectively, profile 1:10 and 1:15 are plotted on top of each other, where the top of the breaker bar or the intersection of still water level and profile are used as reference points. In this way, insight is given into several features analysed in more detail in Section 3.4.1 through Section 3.4.4. The shifted profiles are made dimensionless by dividing the height and length by the offshore water depth (upper plot) and the offshore wave height (lower plot).

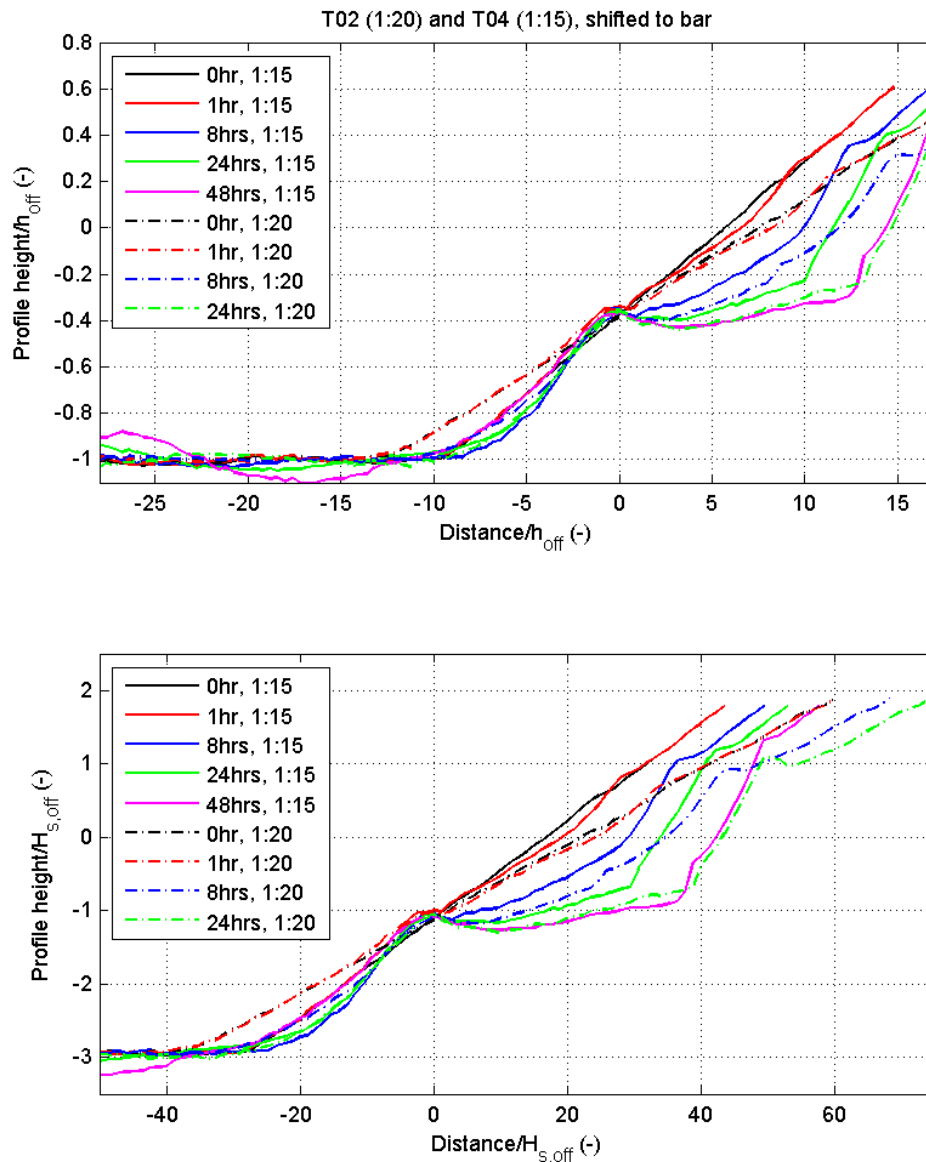


Figure B.1 Dimensionless profiles T02 and T04, shifted on top of breaker bar

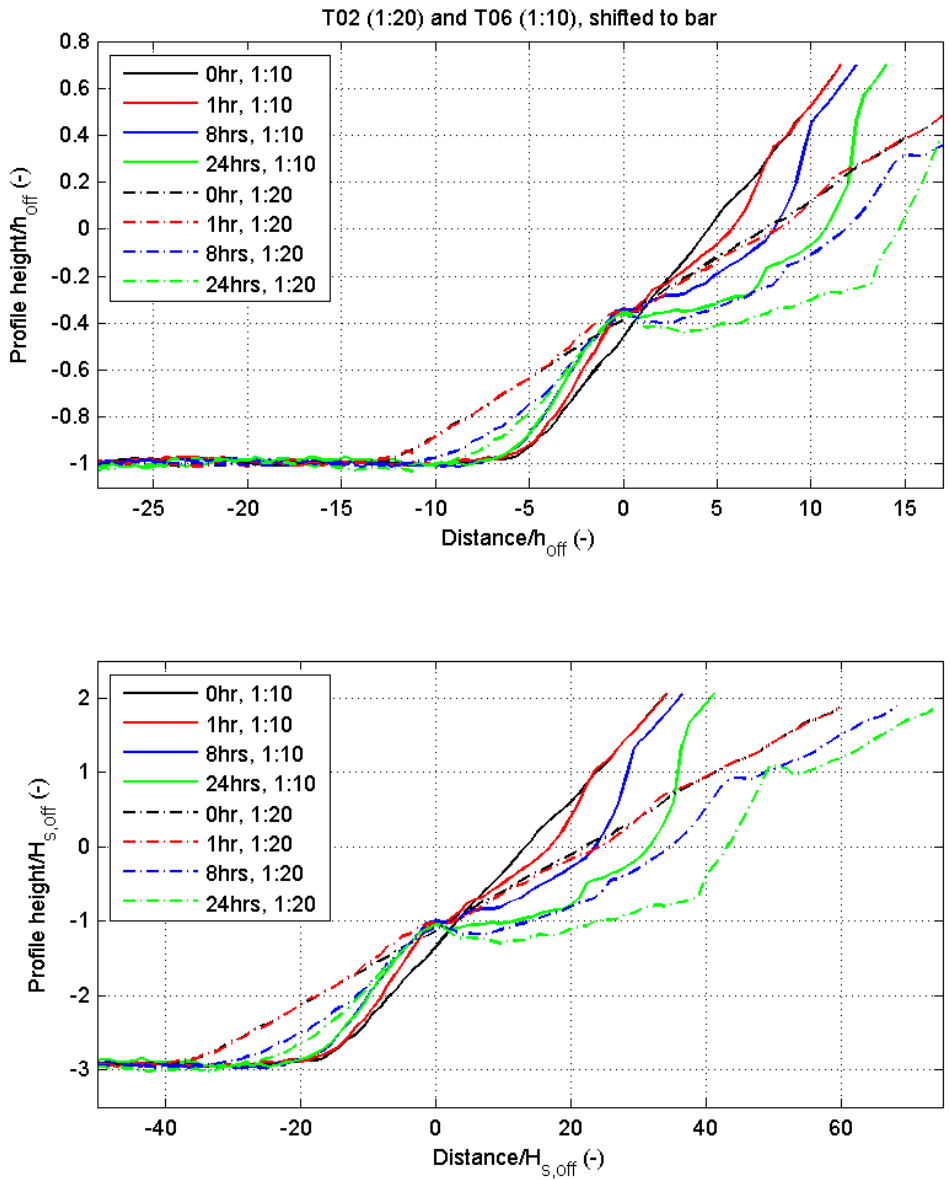


Figure B.2 Dimensionless profiles T02 and T06, shifted on top of breaker bar

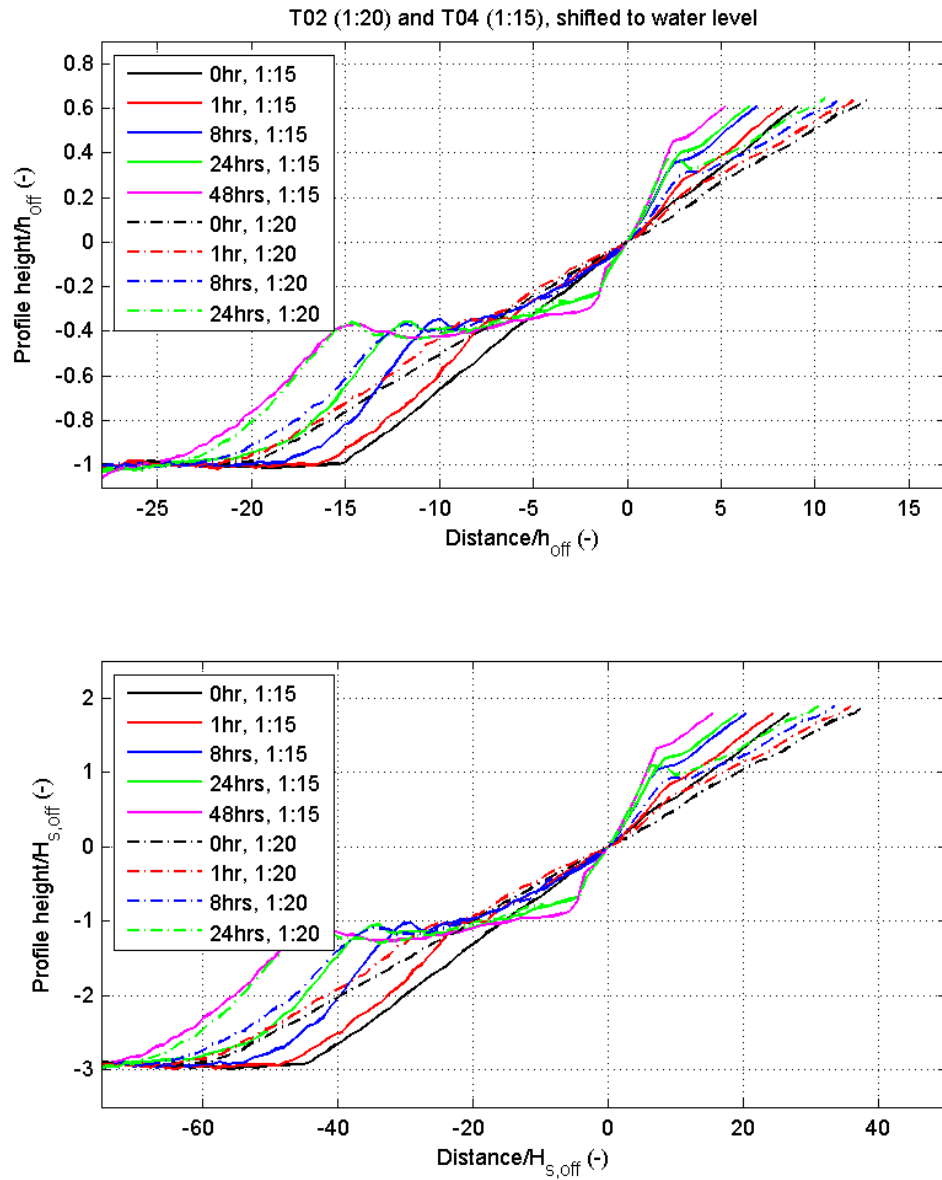


Figure B.3 Dimensionless profiles T02 and T04, shifted to water level

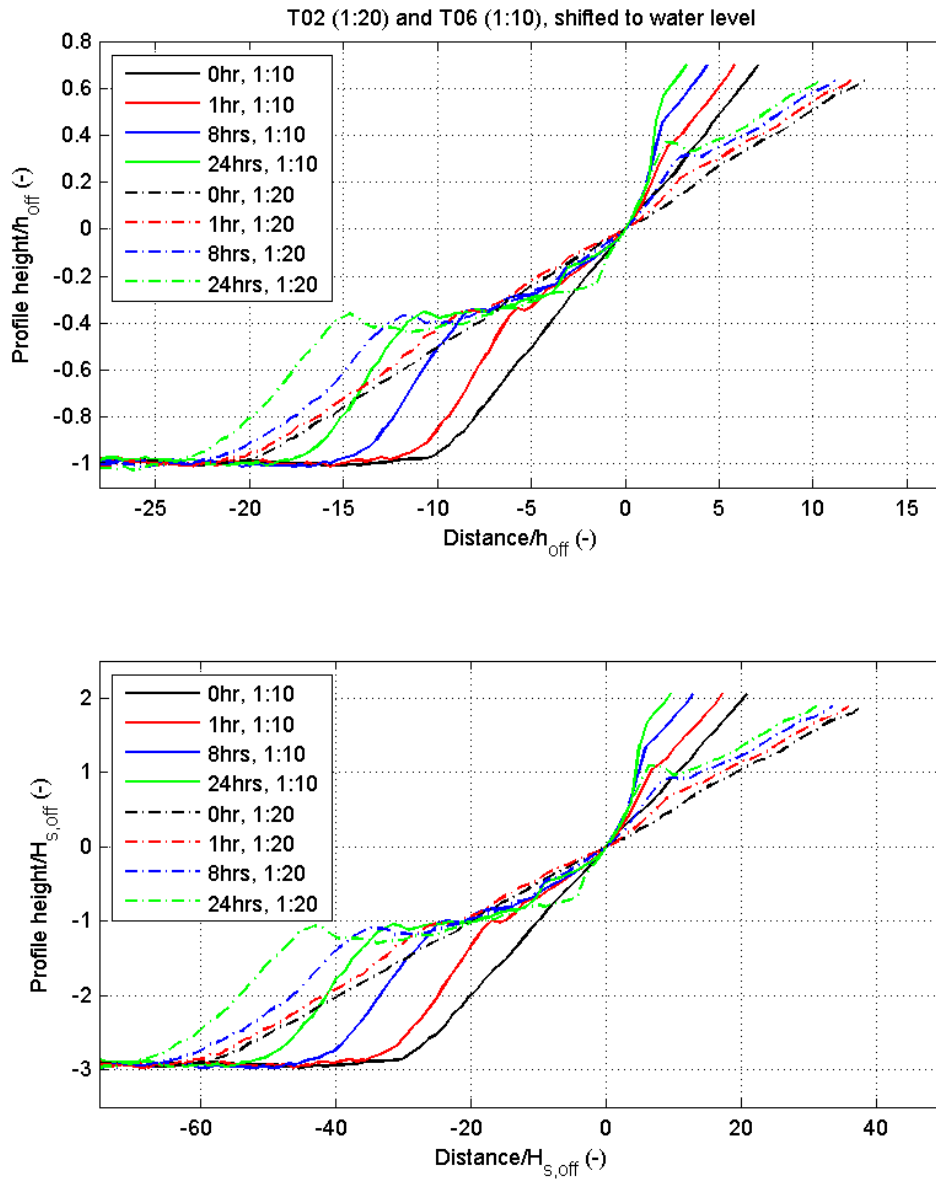


Figure B.4 Dimensionless profiles T02 and T06, shifted to water level

C Sediment transport

Sediment transport is derived from velocity and concentration profiles applying the integral method according to Van Rijn (1991). In this Appendix, this method is explained.

Velocity

The velocities between bed and first measuring point is described by:

$$v = v_1 (z / z_1)^{0.25} \quad \text{for } 0 < z < z_1 \quad (\text{C.1})$$

in which:

v_1 = fluid velocity in first measuring point above the bed

z_1 = height above bed of first measuring point

The velocities between the last measuring point (z_L) and water surface can be taken equal to the velocity in the measuring point.

$$v = v_L \quad \text{for } z_L < z < h \quad (\text{C.2})$$

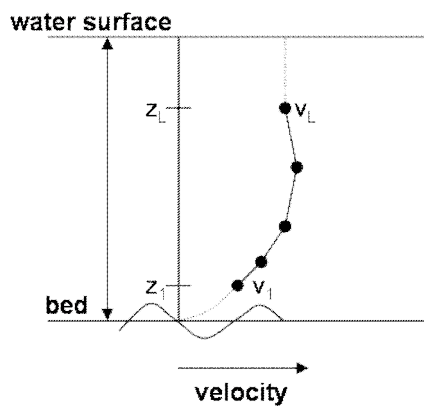


Figure C.1 Extrapolation of velocity profiles

Concentration

The sediment concentrations between last measuring point and water surface are given by a linear function according to:

$$c = [(h - z) / (h - z_L)] c_L \quad \text{for } z_L < z < h \quad (\text{C.3})$$

in which:

c_L = concentration in last measuring point

z_L = height above bed of last measuring point

Three different extrapolation methods are used to represent the concentration profile between bed and lowest measuring point.

Method 1:

Applying the first method the sediment concentrations between bed and lowest measuring point are assumed to be equal to the concentration in the first measuring point:

$$c = c_1 \quad \text{for } 0 < z < z_1 \quad (C.4)$$

Method 2:

The second method computes the sediment concentrations according to:

$$c = AY^B \quad \text{for } 0 < z < z_1 \quad (C.5)$$

in which:

$Y = (h-z)/z$ (dimensionless vertical coordinate)

z = vertical coordinate above bed

h = water depth

A, B = coefficients

Method 3:

Sediment concentrations between bed and first measuring point are represented by:

$$c = e^{AZ+B} \quad \text{for } 0 < z < z_1 \quad (C.6)$$

in which:

z = vertical coordinate above bed

A, B = coefficients

The coefficients in Method 2 and 3 are determined by a regression method applying the measured concentrations in the first three measuring points above the bed.

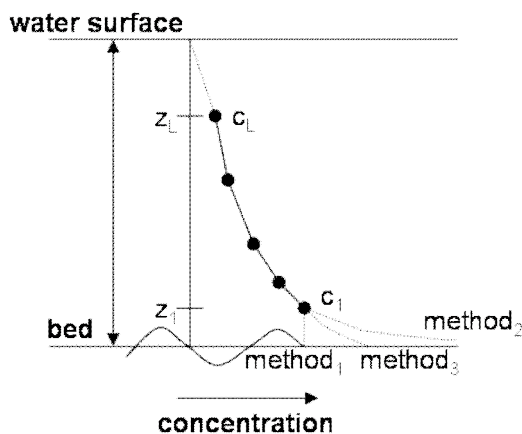


Figure C.2 Extrapolation of concentration profiles

Suspended load transport

Computation of the depth-integrated suspended sediment transport requires measurements of velocities and concentrations at equal elevations. Depth-integrated suspended sediment transport (S_s) is calculated as follows:

$$S_s = \sum^N [0.5(v_i c_i + v_{i-1} c_{i-1})(z_i - z_{i-1})] \quad (C.7)$$

in which:

v_i = fluid velocity at height z above the bed (m/s)

c_i = sediment concentration at height z above the bed (kg/m³)

N = total number of points

D Description of UNIBEST-TC

UNIBEST-TC was developed by WL|Delft Hydraulics. This chapter describes the UNIBEST TC model, based on Bosboom et al. [1997]. Uniform Beach Sediment Transport – Time dependent Cross-shore is a process-based model that incorporates models for hydronamic processes.

D.1 Schematic representation of UNIBEST TC model

The model can be divided into five sub models. The scheme in Figure D.1 shows how these sub models interact with each other. In one time step UNIBEST TC computes first the local wave height according to wave height decay model ENDEC (*Battjes and Janssen, 1978*). From the local wave height, the orbital velocity and mean current are computed. Subsequently separate transport formulations are used for bed load transport and suspended transport. Finally, bottom changes are computed using a sediment mass balance equation, resulting in a new profile, which is used in the next time step.

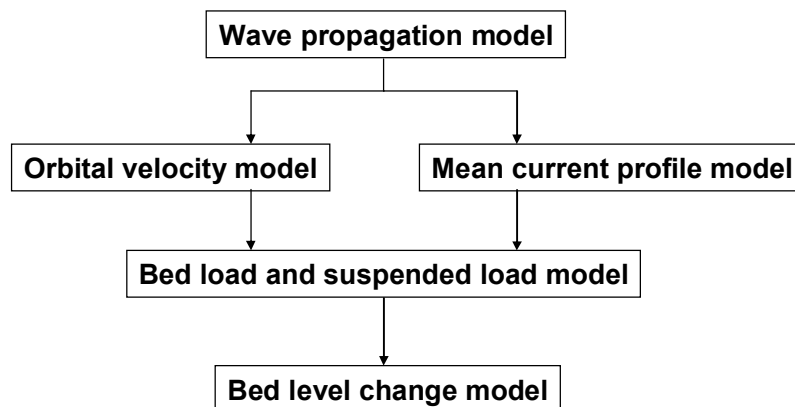


Figure D.1 Set-up of model UNIBEST-TC

The model requires an initial profile, grain sizes and offshore boundary conditions. In the subsequent Sections the sub-models are described.

The models are briefly described in the following sections, which is partly derived from Den Heijer (2005).

D.1.1 Wave propagation model

The wave propagation model solves three first-order differential equations by numerical integration. The equations describe the wave energy balance (Battjes and Janssen, 1978), the energy contained in surface rollers in breaking waves (Nairn et al., 1990) and the horizontal momentum balance.

The energy balance equation yields:

$$\frac{\partial}{\partial x} (E c_g \cos \theta) = -D_w - D_f \quad (\text{D.1})$$

in which,

c_g is the wave group velocity

θ the angle of incidence of the wave field

D_w the dissipation of wave energy due to breaking,

D_f the dissipation due to bottom friction,

E the wave energy.

For the dissipation of wave energy due to breaking an expression by Battjes and Janssen is used:

$$D_w = \frac{1}{4} \frac{\rho g \alpha}{T_p} H_{\max}^2 Q_b \quad (\text{D.2})$$

where,

Q_b is the fraction of breaking waves, calculated from $H_{\text{rms}} / H_{\max}$

α and γ are dissipation coefficients

The model applies a Rayleigh distribution for the non-breaking waves, assuming that waves smaller than H_{\max} are not breaking. H_{\max} is defined according to:

$$H_{\max} = \frac{0.88}{k} \tanh \left(\frac{\gamma k h_r}{0.88} \right) \quad (\text{D.3})$$

For the dissipation of energy due to bottom friction, D_f , the following expression is implemented.

$$D_f = \frac{f_w \rho}{\sqrt{\pi}} u_{orb}^3 \quad (\text{D.4})$$

where,

f_w is a user defined friction factor,

$u_{orbital}$ is the amplitude of the orbital velocity at the bottom, according to linear wave theory and root mean square wave height,

The second equation used for the energy contained in surface rollers in breaking waves was modelled by Nairn:

$$\frac{\partial}{\partial x}(2E_r C \cos \theta) = D_w - Diss \quad (D.5)$$

in which the roller energy E_r represents the amount of kinetic energy in a roller with area A and length L :

$$E_r = \frac{1}{2} \rho c^2 \frac{A}{L} \quad (D.6)$$

The dissipation of roller energy is modelled according to:

$$Diss = \beta \rho g c \frac{A}{L} \quad (D.7)$$

where β is the slope of the face of the wave.

A delay for the breaking of waves was applied, as waves require a certain distance over critically shallow water before breaking occurs.

The third differential equation represents the set-up equation:

$$\frac{\partial \bar{\eta}}{\partial x} = - \frac{1}{\rho g h} \frac{\partial S_{xx}}{\partial x} \quad (D.8)$$

in which:

- η is the mean wave set-up
- ρ the specific weight of water
- g gravitational constant
- h water depth
- S_{xx} , the radiation stress.

D.1.2 Mean current profile model

In UNIBEST TC the modelling of the mean current profile is done according to Roelvink and Reniers (1994), using a quasi-3D model in which effects of wind stress, breaking-induced forcing, surface slope and wave boundary layer are taken into account. The model is derived from a model according to De Vriend and Stive (1987), who identified three layers.

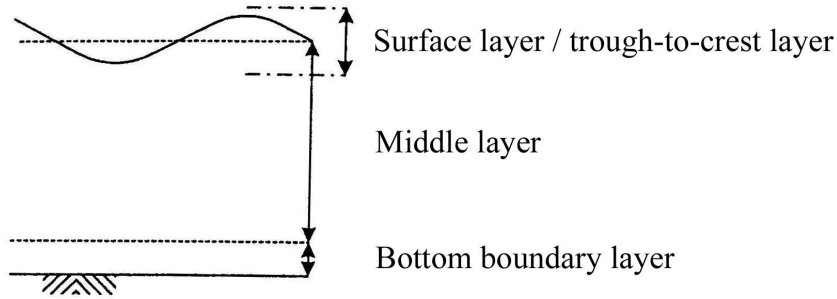


Figure D.2 Three layers, according De Vriend and Stive (1987)

In this model, the surface layer is replaced by a shear stress ($\tau_{s,wave}$) induced by wind and surface rollers and a mass flux (m) for calculation of the net mean flow below trough level.

$$\tau_{s,wave} = \frac{Diss}{c} \quad (D.9)$$

$$m = \frac{E + 2E_r}{c} \quad (D.10)$$

For the two other layers, the shear stress over the water height caused by the forcing on the surface is calculated from which a velocity gradient over the depth can be calculated after the eddy viscosity is established. This velocity gradient is then integrated, resulting in a velocity profile over the depth.

D.1.3 Wave orbital velocity model

The model of the time-variation of the near-bed velocity is based on a concept by Roelvink and Stive (1989). The model consists of two parts:

- A contribution due to wave asymmetry, computed according to the Rienecker and Fenton method.
- A contribution due to long waves, occurring due to grouping of short waves in a random wave field.

The two contributions are implemented separately, and added. The first step is a time series of the near-bed velocity U_1 in case of regular waves, taking into account the wave symmetry contribution:

$$U_1(t) = \sum_{j=1}^n B_j \cos(j\omega t) \quad (D.11)$$

Subsequently a second velocity time series, which is slightly out of phase with U_1 , is added.

$$U_2(t) = \sum_{j=1}^n \cos(j\omega t) \left[\frac{1}{2} (1 + \cos(\Delta\omega t)) \right]^j \quad (\text{D.12})$$

The magnitude of U_2 is corrected to U_2' in such a way, that the third moment of U_2' equals the third moment of U_1 .

$$U_2'(t) = \left(\frac{\frac{1}{T} \int_0^T U_1^3 dt}{\frac{1}{mT} \int_0^{mT} U_2^3 dt} \right) U_2(t) \quad (\text{D.13})$$

Secondly, in case of a random wave field the grouping of the short waves will generate bound long waves. Modelling of a bound long wave is done according to Roelvink and Stive (1989). It is assumed that wave-group related features of a random wave field may be represented by a bichromatic wave train with equal amplitudes a_m and a_n and an accompanying bound long wave with amplitude ξ_a .

In order to find values for $a_m = a_n$ and ξ_a , the wave train is required to have the same total surface variance.

$$m_0 \cong \frac{1}{8} H_{rms}^2 = \frac{1}{2} a_n^2 + \frac{1}{2} a_m^2 + \frac{1}{2} \xi_a^2 \quad (\text{D.14})$$

The long wave amplitude resulting from two waves with equal amplitudes and different frequencies is given by Sands (1982),

$$\xi_a = -G_{nm} \frac{a_n a_m}{d} \quad (\text{D.15})$$

in which G_{nm} is a transfer function.

The long wave velocity U_3 is represented by

$$U_3(t) = \xi_a \frac{\sqrt{gd}}{d} \cos\left(\frac{\omega}{m}t + \varphi\right) \quad (\text{D.16})$$

The phase shift φ is calculated according to an empirical relationship found by Roelvink and Stive (1989).

$$\cos(\varphi) = C_r \left[1 - 2 \left(\frac{H_{rms}}{H_{rms,0}} \right)^2 \right] \quad (\text{D.17})$$

in which,

C_r is the correlation coefficient between the wave envelope and long wave surface variation
 $H_{rms,0}$ is the incoming wave height at the seaward boundary of the model.

Finally, addition of the effects due to short-wave envelope and the bound long wave results in the total orbital velocity:

$$U_4(t) = U_2'(t) + U_3(t) \quad (\text{D.18})$$

D.1.4 Bed load and suspended load transport model

Bed load and suspended load are modelled separately by UNIBEST-TC and added. Bed load is transport of sediment due to grains rolling or jumping over the bed, suspended load is caused by a part of the grains suspended in the water, moving along with the movement of the water.

Bed load transport

For calculation of the bed load transport, UNIBEST-TC applies a non-dimensional bed-load transport vector Φ_{bd} according to Ribberink:

$$\Phi_{bd}(t) = \frac{q_b(t)}{\sqrt{\Delta g D_{50}^3}} = 9.1 \frac{\beta_s}{(1-p)} \left\{ |\theta'(t)| - \theta_{cr} \right\}^{1.8} \frac{\theta'(t)}{|\theta'(t)|} \quad (\text{D.19})$$

which implies the ratio of bed load-transport rate q_b and the square root of a parameter representing the specific under water weight of sand grains. The difference between the dimensionless effective shear stress (θ') and the critical shear stress (θ) determines the transport. The critical shear stress is the shear stress for which the grains on the bed just start to move.

θ' , the effective shear stress due to current and waves represents the sediment forcing as a ratio of the flow drag-force on the grains and the under water weight of grains:

$$\theta'(t) = \frac{\tau_b'(t)}{(\rho_s - \rho) g d_{50}} \quad (\text{D.20})$$

in which

$$\tau_b' = \frac{1}{2} \rho f_{cw}' |u_b(t)| u_b(t) \quad (\text{D.21})$$

where,

f_{cw}' is the weighted friction factor
 u_b is the near bottom velocity at top of the bottom layer.

In the transport formulation the Bagnold parameter β_s is included, taking into account the bottom slope. Grains moved uphill by water movement will cause a smaller transport than grains moved downhill by water movement. This factor therefore decreases uphill transport and increases downhill transport. The magnitude of the factor depends on the difference between the actual bottom slope and the angle of repose. The factor, and therefore the bottom transport, can become infinitely big when these two approach each other. The actual bottom slope is in any case not allowed to exceed the angle of repose.

$$\beta_s = \frac{\tan \varphi}{\tan \varphi + \frac{dz_b}{ds}} \quad (\text{D.22})$$

in which $\frac{dz_b}{ds}$ represent the bottom slope and φ the angle of repose.

Suspended load transport

The suspended transport rate q_s can be computed from the vertical distribution of fluid velocities and sediment concentrations:

$$q_s = \int_a^{h+\eta} VCdz \quad (\text{D.23})$$

in which velocity V and concentration C can be divided in an averaged and a fluctuating component:

$$V = v + \tilde{v} \quad (\text{D.24})$$

$$C = c + \tilde{c} \quad (\text{D.25})$$

Substituting these components, and subsequently averaging over time and space yields

$$\overline{q_s} = \int_a^d vcdz + \int_a^d \tilde{v}\tilde{c}dz = \overline{q_{s,c}} + \overline{q_{s,w}} \quad (\text{D.26})$$

in which,

$q_{s,c}$ is the current related suspended sediment transport

$q_{s,w}$ is the wave related suspended sediment transport.

For the suspended load, the wave-related suspended transport is assumed to be small compared to the current related suspended transport. Therefore, the mean current velocity is used and the suspended load transport in volume per unit time and width inclusive pores is computed as

$$q_{s,c} = \frac{\int_a^h vcdz}{(1-p)\rho_s} \quad (D.27)$$

The concentration is derived by establishing a gradient in concentration over the depth through calculation of sediment stirring up and falling of sediment. A concentration near the bottom is then established, after which this concentration gradient profile can be integrated into a concentration profile over the depth.

The convection diffusion equation yields

$$w_{s,m}c + \varphi_d \varepsilon_{s,cw} \frac{dc}{dz} = 0 \quad (D.28)$$

in which,

$w_{s,m}$ is the fall velocity of suspended sediment in a fluid sediment mixture

φ_d is the damping factor dependent on the concentration

$\varepsilon_{s,cw}$ is the sediment mixing coefficient for combined current and waves, that can be modelled as:

$$\varepsilon_{s,cw} = \sqrt{(\varepsilon_{s,w})^2 + (\varepsilon_{s,c})^2} \quad (D.29)$$

where,

$\varepsilon_{s,c}$ symbolizes the current related mixing coefficient

$\varepsilon_{s,w}$ is the wave related mixing coefficient.

The convection diffusion equation is solved by numerical integration from a near bed reference level a to the water surface. The reference concentration c_a is given by:

$$c_a = 0.015\rho_s \frac{D_{50}}{a} \frac{T^{1.5}}{D_*^{0.3}} \quad (D.30)$$

in which,

T is the dimensionless bed shear stress parameter

D_* is the dimensionless particle diameter

D.1.5 Bed level change model

After the computation of the transport rates along the profile, the bed level changes are computed from the depth integrated mass balance:

$$\frac{\delta z}{\delta t} + \frac{\delta q_{bot+sus}}{\delta x} = 0 \quad (D.31)$$

in which $q_{bot+sus}$ is the combined bed load and suspended transport rate including pores.